The Formation of Novel Sulfur-Containing Natural Product derivatives from Blended Garlic and Cruciferous Plant Preparations

by

Albandary Yahya S Ziyad

A thesis submitted for the degree of Doctor of Philosophy



University of East Anglia

Norwich Research Park, Norwich NR4 7TJ

Supervisor: Dr. Christopher Hamilton

Second Supervisor: Professor A. Ganesan

May 2026

© This copy of the thesis has been supplied on condition that anyone who consults it is understood to recognise that its copyright rests with the author and that use of any information derived therefrom must be in accordance with current UK Copyright Law. In addition, any quotation or extract must include full attribution.

Declaration

I confirm that this is my own work and the use of all material from other sources has been properly and fully acknowledged.

Albandary Ziyad

Dedication

To my beloved husband, Maged,

for your unwavering support, endless patience, and boundless encouragement throughout this journey.

And to my precious children, Sama and Maan,

Your laughter, love, and light gave me strength when I needed it most.

This work is for you, and because of you.

Acknowledgements

First and foremost, I would like to express my deepest and most sincere gratitude to my first supervisor, Dr. Christopher Hamilton. Throughout every stage of this research, Dr. Hamilton has been an exceptional mentor, patient, thoughtful, and genuinely invested in my progress. His door was always open, and his willingness to listen, advise, and encourage me, even during the most challenging moments, made an immeasurable difference to this work and to my confidence as a researcher. His intellectual enthusiasm, meticulous attention to detail, and warm personal support have shaped this thesis in countless ways. I feel truly fortunate to have had such a dedicated and caring supervisor, and I cannot thank him enough for everything he has given to this journey. I would also like to thank my second supervisor, Professor Ganesan, for his advice and support throughout this project.

I am grateful to the staff at the University of East Anglia for their assistance and support during my studies. In particular, I would like to thank Dr. Awis Anwar, my colleague in the laboratory, for his generous assistance with HPLC analyses, and Dr. Morritt for his valuable help with X-ray diffraction experiments. Their technical expertise and willingness to assist were instrumental to this research. Special thanks are also due to Dr. Hill at the John Innes Centre for his kind support with LC-MS analyses. His assistance was greatly appreciated and contributed significantly to the analytical work presented in this thesis.

I would also like to thank my friend in chemistry, Mona Alharbi, for her kind assistance with one of the experiments, her help is gratefully acknowledged. I would also like to extend my sincere thanks to my friend Hadeel Almagthali for her continuous support, encouragement, and help throughout this work. I am also grateful to all my friends and colleagues for their support.

I would like to gratefully acknowledge the financial support provided by King Khalid University and the Royal Embassy of Saudi Arabia, without which this research would not have been possible. I am deeply thankful for the opportunity they have afforded me to pursue my doctoral studies.

On a personal note, my deepest and most heartfelt gratitude goes to my beloved family, whose love and support have been the foundation upon which this achievement was built. To my wonderful husband Maged, words fall short of expressing how truly grateful I am for everything you have given me throughout this journey. Your endless patience, unconditional love, and unwavering belief in me have carried me through every challenge and every moment of doubt. You have been my greatest source of strength, my safe haven, and my constant encouragement. This accomplishment is as much yours as it is mine, and I am endlessly blessed and thankful to have you by my side.

To my precious daughter Sama and my dear son Maan, you are my heart, my joy, and my deepest inspiration. Your smiles, your laughter, and your boundless love have given me the strength to persevere and the reason to strive for the very best. Every step of this journey was taken with you in my heart. I hope that one day this work will inspire you to dream boldly and pursue your passions with dedication and courage. I am, and will always be, immeasurably proud to be your mother.

I would also like to express my deepest love and appreciation to my mother and siblings back home. Their constant emotional support, prayers, and encouragement from afar have sustained me throughout this endeavour, and I am forever grateful for their love and belief in me. To everyone who has contributed in whatever way, to the completion of this thesis; thank you. The last but not least, I want to thank me for believing in me, for doing all this hard work and for never quitting.

Abstract

Organosulfur compounds derived from garlic (*Allium sativum*) and cruciferous vegetables (*Brassica spp*.) are widely recognised for their biological activities, yet no prior study had examined whether their reactive sulfur metabolites could directly interact to generate novel hybrid natural products. This thesis investigates the chemical reactivity between two sulfur-containing compounds allicin and sinigrin hydrolysis intermediate. Each generated enzymatically in plant through the catalytic conversion of their respective precursors alliiin and sinigrin into highly reactive electrophilic species by alliinase and myrosinase, respectively. Under mild aqueous conditions, two previously unreported organosulfur compounds were formed and isolated, alligrin from the reaction of allicin with sinigrin hydrolysis intermediate, and alliphanin from the analogous reaction with glucoraphanin hydrolysis intermediate. Both compounds were fully characterised by NMR spectroscopy, high-resolution mass spectrometry, and for alligrin, single-crystal X-ray diffraction, which confirmed a previously unreported C-S-S-C-C=N-O-SO_3^- connectivity. Smaller quantities of additional rearranged products of alligrin/alliphanin were also identified and structurally characterized from allicin-sinigrin/glucoraphanin mixtures. Formation of both compounds was further confirmed in crude garlic-mustard and garlic-broccoli plants mixtures, demonstrating their relevance under real-world conditions. Antibacterial evaluation revealed that alligrin exhibits selective activity against Gram-positive pathogens including methicillin-resistant Staphylococcus aureus, with a thiol-dependent mechanism of action supported by glutathione reactivity studies. This work establishes inter-family plant sulfur reactivity as a new source of structurally novel bioactive natural products and provides a foundation for future development of plant-derived antimicrobial agents.

Access Condition and Agreement

Each deposit in UEA Digital Repository is protected by copyright and other intellectual property rights, and duplication or sale of all or part of any of the Data Collections is not permitted, except that material may be duplicated by you for your research use or for educational purposes in electronic or print form. You must obtain permission from the copyright holder, usually the author, for any other use. Exceptions only apply where a deposit may be explicitly provided under a stated licence, such as a Creative Commons licence or Open Government licence.

Electronic or print copies may not be offered, whether for sale or otherwise to anyone, unless explicitly stated under a Creative Commons or Open Government license. Unauthorised reproduction, editing or reformatting for resale purposes is explicitly prohibited (except where approved by the copyright holder themselves) and UEA reserves the right to take immediate ‘take down’ action on behalf of the copyright and/or rights holder if this Access condition of the UEA Digital Repository is breached. Any material in this database has been supplied on the understanding that it is copyright material and that no quotation from the material may be published without proper acknowledgement.

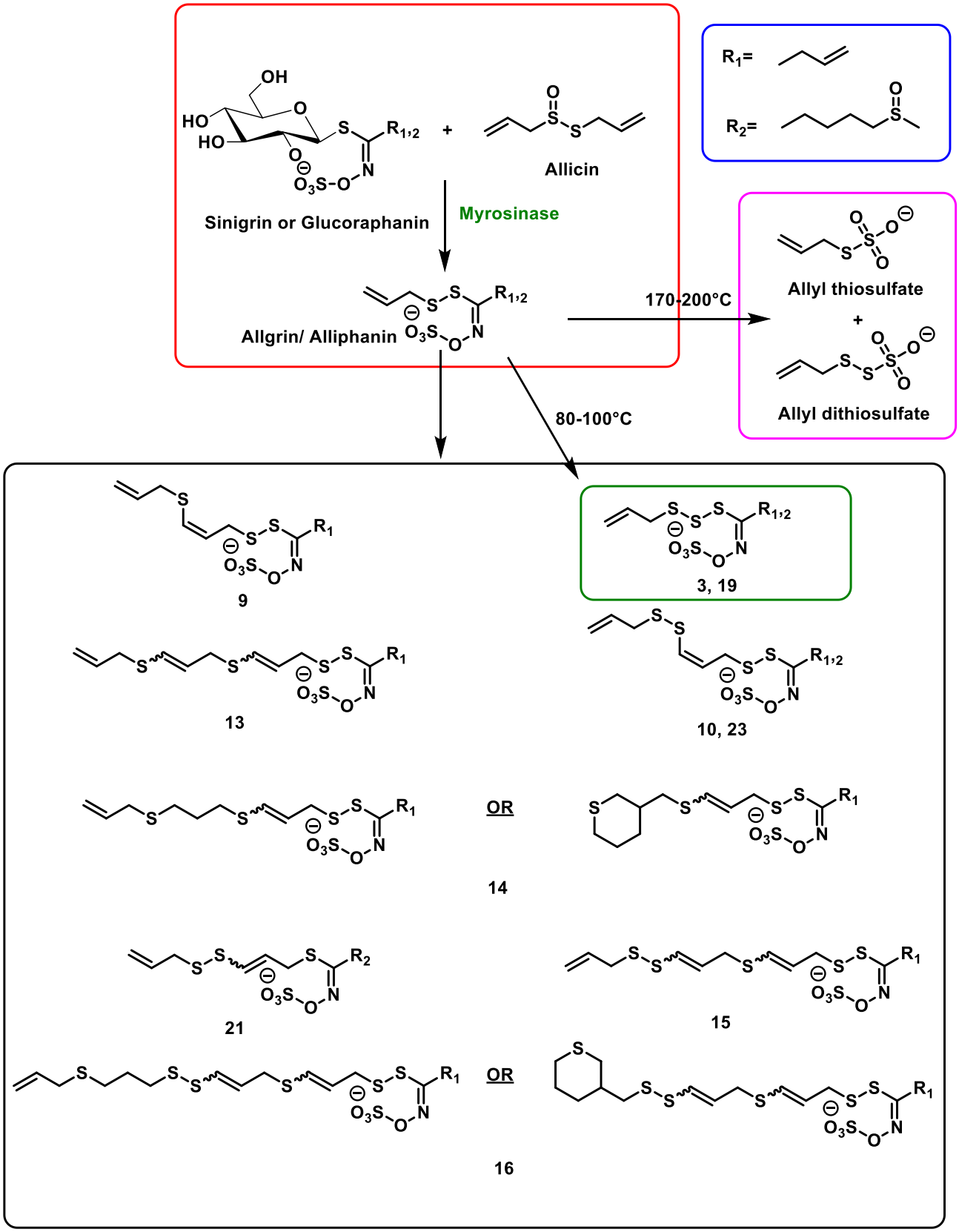
R1=
R2=
Allicin
Sinigrin or Glucoraphanin
Myrosinase
Allgrin/ Alliphanin
170-200°C
Allyl thiosulfate
+
Allyl dithiosulfate
80-100°C
3, 19
9
13
10, 23
OR
14
21
15
OR
16

Conferences and seminar

· **11th International Conference and Exhibition on Natural Products and Medicinal Plants Research** 2023, 2-3 Oct 2023, London, Uk, Poster Presentation: “Novel Natural Product from Mixed Plant Extracts “.

· **UEA School of Chemistry, Pharmacy and Pharmacology, CBBG Postgraduate Symposium** 2024, April 2024, Poster Presentation: “Novel Natural Product from Mixed Plant Extracts “.

· **UEA School of Chemistry, Pharmacy and Pharmacology, PHA Early Career Research Symposium** 2024, June 2024, Poster Presentation: “The discovery and characterisation of the natural product produced when degraded sinigrin reacts with allicin “.

· **UEA School of Chemistry, Pharmacy and Pharmacology Research Day**, September 2024, Poster Presentation: Awarded people’s choice poster prize.

· **UEA School of Chemistry, Pharmacy and Pharmacology seminar, Oral presentation:** November 2024“The discovery and characterisation of natural byproduct produced from blended plants mixtures”.

· **6th Annual Centre for Natural Products Discovery Conference** (2025),23-26 June 2025, Liverpool John Moors University, UK, Oral presentation: “The discovery and characterisation of natural byproduct produced from blended plants mixtures”. Awarded the Kelvin Chan Prize for Best Doctoral Presentation.

Table of contents

1 Introduction 1

1.1 Global impact of infectious diseases 1

1.2 Antimicrobial resistance (AMR): An escalating global threat 1

1.3 Overview of bacterial diversity 2

1.4 Clinically relevant bacterial species 2

1.4.1 Bacteria, associated diseases, and resistance mechanisms 2

1.5 Structural basis of gram-positive and gram-negative bacterial cell walls 5

1.5.1 Mechanisms of antimicrobial resistance 6

1.5.1.1 Intrinsic resistance 7

1.5.1.1.1 Efflux pumps 7

1.5.1.1.2 Reduced permeability 7

1.5.1.1.3 Chromosomally encoded enzymes 8

1.5.1.1.4 Target modification 8

1.5.1.2 Adaptive mechanisms of antimicrobial resistance 8

1.5.1.2.1 Efflux pump upregulation 9

1.5.1.2.2 Reduced number of porins 9

1.5.1.2.3 Epigenetic changes 9

1.5.1.2.4 Persister cells 10

1.5.1.2.5 Biofilm formation 10

1.5.1.3 Acquired resistance 10

1.5.1.3.1 *via* Horizontal gene transfer (HGT) 10

1.5.1.3.2 via Genetic mutations 11

1.6 Resolving antimicrobial resistance 11

1.7 Natural product drug discovery 13

1.7.1 Historical and ethnopharmacological foundations of natural product drug discovery 13

1.7.2 Ecological and evolutionary roles of plant metabolites 14

1.7.3 Major plant-derived bioactive compounds 17

1.8 Literature review 20
1.8.1 Overview of natural organosulfur compounds in plants 20
1.9 Allium family-Garlic 21
1.9.1 Garlic in ancient and traditional medical systems 21
1.9.2 Organosulfur profiles in whole and crushed garlic 22
1.9.2.1 Fates of allicin during cooking or storage 24
1.9.3 Biological activities of organosulfur compounds formed by garlic hydrolysis 24
1.9.3.1 Antimicrobial activity 25
1.9.3.2 Anticancer activity 26
1.9.3.3 Antioxidant activity 26
1.9.3.4 Anti-inflammatory activity 26
1.9.3.5 Immunomodulatory effects 27
1.9.3.6 Cardioprotective effects 27
1.9.3.7 Hepatoprotective effects 27
1.9.3.8 Neuroprotective effects 27
1.10 Brassicaceae family 31
1.10.1 Distribution, botanical characterisation, and phytochemical significance of selected brassicaceae species 31
1.10.2 Historical overview of brassica family and their medicinal uses 32
1.10.3 Organosulfer compounds in brassica family 34
1.10.3.1 The myrosinase-glucosinolate system 41
1.10.3.2 Glucosinolate hydrolysis products 42
1.10.3.2.1 Isothiocyanates, thiocyanate and oxazolidine-2-thiones formation ..43
1.10.3.2.2 Nitriles and epithionitrile formation 43
1.10.3.2.3 Other hydrolysis products 44
1.10.4 Glucosinolates compounds in Brassica plants and the biological activities of their hydrolysis products 45
1.10.4.1 Antimicrobial activity 45
1.10.4.2 Anticancer activity 47
1.10.4.3 Antioxidant activity 47
1.10.4.4 Anti-inflammatory activity 47

1.10.4.5 Ecological and other roles....48
1.11 Thermal degradation pathways of sulfur-containing natural products....48
1.12 Thiol reactive species (RSS)....50
1.12.1 Experimental evidence for thiol trapping of glucosinolate-derived aglycones....52
1.13 Aim and objective of this PhD....53
1.14 Objectives....55
2 Investigating Thiol Reactivity of Intermediates Derived from Garlic and Cruciferous Vegetables: Potential for Novel Antimicrobial Natural By-Products....56
2.1.1 Synthesis of allicin using pre-formed performic acid....56
2.1.2 Structural characterization of sinigrin and its hydrolysis product allyl isothiocyanate via NMR....57
2.1.2.1 Sinigrin structure analysis....58
2.1.2.2 Allyl isothiocyanate structure analysis....59
2.1.2.3 Studying myrosinase catalytic hydrolysis of sinigrin in different solvents....60
2.1.3 Myrosinase catalytic hydrolysis of sinigrin in presence of garlic organosulfur compounds....66
2.1.3.1 Enzymatic reaction in dimethyl sulfoxide (DMSO)/phosphate buffer....66
2.1.3.2 Enzymatic reaction in acetonitrile (MeCN)/phosphate buffer....71
2.1.4 Isolation, purification, and elucidation of the new compound by analytical methods....74
2.1.4.1 Separation and purification by high performance liquid chromatography (HPLC)....74
2.1.4.1.1 Analytical HPLC method development and optimization....74
2.1.4.2 Preparative high performance liquid chromatography (Prep-HPLC)....76
2.1.4.3 Structure elucidation of alligrin....78
2.1.4.3.1 Nuclear magnetic resonance (NMR) spectroscopy....78
2.1.4.4 Liquid chromatography-mass spectrometry (LC-MS)....85
2.1.4.5 Single crystal X-ray diffraction of alligrin....87
2.1.5 Stability profile of alligrin....88
2.1.6 Experimental validation of alligrin rearrangement pathways....110

2.1.7 Thermal treatment of alligrin to mimic cooking process 112
2.1.8 Studying myrosinase catalytic hydrolysis of glucoraphanin in presence of allicin 114
2.1.8.1 HPLC analysis of glucoraphanin activation by myrosinase in phosphate buffer 114
2.1.9 Myrosinase catalytic hydrolysis of glucoraphanin in presence of garlic organosulfur compounds.....115
2.1.9.1 Enzymatic reaction in acetinitrile (MeCN)/phosphate buffer 115
2.1.10 Isolation, purification, and elucidation of alliphanin by analytical methods 116
2.1.10.1 High performance liquid chromatography (HPLC) 117
2.1.10.2 Preparative high performance liquid chromatography (Prep-HPLC) 117
2.1.11 Structure elucidation of alliphanin 118
2.1.11.1 1D-Nuclear magnetic Resonance (1D-NMR).....118
2.1.12 Liquid chromatography-mass spectrometry (LC-MS).....123
2.1.13 Stability profile of alliphanin.....124
2.1.14 Summary and conclusion.....131
3 Investigation of Alligrin and Alliphanin Formation in Crude Plants Mixtures 134
3.1 Introduction 134
3.2 Aims of this chapter 134
3.3 Analytical identification of individual plant extracts and mixture of two plants extract 134
3.3.1 Analytical identification of allicin from crude garlic extract.....134
3.3.1.1 Monitoring the formation, concentration and stability of allicin in fresh garlic 135
3.3.2 Analytical identification of the aglycone intermediate in crude mustard seeds powder extract.....137
3.3.2.1 Monitoring the formation, concentration, and stability of allyl isothiocyanate in mustard seeds powder.....138
3.3.3 Analysis of the garlic-mustard seeds powder mixture for alligrin production.... 140
3.3.3.1 Quantitative assessment of alligrin formation and stability 142

3.3.4 Optimising sinigrin hydrolysis for enhanced alligrin formation 144
3.3.4.1 Influence of external myrosinase on sinigrin degradation and allyl isothiocyanate production from mustard seeds powder 144
3.3.4.2 Effect of sample concentration on alligrin recovery.....146
3.3.5 Analytical identification of the aglycone intermediate in crude broccoli extract 147
3.3.5.1 Monitoring the formation, concentration, and stability of sulforaphane in broccoli crude extract 148
3.3.6 Analysis of the garlic-broccoli mixture for alliphanin production 149
3.4 Summary and conclusion 151

4 Novel Sulfur Metabolites Arising from Garlic-Brassica Interactions: Antibacterial Activity and Mechanistic Insights 153

4.1 Aim of this chapter.....153
4.2 Antibacterial activity of crude plant extracts and mixed plants extract systems..153
4.3 Antibacterial activity of alligrin compared with allicin and sinigrin 157
4.4 Desulfation of alligrin and structure-activity relationship analysis 161
4.4.1 Enzymatic desulfation of alligrin for structure-activity relationship analysis162
4.4.2 Effect of desulfation on the antibacterial activity of alligrin 164
4.4.3 Antibacterial activity of desulfo-alligrin at high concentrations 165
4.5 Proposed mechanism of action of alligrin 167
4.6 Preliminary evaluation of thiol reactivity of alligrin and desulfo-alligrin with glutathione.....169
4.7 Summary and conclusion.....173

5 Alligrin: Crystal Structure, Stereochemical Analysis, and Comparative Study of a Novel Natural Product..... 174

5.1 Introduction and aim 174
5.2 Crystal structure determination of alligrin by single-crystal x-ray diffraction 174
5.3 The disulfide bond: formation, electronic structure, and dihedral angle geometry... 177

5.3.1 Disulfide bonds in proteins: The cystine and glutathione comparison with alligrin 179
5.4 Crystallographic comparison of the C-S-S-C-N=O connectivity in alligrin and synthetic disulfide compound.....182
5.5 Implications of disulfide geometry for the biological activity of alligrin 185
5.6 Crystal structure of sinigrin and comparative analysis with the novel compound alligrin 186
5.6.1 The crystal structure of sinigrin 186
5.6.2 Comparative crystal structure analysis: Sinigrin versus Alligrin 187
5.6.3 Dihedral angle comparison: alligrin vs sinigrin 189
5.7 Summary and conclusion.....190
6 General Conclusion 192
6.1 Discovery and structural elucidation of novel organosulfur hybrid compounds ..193
6.2 Reaction mechanism and chemical characterisation 193
6.3 Formation of novel compounds in crude plants mixture 195
6.4 Antibacterial activity and structure-activity relationships 195
6.5 Crystallographic characterisation and structural significance of alligrin.....196
6.6 Broader scientific significance 196
6.7 Future directions.....197
6.7.1 Mechanistic studies of antibacterial activity 197
6.7.2 Exploration of other plant system combinations 197
6.7.3 Investigation of alligrin formation under physiological and dietary conditions 197
6.7.4 Anticancer and antioxidant activity 198
7 Experimental Procedures and Analytical Methods 199
7.1 Materials 199
7.1.1 Chemicals and reagents 199
7.1.2 Preparation of buffers.....199
7.1.2.1 Potassium phosphate buffer (PPB) 199
7.1.2.2 Ammonium acetate buffer (NH_4OAc) 199

7.1.3 Plant materials 200
7.2 Experimental procedure 200
7.2.1 Synthesis of allicin 200
7.2.1.1 Performic acid pre-formation 200
7.2.1.2 Synthesis of allicin using pre-formed performic acid 200
7.2.2 Enzymatic reactions 200
7.2.2.1 Myrosinase catalytic hydrolysis of sinigrin/ glucoraphanin 200
7.2.2.2 Myrosinase catalytic hydrolysis mixture of sinigrin/ glucoraphanin and allicin 201
7.2.2.2.1 Enzymatic reaction in dimethyl sulfoxide (DMSO)/phosphate buffer 201
7.2.2.2.1.1 Diallyl disulfide experiment: 201
7.2.2.2.1.2 Allicin experiment: 201
7.2.2.2.2 Enzymatic reaction in acetonitrile (MeCN)/phosphate buffer 201
7.2.2.3 Scale-up of the sinigrin-allicin reaction 201
7.2.3 Chromatographic techniques 202
7.2.3.1 Analytical High Performance Liquid Chromatography (HPLC) 202
7.2.3.2 Preparative High Performance Liquid Chromatography (Prep-HPLC) 203
7.2.4 Spectroscopic analysis for structural elucidation 204
7.2.4.1 Nuclear Magnetic Resonance (NMR) 204
7.2.4.2 Liquid Chromatography-Mass Spectrometry (LC-MS) 206
7.2.4.3 X-ray crystallography 207
7.2.4.3.1 Crystallisation 207
7.2.4.3.2 Single Crystal X-ray Diffraction (SCXD) 207
7.2.5 Experimental validation of alligrin rearrangement pathways 208
7.2.6 Thermal treatment of alligrin 209
7.2.7 Plant preparations 209
7.2.7.1 Preparation of individual plant extracts 209
7.2.7.1.1 Preparation of allicin in fresh garlic extract 209
7.2.7.1.2 Preparation of aglycon intermediate in mustard seeds powder/ broccoli 210
7.2.7.2 Preparation of mixed plants extract 210

7.2.7.2.1 Preparation mixture of garlic and mustard seeds powder 210
7.2.7.2.2 Preparation mixture of garlic and broccoli 210
7.2.7.3 Calculation of alligrin content in crude garlic-mustard mixture.....211
7.2.8 Optimisation method of sinigrin hydrolysis for enhanced alligrin formation .....
.....211
7.2.9 Effect of sample concentration on alligrin formation 212
7.2.10 Enzymatic sulfatase assay.....212
7.2.10.1 Reagent preparation.....212
7.2.10.2 General assay procedure 212
7.2.10.3 Solid-phase extraction (SPE) purification of desulfo-alligrin 213
7.2.11 Biological evaluation.....213
7.2.11.1 Maintenance of bacterial strains and growth conditions.....213
7.2.11.2 Inhibition zone determination (Disc Diffusion Assay) 214
7.2.11.3 Evaluation of alligrin/desulfoalligrin reactivity with glutathione 215
8 References..... 216
9 Appendix..... 231

List of figures

Figure 1.1: Structural comparison of Gram-negative and Gram-positive bacterial cell walls. Key differences include the presence of an outer membrane rich in lipopolysaccharides and porins, a thin peptidoglycan layer, and an inner cytoplasmic membrane in Gram-negative bacteria, whereas Gram-positive bacteria lack an outer membrane and are characterized by a thick peptidoglycan layer containing teichoic acids. Created by BioRender.....5

Figure 1.2: Mechanisms of antimicrobial resistance[17].....6

Figure 1.3: Major classes of plant specialised metabolites. This figure was adapted from wu, Northen and Ding, 2023 [47]. 16

Figure 1.4: Allium sativum (garlic) as an example of a species of Allium. 21

Figure 1.5: Biosynthesis of allicin from alliin. 22

Figure 1.6: Transformation of allicin to its derivatives at different condition. 23

Figure 1.7: Mustard seeds and Broccoli as representative members of the Brassicaceae family.....31

Figure 1.8: Core structural features of glucosinolates, consisting of a β-D-thioglucose unit, a sulfur-linked N-hydroximinosulfate group, and a variable amino acid-derived side chain (R). 34

Figure 1.9: Diagram of the myrosinase-glucosinolate defence system in Brassicaceae plants. Tissue damage caused by insects allows glucosinolates and myrosinase to interact, producing isothiocyanates (ITCs) and nitriles that act as natural pest repellents [164].41

Figure 1.10: Enzymatic hydrolysis of glucosinolates by myrosinase and subsequent formation of biologically active degradation products under different biochemical conditions.....42

Figure 1.11: Representative degradation products of indole glucosinolates and their corresponding chemical structures. 44

Figure 1.12: Pathways for the thermal degradation of glucosinolate-derived isothiocyanates and alliin, illustrating the formation of polysulfides and cyclic organosulfur compounds. 49

Figure 1.13: Thiol reactivity of allicin with thiols (R-SH) yields S-thioallylated derivatives (R-S-S-allyl) and water, demonstrating allicin's ability to react with thiol groups. 50

Figure 1.14: Formation of allicin from alliin and its thiol reactivity. Alliinase converts alliin into allyl sulfenic acid, which condenses to form allicin. Allicin subsequently reacts with thiols to generate disulfide products such as diallyl disulfide. 51
Figure 1.15: Myrosinase-catalyzed hydrolysis of glucosinolates, yielding a sulfated thiohydroximate intermediate that rearranges to bioactive isothiocyanates. 52
Figure 1.16: Trapping of the unstable aglycone intermediate generated from sinigrin hydrolysis by 2,2'-dithiodipyridine (2-PDS), yielding a stable conjugate and releasing 2-mercaptopyridine (2-TP). 52
Figure 1.17: Diagram explains the aim of this project. 54
Figure 2.1: Allicin synthesis from diallyl-disulfide (DADS) through oxidation by a peracid generated with H_2O_2 in the reaction mixture. 56
Figure 2.2: ^{1}H-NMR spectrum (500 MHz, DMSO-d) of allicin, confirming structural integrity and purity. 57
Figure 2.3: ^{1}H-NMR spectrum (500 MHz, D_2O) of sinigrin standard. 58
Figure 2.4: Enzymatic hydrolysis of sinigrin by myrosinase, releasing glucose and generating allyl isothiocyanate as the major bioactive product. 59
Figure 2.5: ^{1}H-NMR spectrum (500 MHz, Methanol-d_4) of allyl isothiocyanate standard. 60
Figure 2.6: Monitoring sinigrin hydrolysis to allyl isothiocyanate (AITC) by tracking allylic proton signals in the ^{1}H NMR spectrum. 61
Figure 2.7: ^{1}H-NMR monitoring of sinigrin hydrolysis in 12.5 M methanol/water at different time. 61
Figure 2.8: Comparative hydrolysis of sinigrin in D_2O catalyzed by 1 U and 2 U myrosinase, monitored at 5 minutes and 2880 minutes (48h)." Values are mean ± SD, n = 3". 62
Figure 2.9: Sinigrin hydrolysis to allyl isothiocyanate (AITC) monitored over time (5 min, 60 min, and 2880 min). " Values are mean ± SD, n = 3". 63
Figure 2.10: ^{1}H-NMR monitoring of sinigrin hydrolysis in phosphate buffer, showing 36% conversion after 15 minutes and complete conversion to allyl isothiocyanate after 2 hours. 64
Figure 2.11: ^{1}H-NMR spectra (500 MHz, D_2O) comparing sinigrin and its hydrolysis product allyl isothiocyanate in phosphate buffer-d. 65

Figure 2.12: ^{1}H-NMR spectra (500 MHz, D_2O) of allyl isothiocyanate obtained from sinigrin hydrolysis compared with the authentic allyl isothiocyanate standard. 65
Figure 2.13: Reaction scheme showing the enzymatic interaction between allicin and sinigrin in the presence of 2 U of myrosinase using 25% (v/v) DMSO-d_6 in phosphate buffer (pH 6) as solvent. The reaction yields a novel sulfur-containing compound formed through coupling of the allicin-derived allyl sulfide moiety with the glucosinolate aglycone intermediate. 68
Figure 2.14: ^{1}H-NMR spectrum (500 MHz, D_2O) of the enzymatic reaction mixture containing sinigrin and allicin in the presence of myrosinase under 25% v/v DMSO-d_6 in phosphate buffer-d conditions. 68
Figure 2.15: *HSQC-NMR spectrum (500 MHz, D_2O) of the enzymatic reaction mixture.* 69
Figure 2.16: ^{1}H-NMR spectrum (500 MHz, D_2O) of the enzymatic reaction mixture containing sinigrin and allicin in the presence of myrosinase under 25% v/v acetonitrile/phosphate buffer-d conditions. 72
Figure 2.17: HSQC-NMR spectrum (500 MHz, D_2O) of the enzymatic reaction mixture. 72
Figure 2.18: HPLC chromatogram of the reaction mixture showing the separation of sinigrin, allicin, AITC, and alligrin using optimized method (Phenomenex Spherisorb® column C18, 5µM, 4.6 x 150mm), under a linear gradient elution with acetonitrile/ammonium acetate buffer. Detailed chromatographic conditions are provided in experimental section (7.2.3.1). 75
Figure 2.19: Preparative reversed-phase HPLC chromatogram of the reaction mixture.....77
Figure 2.20: ^{1}H-NMR spectrum (500 MHz, D_2O) of alligrin.....78
Figure 2.21: COSY-NMR spectrum (500 MHz, D_2O) of alligrin.....79
Figure 2.22: ^{13}C-NMR spectrum (125 MHz, D_2O) for alligrin. 80
Figure 2.23: ^{13}C-DEPT 135-NMR (125 MHz, D_2O) of alligrin. 81
Figure 2.24: Chemical structure of alligrin with atom numbering; green = proton (^{1}H) assignments, red = carbon (^{13}C) assignments. 82
Figure 2.25: HSQC-NMR (500 MHz, D_2O) spectrum of alligrin. 83
Figure 2.26: HMBC-NMR (500 MHz, D_2O) spectrum of alligrin. 84
Figure 2.27: LC-MS data of alligrin. 86
Figure 2.28: Single-crystal X-ray structure of alligrin in ammonium acetate. 88

Figure 2.29: Prep-HPLC chromatogram of the sinigrin-allicin with myrosinase reaction mixture. 89
Figure 2.30: LC-ESI-MS2 spectrum of the purified compound **3** ($C_7H_{10}NO_4S_4^-$). 90
Figure 2.31: Proposed plausible mechanism for the formation of compound **3**. 91
Figure 2.32:MS2-LCMS spectrum of compound **9** ($C_{10}H_{14}NO_4S_4^-$). 92
Figure 2.33: Mechanism formation of Ajoene from allicin transformation. 93
Figure 2.34: Proposed mechanistic pathway for the formation of compound **9**. 94
Figure 2.35: ^{1}H NMR (500 MHz, D_2O) of compound **9**. 95
Figure 2.36: MS2-LC-MS spectrum of compound **10** ($C_{10}H_{14}NO_4S_5^-$). 96
Figure 2.37: Proposed mechanism for the formation of compound **10**. 97
Figure 2.38: ^{1}H NMR spectrum (500 MHz, D_2O) of compound **10**. 98
Figure 2.39: LC-ESI-MS^2 spectrum of compound **13** ($C_{13}H_{18}O_4NS_5$). 99
Figure 2.40: Proposed mechanism for the formation of compound **13**. 100
Figure 2.41:LC-ESI-MS^2 spectrum of compound **14** ($C_{13}H_{20}O_4NS_5$). 101
Figure 2.42: Proposed mechanism for the formation of compound **14**. 102
Figure 2.43: Alternative proposed mechanism for the formation of compound **14**. 103
Figure 2.44: LC-ESI-MS^2 spectrum of compound **14** ($C_{13}H_{20}O_4NS_5$). 103
Figure 2.45: LC-ESI-MS^2 spectrum of compound **15** ($C_{13}H_{18}NO_4S_6$). 104
Figure 2.46: Proposed mechanism for the formation of compound **15**. 105
Figure 2.47: LC-ESI-MS^2 spectrum of compound **16** ($C_{16}H_{24}NO_4S_7$). 106
Figure 2.48: Proposed mechanism for the formation of compound **16**. 107
Figure 2.49: Proposed mechanism for the formation of compound **16.** 108
Figure 2.50: LC-ESI-MS^2 spectrum of compound **16** ($C_{16}H_{24}NO_4S_7$). 108
Figure 2.51: Structural overview of alligrin and its secondary rearrangement products. 109
Figure 2.52: HPLC chromatogram of alligrin incubated with allicin at room temperature for 3 hours. 111
Figure 2.53:HPLC chromatograms of alligrin incubated with allicin at 80 °C for 15, 30, and 60 minutes. 111
Figure 2.54:HPLC chromatograms comparing allicin alone and allicin co-incubated with alligrin at 80 °C for 60 minutes. 112

Figure 2.55: Thermal stability profile of alligrin at different temperatures." Values are mean ± SD, n = 3" 113
Figure 2.56: Proposed thermal degradation products of alligrin at 50-100 °C and 170-200 °C. 114
Figure 2.57: Analytical HPLC chromatograms of sulforaphane obtained by hydrolysis of glucoraphanin via myrosinase at retention time 7.2 min. 115
Figure 2.58: Reaction scheme showing the enzymatic interaction between allicin and glucoraphanin in the presence of 2 U of myrosinase using 25% (v/v) acetonitrile in phosphate buffer (pH 6) as solvent. The reaction yields a novel sulfur-containing compound formed through coupling of the allicin-derived allyl sulfide moiety with the glucosinolate aglycone intermediate.....115
Figure 2.59: ^{1}H-NMR spectra (500 MHz, D_2O) of enzyme catalytic mixture reaction of glucoraphanin and allicin with myrosinase. 116
Figure 2.60: HPLC chromatogram of the allicin, glucoraphanin and myrosinase reaction mixture.....117
Figure 2.61: Preparative reversed-phase HPLC chromatogram of the reaction mixture showing the separation of alliphanin and its rearrangement products. The alliphanin fraction was collected between 4.2 and 5.0 minutes using the same optimized preparative HPLC conditions previously established for the sinigrin-allicin reaction...118
Figure 2.62 :^{1}H-NMR spectrum (500 MHz, D_2O) of alliphanin. 119
Figure 2.63: COSY-NMR spectrum (500 MHz, D_2O) of alliphanin 120
Figure 2.64: ^{13}C-NMR spectrum (126 MHz, D_2O) of alliphanin. 121
Figure 2.65: Chemical structure of alliphanin with atom numbering; green = proton (^{1}H) assignments, red = carbon (^{13}C) assignments. 122
Figure 2.66: LC-ESI-MS^2 spectrum of alliphanin. 123
Figure 2.67: Prep-HPLC chromatogram of the glucoraphanin-allicin with myrosinase reaction mixture.....124
Figure 2.68: LC-ESI-MS^2 spectrum of the purified compound **19**.....125
Figure 2.69: Proposed plausible mechanism for the formation of compound **19**. 126
Figure 2.70: LC-ESI-MS^2 spectrum of compound **21**.....127
Figure 2.71: Proposed mechanism for the formation of compound **21**.....128

Figure 2.72: LC-ESI-MS² spectrum of compound **23**. 129
Figure 2.73: Proposed plausible mechanism for the formation of compound **23**. 130
Figure 2.74: Structural overview of alliphanin and its secondary rearrangement products.131
Figure 2.75: Summary of all compounds identified in this chapter. 133
Figure 3.1: HPLC chromatogram of aqueous crude garlic extract 30 min after crushing. 135
Figure 3.2: (a) Time-course analysis of allicin formation and stability in aqueous freshly crushed garlic over 60 minutes. "All measurements were performed in triplicate (n=3)". (b) Allicin calibration graph. 136
Figure 3.3: HPLC chromatogram of aqueous crude mustard seeds powder extract after 15 min. 138
Figure 3.4: (a) Time-course analysis of sinigrin hydrolysis and (c) allyl isothiocyanate (AITC) formation from mustard seed powder over 60 minutes, with corresponding calibration curves for (b) sinigrin and (d) AITC used for quantification. 139
Figure 3.5: HPLC chromatogram of the garlic- mustard seeds powder mixture showing the formation of alligrin. 140
Figure 3.6: Comparison of the garlic- mustard seeds powder mixture before (top) and after (bottom) spiking with purified alligrin. The highlighted peak increases in intensity in the spiked sample, confirming its identity as alligrin. 141
Figure 3.7: LC-MS confirmation of alligrin formation in mustard seed powder extract. 142
Figure 3.8: Calibration curve for alligrin showing the linear relationship between concentration and HPLC peak area. 142
Figure 3.9: Time-course analysis of sinigrin and allyl isothiocyanate (AITC) formation from yellow mustard seed powder (a) in the presence and (b)absence of exogenously added myrosinase enzyme. 145
Figure 3.10: Effect of sample concentration on alligrin formation. 146
Figure 3.11: HPLC chromatogram of crude aqueous broccoli extract. 147
Figure 3.12: (a) Time-course analysis of glucoraphanin hydrolysis and (c) sulforaphane formation in broccoli extract over 60 minutes, with corresponding calibration curves for (b) glucoraphanin and (d) sulforaphane used for quantification. 148

Figure 3.13: HPLC chromatogram of the crude garlic-broccoli mixture showing characteristic peaks for glucoraphanin, allicin, and sulforaphane, with a trace signal at the expected alliphanin retention time below the reliable quantification limit. 150
Figure 3.14: Alliphanin calibration curve showing the linear relationship between alliphanin concentration and HPLC peak area, with the regression equation (y = 3.3984x + 4422.2) and an R^2 value of 0.984. 150
Figure 3.15: LC-MS confirmation of alliphanin in broccoli and garlic crude mixture. 151
Figure 4.1: Enzymatic desulfation of alligrin to desulfo-alligrin by sulfatase. 161
Figure 4.2: HPLC chromatograms of alligrin and desulfo-alligrin. Alligrin eluted at **RT 7.6 min**, while desulfo-alligrin eluted later at **RT 15.5 min**. 162
Figure 4.3: ^{1}H NMR spectra of alligrin and desulfo-alligrin. 163
Figure 4.4:Proposed thiol-dependent mechanism of alligrin activity. 168
Figure 4.5:HPLC chromatogram of alligrin after incubation with glutathione. 169
Figure 4.6: Proposed mechanism of the reactivity of alligrin with glutathione. 170
Figure 4.7: LC-MS spectrum of the alligrin-glutathione incubation mixture showing formation of S-allylmercaptoglutathione. 170
Figure 4.8: Proposed mechanism of the reactivity of alligrin with glutathione. 171
Figure 4.9: LC-MS spectrum of the alligrin-glutathione incubation mixture showing formation of a S-(N-allylthiocarbamoyl) glutathione. 171
Figure 4.10: Proposed mechanism of the reactivity of desulfo-alligrin with glutathione. 172
Figure 4.11: LC-MS spectrum of the desulfo-alligrin-glutathione incubation mixture showing formation of S-allylmercaptoglutathione. 172
Figure 5.1: Crystal structure of alligrin determined by single-crystal X-ray diffraction, revealing the unusual disulfide bridge S8-S9 that covalently connects the allylthio fragment of allicin with the sulfonated oxime fragment of sinigrin. 175
Figure 5.2: Crystal structure of alligrin showing (left) the disulfide bridge bond lengths (C-S = 1.8 Å, S-S = 2.0 Å) and (right) the C-S-S-C dihedral angle of 97.3°, confirming the characteristic gauche geometry of the disulfide linkage. 176
Figure 5.3: Three-dimensional crystal structure of L-cystine (left) and glutathione disulfide (GSSG) (right) showing the C-S-S-C disulfide bridge. 179

Figure 5.4: Bond length measurements (left) and dihedral angle (right) analysis of the L-cystine disulfide bridge. 180
Figure 5.5: Bond length measurements (left) and dihedral angle (right) analysis of glutathione disulfide (GSSG). 181
Figure 5.6: the crystal structure of synthetic backbone disulfide compound 8b determined by single-crystal X-ray diffraction. 183
Figure 5.7: Crystal structure of sinigrin showing the three principal structural domains: the β-D-glucopyranose ring in the $^4C_1$ chair conformation (left), the sulfonated oxime aglucone connected through the thioglycoside bond (centre), and the sulfonate group (right). 186
Figure 5.8: Bond length comparison between sinigrin (left) and alligrin (right), determined by single-crystal X-ray diffraction. 187
Figure 5.9: Dihedral angle comparison between alligrin (left) and sinigrin (right), determined by single-crystal X-ray diffraction. 189
Figure 6.1: Summary of all novel organosulfur natural products identified and characterised in this work.....194
Figure 9.1: HPLC chromatography of alligrin thermal treatment at 50-100 °C showing alligrin and compound **3**. 231
Figure 9.2: LC-MS of alligrin from thermal treatment of alligrin at 50-100 °C showing alligrin. 231
Figure 9.3: LC-MS of compound **3** from alligrin thermal treatment at 50-100 °C showing compound **3.** 232
Figure 9.4: LC-MS of alligrin thermal treatment at 170-200 °C showing allyl thiosulfate ($C_3H_5O_3S_2$, m/z 152.96). 232
Figure 9.5: LC-MS of alligrin thermal treatment at 170-200 °C showing allyl dithiosulfate ($C_3H_5O_3S_3$, m/z 184.93). 232
Figure 9.6: Analytical HPLC chromatography of glucoraphanin standard at retention time 2.6 min. 233
Figure 9.7: ^{1}H NMR (500 MHz, D_2O) of glucoraphanin standard.....233
Figure 9.8: ^{13}C-NMR (500 MHz, D_2O) of glucoraphanin standard. 234
Figure 9.9: COSY-NMR (500 MHz, D_2O) of glucoraphanin standard.....234

Figure 9.10: Analytical HPLC chromatography of sulphoraphane standard at retention time 7.2 min. 235
Figure 9.11: ^{1}H NMR (500 MHz, acetonitrile-d) of sulforaphane standard. 235
Figure 9.12: ^{13}C-NMR (500 MHz, D_2O) of sulforaphane standard. 236
Figure 9.13: ^{13}C- DEPT 135 NMR (500 MHz, D_2O) of sulforaphane standard. 236
Figure 9.14: COSY-NMR (500 MHz, D_2O) of sulforaphane standard. 237
Figure 9.15: ^{1}H-NMR spectra (500 MHz, D_2O) of sulforaphane obtained by hydrolysis of glucoraphanin via myrosinase. 237
Figure 9.16: Calibration curve of synthetic allicin obtained by HPLC, showing a linear relationship between concentration (µg/mL) and peak area (mAU). 238
Figure 9.17: Calibration curve of sinigrin external standard showing the linear relationship between concentration (µg/mL) and HPLC peak area. 238
Figure 9.18: Calibration curve of allyl isothiocyanate (AITC) external standard showing the linear relationship between concentration (µg/mL) and HPLC peak area. 239
Figure 9.19: Calibration curve of purified alligrin showing a strong linear relationship between concentration and HPLC peak area. 239
Figure 9.20: Calibration curve of Glucoraphanin external standard showing the linear relationship between concentration (µg/mL) and HPLC peak area. 240
Figure 9.21: Calibration curve of Sulforaphane external standard showing the linear relationship between concentration (µg/mL) and HPLC peak area. 240
Figure 9.22: Calibration curve of Alliphanin showing the linear relationship between concentration (µg/mL) and HPLC peak area. 241
Figure 9.23: LC-MS data of desulfo-alligrin. 241

List of tables

Table 1.1: Major pathogenic bacteria, the diseases they cause, and their key antimicrobial resistance mechanisms. 3
Table 1.2: Examples of major marketed drugs derived from natural products. 18
Table 1.3: Examples of plant-derived compounds with reported antimicrobial activity [48].19
Table 1.4: Garlic compounds and their biological activities. 28
Table 1.5: Examples of glucosinolates showing variation in the R-side chain, their major Brassica plant sources, and the reported biological activities of their myrosinase-derived hydrolysis products. 35
Table 1.6: Antibacterial activity of selected glucosinolates hydrolysis products (isothiocyanates) and their reported target bacterial species. 46
Table 2.1: ^{1}H-NMR and DEPT-135- ^{13}C-NMR chemical shifts of allicin, sinigrin and the new compound. 70
Table 2.2: ^{1}H-NMR chemical shifts of allicin, sinigrin and the new compound. 73
Table 2.3: Retention times of mixture components (sinigrin, allicin, allyl isothiocyanate, and alligrin). 76
Table 2.4: ^{1}H, ^{13}C, ^{13}C DEPT and COSY- NMR data of alligrin measured at 500 MHZ in D_2O...82
Table 2.5: HSQC- NMR, HMBC-NMR correlations of alligrin Measured at 500 MHZ in D_2O...85
Table 2.6: ^{1}H, ^{13}C and COSY- NMR data of alliphanin measured at 500 MHZ in D_2O. 122
Table 3.1: Quantitative analysis of key compounds in crude garlic-mustard mixture. 144
Table 4.1: Representative agar diffusion plates showing the antibacterial activity of crude plant extracts and mixed extract systems against Gram-positive and Gram-negative bacterial strains using the disc diffusion assay. Note: **Mixture 1** is garlic mixed with mustard seeds powder while **mixture 2** is garlic with broccoli. Discs labelled **Y** represent the aqueous mustard seeds extract alone, and **B** represent the aqueous broccoli extract alone. Sterile water was used as the negative control, and ampicillin served as the positive control. 156
Table 4.2: Antibacterial activity of crude plant extracts and mixed extract systems expressed as inhibition zone diameters (mm). Ampicillin and ciprofloxacin were used as positive controls. 157

Table 4.3: Comparative antibacterial activity of alligrin, allicin, and sinigrin against methicillin-resistant Staphylococcus aureus (MRSA) and Escherichia coli (E.C) determined by the disc diffusion assay. Agar plates were divided into four quadrants to allow direct within-plate comparison. For **alligrin**, discs labelled **2** correspond to 2.6 µmol and **1** to 5.3 µmol. For **allicin**, discs labelled **A5** correspond to 2.6 µmol and **A15** to 5.3 µmol. For **sinigrin**, discs labelled **S20** correspond to 2.6 µmol and **S50** to 5.3 µmol. 70% methanol was used as the negative control, and **ampicillin** was included as the positive control. 159
Table 4.4: Bacterial inhibition zone diameters (mm) produced by alligrin, allicin, and sinigrin. Inhibition zones against (MSSA; Gram-positive) and (E. coli; Gram-negative) measured using the disc diffusion assay. 160
Table 4.5: Comparative antibacterial activity of alligrin and desulfo-alligrin at high concentration against Gram-positive and Gram-negative bacteria. Note The upper quadrants contain alligrin (A1, 10.6 µmol; A2, 5.6 µmol), while the lower quadrants contain desulfo-alligrin (D1, 10.6 µmol; D2, 5.6 µmol). 164
Table 4.6: Bacterial inhibition zone diameters (mm) of alligrin and desulfo-alligrin at the same molar concentrations. Alligrin showed antibacterial activity against Gram-positive bacteria, whereas desulfo-alligrin was inactive against all tested strains, indicating the essential role of the sulfate group in antibacterial activity. 165
Table 4.7: Antibacterial activity of desulfo-alligrin against Gram-positive and Gram-negative bacteria. The disc diffusion assay showing the antibacterial activity of desulfo-alligrin against Gram-positive (Staphylococcus aureus and MRSA) and Gram-negative (Escherichia coli and P. aeruginosa) bacterial strains at high molar concentration. Plates were divided into quadrants to allow direct within-plate comparison. Label “1” corresponds to desulfo-alligrin at 21.13 µmol, while label “2” corresponds to desulfo-alligrin at 10.6 µmol. 166
Table 4.8: Antibacterial activity of desulfo-alligrin at increasing molar concentrations**.** Bacterial inhibition zone diameters (mm) produced by desulfo-alligrin against Staphylococcus aureus (SA), methicillin-resistant S. aureus (MRSA), Escherichia coli (E.C), and Pseudomonas aeruginosa (P.A) determined using the disc diffusion assay. 167
Table 5.1:Dihedral angles describing the geometry of a disulfide linkage[227]. 177

Table 5.2: Crystallographic comparison of the C-S-S-C-N=O connectivity in alligrin and synthetic backbone disulfide compound 8b. 184
Table 5.3: Summarises the disulfide bond geometric parameters of alligrin alongside those of L-cystine, glutathione disulfide (GSSG), and compound 8b, allowing a direct comparison of S-S bond lengths, C-S bond lengths, χ_3 dihedral angles, and handedness across these structurally distinct compounds. 184
Table 5.4: summary of comparative bond lengths of sinigrin and alligrin. 188
Table 5.5: Comparison of key torsion angles in alligrin and sinigrin. 190
Table 7.1: Gradient elution program used for preparative HPLC separation.....204
Table 7.2: HPLC method used during LC-MS analysis.....207
Table 7.3: Gram-positive and negative bacterial strains used for antibacterial evaluation. 214
Table 9.1: Crystal Data and Structure Refinement for Alligrin 242

List of Abbreviations

Abbreviation	Definition
%	Percent
°C	Degree Celsius
2D	Two-dimensional
3D	Three-dimensional
ABC	ATP-binding Cassette
ACN	Acetonitrile
AMR	Antimicrobial Resistance
ATCC	American Type Culture Collection
CD_3OD	Deuterated Methanol
cm	Centimetre
COSY	Correlation Spectroscopy (NMR)
CTX-M	Cefotaximase-Munich (a family of extended-spectrum β-lactamases)
d	Doublet (NMR)
DAD	Diode Array Detector
DCM	Dichloromethane
dd	Doublet of Doublets (NMR)
DEPT	Distortionless Enhancement of Polarisation Transfer (NMR)

Abbreviation	Definition
DMAPP	Dimethylallyl Pyrophosphate
DMSO	Dimethyl Sulfoxide
DMT	N, N-Dimethyltryptamine
DNA	Deoxyribonucleic Acid
ermB	rRNA methyltransferase gene conferring macrolide resistance
ESBL	Extended-Spectrum β-Lactamase
ESP	Epithiospecifier protein
FDA	Food and Drug Administration
g	Gram
GSLs	Glucosinolates
gyrA	Gene encoding DNA gyrase subunit A
HAT	Histone Acetyltransferase
HGT	Horizontal Gene Transfer
HMBC	Heteronuclear Multiple-Bond Correlation Spectroscopy
HPLC	High Performance Liquid Chromatography
Hz	Hertz
IMP	Imipenemase Metallo-β-Lactamase
ITCs	Isothiocyanates

Abbreviation	Definition
J	Spin-spin coupling constant (Hz)
KPC	Klebsiella pneumoniae Carbapenemase
L	Litre
LPS	Lipopolysaccharide
m	Multiplet (NMR)
m/z	Mass-to-charge ratio
MDR	Multi-Drug Resistant
mecA / mecC	Genes encoding altered PBP2a responsible for methicillin resistance
mefA	Macrolide efflux gene
MeOH	Methanol
MexAB-OprM	Multidrug efflux pump system in Pseudomonas aeruginosa
MFS	Major Facilitator Superfamily
mL	Millilitre
mM	Millimolar
MRSA	Methicillin-Resistant Staphylococcus aureus
MS	Mass Spectrometry
MSSA	Methicillin-Susceptible Staphylococcus aureus
NCTC	National Collection of Type Cultures

Abbreviation	Definition
NDM	New Delhi Metallo-β-Lactamase
nm	Nanometre
NMR	Nuclear Magnetic Resonance
NSPs	Nitrile-specifier proteins
OmpF / OmpC / OprD	Outer membrane porin proteins
OXA-48	Oxacillinase-48 (carbapenemase enzyme)
OXA-type	Oxacillinase-type carbapenemases
parC	Gene encoding topoisomerase IV subunit A
PBP	Penicillin-Binding Protein
PBS	Phosphate-Buffered Saline
q	Quartet (NMR)
RNA	Ribonucleic Acid
RND	Resistance Nodulation Division
s	Singlet (NMR)
SCXD	Single-Crystal X-ray Diffraction
SMCSO	S-methylcysteine sulfoxide
t	Triplet (NMR)
TFPs	Thiocyanate-forming proteins

Abbreviation	Definition
TRPV1	Transient receptor potential vanilloid 1
vanA / vanB	Genes conferring vancomycin resistance in Enterococcus species
VIM	Verona Integron-Encoded Metallo-β-Lactamase
VISA	Vancomycin-Intermediate Staphylococcus aureus
VRSA	Vancomycin-Resistant Staphylococcus aureus
δ	Chemical shift
µg	Microgram
µL	Microlitre
µM	Micromolar

1 Introduction

1.1 Global impact of infectious diseases

Microbial infections continue to pose a major global health challenge, remaining one of the leading causes of morbidity and mortality worldwide. Despite advances in sanitation, vaccination, and modern therapeutics, infectious diseases are still responsible for millions of deaths each year, particularly in low- and middle-income countries where access to timely diagnosis, effective antimicrobials, and robust healthcare infrastructure remains limited. Recent global analyses demonstrate that bacterial infections alone were associated with more than seven million deaths in 2019, placing them among the leading causes of preventable mortality globally[1, 2].

Importantly, the burden of bacterial infections extends well beyond traditionally high-risk or resource-limited settings. Globally, severe bacterial diseases persist within human populations regardless of economic status, indicating that pathogenic microorganisms can circumvent host immune defences and exploit limitations in medical care delivery, as well as constraints associated with existing treatment strategies. Clinical conditions such as lower respiratory tract infections, bloodstream infections, and intra-abdominal infections are especially concerning, as they often develop rapidly, spread systemically, and require timely and appropriate antimicrobial therapy[1]. Therefore, these infections create a heavy burden on healthcare resources such as longer hospital stay, higher use of intensive care unit (ICU) care and overall cost of treatment.

1.2 Antimicrobial resistance (AMR): An escalating global threat

Antimicrobial resistance (AMR), particularly resistance among bacterial pathogens, has emerged as a profound global health crisis, threatening the effectiveness of existing treatments and preventive measures. In 2019 alone, an estimated five million deaths were associated with bacterial AMR[1], and this figure is projected to rise dramatically by 2050 if no decisive action is taken. Recent events have further intensified this challenge; for instance, the COVID-19 pandemic led to increased antibiotic consumption, accelerating the selection and spread of resistant organisms[3]. In addition, outbreaks such as the recent U.S. cluster of

extensively carbapenem-resistant *Pseudomonas aeruginosa* linked to contaminated artificial tears demonstrate how resistant pathogens can cause severe ocular and systemic infections with fatal outcomes[4].

1.3 Overview of bacterial diversity

Bacteria are highly diverse prokaryotic microorganisms that inhabit nearly all ecological niches and include many species of clinical importance. Their classification is based on key characteristics such as cell morphology, Gram staining properties, oxygen requirements, and taxonomic grouping, all of which are essential for understanding pathogenicity and antimicrobial susceptibility. Morphologically, bacteria are classified as cocci or bacilli, while Gram staining distinguishes organisms into Gram-positive and Gram-negative groups according to differences in cell wall structure. Further differentiation is achieved by considering aerobic or anaerobic growth and specific structural features such as spore formation[5].

1.4 Clinically relevant bacterial species

Clinically relevant bacterial species frequent in medical settings are Gram-positive bacteria including Staphylococcus aureus, Streptococcus pneumoniae and Enterococcus faecium and Gram-negative pathogens such as Escherichia coli, Klebsiella pneumoniae, Pseudomonas aeruginosa, Acinetobacter baumannii and Salmonella enterica. These bacteria have great clinical significance because of their predominant role in human infections and increasing drug resistance[1] (Table 1.1).

1.4.1 Bacteria, associated diseases, and resistance mechanisms

Table 1.1: Major pathogenic bacteria, the diseases they cause, and their key antimicrobial resistance mechanisms.

Bacterium	Major diseases caused	Key antimicrobial resistance mechanisms	References
Gram-positive bacteria			
Staphylococcus aureus	• Skin and soft tissue infections • Pneumonia • Bloodstream infections	• Methicillin resistance (mecA/mecC → PBP2a; MRSA) • Resistance to macrolides, tetracyclines, fluoroquinolones • VISA/VRSA (cell-wall thickening; vanA acquisition)	[1, 6]
Enterococcus faecalis	• Urinary tract infections • Endocarditis • Bloodstream infections	• Intrinsic cephalosporin resistance • Low-affinity penicillin-binding proteins • Vancomycin resistance (*vanA/vanB*)	[1, 7]
Streptococcus pneumoniae	• Community-acquired pneumonia • Meningitis • Otitis media	• Altered penicillin-binding proteins • Macrolide resistance (ermB, mefA) • Reduced β-lactam susceptibility	[8, 9]
Gram-negative bacteria			
Escherichia coli	• Urinary tract infections • Bloodstream infections • Intra-abdominal infections	• Extended-spectrum β-lactamases (ESBLs, e.g. CTX-M) • Carbapenemases (NDM, KPC, OXA-48) • Fluoroquinolone resistance (gyrA/parC mutations) • Aminoglycoside-modifying enzymes	[1, 10]

Klebsiella pneumoniae	• Hospital-acquired pneumonia • Urinary tract infections • Liver abscesses • Bloodstream infections	• Carbapenemases (KPC, NDM, OXA-48) • ESBLs (CTX-M, SHV) • Aminoglycoside-modifying enzymes • Convergence of hypervirulence and MDR traits	[10, 11]
Pseudomonas aeruginosa	• Ventilator-associated pneumonia • Chronic lung infections • Wound and burn infections	• Low outer-membrane permeability • Overexpression of efflux pumps (MexAB- OprM) • Biofilm formation • Metallo-β-lactamases (VIM, IMP)	[1, 12]
Acinetobacter baumannii	• Ventilator-associated pneumonia • Bloodstream infections • Wound infections	• OXA-type carbapenemases • Efflux pump overexpression • Reduced membrane permeability	[1, 10]
***Salmonella enterica* serotype Typhi**	• Typhoid fever • Systemic bloodstream infection	• Fluoroquinolone resistance (*gyrA* mutations) • Multidrug resistance (Ampicillin, chloramphenicol, trimethoprim-sulfamethoxazole) • ESBL production (emerging)	[1, 13]

1.5 Structural basis of gram-positive and gram-negative bacterial cell walls

Bacterial resistance to antimicrobial agents results from various biochemical and structural responses, the architecture of cell wall being central in intrinsic resistance[14]. The composition of cell envelopes is distinctly different between Gram-negative and Gram-positive bacteria, directly affecting antimicrobial permeability. The cell envelope of Gram-negative bacteria is a multilayered structure that includes an outer membrane, a thin peptidoglycan in the periplasmic space and an inner cytoplasmic membrane. The outer membrane is rich in lipopolysaccharides (LPS) and porins that facilitate passive diffusion of small hydrophilic molecules however it is also a principal permeability barrier for several antibiotics[15]. The peptidoglycan layer is the structural support, and the inner membrane contains proteins necessary for metabolism and transport.

On the other hand, Gram-positive bacteria are characterized by absence an outer membrane and presence of a single cytoplasmic membrane surrounded by a thick peptidoglycan layer. This structure is rigid and provides mechanical strength protecting against environmental stress. The cell walls of Gram-positive species also have teichoic and lipoteichoic acids, anionic polymers that are involved in the integrity of the cell wall, host interaction and susceptibility to antimicrobials[16] (Figure 1.1).

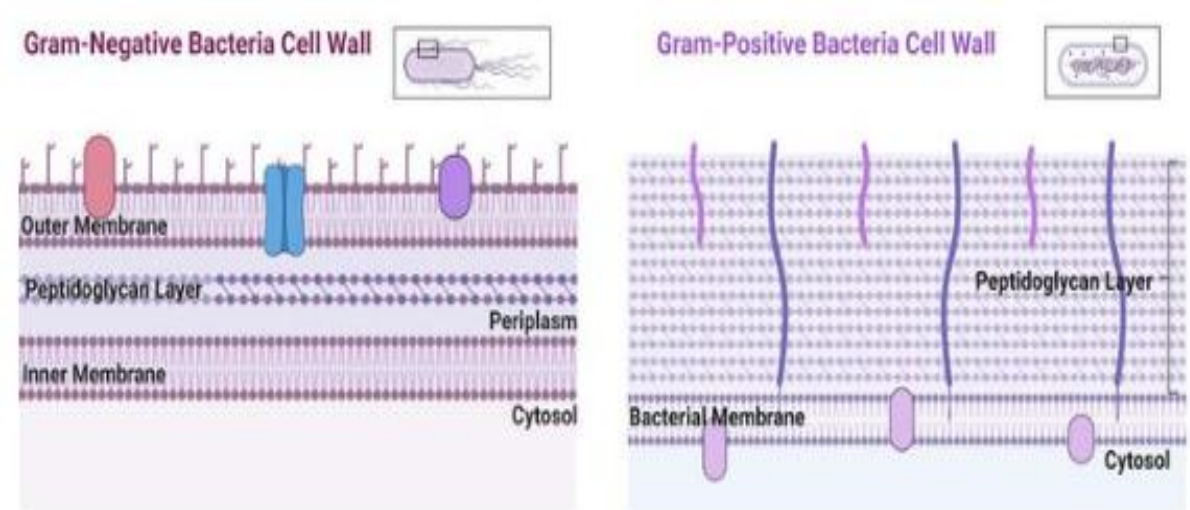

Figure 1.1: Structural comparison of Gram-negative and Gram-positive bacterial cell walls. Key differences include the presence of an outer membrane rich in lipopolysaccharides and porins, a thin peptidoglycan layer, and an inner cytoplasmic membrane in Gram-negative bacteria, whereas Gram-positive bacteria lack an outer membrane and are characterized by a thick peptidoglycan layer containing teichoic acids. Created by BioRender.

1.5.1 Mechanisms of antimicrobial resistance

After the identification of penicillin in 1928, approximately twenty new structural classes of antibiotics were introduced between the 1930s and 1960s. In contrast, the discovery and development of novel antimicrobial classes have markedly declined since the 1980s, resulting in a heavy dependence on existing antibiotics[17]. Bacteria employ a wide range of resistance strategies including reduced membrane permeability, active efflux systems, enzymatic modification or degradation of drugs, alteration of antimicrobial targets, and adaptive responses such as biofilm formation which collectively compromise the effectiveness of nearly all available antibiotics[17] (Figure 1.2). Together, these mechanisms contribute to therapeutic failure and the persistence of bacterial infections.

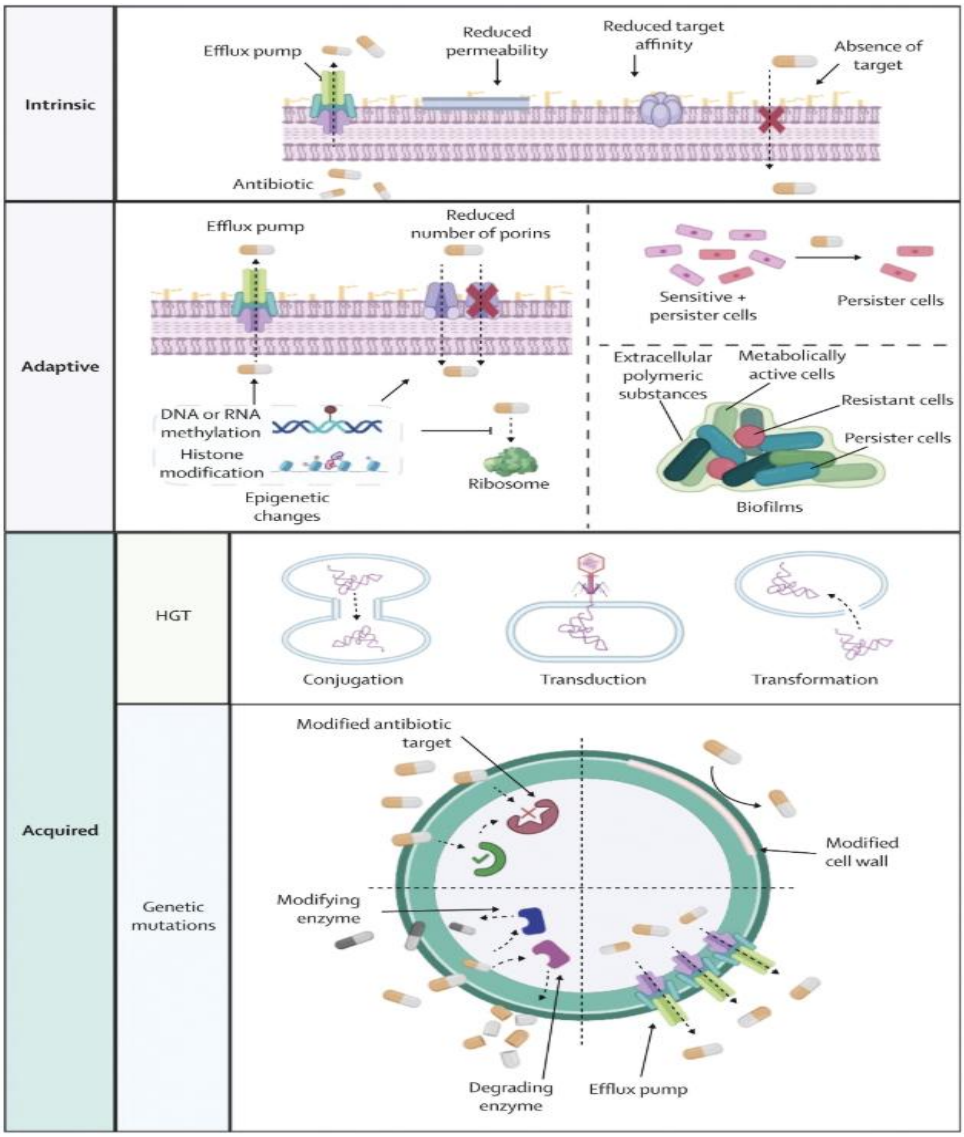

Figure 1.2: Mechanisms of antimicrobial resistance[17].

1.5.1.1 Intrinsic resistance

Intrinsic resistance refers to the natural, baseline ability of bacteria to withstand certain antimicrobial agents due to inherent structural or physiological features. These built-in survival mechanisms include the presence of multidrug efflux pumps that actively transport antibiotics out of the cell, as well as reduced membrane permeability particularly notable in Gram-negative bacteria, whose outer membrane limits antibiotic entry. Additionally, chromosomally encoded enzymes such as β-lactamases can inactivate antibiotics before they reach their targets, while alterations or absence of drug-binding sites can further impair antimicrobial activity[18]. These intrinsic characteristics provide bacteria with a fundamental level of protection against a broad range of antibiotics.

1.5.1.1.1 Efflux pumps

Efflux pumps are transport proteins within the cell membrane which allow bacteria to actively export out antibiotics and other harmful agents from the cell. By decreasing the antimicrobial drug concentration inside the cell, these systems prevent drugs from reaching and binding their targets[19]. A small number of well-characterized efflux pump families RND (Resistance Nodulation Division), MFS (Major Facilitator Superfamily) and ABC (ATP-binding Cassette) are central to multidrug resistance among Gram negative bacteria[20, 21]. The activity of efflux pumps may be a constitutive property of the bacterium or induced by genetic mutations or environmental stress and their overexpression is often a primary mechanism of MDR (multidrug resistance)[22].

1.5.1.1.2 Reduced permeability

Reduced permeability limits the ability of antibiotics to diffuse into bacterial cells. This mechanism is especially important in Gram-negative bacteria, whose asymmetric outer membrane contains lipopolysaccharides (LPS) and porin channels that regulate molecule entry[21]. Alterations in porin proteins such as decreased expression, loss of porins, or structural modifications, restrict antibiotic uptake and significantly decrease susceptibility to

β-lactams, fluoroquinolones, and carbapenems. Reduced permeability often acts synergistically with efflux pumps, leading to high-level multidrug resistance[23].

1.5.1.1.3 Chromosomally encoded enzymes

Some bacteria naturally carry chromosomally encoded enzymes that can modify or break down antibiotics. The most common among them is the β-lactamase, which degrades the β -lactam ring present in penicillins, cephalosporins and carbapenems leading to loss of antimicrobial activity. They can be classified into different classes starting from narrow spectrum penicillinases up to extended spectrum β-lactamases (ESBLs) and carbapenemases such as KPC, NDM, OXA type enzymes[24]. Since these enzymes are encoded on the chromosome, they represent native defence mechanisms of the organism although they may also be transferred horizontally as acquired resistance determinants[18].

1.5.1.1.4 Target modification

Target modification reduces antibiotic binding to its molecular target, thereby diminishing or eliminating drug activity[25]. Bacteria may naturally possess altered versions of essential proteins such as modified penicillin-binding proteins (PBPs), ribosomal subunits, or DNA gyrase that exhibit reduced affinity for antibiotics. For example, intrinsic resistance of *Enterococcus faecium* to cephalosporins arises from low-affinity PBPs[26], while mutations in ribosomal RNA can confer resistance to macrolides or tetracyclines[27]. These intrinsic structural features prevent antibiotics from exerting their inhibitory effects, even at high drug concentrations.

1.5.1.2 Adaptive mechanisms of antimicrobial resistance

Adaptive resistance is a reversible and temporary alteration, that allows for survival of bacteria exposed to the antimicrobial agents in the absence of genetic mutations. This type of resistance is frequently induced by environmental stress factors such as antibiotic pressure[18]. Essential adaptive responses include an increased expression of efflux pumps and a decreased production of membrane porins, both of which limit intracellular antibiotic accumulation. Epigenetic alterations including DNA or RNA methylation and modification of

histone-like proteins may also impact gene expression to help decrease drug uptake or interfere with antibiotics targets.

Another mechanism of adaptive resistance is the development of persister cells, resting bacterial sub-group that can survive high antibiotic doses without growing. Biofilm formation is another key adaptive mechanism, in which bacteria are surrounded by a protective extracellular matrix that protects them from host immune attack while sequestering much of antibiotic penetration. In biofilms, bacteria can communicate within the community through quorum sensing, transfer genetic material and tolerate environmental stresses[28]. Producing biofilm-associated bacteria cells having 10-1000 times increased resistance to antibiotics compared to their planktonic counterparts.

1.5.1.2.1 Efflux pump upregulation

Under antibiotic stress, bacteria can increase the expression or activity of efflux pumps, enabling them to more efficiently export antimicrobial agents out of the cell. This reduces intracellular drug concentrations to sublethal levels. Efflux pump upregulation is rapid and reversible, allowing bacteria to survive antimicrobial exposure even without genetic mutations. This mechanism is especially common in *Pseudomonas aeruginosa*, *Klebsiella pneumoniae*, and *Escherichia coli[21]*.

1.5.1.2.2 Reduced number of porins

In Gram-negative bacteria, outer membrane porins act as channels that allow antibiotics to enter the cell. During adaptive resistance, bacteria can decrease porin expression or close porin channels**,** thereby limiting antibiotic uptake. Reduction of OmpF, OmpC, or OprD porins is a well-characterised mechanism of adaptive resistance in Enterobacterales and *Pseudomonas aeruginosa*, particularly against carbapenems and fluoroquinolones[21].

1.5.1.2.3 Epigenetic changes

Bacteria can undergo epigenetic modifications, such as DNA methylation, RNA methylation, or histone-like protein alterations, which modulate gene expression without altering DNA

sequence[29]. These changes can transiently increase resistance by upregulating efflux pumps, reducing membrane permeability, decreasing expression of antibiotic-binding proteins and altering ribosomal function. Epigenetic regulation allows bacteria to respond quickly to antimicrobial threats and revert once the stress is removed.

1.5.1.2.4 Persister cells

Persister cells are a small, dormant subpopulation of bacteria that tolerate high antibiotic concentrations without growing or dividing. Because most antibiotics target active cellular processes, these metabolically inactive cells survive treatment and later repopulate once antibiotic pressure is removed. Persisters are found both in planktonic cultures and in biofilms and are major contributors to chronic, relapsing infections[30].

1.5.1.2.5 Biofilm formation

Biofilms are the principal adaptive strategy that most bacterial species use to survive. In a biofilm, bacterial cells are enclosed in an extracellular polymeric substance providing a physical protection against antibiotics and host immune factors and reduce antibiotic penetration[31]. This matrix contributes to quorum-sensing communication, metabolic diversity as well as horizontal gene transfer among different bacterial subpopulations. Furthermore, biofilms permit bacteria to resist adverse environmental factors, including nutrient deprivation, pH variation and low oxygen tension[28]. Biofilm-associated bacteria are thus 10 to 1000 times more resistant to antibiotics than their planktonic counterparts, with biofilms a significant clinical problem in chronic wounds and infections related to implanted medical devices, urinary tract infections, and others as found in such conditions as cystic fibrosis[32].

1.5.1.3 Acquired resistance

1.5.1.3.1 *via* Horizontal gene transfer (HGT)

Resistance develops when bacteria acquire new genetic material that allows them to resist the effects of antimicrobial agents. Horizontal gene transfer (HGT) is essential in this process and has three main pathways: conjugation, transduction, and transformation. Conjugation is

when the plasmids containing resistance genes are passed directly from one cell to another. The transduction is brought about by bacteriophages that accidentally transmit DNA between bacteria. Transformation is the process in which free DNA fragments are absorbed from the environment[21]. Bacteria can thereby rapidly acquire resistance determinants across species or genus borders, accelerating the spread of multi-resistance within microbiological communities.

1.5.1.3.2 via Genetic mutations

In addition to HGT, bacteria can also develop antimicrobial resistance through spontaneous genetic mutations. Such mutations may alter membrane composition such as changes to lipopolysaccharides or porin proteins reducing antibiotic penetration or altering susceptibility. Mutations can also influence the regulation or structure of efflux pumps, increasing their ability to expel antimicrobial agents[14].

Bacteria may also acquire genes encoding enzymes that chemically modify antibiotics. These enzymes can phosphorylate, acetylate, adenylate, oxidise, hydroxylate, or otherwise alter antibiotics, preventing them from binding to their intended targets[33]. Degradation enzymes, including extended-spectrum β-lactamases (ESBLs), directly hydrolyse β-lactam rings, conferring resistance to penicillins, cephalosporins, and related β-lactam antibiotics[34]. Additionally, mutations affecting antibiotic target sites can reduce the affinity of drugs for their targets or enable alternative metabolic pathways, effectively bypassing the action of the antimicrobial agent[17, 18].

1.6 Resolving antimicrobial resistance

Addressing antimicrobial resistance (AMR) requires a coordinated and comprehensive strategy that integrates targeted research priorities with strong public health interventions. The complexity of AMR cannot be effectively managed through isolated or single interventions, as it is raised by interconnected biological, clinical, environmental, and behavioural factors. Consequently, comprehensive efforts encompassing antimicrobial stewardship, therapeutic innovation, enhanced surveillance, public and professional

education, and evidence-based policy implementation are essential to limit the emergence and dissemination of resistant pathogens [35].

From the public health perspective, antibiotic stewardship is an essential factor in AMR control, promoting a responsible use of antibiotics through acceptable prescription choice, dose and duration. Education and public awareness programmes that should aim to reduce misuse or overuse of antibiotics by healthcare professionals. Alongside, comprehensive surveillance systems are necessary to monitor patterns of resistance in real-time that guide treatment recommendations and can facilitate early detection of novel threats[36]. Such actions are known to work, although they need long-term investment and behavioural change as well as coordinated international agreements.

At the research and therapeutic level, the development of new antibiotics targeting novel bacterial pathways remains a priority, although high costs and lengthy development timelines. In addition, Combination therapies can improve antimicrobial effectiveness and resistance suppression, while phage therapy provide a highly targeted approach against specific bacterial strains. Moreover, probiotics and prebiotics support host microbiota resilience, reducing pathogen colonisation, whereas immunotherapeutic approaches aim to strengthen host immune responses to infection[37]. Drug repurposing is an economical approach to identify new antimicrobial uses for existing drugs such as antimicrobial peptides, bacteriocins, and nanomaterials, offer novel mechanisms that may avoid traditional resistance pathways[38].

Collectively, integrating research priorities with organized public health actions provides a strong framework for addressing antimicrobial resistance. However, the continued rise of resistance and the limited development of new antibiotics highlight the urgent need for alternative and sustainable antimicrobial sources. In this context, natural product drug discovery remains one of the most successful approaches in modern pharmacology and represents a promising strategy for identifying novel agents capable of overcoming antimicrobial resistance.

1.7 Natural product drug discovery

Natural product drug discovery has long served as one of the most effective and continuing strategies in modern pharmacology. Natural products are small molecules produced by microorganisms, plants, and marine organisms propose structural diversity and biological relevance[39]. Their evolutionary optimisation within ecological systems gives them unique pharmacophores, stereochemical complexity, and a wide range of biological activities that synthetic libraries struggle to replicate[40, 41]. Most clinically used antibiotics, anticancer agents, immunomodulators, and antiparasitic drugs trace their origins to natural scaffolds, highlighting their indispensable role in drug development[39]. Advances in chromatographic techniques, genome mining, metabolomics, and computational chemistry have renewed interest in natural products as a source of next-generation therapeutics, particularly in the context of antimicrobial resistance[42].

1.7.1 Historical and ethnopharmacological foundations of natural product drug discovery

Natural products have played a central role in the development of therapeutics throughout human history, long before the emergence of modern chemistry and molecular pharmacology. Early human societies relied extensively on plants, minerals, and animal-derived substances to treat illness, guided by empirical observation and the gradual accumulation of traditional knowledge. These practices laid the foundations of ethnopharmacology and provided the earliest conceptual frameworks for systematic drug discovery[43].

As human societies evolved, empirical knowledge of medicinal plants transitioned from opportunistic use to regulated therapeutic practice. The earliest known written documents on the use of medicinal plants are from Mesopotamia and Egypt document the systematic application of plant-derived substances for medical purposes. Similar developments occurred independently in Asia, where successive Chinese medical textbooks contained long lists of plant-derived drugs, and laid the groundwork for traditional Chinese medicine. Meanwhile, Greco-Roman scholars formalised botanical medicine through detailed descriptions of plant

identification, preparation, and therapeutic use. This collective knowledge was preserved, expanded, and synthesised during the medieval period, particularly through Arab scholars who integrated medical traditions from multiple cultures and established early pharmaceutical practices[43, 44].

The enduring impact of natural products on modern therapeutics is further illustrated by several landmark plant-derived drugs. Aspirin, a semi-synthetic anti-inflammatory agent, was developed from salicin isolated from the bark of *Salix alba*. Investigation of *Papaver somniferum* led to the isolation of morphine in the early nineteenth century, followed by the development of clinically important derivatives such as codeine. Similarly, digitoxin from *Digitalis purpurea* became a widely used cardiotonic agent, while quinine from *Cinchona* species was employed for centuries in the treatment of malaria before its formal adoption in Western medicine. Pilocarpine, isolated from *Pilocarpus jaborandi*, has been used clinically for over a century in the management of glaucoma and was later approved for the treatment of xerostomia and Sjögren's syndrome[43]. Collectively, these examples highlight how traditional plant-based remedies have repeatedly served as critical starting points for the discovery and development of clinically important drugs.

Despite advances in synthetic chemistry, natural products continue to play a central role in healthcare. The World Health Organization estimates that a significant proportion of the global population still relies on traditional plant-based medicines, and many approved drugs retain direct links to ethnopharmacological knowledge[43]. This sustained relevance reflects the long evolutionary history of plants, during which they developed structurally diverse secondary metabolites to mediate ecological interactions and defence. These compounds provide a biologically validated foundation for modern drug discovery and continue to inform the search for new therapeutic agents.

1.7.2 Ecological and evolutionary roles of plant metabolites

Plant natural products play critical ecological roles that are closely linked to their evolutionary and structural diversification. Primary metabolites, such as sugars, amino acids, and lipids, are essential for growth and reproduction and are therefore highly conserved due to strong

evolutionary constraints. In contrast, secondary (specialised) metabolites exhibit extensive structural diversity and species specificity, reflecting their evolution under selective pressures imposed by biotic and abiotic stresses [45]. Major classes of secondary metabolites include alkaloids, terpenoids, phenylpropanoids and glucosinolates, which collectively function in plant defence, signalling, and environmental adaptation by mediating interactions with herbivores, pathogens, pollinators, and symbiotic organisms (Figure 1.3).

The structural evolution of secondary metabolites has been driven by gene duplication, enzyme promiscuity, and pathway diversification, enabling plants to generate a wide array of bioactive molecules from common biosynthetic precursors [46]. Abiotic factors such as drought, salinity, ultraviolet radiation, and heavy metal exposure further shape specialised metabolism by inducing stress-responsive chemical defences. This ecological optimisation of plant secondary metabolites underpins their biological potency and helps explain their frequent relevance as pharmacologically active compounds in human medicine [45, 47].

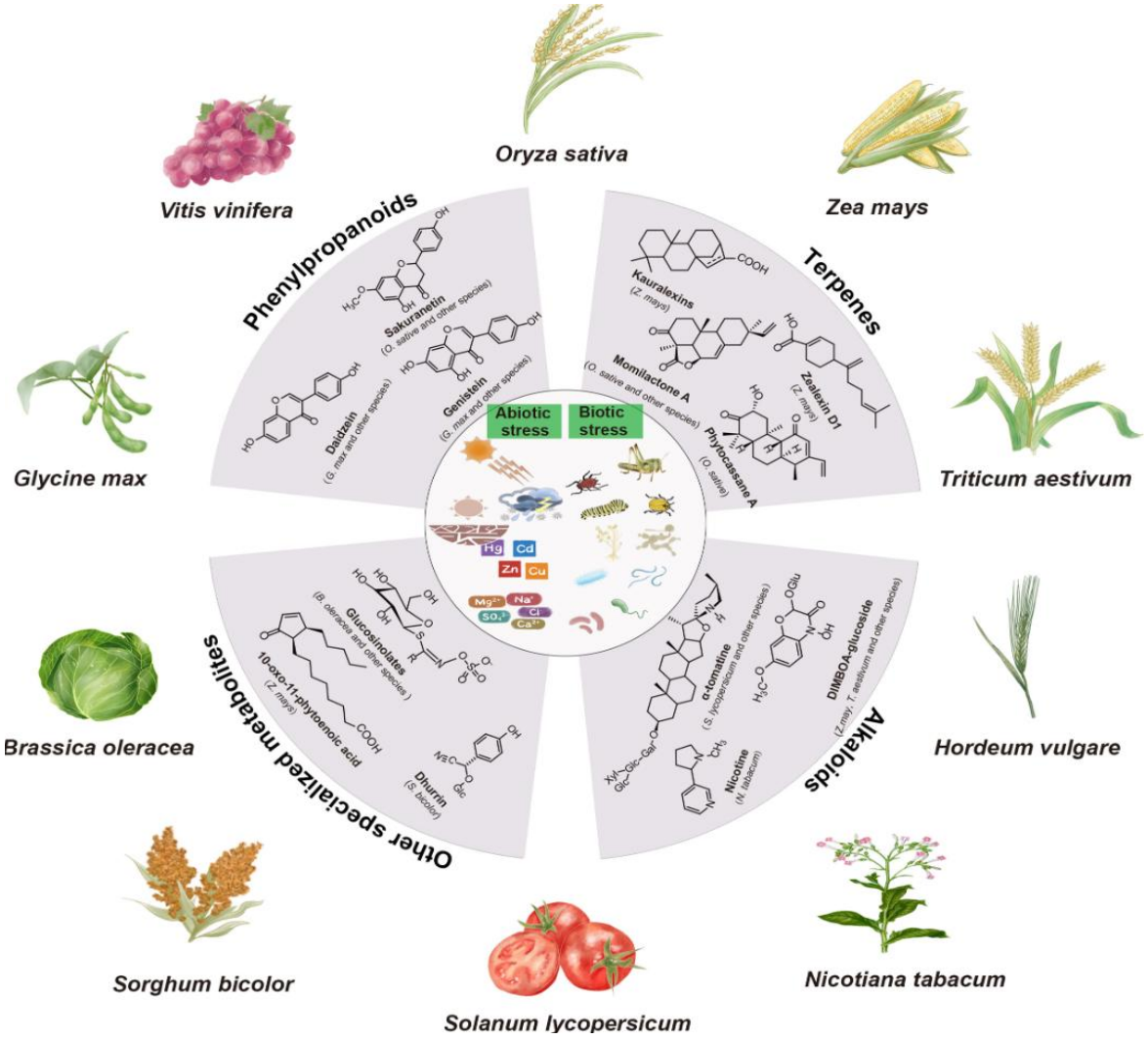

Figure 1.3: Major classes of plant specialised metabolites. This figure was adapted from wu, Northen and Ding, 2023 [47].

The evolutionary adaptation of plants has led to the development of highly specialised biosynthetic pathways, enabling the production of diverse bioactive natural products. This chemical diversity provides a clear explanation for the significant medicinal value of natural sources. Such compounds have been utilised by humans for centuries and continue to support both traditional remedies and modern pharmacotherapy. Building on this evolutionary and historical context, the following section outlines key plant-derived natural products that have demonstrated antimicrobial and other biological activity.

1.7.3 Major plant-derived bioactive compounds

Plants are one of the richest and most chemically diverse sources of bioactive natural products, and their secondary metabolites have contributed extensively to the development of modern therapeutics. Many clinically important drugs currently in use originate directly from plant-derived compounds or have been developed through structural modification of natural core structures. These metabolites include several chemical classes and therapeutic uses, reflecting their diverse biosynthetic origins and biological functions. The following table presents representative examples of major marketed drugs derived from plant natural products (Table 1.2).

Plant secondary metabolites constitute an important source of antimicrobial agents and have attracted sustained interest due to their broad-spectrum activity against clinically relevant pathogens. Numerous compounds isolated from medicinal plants have demonstrated antibacterial and antifungal properties, supporting their potential as leads for antimicrobial drug discovery. The following table presents selected plant-derived compounds with reported antimicrobial activity, together with their botanical sources and documented targets (Table 1.3).

Table 1.2: Examples of major marketed drugs derived from natural products.

Therapeutic class	Trivial name, chemical structure and plant source	Reference
Analgesic	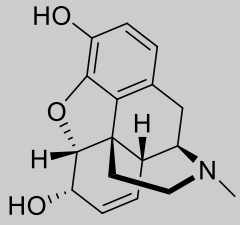 **Morphine** (Opioid) - *Papaver somniferum* (opium poppy)	[43] [39]
Antimalarial	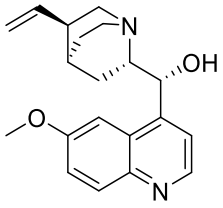 **Quinine** - *Cinchona spp.* 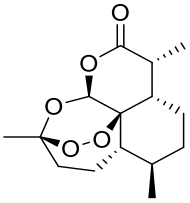 **Artemisinin** - *Artemisia annua*	[40] [39]
Anticancer	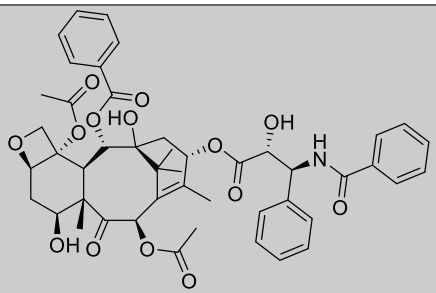 **Paclitaxel (Taxol®)** - *Taxus brevifolia* (Pacific yew)	[39]
Cardiotonic	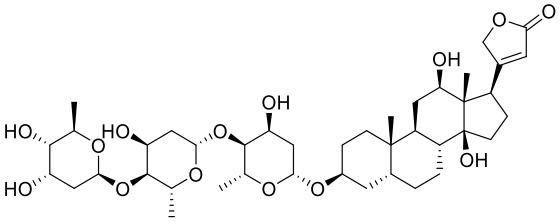 **Digoxin** - *Digitalis lanata*	[43]
Cholinergic agonist	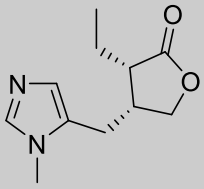 **Pilocarpine** - *Pilocarpus jaborandi*	[43]

Table 1.3: Examples of plant-derived compounds with reported antimicrobial activity [48].

Trivial name and its structure	Plant species	Active against	Refs.
Allicin 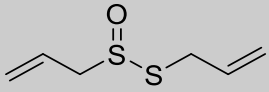	*Allium sativum* (Garlic)	Broad-spectrum antibacterial	[49]
Berberine 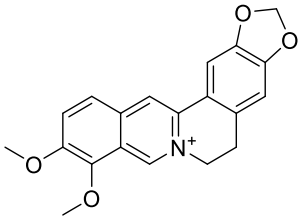	*Berberis vulgaris* (Barberry)	Broad-spectrum antibacterial	[50]
Catechins 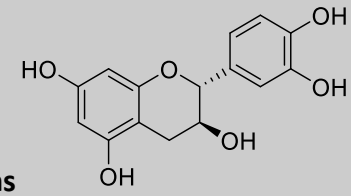	*Glycyrrhiza glabra* (Green tea)	*Staphylococcus aureus*, *Mycobacterium tuberculosis*	[51]
Curcumin 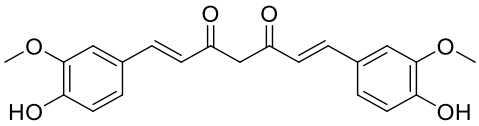	*Curcuma longa* (Tumeric)	Antibacterial	[52]
Eugenol 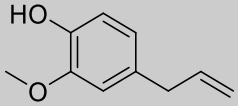	*Syzygium aromaticum* (Clove)	Broad-spectrum antibacterial	[53]
Glabridin 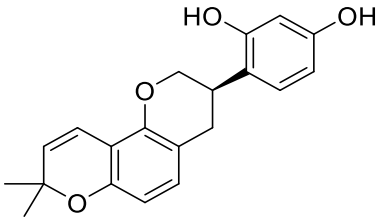	*Glycyrrhiza glabra* (Liquorice)	*Staphylococcus aureus*, *Mycobacterium tuberculosis*	[54]
Piperine 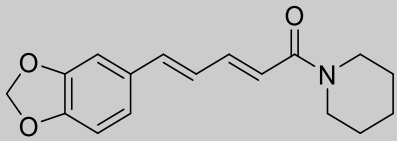	*Piper nigrum* (Black pepper)	*Lactobacillus*, *Micrococcus*, *Escherichia-coli*, *Enterococcus faecalis*	[55]
Thymol 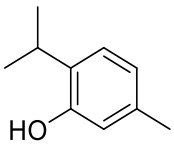	*Thymus vulgaris* (Thyme)	*Antibacterial*	[56]

The plant-derived compounds discussed above illustrate the diversity of secondary metabolites that have been reported to possess antimicrobial activity. However, most existing studies have focused on the isolation and evaluation of individual bioactive constituents, often overlooking the chemical reactivity and potential interactions that may occur between metabolites originating from different plant sources. reactive intermediates generated during enzymatic processes that occur during plant processing, preparation, or consumption remain an underexplored aspect of natural product chemistry. A more integrated understanding of how such intermediates interact with other plant-derived compounds is therefore needed. The following section reviews the chemistry of organosulfur compounds from selected plants, providing a foundation for identifying gaps in current knowledge and for contextualising the aims and objectives of the present study.

1.8 Literature review

1.8.1 Overview of natural organosulfur compounds in plants

Organosulfur compounds are a chemically diverse and complex group of secondary metabolites distributed among higher plant species. They are especially abundant in edible plants from the Allium genus (e.g., garlic, onion, and leek) and Brassicaceae or cruciferous family (e.g., broccoli, cabbage, mustard seed and radish). These sulphur-containing metabolites impart characteristic aromas and pungent flavours to these vegetables. They also play crucial roles in the plants for resistance against pathogens, herbivores and environmental stresses. In addition, organosulfur metabolites have been widely studied for their beneficial effects on human health such as antimicrobial, antioxidant and anticancer activities. They are therefore a major target of research in the fields of natural product chemistry, plant ecology, and nutritional science.

Plant-derived organosulfur compounds constitute a chemically diverse and biologically significant group of natural products. Among the major plant families producing these metabolites, the Allium and Brassicaceae families are particularly notable for generating distinct classes of sulfur-containing compounds with well-characterised biosynthetic pathways and documented biological activities. The *Allium* genus, and garlic (*Allium sativum*) in particular, is a prominent source of thiosulfinates such as allicin, which are formed

enzymatically following tissue disruption. In contrast, members of the Brassicaceae family biosynthesise a wide range of glucosinolates, sulfur-rich precursors that are enzymatically converted into bioactive products, including isothiocyanates. These two plant families form the focus of the present study. An integrated review of their chemical diversity, biosynthesis, ecological functions, and biological activities provides important insight into sulfur reactivity in plant defence systems. Understanding these sulfur-based chemical processes may also inform the discovery of novel natural products and open new avenues for the development of innovative bioactive compounds with potential therapeutic applications.

1.9 Allium family-Garlic

1.9.1 Garlic in ancient and traditional medical systems

Allium sativum L. (garlic) is a perennial bulbous plant in the *Amaryllidaceae* family, distinguished by its strong odour and pungent taste from sulfur-containing compounds [57]. Originating in Central Asia and now cultivated worldwide, it is among the oldest known culinary spices and medicinal herbs [58], with recorded usage at least 5000 years ago [59].



Figure 1.4: Allium sativum (garlic) as an example of a species of Allium.

Historically, garlic held significant cultural and medicinal importance across ancient Egypt, India, China, Greece, and Rome [60, 61]. In Egypt, it was placed in pharaohs' tombs and given to pyramid builders for strength [60]. In addition, Hippocrates prescribed it for numerous ailments, while Greek and Roman soldiers and athletes consumed it to boost stamina [60, 61]. As garlic spread across continents, it became integrated into Mediterranean and European cuisine and folk medicine [59]. Garlic (*Allium sativum*) has been acknowledged in

traditional and alternative medicine as a “cure-all,” because of its wide range of bioactive functions [62]. Garlic provides a range of health benefits from its vitamins, minerals, antioxidants, and particularly its organosulfur compounds, which exhibit a range of biological activities including antibacterial [63], antifungal [64], antiviral [65], antiprotozoal [66], reducing cholesterol levels and hypolipidemia [67], antithrombotic [68], antioxidant [69], as well as anticancer activity [70, 71].

1.9.2 Organosulfur profiles in whole and crushed garlic

Whole garlic cloves contain mainly non-volatile stable organosulfur precursors, such as γ-glutamylcysteines peptides and S-allyl-L-cysteine sulfoxide (alliin), in intact cells. These compounds are stored in separate cellular locations from the alliinase enzyme to avoid early enzymatic reactions and formation of reactive sulfur species, Alliin, chemically designated as (+)-S-(2-propenyl)-L-cysteine sulfoxide, is an odourless organosulfur compound present in garlic representing approximately 80% of total garlic sulfoxides. It serves as the primary biosynthetic precursor to allicin, remaining inert until cellular disruption triggers enzymatic conversion [72]. This conversion is catalysed by alliinase localised within vacuoles of intact garlic cells and accounting for up to 10% of total garlic clove protein [73]. On mechanical damage such as crushing, chopping or chewing, the cell compartments will destroy and alliinase rapidly hydrolyses alliin to produce allyl sulfenic acid that then rearranges into allicin within a few seconds [74, 75] (Figure 1.5). The resultant allicin (S-(2-propenyl)-2-propene-1-sulfinothioate) constitutes approximately 70% of the thiosulfinate fraction in crushed garlic [49, 57]. It is a colourless, volatile, poorly water-soluble compound (2.5% solubility) responsible for garlic's characteristic pungent odour and taste [63].

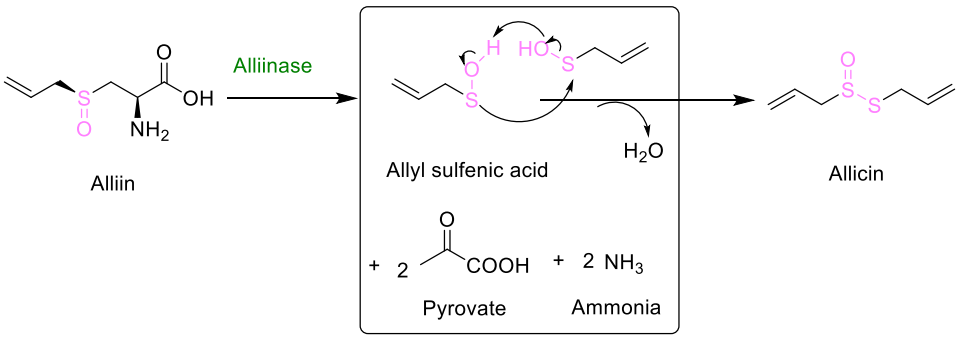

Figure 1.5: Biosynthesis of allicin from alliin.

Allicin is a highly reactive and thermolabile thiosulfinate responsible for the characteristic pungent flavour of fresh garlic. Due to its chemical instability, it undergoes rapid decomposition at room temperature, serving as a precursor to a broad spectrum of biologically active organosulfur metabolites [49, 76]. Decomposition of allicin yields a complex mixture of diallyl polysulfides, with diallyl disulfide (DADS) as the predominant product (66.7%), followed by diallyl trisulfide (DATS, 14.6%), diallyl sulfide (DAS, 13.3%), and diallyl tetrasulfide (5.4%). Higher order polysulfides, including diallyl penta-, hexa-, and heptasulfide are also formed, even though in considerably smaller quantities [77, 78]. In the presence of organic solvents or oil, allicin is additionally converted to ajoene and vinyl dithiins. Each of these secondary metabolites exhibits distinct physicochemical properties and bioactive profiles, collectively contributing to the wide-ranging biological activities attributed to garlic [79](Figure 1.6).

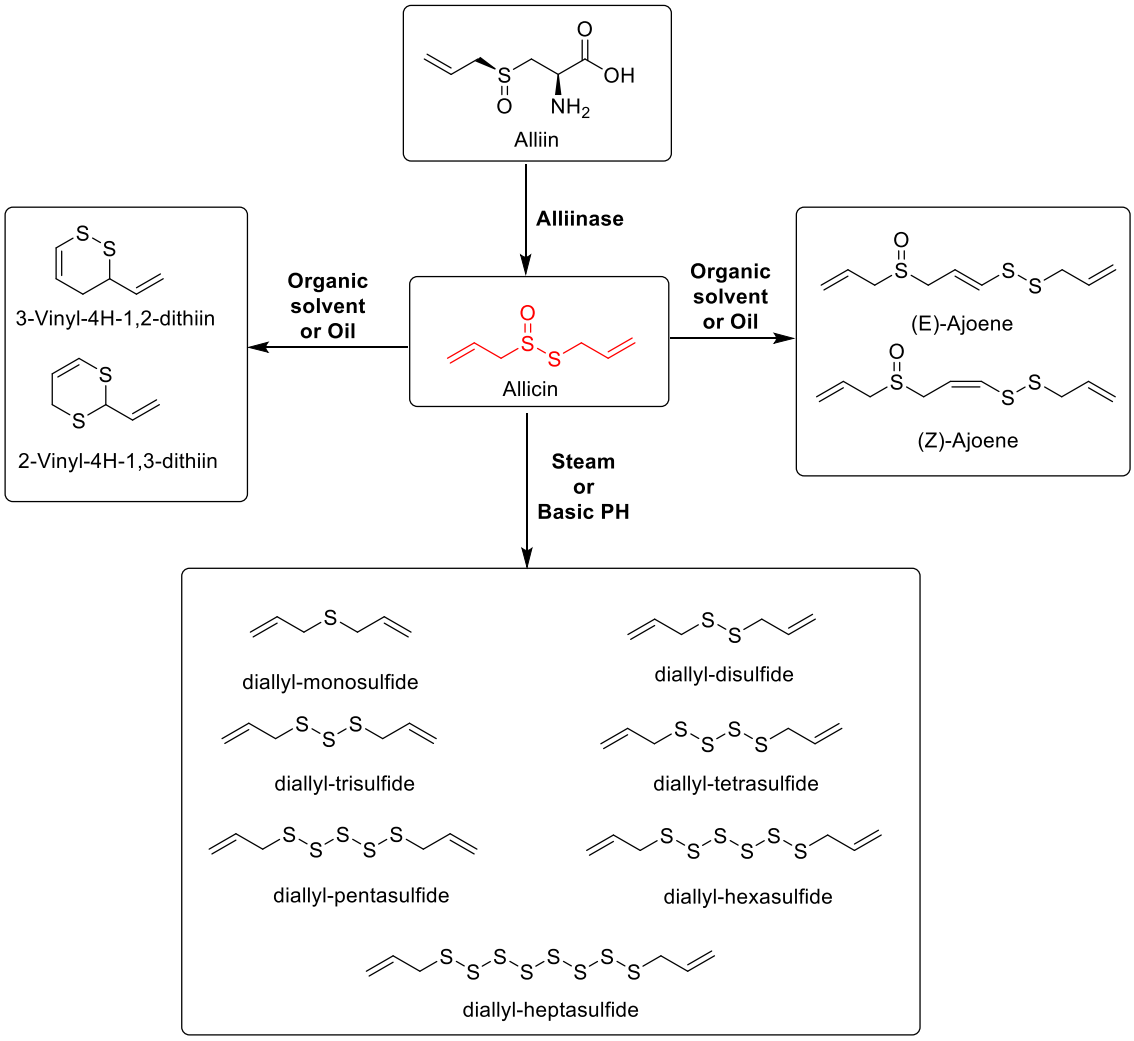

Figure 1.6: Transformation of allicin to its derivatives at different condition.

The content of these volatile sulfur compounds is related to several factors including temperature, pH, and mechanical processing conditions, all of them that would affect how fast allicin will degrade and formation rate of sulfur metabolite compounds [72].

1.9.2.1 Fates of allicin during cooking or storage

Allicin is entirely absent in intact garlic bulbs, forming only upon mechanical tissue disruption that brings alliinase into contact with alliin. once synthesised, it degrades rapidly at room temperature within hours. Thermal processing including boiling, frying, and microwaving further diminishes allicin content by inactivating alliinase before conversion can occur, with losses proportional to temperature and heating duration [80]. Allowing crushed garlic to rest for approximately 10 minutes prior to cooking has been proposed to partially preserve bioactive yield by permitting allicin synthesis before enzymatic denaturation [81]. Additional stability is influenced by humidity, oxygen, light, and storage duration, with refrigeration shown to retard but not prevent decomposition. Consequently, processed garlic preparations such as aged garlic extract, garlic oil, and enteric-coated supplements possess markedly different organosulfur profiles, reflecting the substantial transformation or absence of allicin incurred during their manufacture [49].

From the nutritional and biological point of view, cooking or inappropriate storage dramatically decreases the content of allicin with a consequent reduction of its well-established antimicrobial, cardioprotective and chemo-preventive effects. For the preservation of allicin benefits, suggestions are including eating raw garlic, letting crushed garlic resting before heating, as well as preserving under proper conditions [49, 62].

1.9.3 Biological activities of organosulfur compounds formed by garlic hydrolysis

Garlic possesses multiple pharmacological activities, which is primarily associated with its bioactive organosulfur compounds. These components exhibit various bioactivities and have been reported to prevent or treat a range of chronic diseases. Studies have reported that garlic shows antioxidant, anti-inflammatory, antimicrobial, immunomodulatory, cardioprotective, anticancer, hepatoprotective, and neuroprotective activities. The following

sections show the main biological effects related to garlic and the major substances contributing to these activities.

1.9.3.1 Antimicrobial activity

Garlic aqueous extracts exhibit broad-spectrum antibacterial activity against both Gram-positive and Gram-negative organisms, with documented susceptible species including *Helicobacter pylori*, *Bacillus subtilis*, *Escherichia coli*, *Listeria monocytogenes*, *Pseudomonas aeruginosa*, *Salmonella typhimurium*, *Staphylococcus aureus*, and *Vibrio parahaemolyticus*. Notably, inhibitory effects have been consistently reported to be greater against Gram-positive than Gram-negative species, a differential likely attributable to structural differences in cell wall architecture and membrane permeability. Among the various extract types investigated, ethanolic preparations have demonstrated superior antibacterial efficacy, particularly against *E. coli* and *Salmonella typhi*, whereas non-polar solvents such as hexane, chloroform, and ethyl acetate yielded no significant activity [57].

The principal mediator of garlic's antimicrobial activity is allicin, which exerts its bactericidal effects primarily through rapid covalent interaction with thiol groups (-SH) of essential microbial enzymes, including alcohol dehydrogenase, thioredoxin reductase, and RNA polymerase, thereby disrupting critical metabolic processes. In certain pathogens such as *Entamoeba histolytica*, allicin additionally inhibits cysteine proteinase activity, a key virulence determinant [49, 82]. Beyond direct bactericidal action, allicin has been demonstrated to suppress biofilm formation through interference with bacterial quorum sensing, a mechanism central to both biofilm development and the emergence of antibiotic resistance [83, 84]. Furthermore, garlic extracts inhibit enterotoxin production by intestinal pathogens, including enterotoxigenic *E. coli*, suggesting a protective role against diarrhoeal disease [85].

Secondary organosulfur metabolites derived from allicin degradation further broaden the antimicrobial spectrum. Ajoene exhibits potent activity against methicillin-resistant *Staphylococcus aureus* (MRSA), disrupting bacterial adhesion and biofilm integrity while demonstrating synergism with conventional antibiotics [86]. Diallyl trisulfide (DATS) and related polysulfides exert bactericidal effects by penetrating bacterial cell membranes, inducing oxidative stress and structural membrane damage [49]. Antimicrobial potency among these compounds has been reported to correlate positively with the number of sulfur

atoms per molecule, with DATS and diallyl tetra-sulfide exhibiting activity comparable to that of allicin itself [77]. Collectively, these organosulfur constituents retain activity against several multidrug-resistant strains, supporting their potential as adjuvant or alternative therapeutic agents in the context of escalating antimicrobial resistance

Despite this considerable antimicrobial potential, allicin's inherent chemical instability, constrains its systemic therapeutic application. Current research efforts are therefore directed towards the development of stabilised allicin derivatives and synergistic combinations with established antibiotics, while topical and inhalational routes of administration represent promising near-term clinical avenues[49, 87].

1.9.3.2 Anticancer activity

Garlic's anticancer properties involve multiple mechanisms including detoxification of carcinogens, induction of apoptosis, cell cycle arrest, and inhibition of tumour angiogenesis. Organosulfur constituents, particularly diallyl sulfides and ajoene, modulate signaling pathways to suppress proliferation and enhance programmed cell death in various cancer cell lines[62, 77].

1.9.3.3 Antioxidant activity

Garlic exhibits potent antioxidant activity primarily due to its organosulfur compounds such as allicin, diallyl disulfide (DADS), and S-allyl cysteine (SAC). These compounds help scavenge reactive oxygen species (ROS) and reduce oxidative stress in cells, thereby protecting lipids, proteins, and DNA from oxidative damage. SAC, especially prevalent in aged garlic extract, has demonstrated strong free radical scavenging capacity and enhancement of endogenous antioxidant enzymes such as superoxide dismutase and glutathione peroxidase[62, 72].

1.9.3.4 Anti-inflammatory activity

Garlic-derived sulfur compounds modulate inflammatory pathways by inhibiting the production of pro-inflammatory cytokines such as tumour necrosis factor-alpha (TNF-α), interleukin-6 (IL-6), and nuclear factor kappa B (NF-κB). Allicin and ajoene notably exhibit inhibitory effects on key enzymes like cyclooxygenase (COX) and lipoxygenase (LOX), attenuating inflammatory responses. These anti-inflammatory effects contribute to garlic's efficacy in managing chronic inflammatory diseases[62].

1.9.3.5 Immunomodulatory effects

Garlic's organosulfur compounds influence both innate and adaptive immunity by enhancing macrophage function, natural killer cell activity, and modulating cytokine secretion. S-allyl cysteine (SAC) and other sulfur compounds stimulate immune responses while maintaining immune homeostasis, potentially benefiting autoimmune and infectious disease management[72, 88].

1.9.3.6 Cardioprotective effects

Garlic consumption is linked to reduced cardiovascular risk through mechanisms including lowering total cholesterol, LDL cholesterol, and blood pressure. Organosulfur compounds such as allicin inhibit platelet aggregation, improve endothelial function, and exhibit vasodilatory effects. These actions contribute to improved lipid profiles and prevention of atherosclerosis[62, 72].

1.9.3.7 Hepatoprotective effects

Studies show that garlic organosulfur compounds protect the liver against toxins by enhancing antioxidant defences and modulating detoxifying enzymes. S-allyl cysteine and allicin reduce lipid peroxidation and inflammatory mediator release in liver injury models, thereby exerting hepatoprotective effects[62].

1.9.3.8 Neuroprotective effects

Garlic’s neuroprotective actions are attributed to its antioxidant and anti-inflammatory sulfur compounds, which reduce neuroinflammation and oxidative stress implicated in neurodegenerative diseases. SAC has shown promise in models of Alzheimer’s and Parkinson’s disease through its ability to attenuate neuronal damage[72].

Table 1.4: Garlic compounds and their biological activities.

Chemical structure	Compound name	Biological activities	References
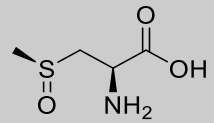	Methiin	Anticancer/ Antioxidant	[72]
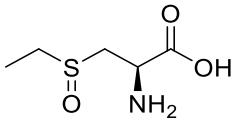	Ethiin	Anticancer/ Anti-inflammatory/ Antimicrobial/ Antioxidant	[72]
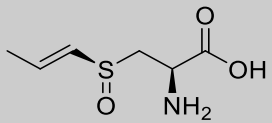	Isoalliin	Anticancer Antimicrobial Antioxidant	[72]
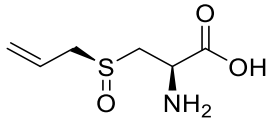	Alliin	Antithrombotic/ Hypolipidemic/ Anticancer/ Hypoglycaemic/ Antiviral	[65, 68, 89]
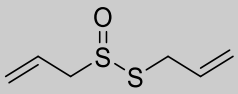	Allicin	Antibacterial/ Antiproliferative/ Antidiabetic/ Reduce cholesterol/ Antiprotozoal/Antioxidant/ Antifungal	[63, 90] [57, 91] [64, 66, 67]

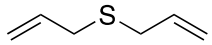	Diallyl-sulfide	Antitumor/ Antioxidant/ Antibacterial	[92-94] [95-97]
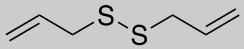	Diallyl-disulfide	Antimicrobial/ Antiviral/ Anticancer/ Antifungal	[65, 98] [94, 99, 100]
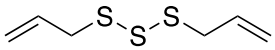	Diallyl-trisulfide	Antiviral/ Anticancer/ Antimicrobial/ Antifungal/Antimycobacterial-Hepatoprotective agent/Antiprotozoal/ Antioxidant	[65, 66, 69, 71, 90, 94, 95, 98, 101]
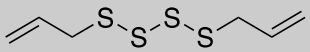	Diallyl-tetrasulfide	Antimycobacterial/ Hepatoprotective agent/ Antioxidant/ Antibacterial/ Antifungal/ Anticancer	[90, 95, 101, 102]
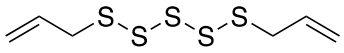	Diallyl-pentasulfide	Antifungal	[103]
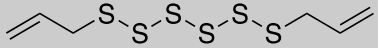	Diallyl-hexasulfide	Antimicrobial Anticancer	[78, 95]
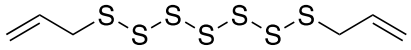	Diallyl-heptasulfide	Antimicrobial	[78, 95]
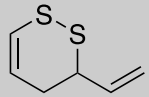	Dithiins 3-vinyl-3,4-dihydro-1,2-dithiin	Antioxidant/ Anti-inflammatory	[62, 95]

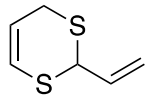	2-vinyl-2,4-dihydro-1,3-dithiin	Antioxidant/ Anti-inflammatory	[62, 95]
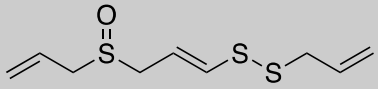	E-ajoene	Anti-obesity/ Reduce cholesterol synthesis/ Anticancer/ Antimicrobial/ Anti-fungal/ Anti-inflammatory	[67, 104, 105] [90, 106, 107]
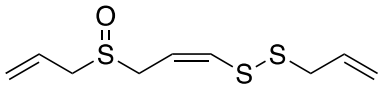	Z-ajoene	Anti-obesity/ Anti-pancreatic cancer/ Antimicrobial/ Anti-inflammatory	[104, 108] [90, 106]
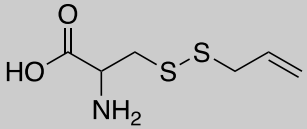	S-allyl-mercapto cystein	Anticancer	[109]
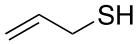	Allyl-mercaptan	Antioxidant/ Antimicrobial/ Anti-inflammatory/ Anticancer	[110, 111]
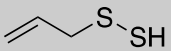	Allyl perthiol	Antioxidant/ Cytoprotective/ Anti-inflammatory Cardiovascular benefits	[95]
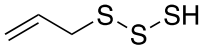	Allyl hydro-trisulfide	Antimicrobial/ Anticancer/ Antioxidant	[95]

Having examined the bioactivity of organosulfur compounds in garlic, attention now shifts to Brassica vegetables. Like garlic, Brassica species such as broccoli and mustard rely on enzymatic hydrolysis to produce potent sulfur-containing metabolites, but through distinct pathways involving glucosinolates. The next section will review the chemistry, metabolism, and health effects of these compounds in Brassica plants, drawing key comparisons and contrasts with garlic.

1.10 Brassicaceae family

1.10.1 Distribution, botanical characterisation, and phytochemical significance of selected brassicaceae species

The Brassicaceae (also known as Cruciferae or the mustard family) comprises approximately 338 genera and over 3,700 species distributed worldwide [112], with the highest diversity found in Europe and the Middle East. The family encompasses numerous economically and nutritionally significant plants, many of which are cultivated for their seeds which used as condiments and spices, and their leaves serve as nutritious vegetables[113, 114]. Three representative Brassicaceae species are investigated in the present study: yellow mustard (*Sinapis alba* L.), brown mustard (*Brassica juncea* L.), and broccoli (*Brassica oleracea* L. var. *italica*).



Figure 1.7: Mustard seeds and Broccoli as representative members of the Brassicaceae family.

Sinapis alba is an annual herb native to the Mediterranean region and Western Asia, now widely cultivated for its pale-yellow seeds, which are characteristically rich in the glucosinolate sinalbin. The seeds are hard, round, and slightly mucilaginous, measuring approximately 1-2 mm in diameter [115-117]. *Brassica juncea,* believed to have originated in

Central Asia through natural hybridisation of B. rapa and B. nigra, is extensively cultivated across Asia, Europe, and North America and is distinguished by its dark brown seeds with a notably high sinigrin content [118]. Together with *B. nigra*, these three mustard species are regarded as the most economically significant within the family, owing to their high seed yield and distinctive flavour profiles [115].

Broccoli (*Brassica oleracea* var. *italica*), a Mediterranean-derived cultivar of *B. oleracea*, is widely recognised as one of the richest dietary sources of glucoraphanin, the direct biosynthetic precursor to sulforaphane [119]. Botanically, it is an herbaceous annual characterised by a thick green stalk supporting broad, leathery blue-green leaves and a large, branching head composed of dense, tightly packed unopened flower buds.

The characteristic sharp pungency of mustard is primarily attributed to four isothiocyanates, allyl isothiocyanate, 4-hydroxybenzyl isothiocyanate, and *p*-hydroxybenzyl isothiocyanate. These compounds elicit their sensory effects by activating the transient receptor potential vanilloid 1 (TRPV1) ion channel in the oral cavity and nasal passages, producing the well-known burning sensation associated with mustard consumption. Other isothiocyanates present in Brassicaceae, including phenethyl isothiocyanate, benzyl isothiocyanate, and sulforaphane, contribute to a lesser extent to overall pungency. Sulforaphane, which bears a sulfoxide functional group (CH_3-SO-$(CH_2)_4$-N=C=S) with structural similarity to thiol compounds (R-SH), imparts an organoleptic character reminiscent of onion or garlic, thereby adding a distinct aromatic dimension to the flavour profile of broccoli and related Brassica vegetables [120].

1.10.2Historical overview of brassica family and their medicinal uses

Glucosinolates are the principal secondary metabolites characteristic of the Brassicaceae family, including plants such as mustard, horseradish, broccoli, and cabbage, which have a long history of use in traditional medicine across diverse cultures. Since ancient times, these plants have been valued both as food sources and for their medicinal properties, including digestive stimulation, treatment of respiratory disorders, and topical applications for inflammation and musculoskeletal pain[121, 122]. In ancient Greece, Rome, and cross Asia, mustard seed and horseradish preparations were employed as herbal remedies, their

therapeutic effects attributed to the pungent and irritant properties of their bioactive breakdown products [122].

The scientific elucidation of glucosinolate chemistry began in 1956 with the isolation and characterisation of sinigrin, the first glucosinolate to be chemically defined [123]. The term *glucosinolates* was formally introduced a few years later in 1961 [124]. Since then, over 130 distinct GSLs have been characterized, with their structural diversity largely determined by the amino acid derived side chains [125]. It became apparent that the biological and medicinal effects traditionally attributed to these plants depend on the hydrolysis of glucosinolates by the endogenous enzyme myrosinase into biologically active compounds such as isothiocyanates, thiocyanates, and nitriles[123, 126].

These hydrolysis products have been studied for their biological activities such as antimicrobial, anti-inflammatory, and chemo-preventive activities. Such activity supports their historical use as topical antiseptics and remedies for infections and inflammatory disorders[127]. In traditional medicine, mustard seed oil has been used topically to relieve muscle pain, rheumatism, arthritic discomfort, chest congestion, and for its counter-irritant effects. It has also been applied in digestive remedies, for treating dyspepsia, and for stimulating peripheral blood flow [116, 128]. Although broccoli is primarily valued for its health-related properties, it has also been used in traditional medicine. For instance, juice extracted from broccoli leaves has been applied topically for the treatment of warts in certain Mediterranean communities [129].

Throughout the 20th and 21st centuries, research has expanded on the molecular mechanisms underlying the health benefits of glucosinolate derivatives. For example, sulforaphane, a hydrolysis product of glucoraphanin from broccoli, has been extensively studied for its potent chemo-preventive and antioxidant effects, validating earlier empirical findings[121, 122]. Similarly, allyl isothiocyanate, derived from sinigrin in mustard, continues to be recognized for its antimicrobial and anti-inflammatory properties[130]. These advances in understanding have transformed glucosinolate-rich Brassica plants into valuable functional foods and nutraceutical agents in modern medicinal approaches.

1.10.3Organosulfer compounds in brassica family

Brassicaceae plants harbour two biologically significant classes of organosulfur phytochemicals: glucosinolates (GSLs) and S-methylcysteine sulfoxide (SMCSO). SMCSO is a cysteine-derived sulfoxide also present in Allium species that, upon enzymatic degradation by cysteine lyases, yields volatile organosulfur compounds including dimethyl disulfide and dimethyl trisulfide, with reported antioxidant and hypolipidemic properties [131]. However, glucosinolates represent by far the predominant and most pharmacologically significant organosulfur class in Brassicaceae and constitute the primary focus of the present study.

Chemically, glucosinolates are defined as anionic sulfur- and nitrogen-containing secondary metabolites, comprising a *β-D-thioglucose moiety (glycone*) linked via a sulfur atom to an *N-hydroximinosulfate ester* (aglycone) with a variable R-side chain derived from different amino acids [123, 124, 132, 133]. Their general structure can therefore be described as a *β-thioglucoside-N-hydroxysulfate,* also known by other chemical names such as *cis-N-hydroximinosulfate esters* or *S-glucopyranosyl thiohydroximates* (Figure 8) [133-135]. Structural diversity within this class arises from variation in the amino acid-derived R-side chain, giving rise to three major subclasses aliphatic, aromatic, and indole glucosinolates, each contributing differently to the plant's defence chemistry, flavour profile and range of bioactive hydrolysis products (Table 1.5).

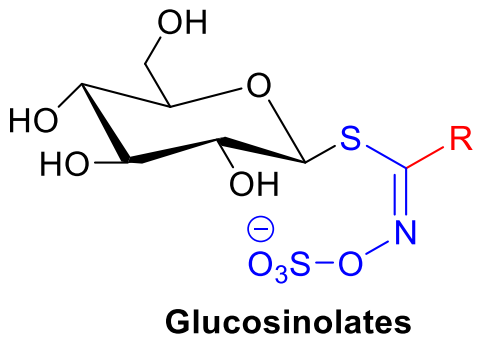

Figure 1.8: Core structural features of glucosinolates, consisting of a β-D-thioglucose unit, a sulfur-linked N-hydroximinosulfate group, and a variable amino acid-derived side chain (R).

Table 1.5: Examples of glucosinolates showing variation in the R-side chain, their major Brassica plant sources, and the reported biological activities of their myrosinase-derived hydrolysis products.

The general hydrolysis reaction of glucosinolates

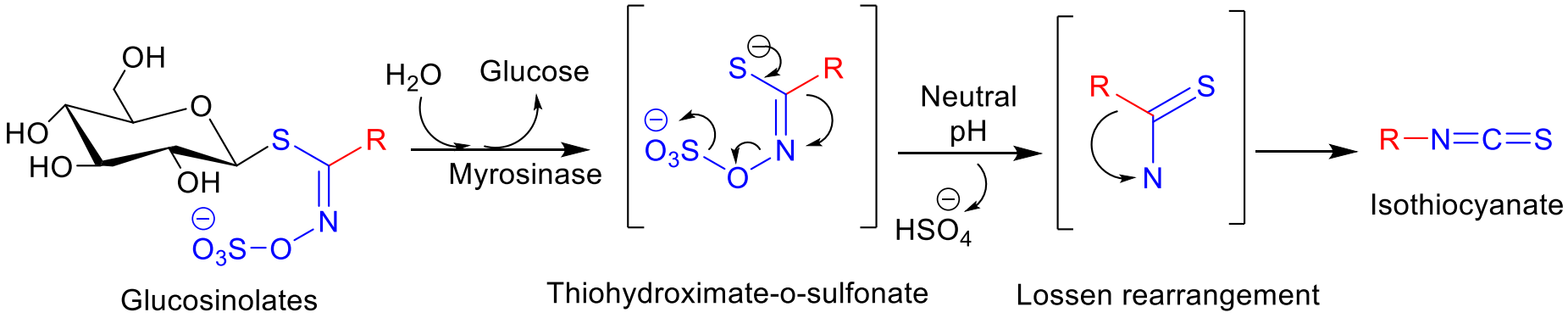

An example of R- moiety in glucosinolate and the product of its hydrolysis

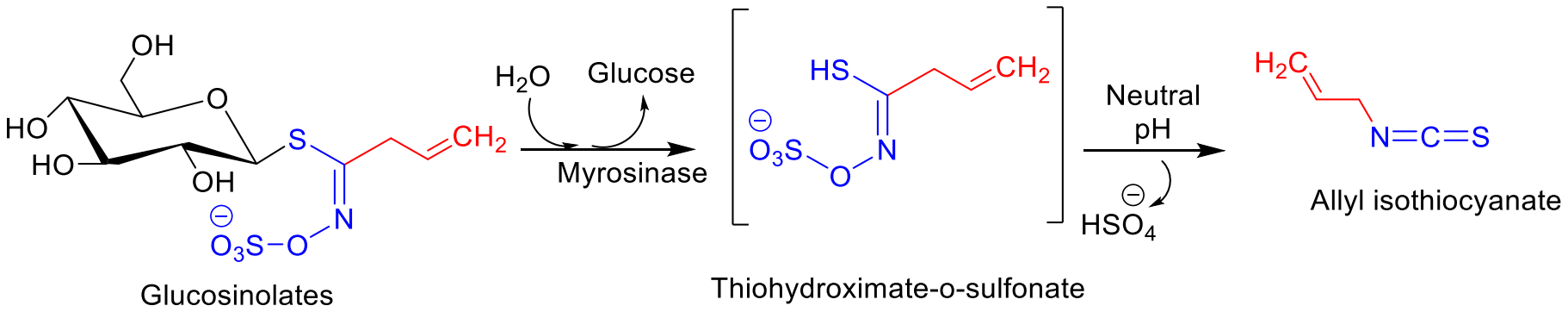

	R-functional group of glucosinolates	Trivial name	Brassica crops	Biological activities of glucosinolate hydrolysis products	References
			Aliphatic glucosinolates		
1		Sinigrin	Mustard, rockets, cabbage, cauliflower, Brussel sprouts, collards, kale, Broccoli, kohlrabi	Antibacterial, Antioxidant, hypoglycaemic, hypolipidemic and Antifungal	[136-140]
2		gluconapin	Cabbage, Brussel sprouts, kale, Broccoli, rockets	Antibacterial and Antifungal	[136, 137, 139, 140]
3	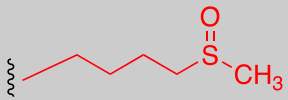	Glucoraphanin	Broccoli, Cabbage and kale	Antibacterial, Antioxidant and Anticancer	[136, 137],[139, 141-143]
4	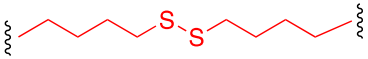	-	Rockets	Antioxidative and Antimutagenic	[136, 144]
5		Glucoerucin	Rockets, Broccoli, Cabbage, collards and Turnip	Antihypertensive,	[145, 146]

				Chemo-preventive agent and Antibacterial	[145,177, 178]
6	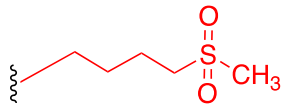	Erysolin	Rockets	Antitumor and Antimicrobial	[147], [148]
7		Camelinin	Camelina	Alleopathic	[149]
8	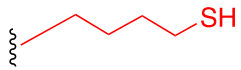	Glucosativin	Rockets	Cytotoxic	[150]
9		Glucolepiidin	Radish	Antifungal	[114, 137, 140]
10		Dihydrogluconapin	Cabbage	-	[114, 137] [151]
11	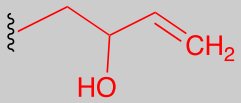	Progoitrin/ epiprogoitrin	Broccoli, Cauliflower, kohlrabi Cabbage and kale	Antiproliferative and Antioxidant	[152] [139, 141]

12		-	Rockets	-	[137]
13		Glucobrassicanapin	Cabbage, Broccoli, and Turnip	Antioxidant and Antifungal	[139-141]
14	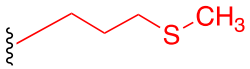	Glucoiberverin	Cauliflower, kohlrabi Cabbage, Brussel sprouts and kale	Antimicrobial and Cytotoxic	[139, 153]
15		Glucoalyssin	Cabbage, Broccoli and kohlrabi	Anticancer	[139, 154]
16	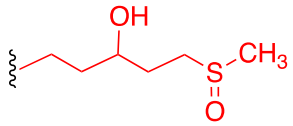	-	Rockets	-	[114]
17		Glucoibarin	Cauliflower, kohlrabi, Cabbage Brussel sprouts, kale and broccoli	Antimicrobial and Cytotoxic	[139, 153]
18	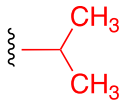	Glucoputranjivin	Mustard seeds	-	[114, 137]

			Aromatic glucosinolates		
22	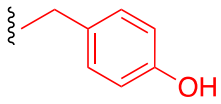	Glucosinalbin/ Sinalbin	white mustard	Antiproliferative Antifungal	[152, 155]
23	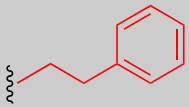	Gluconasturtiin	Watercress, radishes, Turnips, broccoli, Cabbage	Antibacterial Cytotoxic activity	[139, 156]
25	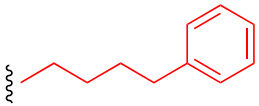	Glucoamoracin	Rockets	-	[114, 157]
26	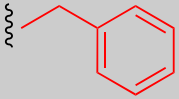	Glucotropaeolin	Cress and Watercress	Antiproliferative and Antifungal	[140, 152]
27	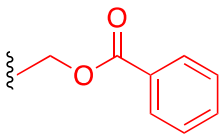	-	Rockets	-	[114]

		Indole glucosinolate			
28	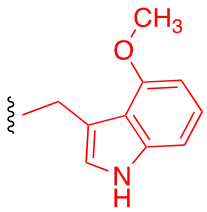	DS-4-methoxyglucobrassicin	Brussel sprouts, Broccoli, Cabbage, kale, kohlrabi, and Turnip	Anti-inflammatory	[114, 137, 139, 158]
29	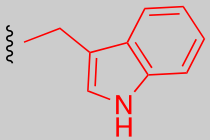	Glucobrassicin	Collards, cauliflower, kohlrabi, cabbage, Brussel sprout, kale, broccoli, turnip.	Anticancer Antioxidant	[159] [139, 141, 143]
30	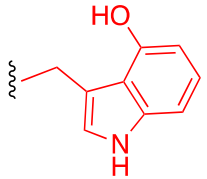	4-Hydroxyglucobrassicin	Cabbage, kale, broccoli, kohlrabi, and Turnip	-	[139, 160]
31	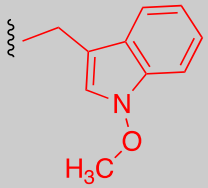	Neoglucobrassicin	Cauliflower, kohlrabi Cabbage, kale, Brussel sprouts, broccoli, and Turnip	Antioxidant Anticancer Anti-inflammatory	[161] [139, 154, 158]

1.10.3.1 The myrosinase-glucosinolate system

Glucosinolates are biologically inactive in their native state and require enzymatic activation by myrosinase to generate their characteristic spectrum of bioactive hydrolysis products. In intact plant tissues, glucosinolates and myrosinase coexist but are maintained in strict spatial separation to prevent premature hydrolysis. Glucosinolates are primarily localised within sulfur-rich S-cells in the cytoplasm, whereas myrosinase is sequestered in specialised myrosin cells, typically positioned adjacent to guard cells or vascular tissues (Figure 1.9). Upon tissue disruption whether through herbivore attack, mechanical damage, chewing, or environmental stress, this physical separation is disrupted, enabling direct enzyme-substrate to contact and initiating rapid hydrolysis [162, 163].

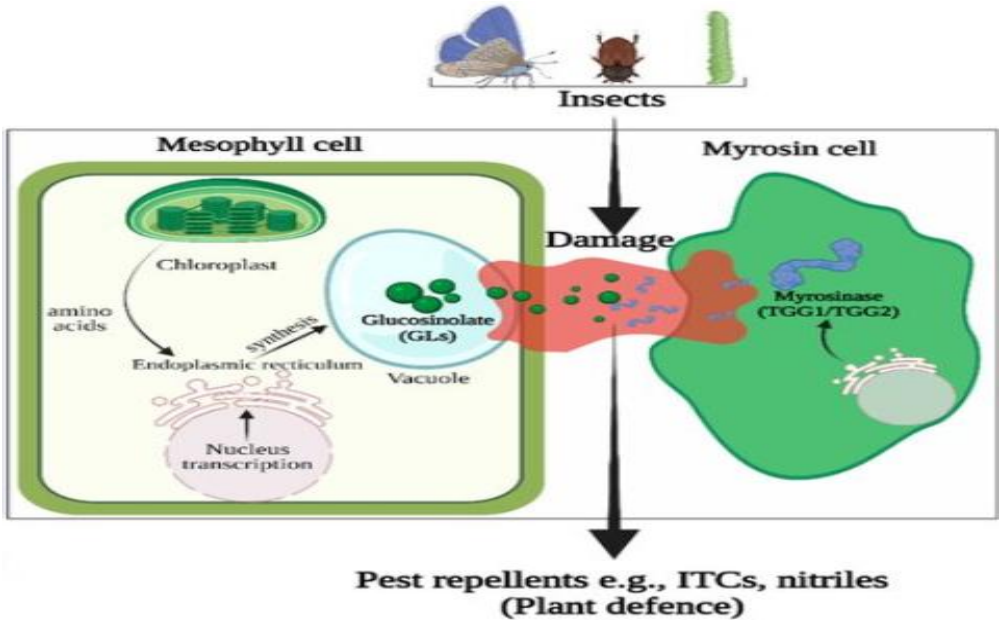

Figure 1.9: Diagram of the myrosinase-glucosinolate defence system in Brassicaceae plants. Tissue damage caused by insects allows glucosinolates and myrosinase to interact, producing isothiocyanates (ITCs) and nitriles that act as natural pest repellents [164].

Myrosinase is a member of the glycosyl hydrolase family and is broadly distributed across diverse biological taxa, including plants, fungi, bacteria, and insects [165, 166]. In the literature, the enzyme is referred to under several alternative nomenclature, including ''*thioglucosidase, sinigrinase, sinigrase, glucosinolase,* or *thioglucoside glucohydrolase*'' [125, 162]. Notably, myrosinase-like activity has also been identified within the human gut microbiota, indicating that the conversion of dietary glucosinolates into bioactive metabolites can proceed in the gastrointestinal tract independently of plant-derived enzyme activity, a

finding with important implications for the bioavailability and systemic health effects of cruciferous vegetable consumption.[134].

1.10.3.2 Glucosinolate hydrolysis products

During glucosinolate hydrolysis, myrosinase catalyses cleavage of the thioglucosidic bond resulting in the release of D-glucose and the formation of an unstable aglycone intermediate, commonly referred to as a sulfated thiohydroximate [124, 125, 134]. This highly reactive intermediate undergoes rapid spontaneous rearrangement to generate a range of biologically active degradation products, including isothiocyanates (ITCs), nitriles, thiocyanates, and epithionitriles (Figure 1.10). The specific profile of hydrolysis products is influenced by multiple factors, including pH, the presence of ferrous ions (Fe^{2+}), and endogenous specifier proteins such as epithiospecifier protein (ESP) [167, 168].

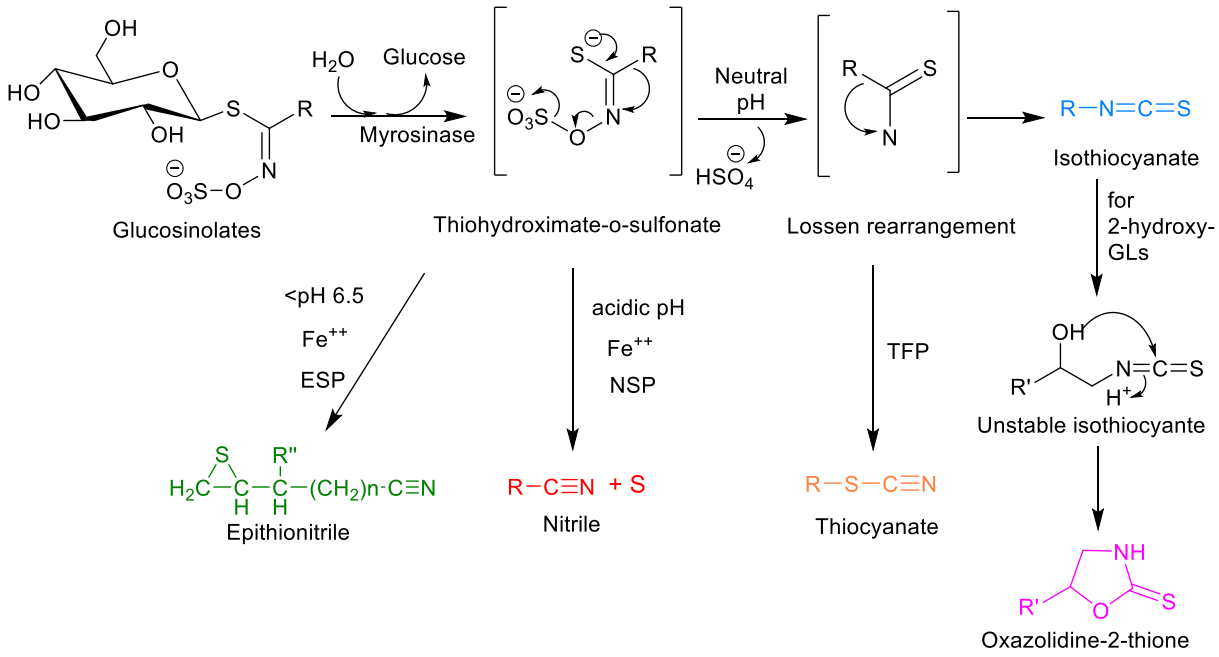

Figure 1.10: Enzymatic hydrolysis of glucosinolates by myrosinase and subsequent formation of biologically active degradation products under different biochemical conditions.

The glucosinolate hydrolysis products are chemically reactive compounds that play critical roles in both plant defence and human health. In plants, these metabolites act as effective deterrents against herbivores and microbial pathogens, forming an integral component of the plant's chemical defence system. In humans, glucosinolate-derived compounds have been extensively studied and are widely recognised for their antimicrobial, anti-inflammatory, antioxidant, and chemo-preventive activities [169, 170]. In addition, these degradation

products are responsible for the characteristic pungent aroma and bitter taste of cruciferous vegetables, contributing to their sensory properties and dietary significance [124, 171]. The factors governing the selective formation of each hydrolysis product class are examined in detail in the sections that follow.

1.10.3.2.1 Isothiocyanates, thiocyanate and oxazolidine-2-thiones formation

Isothiocyanates (ITCs) are among the major biologically active hydrolysis products of glucosinolates and have been widely recognized for their anticancer properties against several cancer types, including leukaemia, lung, liver, colon, and prostate cancers [124]. The formation of ITCs is strongly influenced by pH and temperature. Under neutral conditions (pH 6-7), myrosinase-catalyzed glucosinolate hydrolysis predominantly yields isothiocyanates (Figure 10) [134, 168]. At high temperatures and hydration levels also promote ITC generation by accelerating enzymatic and non-enzymatic transformations [124].

In the presence of thiocyanate-forming proteins (TFPs), the hydrolysis pathway can shift toward the formation of thiocyanates rather than ITCs. This alternative reaction occurs with specific glucosinolates such as sinigrin, glucoerucin, and glucotropaeolin, producing thiocyanates as minor but biologically relevant products [172, 173]. Additionally, oxazolidine-2-thiones are produced through the intramolecular cyclization of unstable β-hydroxy isothiocyanate intermediates, a reaction that typically occurs under mild alkaline conditions (Figure 10) [135].

1.10.3.2.2 Nitriles and epithionitrile formation

Isothiocyanates and nitriles are the main hydrolysis products formed during glucosinolate breakdown. The pathway that a glucosinolate follows is strongly influenced by pH, metal ions, and specifier proteins. Under acidic conditions and in the presence of ferrous ions (Fe^{2+}) or nitrile-specifier proteins (NSPs), the reaction changes from isothiocyanate formation to the production of nitriles [124, 134, 168, 174, 175]. Conversely, when epithiospecifier proteins (ESPs) are present alongside Fe^{2+} ions, the hydrolysis of certain aliphatic glucosinolates yields epithionitriles, which result from the intramolecular incorporation of a sulfur atom into the nitrile structure. (Figure 10) [139, 172]. These protein- and pH-dependent pathways highlight

the biochemical flexibility of the glucosinolate-myrosinase system and contribute to the chemical diversity of glucosinolate degradation products.

1.10.3.2.3 Other hydrolysis products

Indole glucosinolates, such as neoglucobrassicin and glucobrassicin, undergo hydrolysis to form an unstable indole isothiocyanate intermediate. This reactive intermediate rapidly rearranges to yield a range of biologically active compounds, including 3-indolyl carbinol, 3-indoleacetonitrile, and 3,3'-diindolylmethane (DIM), which are summarised in Figure 1.11 [124, 176, 177]. These products are characteristic of indole glucosinolate degradation and contribute significantly to the antimicrobial, anti-inflammatory, and chemo-preventive activities associated with cruciferous vegetables.

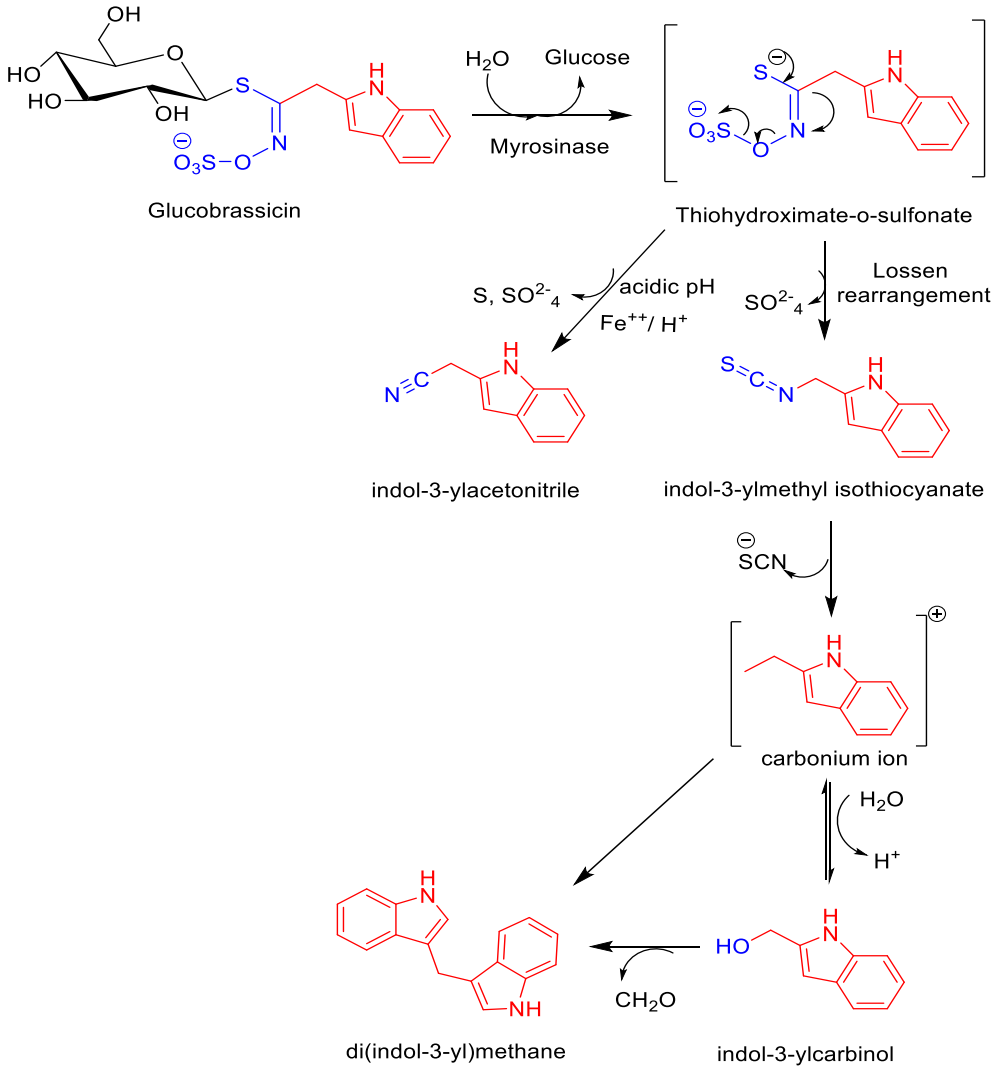

Figure 1.11: Representative degradation products of indole glucosinolates and their corresponding chemical structures.

1.10.4Glucosinolates compounds in Brassica plants and the biological activities of their hydrolysis products

Brassica plants have a different glucosinolate profile that varies between species, cultivars, and plant tissues. These sulfur and nitrogen-containing compounds are stored as inactive precursors and become biologically active only after enzymatic hydrolysis, producing structurally diverse compounds with important ecological and pharmacological roles. The biological activities of *Brassica* plants depend on the composition and amount of glucosinolate hydrolysis products. For example, Isothiocyanates such as allyl isothiocyanate and sulforaphane, are the most extensively studied compounds due to their strong biological activities such as anticancer, anti-inflammatory, antioxidant, and antimicrobial. Although nitriles and thiocyanates have lower bioactivity in humans, they are essential components of plant defence and significantly influence the chemical diversity of *Brassica* species. The following section discusses in detail the biological activities of glucosinolate-derived compounds.

1.10.4.1 Antimicrobial activity

Isothiocyanates (ITCs) derived from Brassicaceae species exhibit potent broad-spectrum antimicrobial activity against a diverse range of pathogenic microorganisms, including Gram-positive bacteria (*Staphylococcus aureus*, *Bacillus subtilis*), Gram-negative bacteria (*Escherichia coli*, *Pseudomonas aeruginosa*, *Salmonella* spp.), fungi (*Candida albicans*), and certain viruses [121]. Their antimicrobial efficacy operates through two principal and complementary mechanisms. The first involves disruption of microbial cell membranes, leading to altered intracellular ATP concentrations, reduced intracellular pH, increased membrane permeability, leakage of cellular contents, and ultimately cell death [178].The second involves direct interaction with intracellular targets, whereby the electrophilic isothiocyanate group reacts covalently with thiol groups (-SH) on cysteine residues of key microbial enzymes, impairing bacterial metabolism, redox balance, and stress response pathways [123, 179]. This dual mechanism not only exerts direct bactericidal effects but simultaneously increases microbial susceptibility to oxidative stress.

Beyond direct antimicrobial action, several ITCs demonstrate significant antibiofilm and anti-virulence properties. Allyl isothiocyanate (AITC) has been shown to inhibit biofilm formation

and disrupt established biofilms, which are highly resistant microbial communities central to chronic infections and antimicrobial resistance [180]. Sulforaphane, derived from glucoraphanin in broccoli, similarly demonstrates antibiofilm activity and has been reported to suppress quorum sensing (the bacterial communication mechanism governing virulence gene expression and resistance) substantially extending its antimicrobial efficacy beyond simple bactericidal properties[181]. Furthermore, ITCs exhibit immunomodulatory properties that augment innate immune responses, contributing to enhanced host defence against infection [169]. The most extensively investigated antimicrobial isothiocyanates including AITC, sulforaphane, 2-phenylethyl isothiocyanate, 3-butenyl isothiocyanate, and bis(4-isothiocyanatobutyl) disulfide are summarised alongside their reported activities in Table 1.6 [136, 182-185].

Table 1.6: Antibacterial activity of selected glucosinolates hydrolysis products (isothiocyanates) and their reported target bacterial species.

	Glucosinolate chemical structures	Bacteria	References
1	allylisothiocyanate (AITC) 	*E. coli, P. aeruginosa, S. aureus, L. monocytogenes, S. flexneri, and B. subtilis*	[183] [136]
2	2-phenylethylisothiocyanate (PEITC) 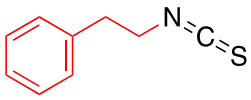	*E. coli, P. aeruginosa, S. aureus, L. monocytogene, S. flexneri,* and *B. subtilis*	[183] [136]
3	3-Butenyl isothiocyanate 	*E. coli, P. aeruginosa, S. flexneri S. aureus, and B. subtilis*	[136]
4	Sulforaphane 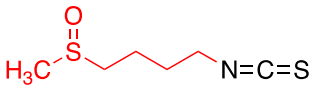	*E. coli, P. aeruginosa and S. flexneri S. aureus, and B. subtilis*	[136]
5	Bis (4-iso thiocyanatobutyl) disulphide 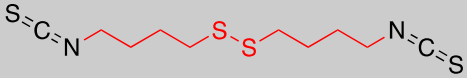	*E. coli, P. aeruginosa, S. flexneri S. aureus, and B. subtilis*	[136]

1.10.4.2 Anticancer activity

The isothiocyanate sulforaphane, derived from the glucosinolate glucoraphanin in broccoli, is extensively studied for its chemo-preventive properties. Sulforaphane induces phase II detoxification enzymes such as quinone reductase and glutathione S-transferase, which enhance the elimination of carcinogens and protect cells from DNA damage. It also promotes apoptosis and inhibits tumour angiogenesis and proliferation in various cancer cell lines [186]. Compared to sulforaphane, its hydrolysis product sulforaphane nitrile shows much weaker activity, underscoring the importance of directing glucoraphanin hydrolysis toward sulforaphane formation for effective anticancer potential [187]. Mustard seed contains sinigrin, which upon hydrolysis produces allyl isothiocyanate (AITC), another compound demonstrating anticancer effects by similar mechanisms including apoptosis induction and tumour growth inhibition [123, 188].

1.10.4.3 Antioxidant activity

Glucosinolate hydrolysis products activate the Nrf2 (nuclear factor erythroid 2-related factor 2) pathway, a key regulator of antioxidant responses within cells. Sulforaphane and related isothiocyanates upregulate endogenous antioxidant enzymes such as glutathione peroxidase, catalase, and superoxide dismutase, reducing oxidative stress and protecting cellular macromolecules from damage. These antioxidant effects contribute to overall cellular homeostasis and have implications in preventing chronic diseases related to oxidative damage [189, 190].

1.10.4.4 Anti-inflammatory activity

Isothiocyanates derived from glucosinolates show anti-inflammatory effects by inhibiting pro-inflammatory signalling pathways such as NF-κB and reducing the production of inflammatory cytokines like TNF-α and IL-6. Through these mechanisms, sulforaphane and allyl isothiocyanate can modulate inflammatory responses, potentially benefiting conditions associated with chronic inflammation [191].

1.10.4.5 Ecological and other roles

Beyond human health, glucosinolate hydrolysis products serve as natural defence agents in plants. Their antimicrobial and insect-deterrent properties help protect these plants from pathogens and herbivores.

Following an understanding of the chemistry and biological activities of organosulfur compounds, it is important to consider the stability of sulfur-containing metabolites under processing conditions. Thermal treatment can markedly alter their composition, reactivity, and bioactivity. Examining the thermal behaviour of sulfur compounds derived from garlic and glucosinolate-containing plants therefore provides essential context for interpreting changes in biological activity, sensory properties, and potential synergistic effects. The following section outlines the effects of thermal processing on organosulfur compounds in both garlic and cruciferous vegetables.

1.11 Thermal degradation pathways of sulfur-containing natural products

Thermal degradation of sulfur-containing natural products particularly those derived from garlic and cruciferous vegetables, greatly alters their chemical composition and bioactivity. Although these molecules differ chemically and arise from distinct pathways, upon heating they undergo decomposition and rearrangement reactions that yield similar types of organosulfur metabolites. For example, in garlic allicin, the principal reactive sulfur compound formed enzymatically from alliin upon tissue disruption is notably thermally unstable. Even mild heating at 75 °C causes a significant reduction in allicin content, initiating its rapid conversion into various organosulfur derivatives such as diallyl disulfide (DADS), diallyl trisulfide (DATS), and cyclic sulfur compounds including vinyl-dithiins and thiophenes, which are absent in fresh garlic but contribute to the physical characteristic aroma and flavour of cooked garlic[192]. Extended heating furthermore enhances the transformation of allicin into a diverse suite of organosulfur compounds, with significant impact on both the qualities and biological activities of garlic (Figure 1.12) [193-195].

In cruciferous vegetables, the sulfur-containing profile focuses on glucosinolates and their enzymatic hydrolysis products. Thermal processing techniques such as boiling, blanching, or steaming induce significant losses of glucosinolates up to 70% under intense conditions due

to their thermal sensitivity and enzyme denaturation, which alters the yield and composition of hydrolysis products. Allyl isothiocyanate (AITC), a bioactive isothiocyanate predominantly derived from glucosinolate hydrolysis, exemplifies this instability. When subjected to boiling or extended heating in aqueous media at 100 °C for an hour, AITC may degrade by approximately 75%, producing an array of sulfur-containing by-products including diallyl sulfide, diallyl disulfide, and cyclic compounds such as dithiin and tri-thiin derivatives[196]. These degradation pathways not only reduce the bioavailability of isothiocyanates but also shift the physical characteristics from a typical pungent, mustard-like aroma to more garlic-like or sulfureous notes (Figure 1.12) [193, 197].

Overall, thermal processing substantially reshapes the profile of sulfur-containing metabolites in garlic and cruciferous vegetables by inducing the conversion of unstable, highly reactive precursors such as allicin and glucosinolates into more thermally stable polysulfides and cyclic sulfur compounds. As a result, heat treatment alters both the chemical composition and the biological activity of sulfur-rich foods, with important implications for their functional efficacy and physical properties. These transformations highlight the need to optimize processing and cooking conditions to preserve key bioactive constituents.

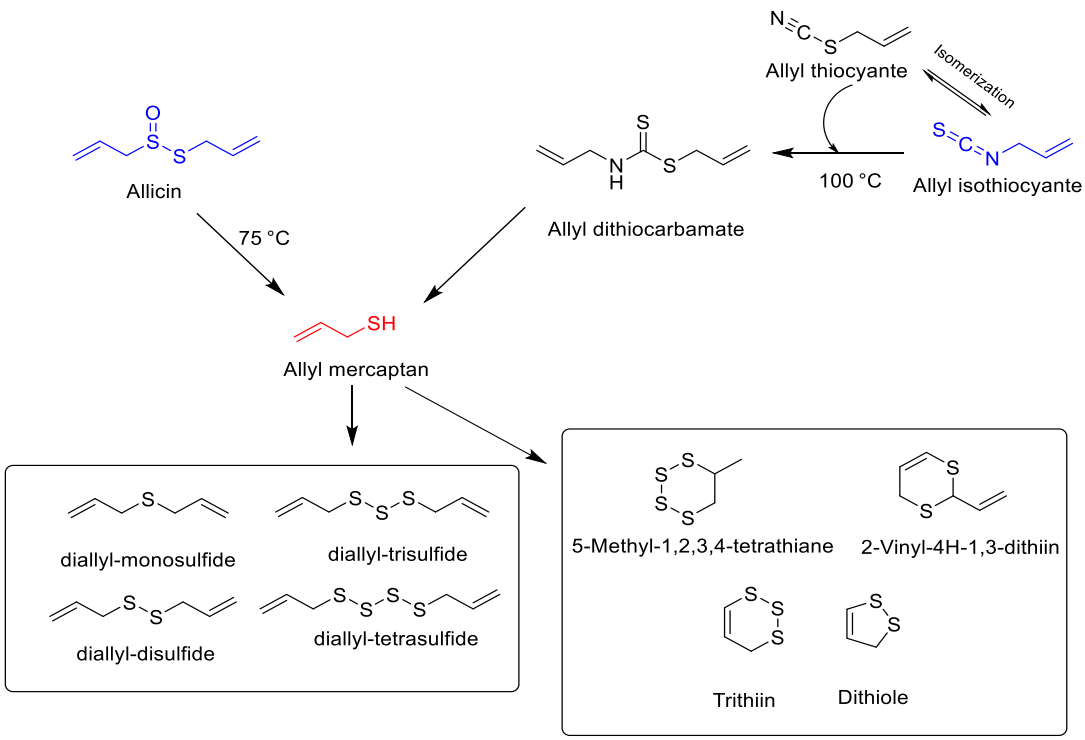

Figure 1.12: Pathways for the thermal degradation of glucosinolate-derived isothiocyanates and alliin, illustrating the formation of polysulfides and cyclic organosulfur compounds.

While the previous sections have outlined the chemistry, biological activity, and stability of sulfur-containing metabolites, a primary understanding of their thiol reactivity is essential to integrate these concepts mechanistically. Many organosulfur compounds produce their biological effects through direct interactions with thiol groups present in small molecules and proteins, making thiol reactivity a central feature of their chemical behaviour. Establishing this foundation is necessary before defining the aim and objectives of this thesis, which are focused on investigating thiol-mediated interactions between organosulfur compounds derived from garlic and glucosinolate-containing plants.

1.12 Thiol reactive species (RSS)

One common characteristic of sulfur-containing compounds in Cruciferae vegetables and Alliums is that their degradation products are highly reactive to thiol-containing substances. Allicin is a well-known thiol-reactive compound of garlic, which is an unstable organosulfur compound produced enzymatically after tissue disrupt. Allicin contains a sulfinyl functional group attached to a disulfide bond that imparts very strong electrophilic nature, which leads to its high reactivity towards nucleophilic (-SH) thiols found in biomolecules as cellular thiol such as glutathione and cysteines [198] (Figure 1.13).

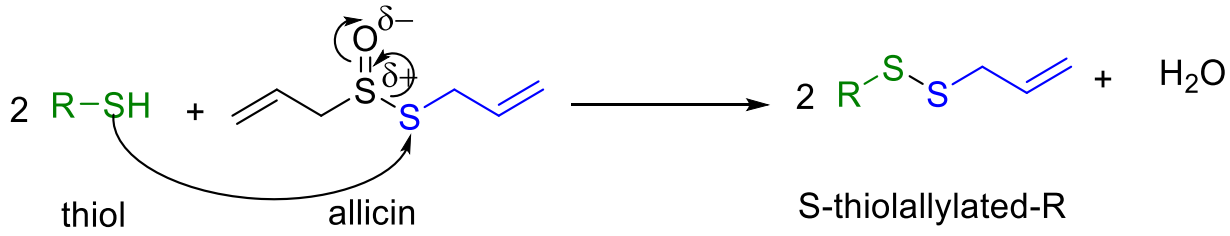

Figure 1.13: Thiol reactivity of allicin with thiols (R-SH) yields S-thioallylated derivatives (R-S-S-allyl) and water, demonstrating allicin's ability to react with thiol groups.

Allicin has significant reactivity with low molecular weight thiols, including glutathione, cysteine and a range of small thiol-containing molecules. This reactivity allows allicin to participate in thiol-disulfide exchange while (-S-R) group of allicin reacts with the free thiol (-SH) groups of these molecules. As result, mixed disulfides and other sulfur compounds are produced including allyl mercaptan and diallyl disulfide (Figure 1.14). Allicin shows potent antimicrobial activity by interacting with cysteine thiol groups in enzymes and proteins, leading to changes in the redox balance and functional activity of cellular thiols thereby

affecting enzyme function and cell signalling. This reactivity in biological systems allows allicin to disrupt microbial metabolism via interaction with thiol-dependent enzymes as well as antioxidant molecules such as glutathione, illustrating the wide-spectrum antimicrobial activity of allicin.

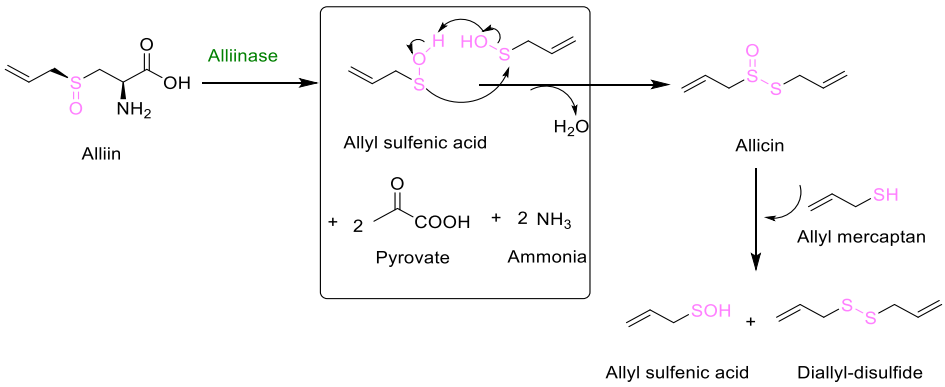

Figure 1.14: Formation of allicin from alliin and its thiol reactivity. Alliinase converts alliin into allyl sulfenic acid, which condenses to form allicin. Allicin subsequently reacts with thiols to generate disulfide products such as diallyl disulfide.

Understanding the thiol reactivity of allicin is essential for elucidating the biochemical basis of garlic's medicinal properties and forms a foundation for exploring its interaction with other sulfur-containing phytochemicals.

Likewise, glucosinolates are the most abundant secondary sulfur-containing metabolites in cruciferous vegetables, which hydrolysed by myrosinase upon mechanical damage of plant tissue such as during chewing. This reaction leads to break down the S-glucose bond and producing an unstable highly reactive aglycone intermediate characterized by electrophilic thiohydroximate-O-sulfate moiety. This highly reactive aglycone spontaneously rearranges to form a numerous of degradation compounds, isothiocyanate (R-N=C=S) are the most prominent. These compounds have been extensively studied for their antimicrobial properties and their potential contribution to the health-promoting effects of cruciferous vegetables (Figure 1.15) [193, 199].

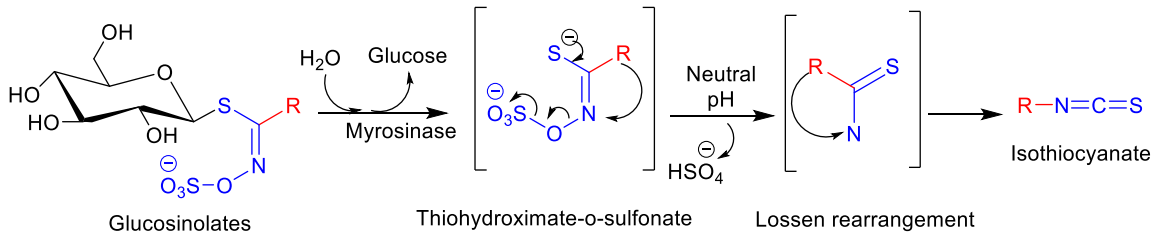

Figure 1.15: Myrosinase-catalyzed hydrolysis of glucosinolates, yielding a sulfated thiohydroximate intermediate that rearranges to bioactive isothiocyanates.

1.12.1 Experimental evidence for thiol trapping of glucosinolate-derived aglycones

The enzymatic hydrolysis intermediates of glucosinolates have shown chemical ability to react with nucleophilic thiols. In experiment designed to investigate the stability and lifetime of these aglycones' intermediates, it was found that the allyl aglycone remained stable for approximately one minute before being rapidly trapped by 2,2'-dithiodipyridine (2,2'-DTDP). This result can obviously prove the capability of the aglycone intermediate to react with thiol-reactive compounds, supporting the hypothesis that these sulfur intermediates can be chemically react with thiol nucleophiles (Figure 1.16) [200].

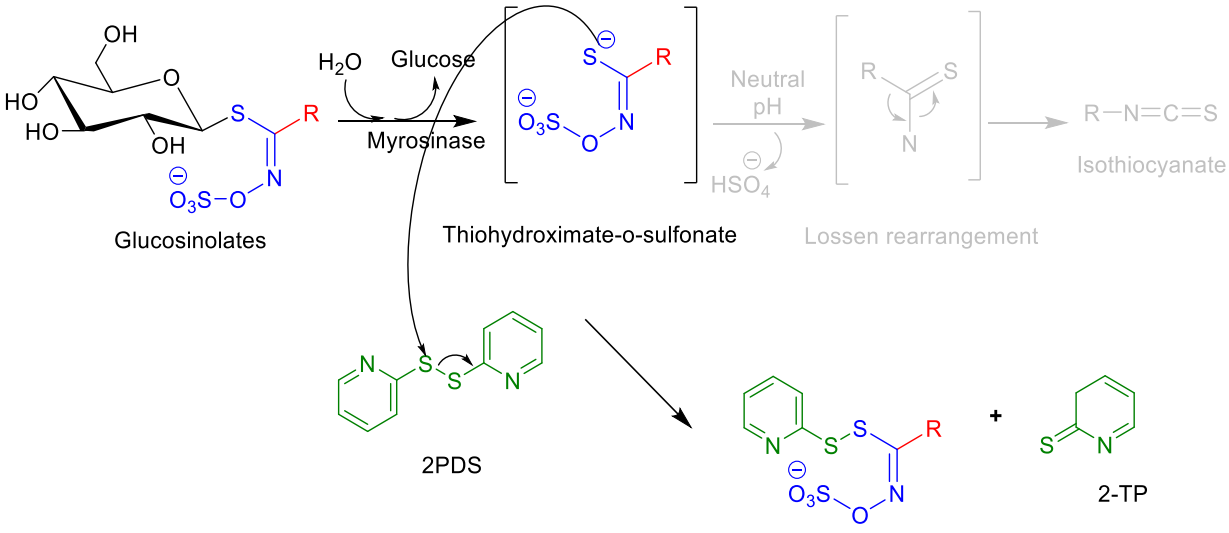

Figure 1.16: Trapping of the unstable aglycone intermediate generated from sinigrin hydrolysis by 2,2'-dithiodipyridine (2-PDS), yielding a stable conjugate and releasing 2-mercaptopyridine (2-TP).

This reactivity emphasizes the possibility that the aglycone can be trapped by different sulfur nucleophiles, including bioactive compounds such as allicin from garlic leading to the formation of new S-linked conjugates. The ability to form such conjugates supports the core

hypothesis of this thesis, that the reactive glucosinolate-derived aglycone intermediates can be selectively trapped by sulfur-containing phytochemicals, leading to the formation of novel natural by-products. Exploration of this thiol trapping mechanism will help to identify new bioactive compounds with increased antimicrobial activities, thus facilitating the search for multifunctional natural agents that could take advantage of the unique chemistry associated with garlic and cruciferous vegetable metabolites.

No studies to date have discovered that sulfur-containing hydrolysis intermediates from garlic and cruciferous vegetables might interact to form novel bioactive products. Currently, these metabolites have been extensively studied focusing on their individual bioactivities and reactivity profiles. Investigations of garlic-derived thiol reactivity have focused on low molecular weight thiols such as glutathione and cysteine with no examination for possible cross-reactivity towards glucosinolate-derived intermediates from cruciferous plants. This gap highlights an unexplored avenue for the discovery of hybrid sulfur-containing compounds with unique biological properties.

1.13 Aim and objective of this PhD

A highly reactive aglycone intermediate fragment produced during glucosinolates hydrolysis, that has the potential to be trapped by allicin, the bioactive sulphur-containing compound found in garlic extracts. The aim of this work is to investigate whether the interactions of these intermediates can lead to the formation of novel conjugated compounds with enhanced biological activity. Such a reaction might combine the unique antimicrobial properties of both plants, potentially resulting in a synergistic effect. These hybrid products might not only exhibit broad-spectrum antimicrobial activity but also serve as innovative natural compounds with applications in combating microbial resistance and improving food preservation. Exploring this interaction further could open new avenues for the development of multifunctional natural antimicrobials with significant therapeutic and agricultural potential (Figure 1.17).

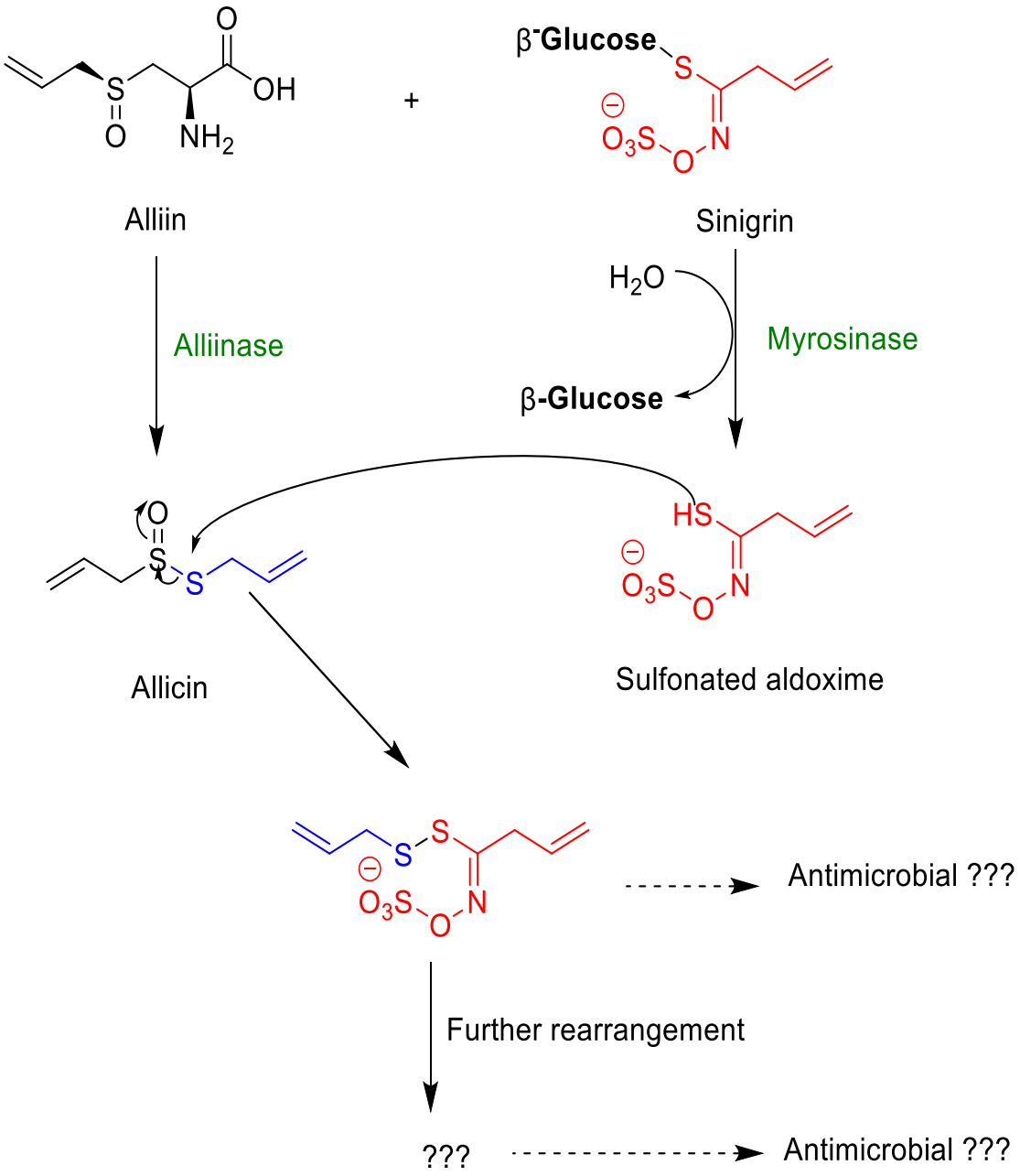

Figure 1.17: Diagram explains the aim of this project.

1.14 Objectives

To achieve the aim of this thesis, the following specific objectives are defined:

1. To investigate the thiol reactivity of allicin with reactive intermediates generated during glucosinolate hydrolysis, and to determine whether these interactions lead to the formation of novel sulfur-containing conjugated compounds, including their subsequent chemical rearrangements and structural characterisation (Chapter 2).
2. To detect, identify, and confirm the formation of these novel sulfur-containing compounds in crude mixed plant extracts, produced from combinations of garlic and glucosinolate-containing plant materials (Chapter 3).
3. To assess the antibacterial activity of the newly formed sulfur-containing compounds and the corresponding crude plant mixture extracts, to evaluate their potential as enhanced or synergistic antimicrobial agents (Chapter 4).
4. To investigate the structural properties and stereochemical features of the newly identified sulfur-containing compound (alligrin), and to compare these features with established disulfide-containing compounds to elucidate differences in disulfide geometry, electronic structure and conformational preferences, and to evaluate how these variations influence molecular reactivity stability, and potential biological interactions (Chapter 5).

2 Investigating Thiol Reactivity of Intermediates Derived from Garlic and Cruciferous Vegetables: Potential for Novel Antimicrobial Natural By-Products

The aim of this chapter is to investigate the thiol reactivity of allicin with glucosinolate-derived hydrolysis intermediates, and to determine whether these interactions lead to the formation of new sulfur-containing compounds and their subsequent rearrangements. To achieve this, the chapter begins with a structural characterisation of allicin, selected glucosinolates (sinigrin and glucoraphanin), and their enzymatic hydrolysis products, allyl isothiocyanate (AITC) and sulforaphane, using nuclear magnetic resonance (NMR) spectroscopy. The reactivity of allicin with these intermediates is then examined under controlled conditions, with experiments designed to monitor and evaluate the outcomes of these interactions. Taken together, this work aims to provide experimental evidence for a previously unreported mechanism by which metabolites from Allium (garlic) and cruciferous vegetables react to generate new sulfur-containing bioactive compounds.

2.1.1 Synthesis of allicin using pre-formed performic acid

Allicin was synthesized through a well-established two-step oxidation method (Figure 2.1) [201]. First step, the organic peracid typically performic acid is generated by the oxidation of formic acid with hydrogen peroxide (H_2O_2). In the second step, diallyl disulfide (DADS) is oxidized by the freshly prepared peracid, the reaction is conducted at 0 °C under controlled conditions to minimize side reactions and by-product formation. Upon completion, the reaction is quenched by adding five volumes of water, then the products including allicin and unreacted DADS, are extracted with dichloromethane (DCM).

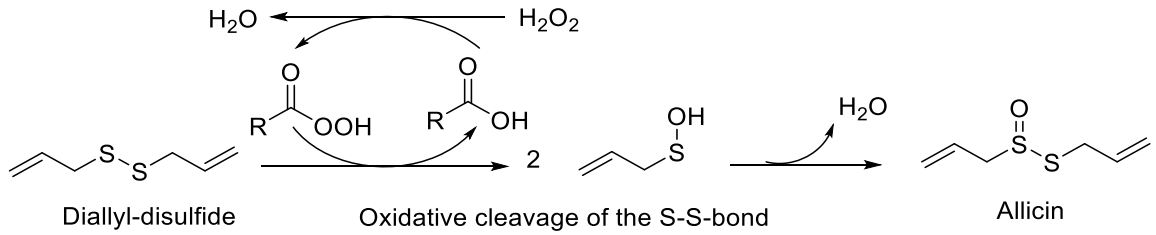

Figure 2.1: Allicin synthesis from diallyl-disulfide (DADS) through oxidation by a peracid generated with H_2O_2 in the reaction mixture.

Reaction progress and product purity were monitored by high-performance liquid chromatography (HPLC). Allicin was obtained in 97% yield (0.54 g, 3.33 mmol, calculated on the basis of DADS; MW 162.27 g/mol) with an HPLC purity of 99.3%. The structural identity of the synthesized allicin was further validated through ^{1}H-NMR analysis (Figure 2.2), where the observed chemical shifts and coupling patterns were in full agreement with the expected values, confirming both the identity and structural integrity of the compound [201].

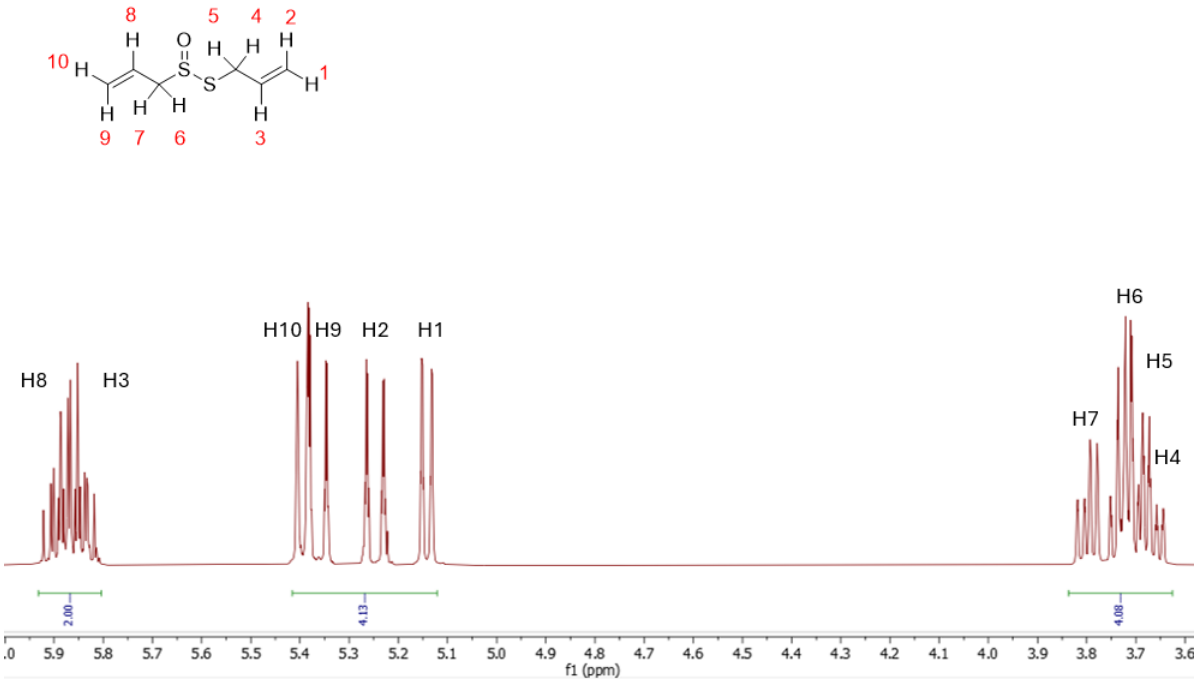

Figure 2.2: ^{1}H-NMR spectrum (500 MHz, DMSO-d) of allicin, confirming structural integrity and purity.

The structural properties of sinigrin and its principal hydrolysis product, allyl isothiocyanate (AITC), are examined in the following section, as these directly inform the reactivity anticipated in the planned reaction.

2.1.2 Structural characterization of sinigrin and its hydrolysis product allyl isothiocyanate via NMR

To achieve the main objective of this study, exploring the interaction between allicin and glucosinolates leading to the formation of novel sulfur-containing compounds, it was first necessary to establish a structural reference. Sinigrin and its enzymatic hydrolysis product allyl isothiocyanate were characterized using NMR to confirm their identities and spectral features. These well-defined standards provided essential guide for interpreting later

enzymatic reactions with allicin and formed the basis for understanding the structural and mechanistic aspects of new sulfur compound formation.

2.1.2.1 Sinigrin structure analysis

Sinigrin is a naturally existing glucosinolate found in many plants of the Brassicaceae family including Brassica nigra (black mustard), Brassica juncea (Indian mustard), brussels sprouts, and broccoli. Sinigrin (allyl glucosinolate) is a glucosinolate found predominantly in Brassica plants. The structure of sinigrin consists of a β-D-glucopyranose ring linked via a sulfur atom to an allyl group, with the nitrogen bearing an O-sulfonate group (O-SO_3^-), forming a thiohydroximate (C=N-O-SO_3^-) fragment [202]. The structure of sinigrin was confirmed by ^{1}H NMR spectroscopy (500 MHz, D_2O), with all proton assignments for both the glucose and aglycone moieties in full agreement with previously reported data (Figure 2.3), including the characteristic signals of the allyl group (7a/7b, H8, H9a/9b), the anomeric proton (H1), and the glucopyranose ring protons (H2-H6a/6b) [174].

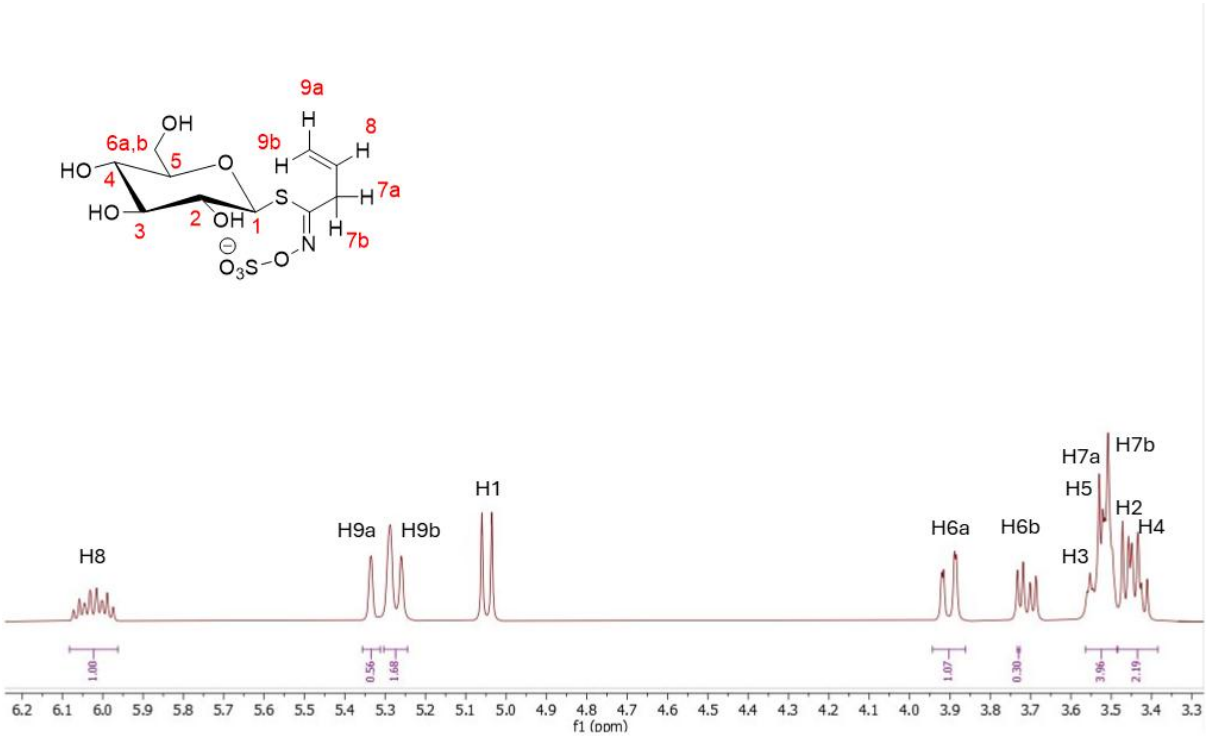

Figure 2.3: ^{1}H-NMR spectrum (500 MHz, D_2O) of sinigrin standard.

Sinigrin is a water-soluble anion in general, and after tissue damage it is enzymatically hydrolysed by myrosinase when combined with water resulting in the formation of biologically active products known as isothiocyanates, thiocyanates or nitriles (Figure 2.4).

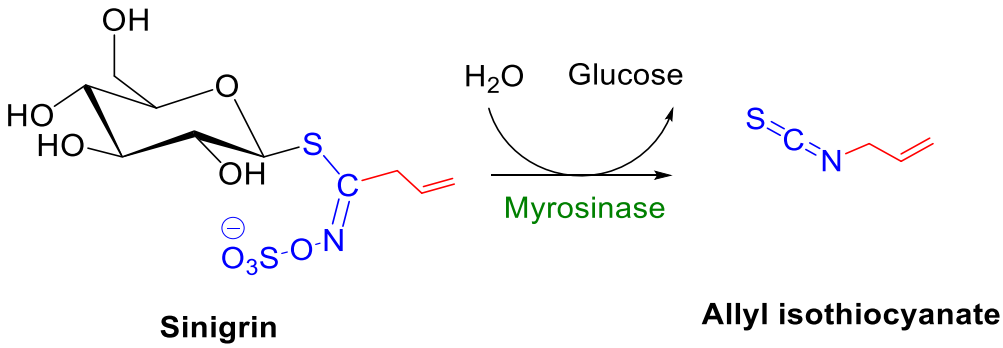

Figure 2.4: Enzymatic hydrolysis of sinigrin by myrosinase, releasing glucose and generating allyl isothiocyanate as the major bioactive product.

Sinigrin mainly hydrolysed to allyl isothiocyanates (AITC), a compound responsible for the pungency of mustard as well as known antimicrobial and therapeutic effects. The hydrolysis of sinigrin does not produce only allyl isothiocyanates (AITC) as allyl thiocyanate (AT) is also generated. The ratio of AITC to AT is known to be influenced by environmental conditions particularly soil pH, under neutral conditions (pH>5) favoured the creation of AITC (>90%) while at acidic conditions of (pH<5), AT yield was increased[174].

2.1.2.2 Allyl isothiocyanate structure analysis

Isothiocyanates (ITCs) are naturally occurring phytochemicals released from cruciferous vegetables through enzymatic hydrolysis of glucosinolates and have received considerable attention due to their wide range of health-promoting biological activities. Among these compounds, allyl isothiocyanate (AITC) formed specifically as the hydrolysis product of sinigrin, a major glucosinolate found in plants such as mustard, horseradish and various Brassica species, which is characterised by a (N=C=S) linked to both an alkyl and an aryl chain. The structure of AITC was confirmed by ^{1}H NMR spectroscopy , with all proton assignments fully consistent with the reported literature values (Figure 2.5) [174], including the characteristic signals of the terminal vinyl protons (H6a, H6b), the internal vinyl proton (H5), and the methylene protons adjacent to the isothiocyanate group (H4a, H4b).

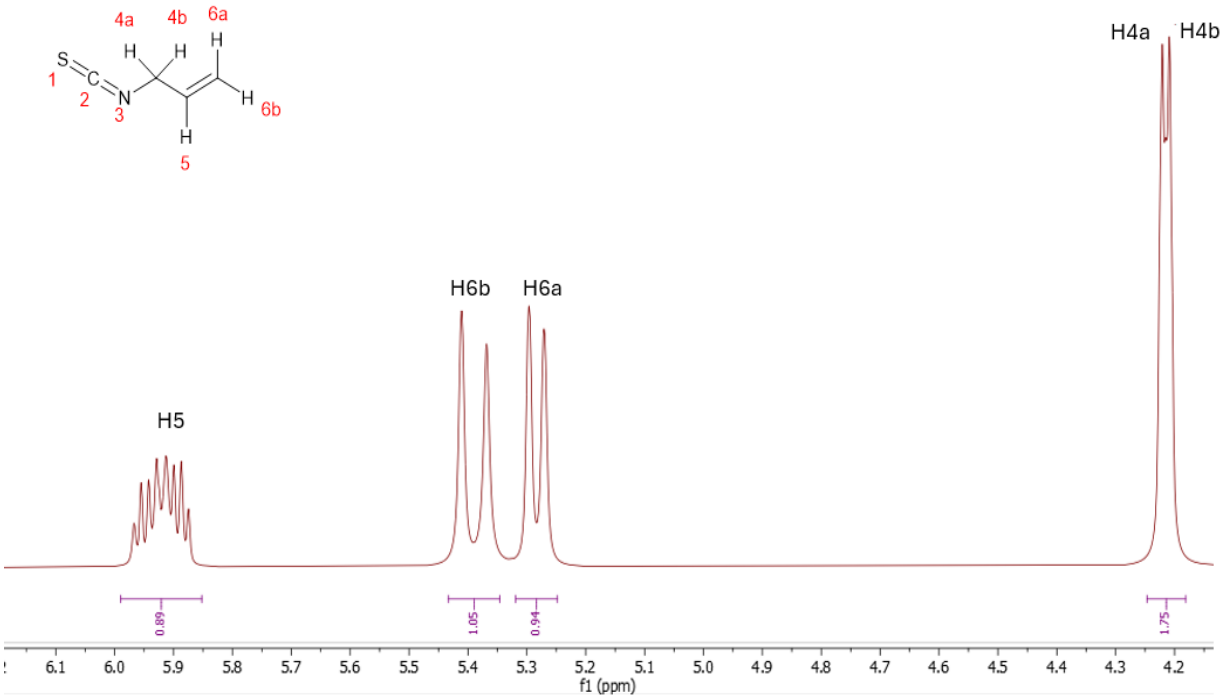

Figure 2.5: ^{1}H-NMR spectrum (500 MHz, Methanol-d_4) of allyl isothiocyanate standard.

2.1.2.3 Studying myrosinase catalytic hydrolysis of sinigrin in different solvents

The enzymatic hydrolysis of sinigrin by myrosinase was monitored in real time by ^{1}H NMR spectroscopy to establish optimal reaction conditions in the presence of various organic solvents. The internal vinyl proton was selected as the diagnostic signal for monitoring reaction progress and quantifying reaction yield, as it appears as a well-resolved and clearly distinguishable signal in the ^{1}H NMR spectra of both compounds (Figure 2.6). Specifically, the internal vinyl proton H8 of sinigrin (δ 5.9 ppm) and its corresponding signal H5 in AITC were tracked throughout the reaction, as these signals reflect the characteristic chemical shift change upon cleavage of the thioglucosidic bond and Lossen-type rearrangement to the isothiocyanate, enabling quantitative monitoring of substrate consumption and product formation.

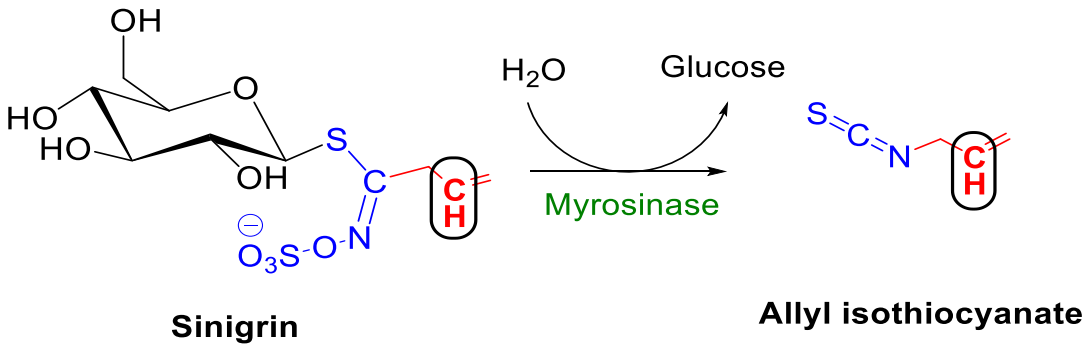

Figure 2.6: Monitoring sinigrin hydrolysis to allyl isothiocyanate (AITC) by tracking allylic proton signals in the ^1H NMR spectrum.

The effect of solvent composition on myrosinase-catalysed hydrolysis of sinigrin was investigated using ^1H NMR spectroscopy across three reaction media, methanol/water (12.5 M), ethanol/water (4.3 M) and deuterium water (D_2O). In methanol/water, addition of one unit of myrosinase presented 22% conversion of sinigrin to AITC within 5 minutes, which remained essentially unchanged at 23% after 2 days, indicating that the reaction reached a plateau rapidly with no significant further hydrolysis over the extended monitoring period (Figure 2.7). Under comparable conditions in ethanol/water, the initial conversion yield was lower at 11%, similarly stagnating at 17% after 2 days (Figure 2.9).

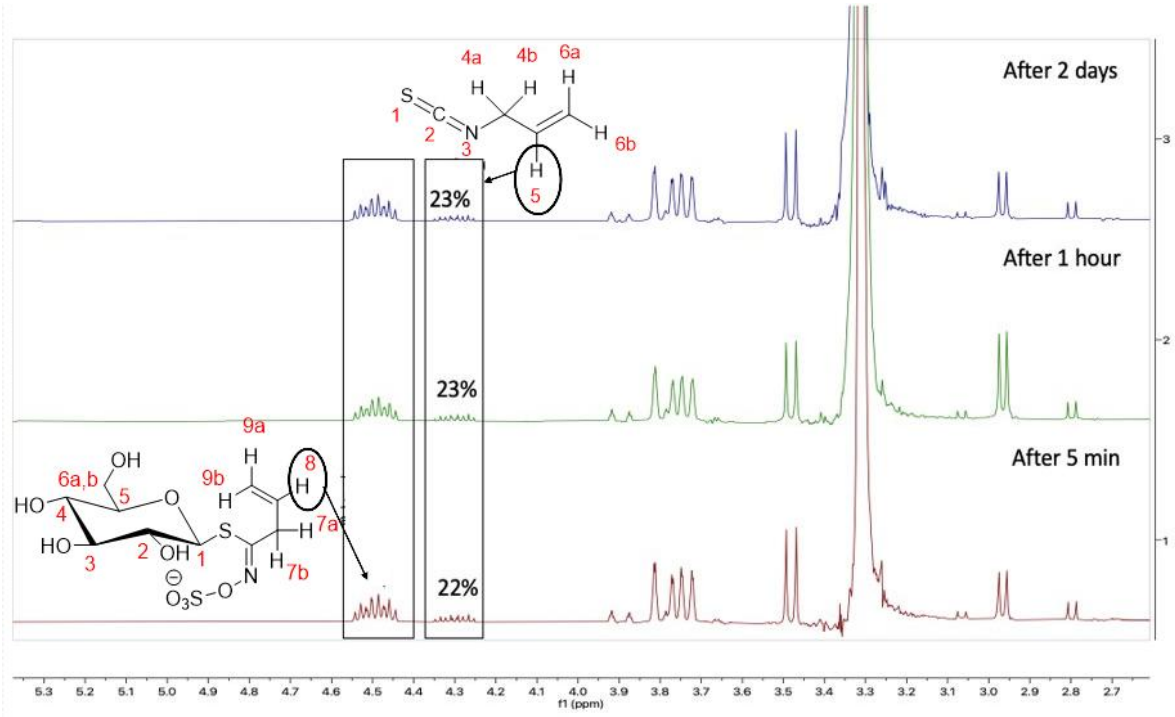

Figure 2.7: ^1H-NMR monitoring of sinigrin hydrolysis in 12.5 M methanol/water at different time.

Notably, doubling the enzyme loading from one to two units did not meaningfully improve the overall conversion in either organic solvent, with final hydrolysis yields after two days reaching only 24% in methanol and 17% in ethanol (Figure 2.8). These results collectively indicate that both methanol and ethanol significantly inhibit myrosinase activity under the tested conditions, most likely through partial enzyme denaturation or solvent-induced conformational changes that reduce catalytic efficiency. This is consistent with previous reports demonstrating that exposure of myrosinase to high methanol concentrations (up to 12.5 M) results in approximately 50% reduction in enzyme activity and stability [203].

Due to the limitations associated with organic co-solvents, D_2O was subsequently evaluated as an alternative reaction medium to separate solvent inhibition effects from intrinsic enzymatic activity. Hydrolysis in D_2O proceeded more efficiently than in either organic solvent system, achieving 32% conversion with one unit of myrosinase after two days, which increased to 41% upon doubling the enzyme concentration to two units (Figure 2.8, 2.9).

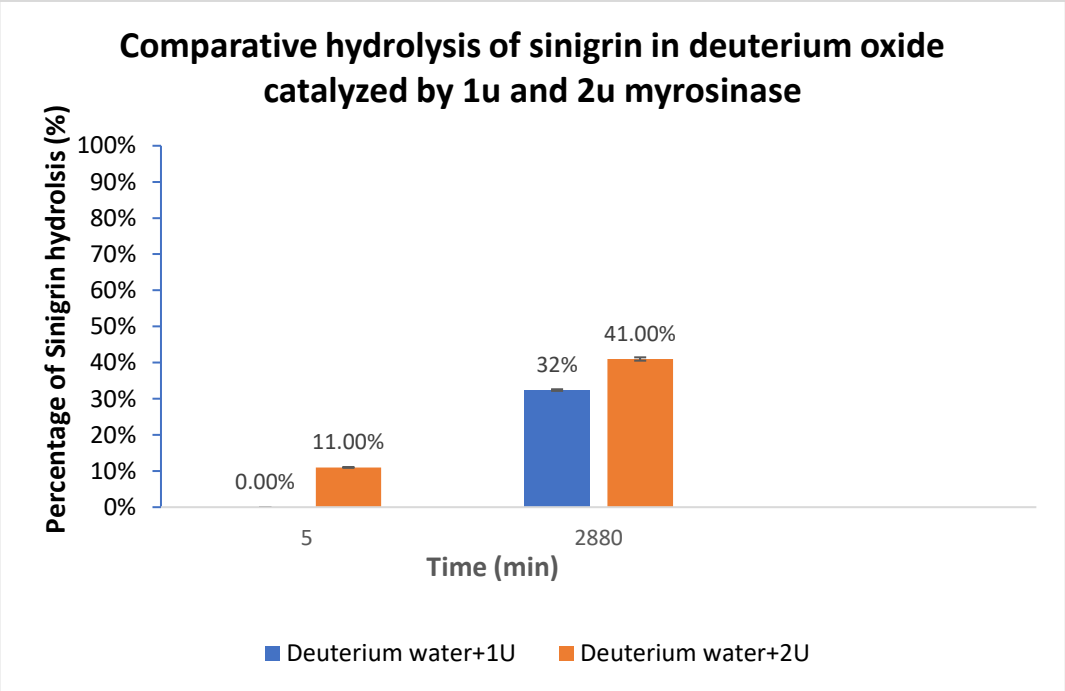

Figure 2.8: Comparative hydrolysis of sinigrin in D_2O catalyzed by 1 U and 2 U myrosinase, monitored at 5 minutes and 2880 minutes (48h)." Values are mean ± SD, n = 3".

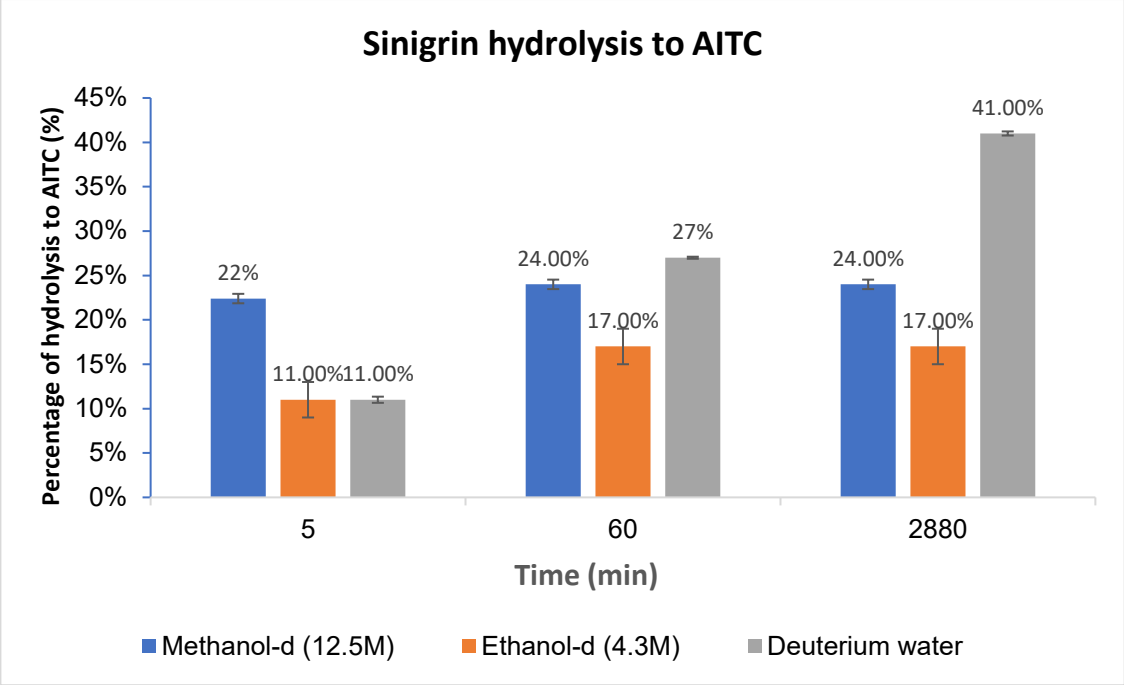

Figure 2.9: Sinigrin hydrolysis to allyl isothiocyanate (AITC) monitored over time (5 min, 60 min, and 2880 min). " Values are mean ± SD, n = 3".

Complete conversion was not achieved under any of the conditions tested, suggesting that either the enzyme quantity was insufficient or that D_2O itself slows the reaction through a inhibitory effect on the catalytic mechanism. Overall, these findings show that the solvent environment has a significant influence on myrosinase-catalysed sinigrin hydrolysis, with D_2O proving to be a better reaction medium than methanol/water or ethanol/water mixtures, though further optimisation of enzyme loading and reaction conditions will be needed to achieve full substrate conversion.

To identify reaction conditions more closely aligned with the enzyme's native aqueous environment, sinigrin hydrolysis was evaluated in potassium phosphate buffer (pH 6.0), which falls within the well-established pH optimum of myrosinase (pH 5.0-7.0) [168, 204]. This buffer system was selected because its buffering capacity and ionic strength help stabilise the enzyme's native structure, maintain a consistent reaction pH and reduce the formation of competing by-products such as nitriles and epithionitriles, which tend to predominate under acidic or alkaline conditions [162, 204, 205]. Myrosinase activity is also influenced by temperature, with optimal catalytic performance reported between 20-30 °C [205], and by differences in isoform expression across plant species, which can affect substrate specificity and hydrolytic capacity [200, 204].

Upon addition of one unit of myrosinase, approximately 36% conversion of sinigrin to AITC was observed within 15 minutes, as indicated by the appearance of characteristic AITC vinyl proton signals and the associated release of both α- and β-glucose anomeric proton signals in the ^{1}H NMR spectrum (Figure 2.10). Continued incubation resulted in complete substrate consumption with 100% conversion achieved within two hours, confirmed by the complete disappearance of sinigrin signals and exclusive presence of AITC resonances (Figures 2.10 and 2.11). The identity of enzymatically produced AITC was further verified by direct comparison with an authentic standard, showing complete agreement in chemical shifts and multiplicities for all diagnostic protons H5, H6a, H6b, and H4a/4b (Figure 2.12) [174, 206]. As well, glucose release was confirmed by the characteristic β-anomeric proton signal at δ 4.6 ppm, consistent with the retaining mechanism of myrosinase (Figure 2.11).

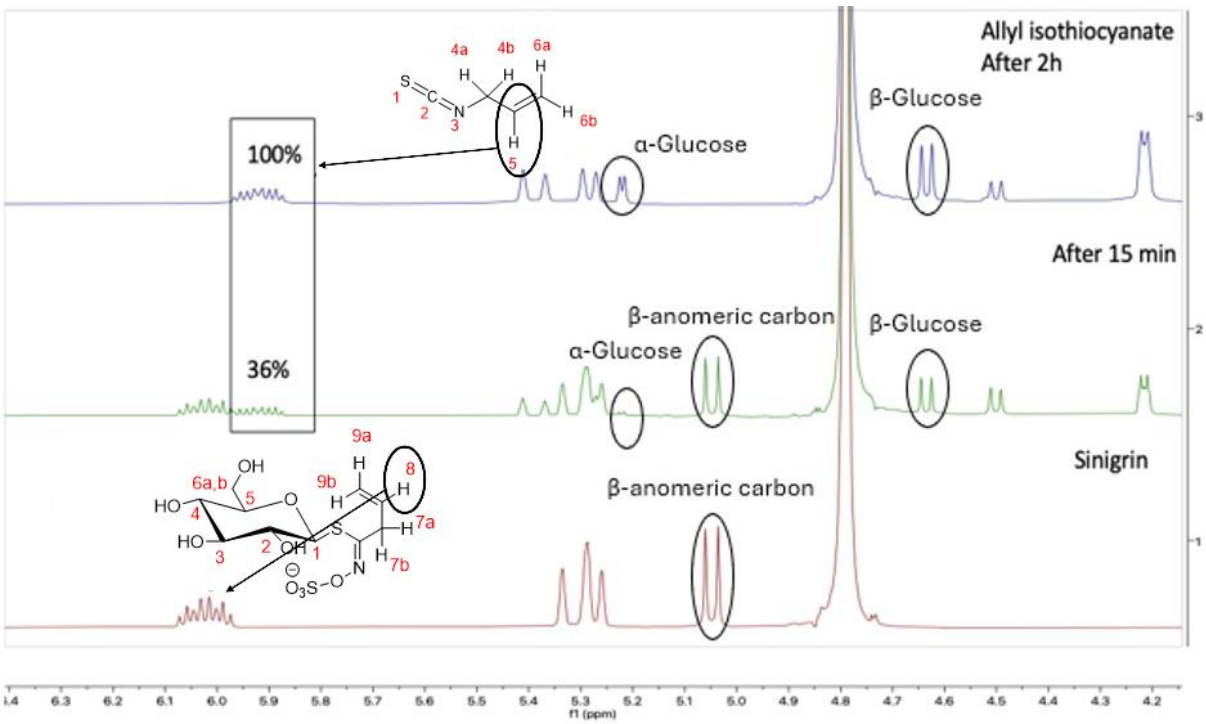

Figure 2.10: ^{1}H-NMR monitoring of sinigrin hydrolysis in phosphate buffer, showing 36% conversion after 15 minutes and complete conversion to allyl isothiocyanate after 2 hours.

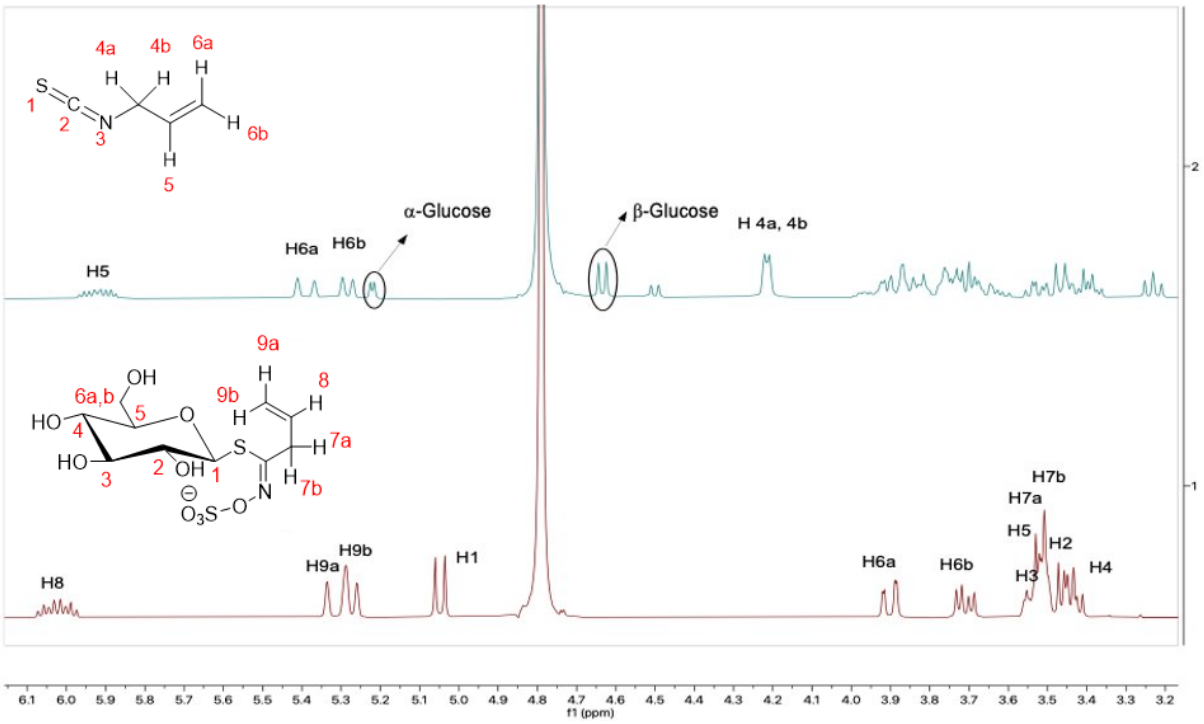

Figure 2.11: ^{1}H-NMR spectra (500 MHz, D_2O) comparing sinigrin and its hydrolysis product allyl isothiocyanate in phosphate buffer-d.

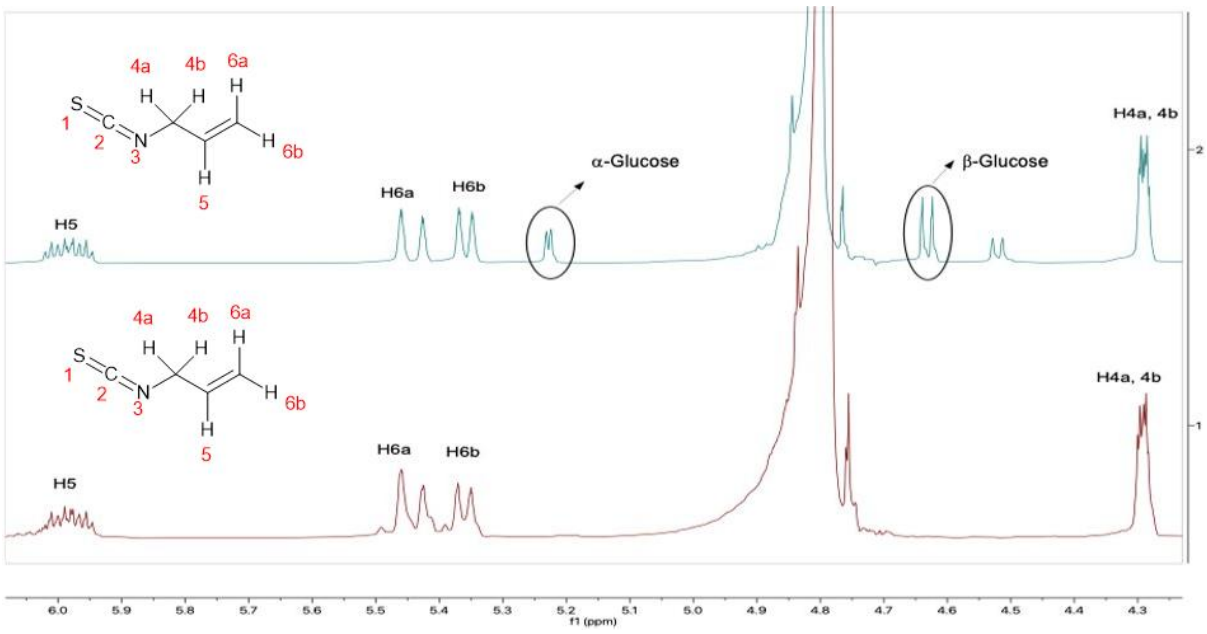

Figure 2.12: ^{1}H-NMR spectra (500 MHz, D_2O) of allyl isothiocyanate obtained from sinigrin hydrolysis compared with the authentic allyl isothiocyanate standard.

The complete hydrolysis observed in phosphate buffer contrasts with the partial limited conversions obtained in organic solvent systems and is consistent with previous reports of maximal myrosinase activity in phosphate or citrate buffers at pH 4-7 [168, 204].

These findings establish potassium phosphate buffer (pH 6.0) as the optimal medium for rapid and complete myrosinase-catalysed hydrolysis of sinigrin to AITC. This is providing a critical experimental foundation for next investigations into the reactivity of enzymatically generated sinigrin intermediate with allicin potentially yielding novel bioactive products.

2.1.3 Myrosinase catalytic hydrolysis of sinigrin in presence of garlic organosulfur compounds

2.1.3.1 Enzymatic reaction in dimethyl sulfoxide (DMSO)/phosphate buffer

To investigate potential interactions between garlic organosulfur compounds and the hydrolysis intermediate of sinigrin, it was essential to employ a solvent system capable of solubilising both reactants. garlic organosulfur compounds are poorly soluble in aqueous media and require dissolution in an organic solvent. Initial attempts to use methanol and ethanol as co-solvents were unsuccessful due to complete loss of myrosinase catalytic activity in these media, indicating that these alcohols are incompatible with the enzymatic reaction. Consequently, a mixed-solvent approach was adopted, using deuterated dimethyl sulfoxide (DMSO-d_6) to dissolve garlic organosulfur compounds and a deuterated potassium phosphate buffer to dissolve sinigrin. This combination was selected to maintain enzyme activity while ensuring adequate solubility of both substrates, thereby enabling simultaneous enzymatic hydrolysis of sinigrin and potential cross-reactivity with garlic organosulfur compounds under NMR-monitored conditions.

The initial objective was to evaluate the catalytic activity of myrosinase in the presence of varying concentrations of dimethyl sulfoxide-d_6 (DMSO-d_6) by monitoring the hydrolysis of sinigrin to allyl isothiocyanate (AITC) via ^{1}H-NMR spectroscopy. The results demonstrated a complete inhibition of myrosinase activity at 50% v/v DMSO-d_6/phosphate buffer-d, with no detectable AITC formation under these conditions. At a reduced concentration of 25% v/v DMSO-d_6/phosphate buffer-d only 23% of the reaction was completed within the same timeframe (2 hrs) when using a single unit (1 U) of myrosinase, suggesting that the high concentration of DMSO-d_6 may partially inhibit enzyme activity. Increasing the enzyme concentration to two units (2 U) under 25% v/v solvent conditions resulted in complete (100%) conversion to AITC within two hours.

Following the optimisation of solvent and enzyme concentration, the next stage involved monitoring a mixture reaction via ^{1}H-NMR to detect any novel peaks or changes in chemical shifts that might indicate the formation of new products. The strategy aimed to explore possible interactions between the reactive aglycone intermediate, generated from myrosinase-catalysed sinigrin hydrolysis, and organosulfur compounds found in garlic. Diallyl disulfide (DADS) was initially selected as a model garlic-derived, thiol-reactive compound. In this experiment, DADS was dissolved in DMSO and sinigrin in phosphate buffer. As a result, no detectable changes were observed in the ^{1}H NMR spectra throughout the reaction period, suggesting that DADS lacks sufficient rapid reactivity toward the glucosinolate-derived aglycone under the tested conditions.

The lack of reactivity observed for diallyl disulfide (DADS) can be attributed to its inherently low thiol reactivity compared with allicin. Diallyl disulfide (DADS) contains a simple disulfide bond (R-S-S-R) that is chemically stable and shows low electrophilicity, making it less reactive toward nucleophilic attack under mild conditions. In contrast, allicin, a diallyl thiosulfinate (R-S(=O)-S-R), has a sulfinyl (S=O) group that polarizes the adjacent S-S bond, increasing its electrophilicity and making it more susceptible to nucleophilic substitution and contributing to its greater biological activity compared to DADS [199]. Consequently, allicin undergoes rapid thiol-disulfide exchange and oxidative modification, enabling it to react readily with reactive intermediates from sinigrin hydrolysis. Due to its greater electrophilicity and biological activity, allicin was employed in place of DADS. When the sinigrin-allicin mixture was incubated in 25% v/v DMSO-d_6/phosphate buffer with 2 U of myrosinase at room temperature, complete hydrolysis to allyl isothiocyanate (AITC) and formation of new products occurred within three hours. Continuous ^{1}H NMR monitoring confirmed the disappearance of sinigrin and the presence of the expected hydrolysis products and glucose.

From these results, it can be concluded that the optimal conditions for conducting the mixed sinigrin-allicin reaction in this study involve dissolving allicin in DMSO-d_6, preparing sinigrin in phosphate buffer (pH 6), and employing two units of myrosinase. These conditions maximise both enzyme activity and solvent compatibility while enabling the study of potential cross-reactivity between glucosinolate hydrolysis products and reactive organosulfur species. The use of ^{1}H-NMR for real-time monitoring proved valuable for detecting slight spectral changes,

providing a direct and non-destructive method for exploring novel product formation (Figure 2.13-2.14).

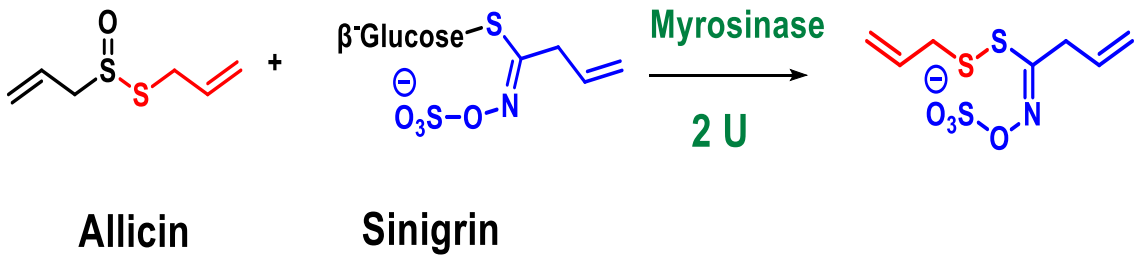

Figure 2.13: Reaction scheme showing the enzymatic interaction between allicin and sinigrin in the presence of 2 U of myrosinase using 25% (v/v) DMSO-d_6 in phosphate buffer (pH 6) as solvent. The reaction yields a novel sulfur-containing compound formed through coupling of the allicin-derived allyl sulfide moiety with the glucosinolate aglycone intermediate.

^{1}H-NMR data revealed the appearance of new signals and noticeable chemical shift changes in several proton environments, indicating the formation of new reaction products (Figure 2.14) explained more in HSQC-NMR data.

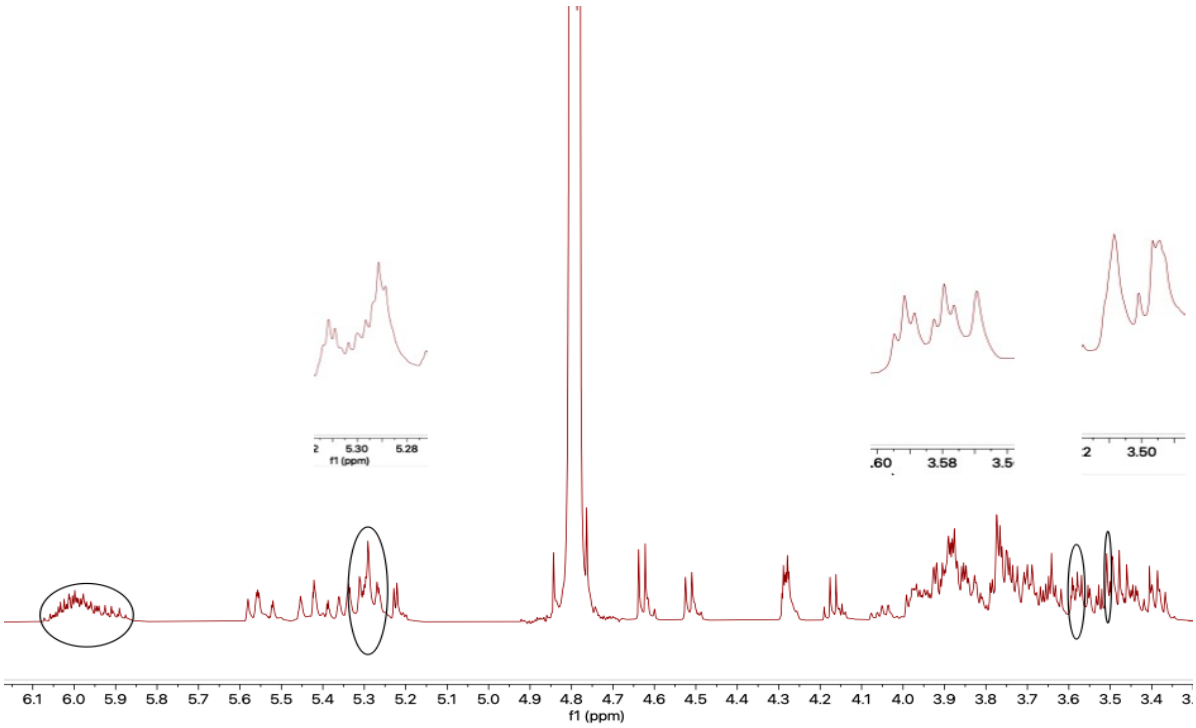

Figure 2.14: ^{1}H-NMR spectrum (500 MHz, D_2O) of the enzymatic reaction mixture containing sinigrin and allicin in the presence of myrosinase under 25% v/v DMSO-d_6 in phosphate buffer-d conditions.

The HSQC-NMR analysis of the reaction mixture revealed several diagnostic protons-carbon correlations that are absent in the spectra of the individual reactants, indicating the formation

of a new compound. Key cross peaks were observed at δH/δC 3.58/34.61 ppm, 3.50/42.06 ppm, and 5.27/120.10 ppm, which are not attributable to either unreacted allicin or sinigrin. In addition, notable chemical shift changes were detected in several resonances. For instance, the allicin signal at δH/δC 5.91/125.58 ppm shifted to 6.00/125.00 ppm in the product, while two sinigrin hydrolysis-associated signals at δH/δC 5.90/131.11 ppm and 5.20/117.00 ppm shifted to 5.91/131.92 ppm and 5.30/118.80 ppm, respectively (Figures 2.15). These changes suggest modifications to the electronic environment of the allyl moiety, consistent with covalent structural rearrangement during the reaction.

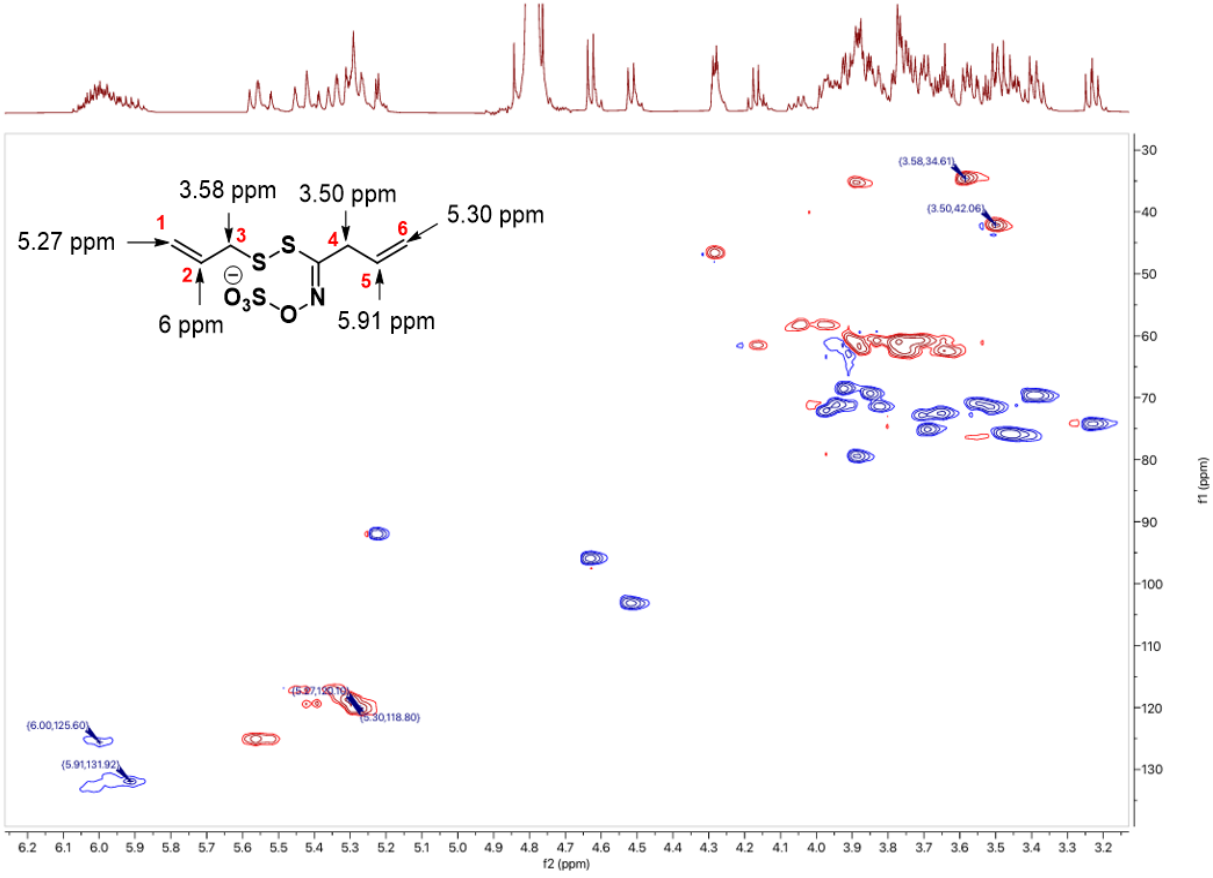

Figure 2.15: *HSQC-NMR spectrum (500 MHz, D_2O) of the enzymatic reaction mixture.*

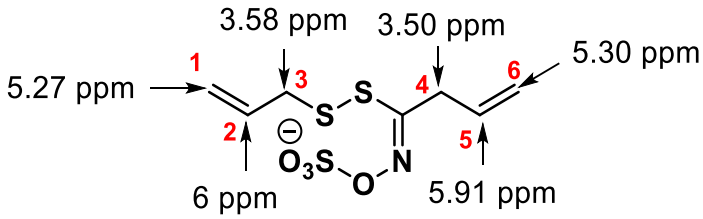

Table 2.1: ^{1}H-NMR and DEPT-135- ^{13}C-NMR chemical shifts of allicin, sinigrin and the new compound.

	Allicin chemical shifts (ppm)		**Sinigrin chemical shift (ppm)**		**New compound chemical shifts (ppm)**	
	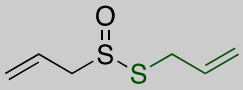		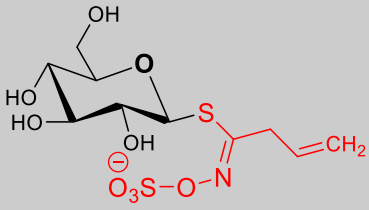		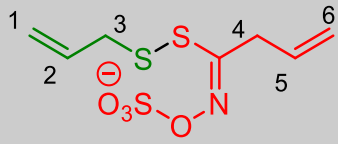	
	^{1}H	DEPT-135- ^{13}C	^{1}H	DEPT-135- ^{13}C	^{1}H	DEPT-135- ^{13}C
1	5.3	119.4			5.27	120.10
2	5.91	125.58			6	125
3	3.7	35.79			3.58	34.61
4	3.9	58.7	3.5-3.52	46.8	3.50	42.06
5	5.94	133.36	6.1	131.11	5.91	131.92
6	5.47	124.9	5.3-5.2	117	5.30	118.80

The two signals at δH 5.30 and 5.27 ppm are of particular interest, as this chemical shift region is characteristic of allylic protons in both allicin and sinigrin. Their presence in the reaction product strongly indicates that at least one allyl group remains intact after the reaction. Meanwhile, the downfield shifts observed for carbons C3 and C4 (34.61 and 42.06 ppm) suggests that a new linkage involving the allyl sulfur and sinigrin-derived moieties has formed, altering the electronic environment of these carbons.

Several proton signals show considerable overlap, making accurate spectral assignment challenging. Therefore, isolation and purification of the reaction product are necessary to allow comprehensive 2D NMR analyses (such as COSY, HSQC, and HMBC) for definitive structural characterization. Nevertheless, the appearance of new signals and chemical shift changes, in combination with the presence of allyl-related signals, supports the hypothesis that the new compound is a conjugate formed between an allicin-derived allyl sulfide fragment and a sinigrin-hydrolysis intermediate.

2.1.3.2 Enzymatic reaction in acetonitrile (MeCN)/phosphate buffer

One drawback of using dimethyl sulfoxide (DMSO) as a co-solvent in this reaction system was the inability to completely remove residual solvent from the product mixture, even after rotary evaporation. Because DMSO has a high boiling point (189 °C), complete removal at elevated temperatures could result in thermal degradation of the newly formed product from the reaction mixture.

To overcome this limitation, DMSO was replaced with acetonitrile as water miscible organic co-solvent. Acetonitrile, being more volatile with a lower boiling point (82 °C), allowed efficient solvent removal under mild conditions. This substitution facilitated product isolation and improved spectral resolution, making acetonitrile a more suitable solvent for reactions requiring clean product recovery and high-quality NMR analysis.

The same experimental procedure previously conducted with DMSO-d_6 was repeated using acetonitrile (Figure 2.16). The resulting HSQC-NMR spectrum revealed the same distinctive proton-carbon cross peaks observed in the DMSO-d_6 system, specifically at $\delta^1H/\delta^{13}C$ 3.65/34.49 ppm, 3.56/42.27 ppm, and 5.34/120.07 ppm, confirming the formation of the same novel product. Minor variations in the chemical shifts of certain protons were noted when compared to the DMSO-d_6 spectra, likely reflecting solvent-induced differences in chemical environment. These included shifts in signals corresponding to allylic protons from allicin and sinigrin, as detailed in Figures 2.16 and 2.17.

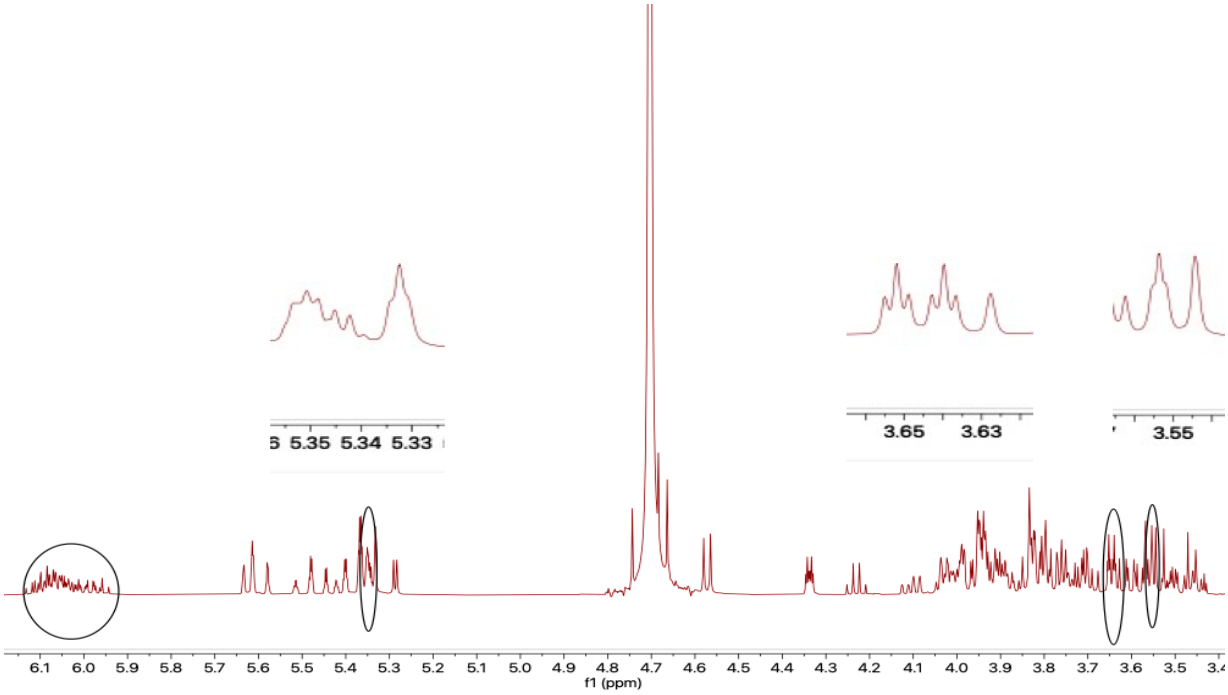

Figure 2.16: ^{1}H-NMR spectrum (500 MHz, D_2O) of the enzymatic reaction mixture containing sinigrin and allicin in the presence of myrosinase under 25% v/v acetonitrile/phosphate buffer-d conditions.

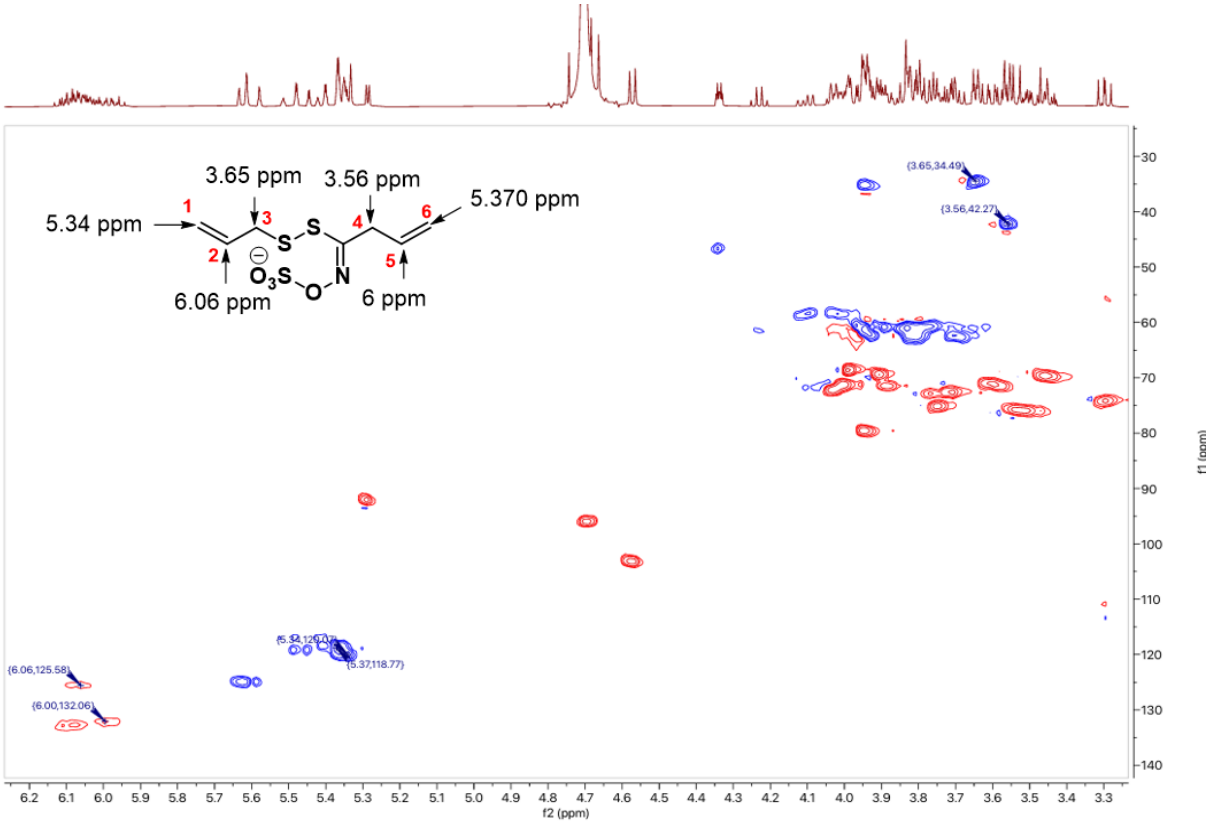

Figure 2.17: HSQC-NMR spectrum (500 MHz, D_2O) of the enzymatic reaction mixture.

Table 2.2: ^{1}H-NMR chemical shifts of allicin, sinigrin and the new compound.

	Allicin chemical shifts (ppm)		Sinigrin chemical shift (ppm)		New compound chemical shifts (ppm)	
	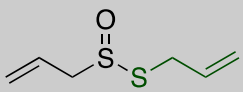		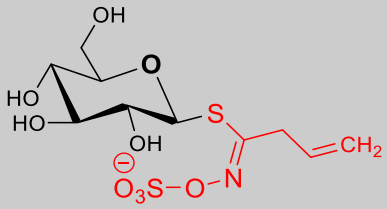		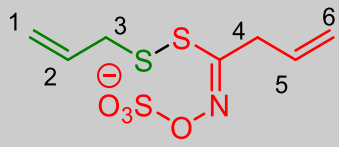	
	^{1}H	DEPT-135-^{13}C	^{1}H	DEPT-135-^{13}C	^{1}H	DEPT-135-^{13}C
1	5.3	119.4			5.27	120.10
2	5.91	125.58			6	125
3	3.7	35.79			3.58	34.61
4	3.9	58.7	3.5-3.52	46.8	3.50	42.06
5	5.94	133.36	6.1	131.11	5.91	131.92
6	5.47	124.9	5.3-5.2	117	5.30	118.80

To evaluate whether increasing enzyme concentration could enhance reaction yield or product formation, the myrosinase loading was raised to 4 units and then to 6 units under identical conditions. No significant changes were observed in the extent of sinigrin hydrolysis or in the intensity of product-related NMR signals compared with the reaction performed with 2 units of enzyme. This outcome is consistent with the principle that beyond a certain enzyme concentration, the reaction rate is constrained by substrate availability rather than catalytic activity. In this study, the concentration of sinigrin appears sufficient to saturate 2 U of myrosinase, meaning that additional enzyme offers no kinetic benefit.

Following the optimisation of the reaction between the sinigrin hydrolysis intermediate and allicin, the focus shifted to isolating and characterising the newly formed compounds. The

optimised conditions ensured reproducible production of the target molecule, enabling its separation by preparative chromatography and subsequent purification and structural elucidation using advanced analytical techniques.

2.1.4 Isolation, purification, and elucidation of the new compound by analytical methods

The isolation and structural elucidation of the novel compound formed from the myrosinase-catalysed reaction between sinigrin, and allicin were accomplished using a combination of complementary analytical techniques, including HPLC, preparative HPLC, 1D and 2D-NMR, and high-resolution LC-MS (Q-Exactive). Where possible, single-crystal X-ray diffraction was also attempted to further confirm the three-dimensional structure, stereochemistry, and atomic connectivity of the novel compound. The compound formed in this reaction, [(Z)-[1-(prop-2-en-1-yldisulfanyl) but-3-en-1-ylidene] amino] sulfate, was named **alligrin**, derived from ‘alli-’ (allicin) and ‘-grin’ (sinigrin). This name reflects its origin from two distinct plant-derived sulfur metabolites.

2.1.4.1 Separation and purification by high-performance liquid chromatography (HPLC)

2.1.4.1.1 Analytical HPLC method development and optimization

Developing and optimizing HPLC method was crucial in this study to achieve efficient separation and quantification of alligrin within the reaction mixture. The aim was to establish a single chromatographic protocol capable of separating and quantifying sinigrin, allyl isothiocyanate (AITC), allicin and the newly formed compound alligrin. This method allows reliable peak identification for structural analysis and providing accurate quantification of each component in the mixture.

Following extensive chromatographic optimisation trials, the finalised HPLC method was established as the definitive analytical approach employed consistently throughout all subsequent analyses. This method used a linear gradient elution program, which provided more controlled and gradual changes in solvent composition compared to the stepwise gradients (Figure 2.18). The extended analysis time (40 minutes) combined with a reduced flow rate (0.5 mL/min) allowed for improved interaction between analytes and the stationary

phase, thereby enhancing resolution and minimizing peak overlap. The linear gradient from 25% to 100% acetonitrile over 30 minutes, followed by an isocratic hold, achieved excellent separation of all reaction components, including sinigrin, allicin, AITC, and the target compound alligrin. This optimization enabled the accurate isolation and purification of alligrin for subsequent spectroscopic and structural analysis, while confirming that the method is well-suited for preparative-scale separations, offering high analytical accuracy and reproducible performance.

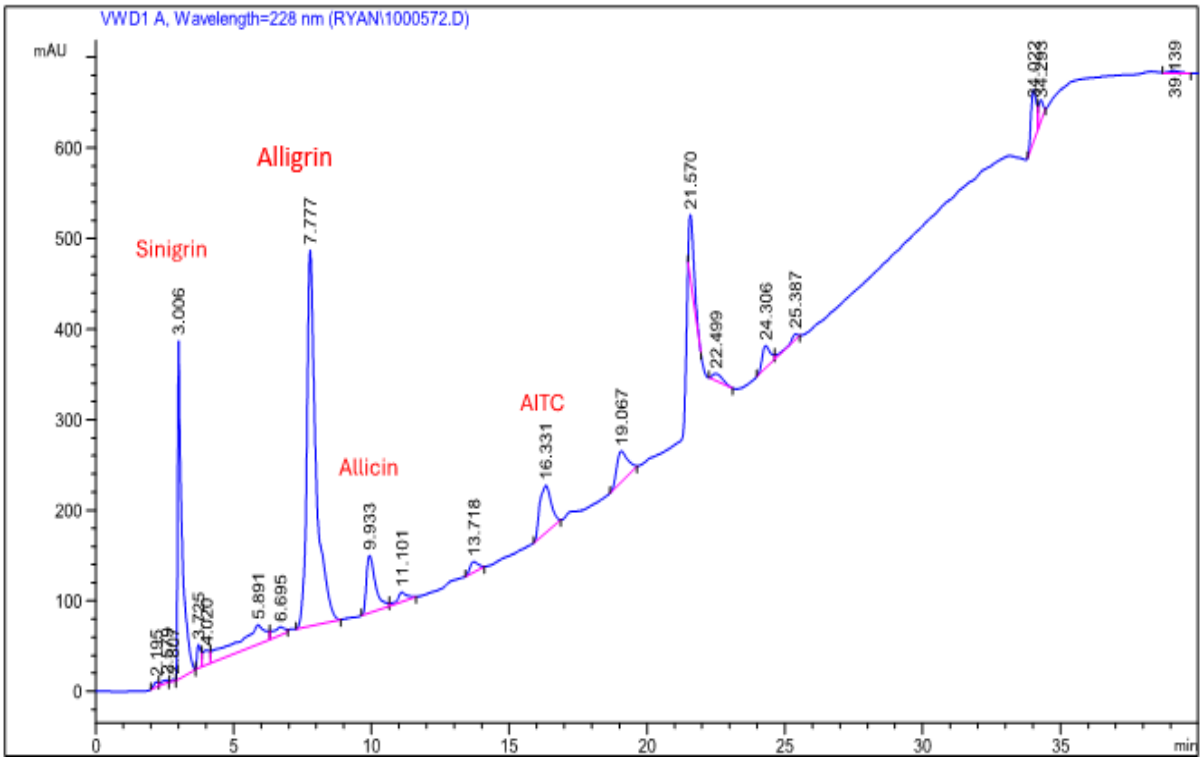

Figure 2.18: HPLC chromatogram of the reaction mixture showing the separation of sinigrin, allicin, AITC, and alligrin using optimized method (Phenomenex Spherisorb® column C18, 5µM, 4.6 x 150mm), under a linear gradient elution with acetonitrile/ammonium acetate buffer. Detailed chromatographic conditions are provided in experimental section (7.2.3.1).

The retention times obtained reflect the relative polarity of each compound and confirm a consistent elution order throughout all analyses (Table 2.3). Sinigrin eluted first (3 min) due to its highly polar glucosinolate structure, followed by alligrin (7.7 min) and allicin (9.9 min), whose close elution reflects their structural similarity as organosulfur compounds, and finally allyl isothiocyanate (16.3 min) as the most hydrophobic component. This elution profile validated the selectivity and reproducibility of the finalised HPLC method for the accurate separation of all reaction components.

Table 2.3: Retention times of mixture components (sinigrin, allicin, allyl isothiocyanate, and alligrin).

	Compound	Retention time (min)
1	Sinigrin	3
2	Allicin	9.9
3	Allyl isothiocyanate	16.3
4	Alligrin	7.7

The successful development and optimization of analytical HPLC methods provided foundation for scaling up to preparative HPLC applications.

2.1.4.2 Preparative high-performance liquid chromatography (Prep-HPLC)

The optimized parameters including mobile phase, gradient profile, and column temperature were reformed for preparative-scale operation to enable efficient compounds isolation and purification. Scaling up required proportional adjustments to flow rate, injection volume and column dimensions while maintaining the same chromatographic selectivity and retention behaviour established during analytical method development.

The preparative HPLC separation successfully resolved the target compound from the crude mixture, as demonstrated in (Figure 2.19). The chromatogram shows clear baseline separation of multiple peaks, with the target compound alligrin eluting at approximately 7.6 minutes. The alligrin peak was well-separated from the other compounds in the mixture reaction, indicating that the separation conditions were effective.

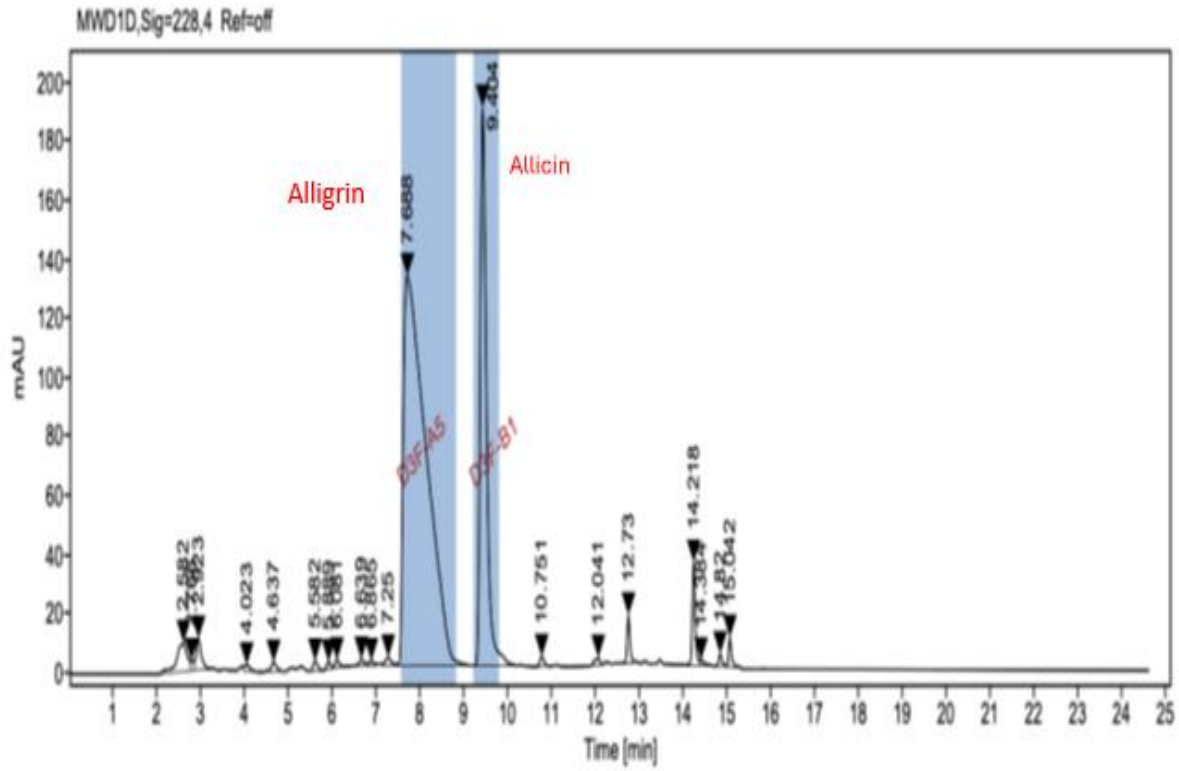

Figure 2.19: Preparative reversed-phase HPLC chromatogram of the reaction mixture.

Injection volume optimization showed that 750 µL provided the best balance between sample loading and separation efficiency. At this volume, the target compound alligrin eluted at 7.68 minutes with complete baseline separation from adjacent peaks, maintaining excellent peak shape and resolution comparable to analytical-scale conditions, yielding 1.5 mg. At 750 µL, the column operated near its optimal capacity, avoiding overloading effects that cause peak broadening. In contrast, increasing the injection volume to 1000 µL led to noticeable weakening in separation performance, including peak broadening and merging of previously separated compounds. These findings emphasize the critical importance of injection volume optimization to preserve resolution and product purity in preparative-scale chromatography. The successful preparative separation enables the isolation of pure target compound (alligrin) for further structural characterization and biological activity.

2.1.4.3 Structure elucidation of alligrin

2.1.4.3.1 Nuclear magnetic resonance (NMR) spectroscopy

The ^{1}H-NMR (500 MHz, D_2O) spectrum of the isolated compound displayed characteristic multiplets at δ 5.96 (1H), corresponding to the vinylic proton of the allyl group derived from the sinigrin fragment, while the signal at δ 5.26 (2H) was assigned to the terminal methylene protons (-CH=CH_2) of the same allyl group. A separate resonance at δ 5.87 (1H) was attributed to the vinylic proton of the allyl group originating from the allicin-derived fragment, and the multiplet at δ 5.22 (2H) represented its corresponding terminal methylene protons (-CH=CH_2). The presence of allyl group signals indicates two different allyl environments within the molecule, consistent with the conjugation of sinigrin and allicin moieties. The downfield chemical shifts of these protons reflect deshielding effects associated with neighbouring sulfur atoms, characteristic of disulfide linkages. Additionally, the doublets of triplets at δ 3.56 (J = 6.12, 1.60 Hz, 2H) and δ 3.45 (J = 7.39, 1.00 Hz, 2H) correspond to methylene protons adjacent to sulfur atoms, further confirming the presence of allylic sulfide bonds and supporting the proposed structural connectivity of the novel sulfur-containing compound (Figure 2.20).

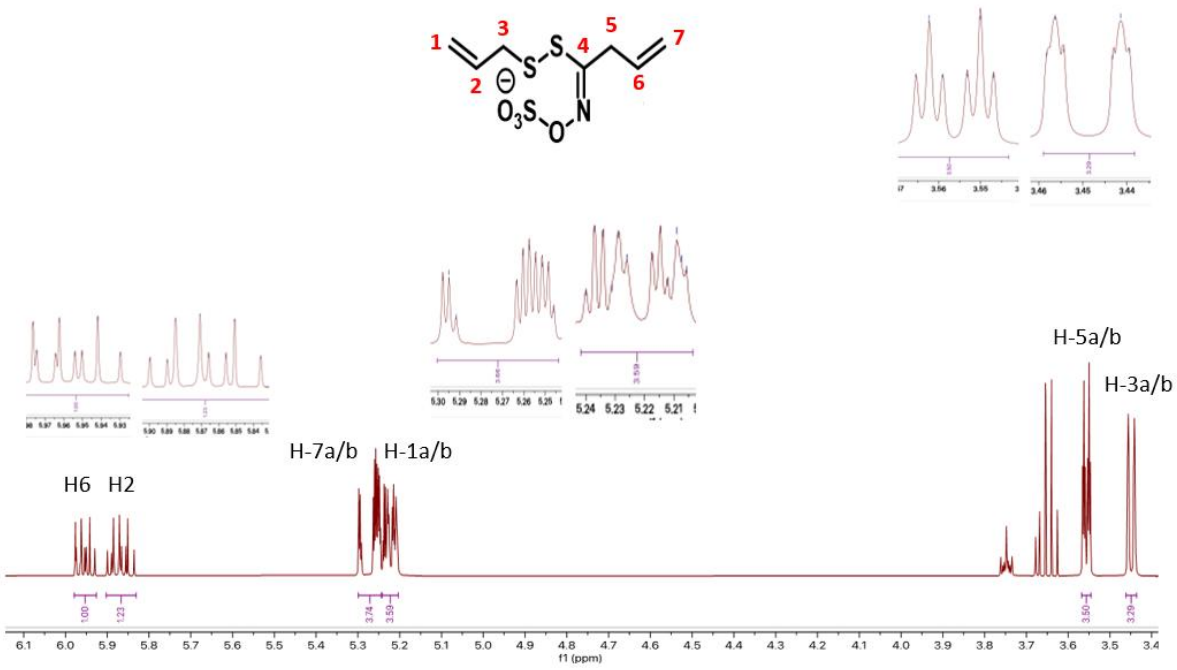

Figure 2.20: ^{1}H-NMR spectrum (500 MHz, D_2O) of alligrin.

The COSY-NMR (500 MHz, D_2O) spectrum revealed key ^1H-^1H correlations that traced the connectivity within each allyl system. Notable correlations included H-7a/b /H-6 and H-1a/b /H-2, confirming the integrity of both allyl chains. Additionally, correlations between H-5a/b /H-6 and H-3a/b /H-2 established the connection between the methylene groups and their respective vinyl systems (Figure 2.21).

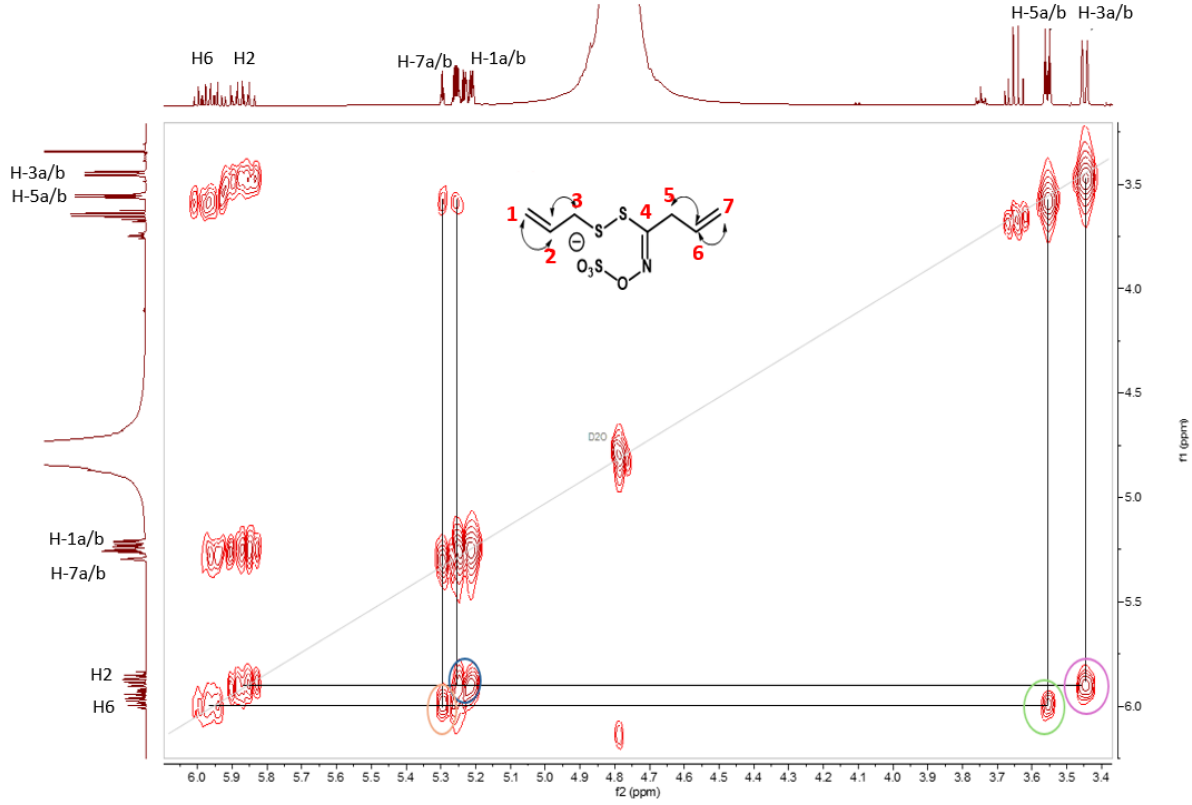

Figure 2.21: COSY-NMR spectrum (500 MHz, D_2O) of alligrin.

The ^{13}C NMR (125 MHz, D_2O) spectrum of alligrin provided further structural confirmation of the proposed structure. The signal observed at δ 167.57 (C4) was attributed to a quaternary carbon directly bonded to sulfur, confirm with the presence of C-S bond from sinigrin fragment. The signals at δ 132.13 (C6) and δ 131.69 (C2) correspond to internal vinylic carbons, while δ 119.96 (C1) and δ 118.30 (C7) were assigned to terminal vinylic carbons of the allyl moieties. The downfield chemical shifts of carbons further indicate deshielding caused by adjacent sulfur atoms. In the aliphatic region, peaks at δ 42.24 (C3) and δ 34.65 (C5) were assigned to methylene carbons adjacent to sulfur, supporting the presence of disulfide linkages (Figure 2.22).

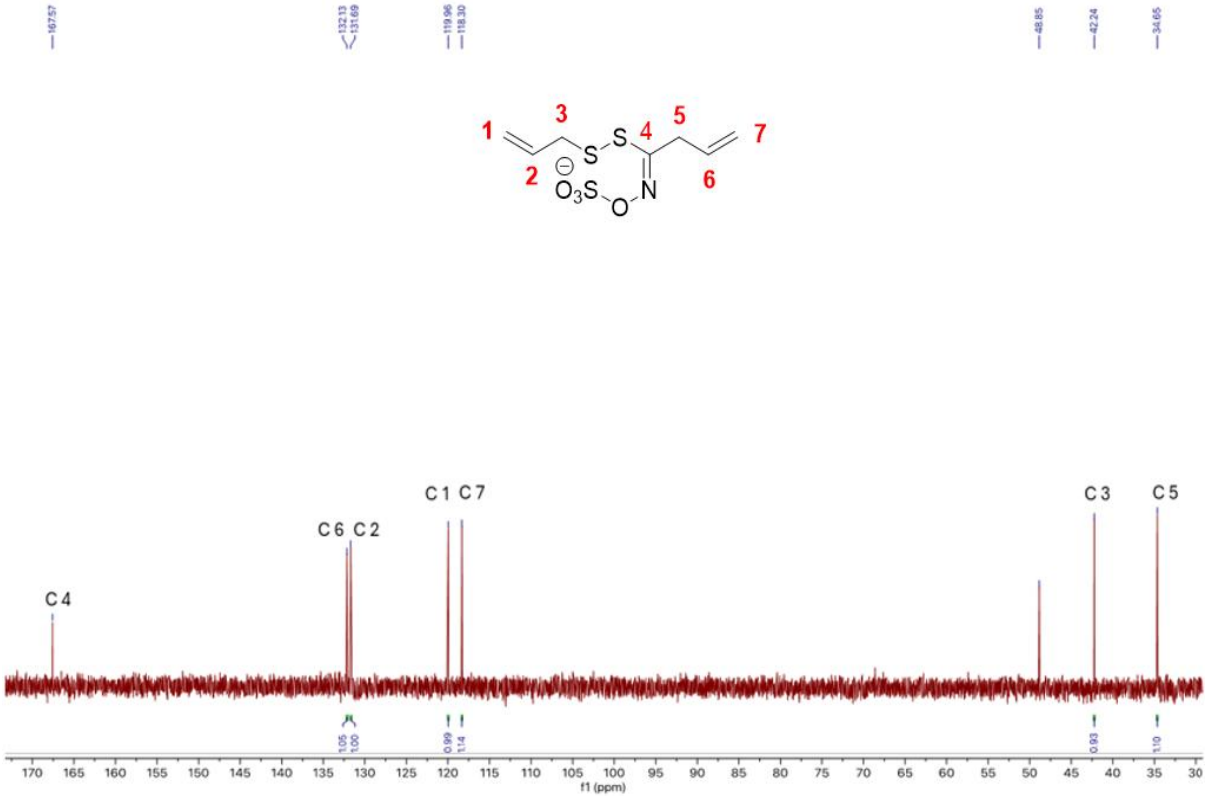

Figure 2.22: ^{13}C-NMR spectrum (125 MHz, D_2O) for alligrin.

The ^{13}C-DEPT NMR (125 MHz, D_2O) spectrum provided detailed insights into the carbon structure of alligrin. signals at δ 132.13 (C6), 131.69 (C2), 119.96 (C1), and 118.30 (C7) were assigned to vinylic carbons of the allylic groups, while signals at δ 42.24 (C3) and 34.65 (C5) corresponded to methylene (CH_2) *carbons* adjacent to sulfur atoms. The DEPT-135 experiment confirmed the multiplicity of these signals, with CH_2 carbons appearing as negative peaks (down) and CH carbons as positive peaks (up), thereby allowing clear differentiation of carbon types and verifying the absence of CH_3 groups within the structure (Figure 2.23).

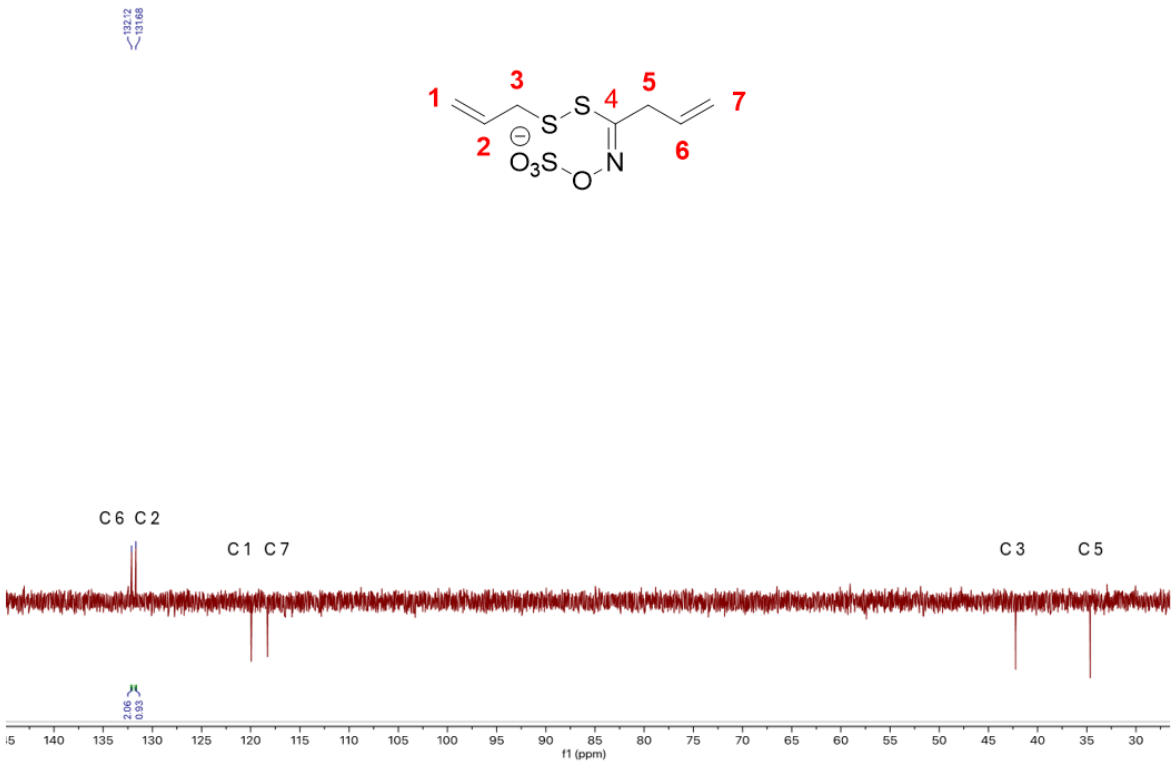

Figure 2.23: ^{13}C-DEPT 135-NMR (125 MHz, D_2O) of alligrin.

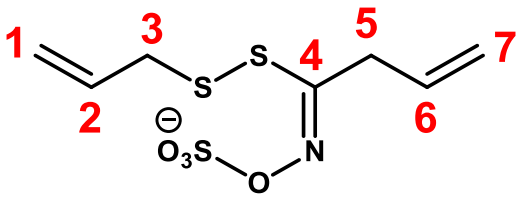

Figure 2.24: Chemical structure of alligrin with atom numbering; green = proton (^{1}H) assignments, red = carbon (^{13}C) assignments.

Table 2.4: ^{1}H, ^{13}C, ^{13}C DEPT and COSY- NMR data of alligrin measured at 500 MHZ in D_2O.

	^{1}H	^{13}C	^{13}C-DEPT 135	COSY
Position	**δ H (J in Hz)**	**δ C (Hz)**	**δ C (Hz)**	J_{HH}
1 $=CH_2$	(H1,2) 5.22 (m, 2H) ppm	118.30 ppm	CH_2	H-1a/b and H-2
2 =CH-	(H3) 5.87 (m, 1H) ppm	131.69 ppm	CH	H2 and H-3a/b
3 $-CH_2-$	(H4,5) 3.45 ppm (dt, J=7.39, 1 Hz, 2H)	42.24 ppm	CH_2	-
4 -C-	-	167.57 ppm	-	-
5 $-CH_2-$	(H6,7) 3.56 ppm (dt, J=6.12, 1.60 Hz, 2H)	34.65 ppm	CH_2	H-5a/b and H-6
6 =CH-	(H8) 5.96 (m, 1H) ppm	132.13 ppm	CH	-
7 $=CH_2$	(9,10) 5.26 (m, 2H) ppm	119.96 ppm	CH_2	H-7a,b and H-6

The HSQC-NMR (500 MHz, D_2O) spectrum provided direct one-bond ^{13}C-^{1}H correlations, clearly assigning each proton to its directly attached carbon. The correlations observed were H-6a/b (δ 5.96) to C-6 (δ 132.13), H-2 (δ 5.87) to C-2 (δ 131.69), H-7a/b (δ 5.26) to C-7 (δ 118.30), H-1a/b (δ 5.22) to C-1 (δ 119.96), H-5a/b (δ 3.56) to C-5 (δ 34.65), and H-3a/b (δ 3.45) to C-3 (δ 42.24). These correlations confirmed the direct bonding relationships and validated the carbon assignments (Figure 2.25).

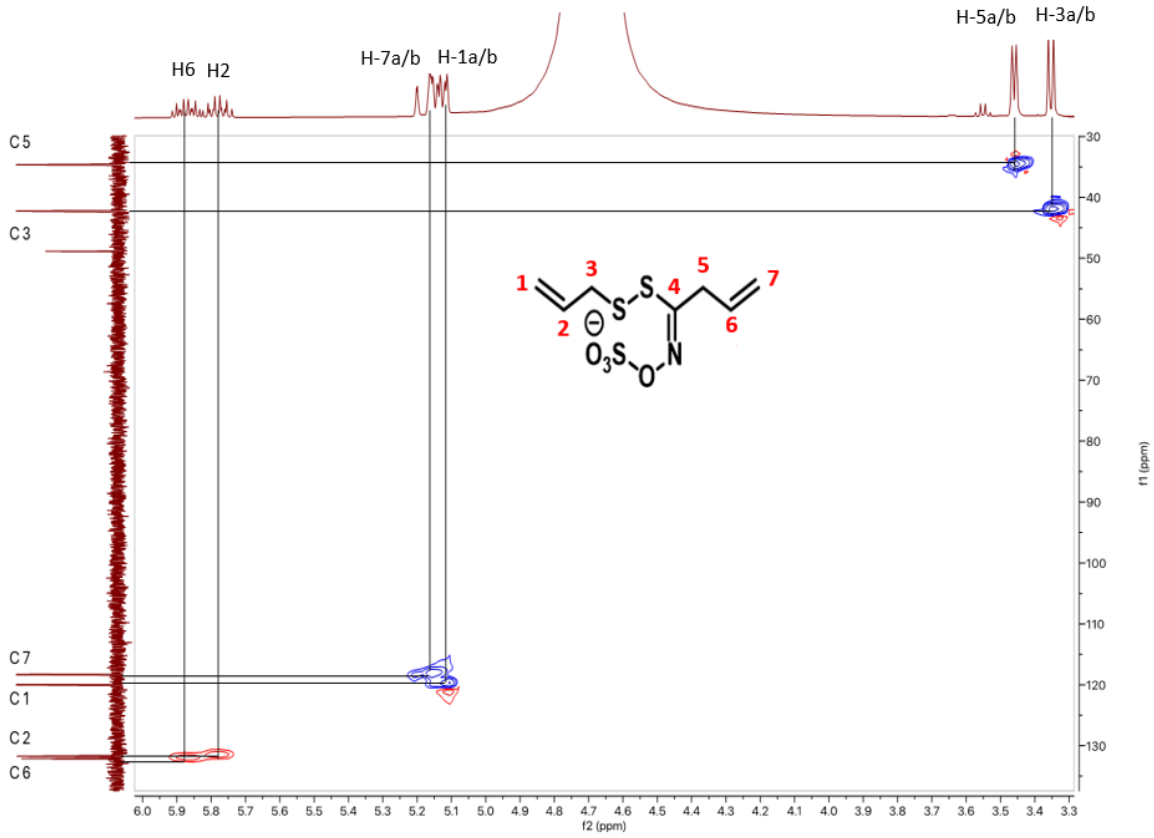

Figure 2.25: HSQC-NMR (500 MHz, D_2O) spectrum of alligrin.

The HMBC (^{1}H-^{13}C) NMR (500 MHz, D_2O) spectrum provided long-range coupling information (^{2}J and ^{3}J correlations) that established the key structural linkages within *alligrin*. Significant correlations were observed between H-3a/b (δH 3.45) and C-1/C-2 (δC 119.96, 131.69), confirming the connectivity between the methylene and vinylic carbons of the allicin-derived fragment. Further, H-1a/b (δH 5.22) correlated with C-2 (δC 131.69), while correlations of H-5a/b (δH 3.56) to C-4, C-6, and C-7 (δC 167.57, 132.13, 118.30), H-6 (δH 5.96) to C-4 (δC 167.57), and H-7a/b (δH 5.26) to C-5 and C-6 (δC 34.65, 132.13) collectively confirmed the conjugation between the allyl moieties (Figure 2.26).

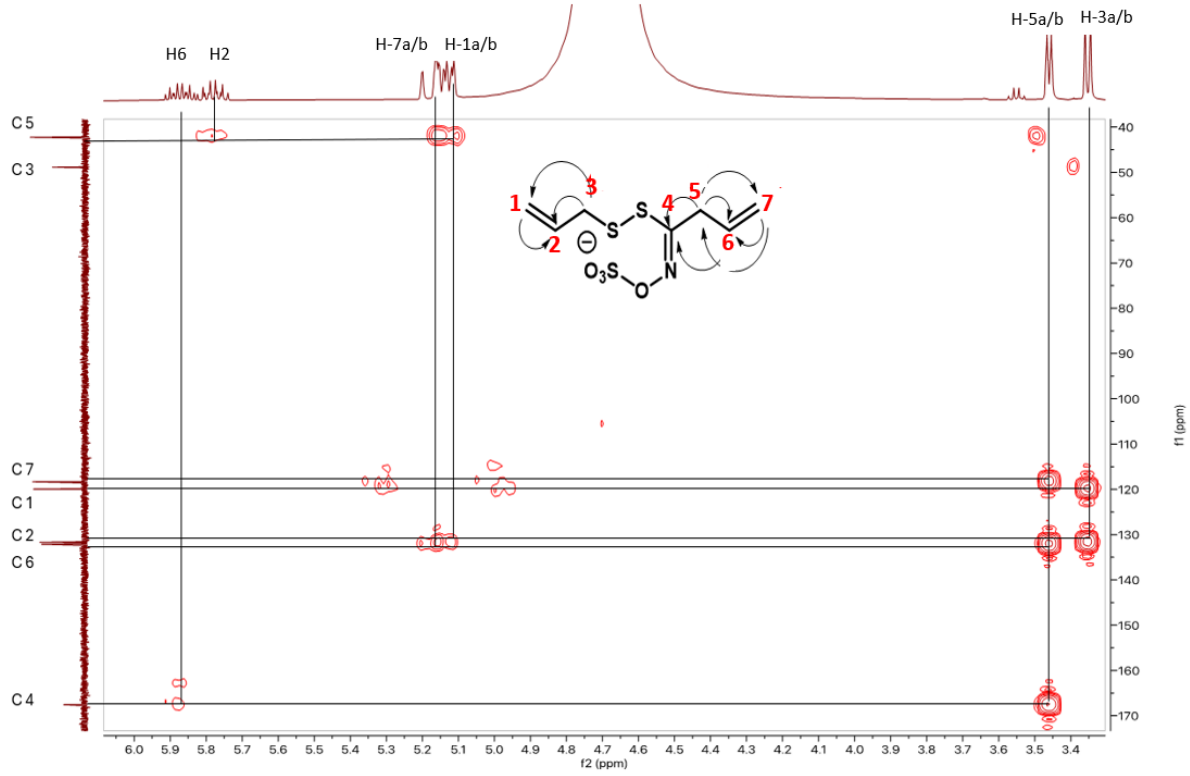

Figure 2.26: HMBC-NMR (500 MHz, D_2O) spectrum of alligrin.

Table 2.5: HSQC- NMR, HMBC-NMR correlations of alligrin Measured at 500 MHZ in D_2O.

	HSQC		HMBC	
Position	**^{1}H NMR**	**DEPT-135- ^{13}C NMR**	**^{2}J**	**^{3}J**
1 =CH_2	H-1a/b	C 1	C 2	-
2 -CH-CH_2	H-2	C 2	-	-
3 CH-CH_2-	H-3a/b	C 3	C 2	C 1
4 -C	-	C 4	-	-
5 CH-CH_2-	H-5a/b	C 5	C 4, C 6	C 7
6 -CH-CH_2	H-6	C 6	-	C 4
7=CH_2	H-7a/b	C 7	C 6	C 5

The combined NMR data confirms that the retention of both allyl groups and the presence of the characteristic quaternary carbon signal confirm that the reaction proceeds through sulfur-sulfur bond formation while preserving the essential structural features of both precursor molecules. The structural insights obtained from NMR spectroscopy were further corroborated by LC-MS analysis, which provided complementary data on molecular weight and fragmentation pattern.

2.1.4.4 Liquid chromatography-mass spectrometry (LC-MS)

Alligrin was isolated as a white crystal and subjected to comprehensive structural characterization using liquid chromatography high-resolution electrospray ionization mass spectrometry (LC-HR-ESI-MS) in negative ion mode (Figure 2.27). The mass spectrum exhibited a prominent molecular ion peak at m/z 267.9777 $[M-H]^-$, which demonstrated

excellent agreement with the calculated theoretical value for the molecular formula $C_7H_{10}S_3NO_4^-$ (calculated: 267.9777 Da) provides definitive confirmation of the molecular formula and structural characteristics of alligrin.

The ESI-MS spectrum (Figure 2.27) also showed several significant fragment ions, providing valuable insights into the structural features of alligrin. The fragment at *m/z* 95.95 $[M-H]^-$ with 100% relative abundance likely corresponds to a sulfonate fragment $HO\text{-}SO_3^-$, consistent with the characteristic peak commonly observed in glucosinolates due to cleavage of the sulfonated moiety [207]. This fragmentation pattern supports the presence of labile sulfur-oxygen bonds within the molecule.

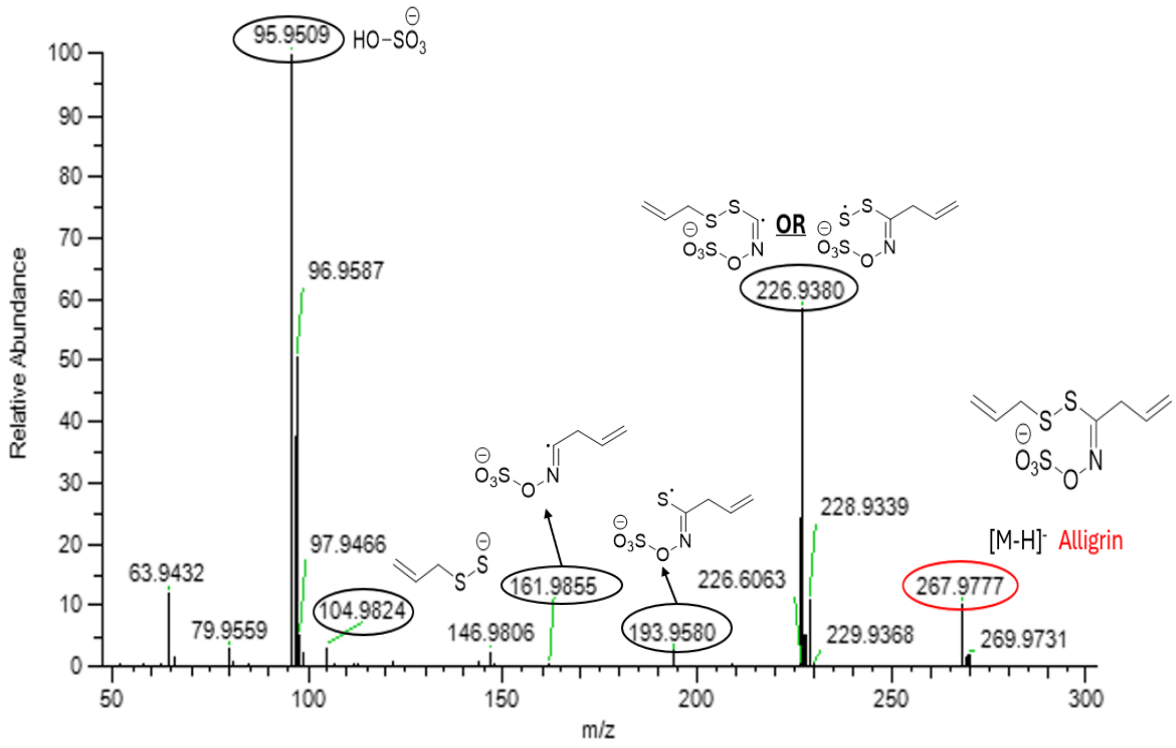

Figure 2.27: LC-MS data of alligrin.

The fragment ion observed at *m/z* 226.93 $[M-H]^-$ is indicative of the loss of an allyl moiety (CH_2-CH=CH_2) from the parent molecule. The isotopic distribution of the *m/z* 226.93 ion further supports the presence of two sulfur atoms within this fragment. Sulfur exhibits characteristic isotopes ^{32}S (100%), ^{33}S (0.78%), and ^{34}S (4.40%) which generate an *M+2* peak approximately 4% of the main M^+ signal for each sulfur atom. Accordingly, a compound containing two sulfur atoms would display an *M+2* peak around 8% of the base peak intensity,

consistent with the experimental spectrum. This isotopic pattern provides additional confirmation that the fragment retains both sulfur atoms, consistent with a disulfide containing structure.

The fragment ion at m/z 104.98 corresponds to $C_3H_5S_2^-$, consistent with an allyl disulfide anion arising from cleavage at the sulfur linkage. The fragment at m/z 161.99 corresponds to (O_3S-O-N=C•-allyl) $^-$, arising from C-S bond cleavage on the oxime side of the disulfide bridge, while the fragment at m/z 193.96 corresponds to (O_3S-O-N=C-allyl-S•) $^-$, consistent with cleavage of the central S-S bond. Together, these fragments confirm the presence of both the allyl disulfide and sulfonated oxime motifs within the same molecule, providing strong evidence for the proposed structure of alligrin.

While NMR and LC-MS data confirmed the structure and purity of alligrin, definitive structural confirmation was achieved through single crystal X-ray diffraction analysis of crystals obtained unexpectedly during isolation, providing clear determination of the three-dimensional molecular structure.

2.1.4.5 Single crystal X-ray diffraction of alligrin

White single crystals of alligrin were obtained by chance via slow evaporation of acetonitrile and ammonium acetate buffer. Subsequent single-crystal X-ray diffraction (SXRD) (Figure 2.28) analysis confirmed its complete three-dimensional structure and molecular formula as $C_7H_{10}S_3NO_4^-$, providing a definitive foundation for understanding its atomic connectivity, chemical reactivity and physicochemical properties with further details discussed in Chapter 5.

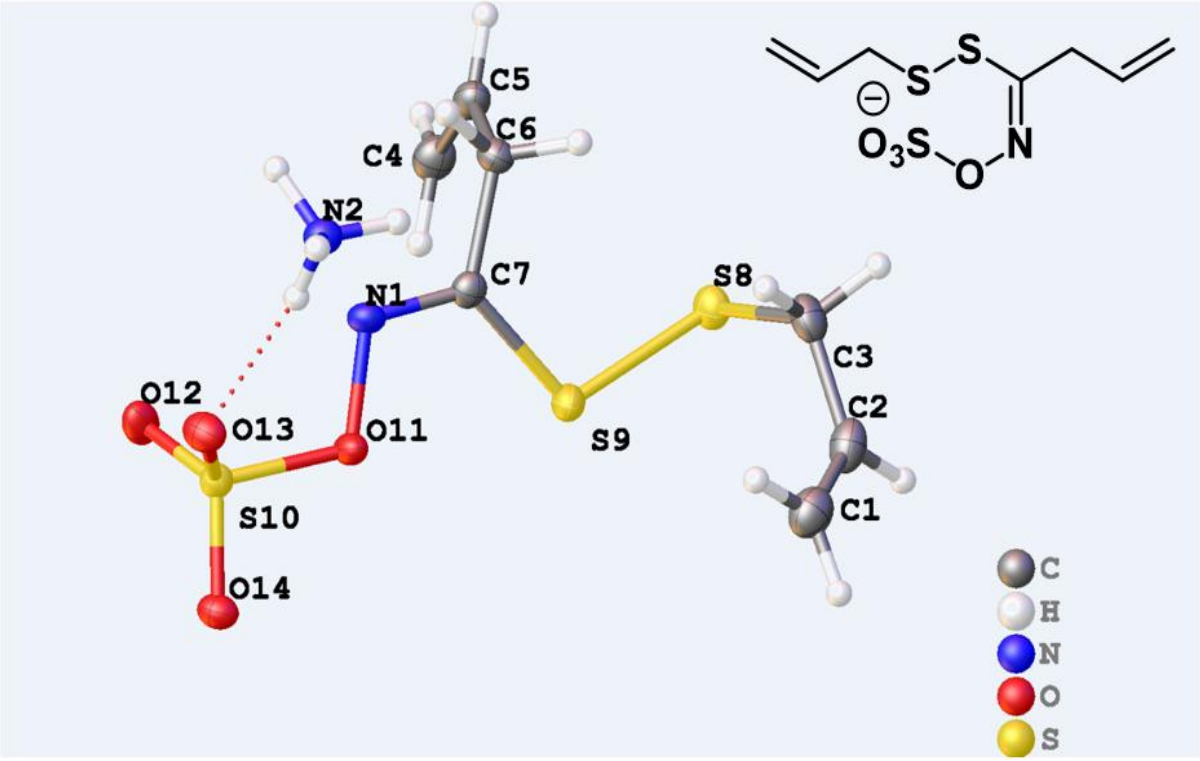

Figure 2.28: Single-crystal X-ray structure of alligrin in ammonium acetate.

Following the confirmation of alligrin's molecular structure through single-crystal X-ray diffraction, the next step was to evaluate its chemical stability at certain condition. Evaluating the stability profile of alligrin is essential for assessing its potential biological relevance and practical applicability. Sulfur-containing compounds are often susceptible to oxidation, rearrangement, or decomposition. Therefore, stability studies were required to determine how factors such as temperature, and storage time influence the integrity and persistence of alligrin.

2.1.5 Stability profile of alligrin

When isolated and stored as a pure compound, alligrin remains stable for approximately one week at room temperature after which gradual degradation begins, whereas storage at -20 °C preserves its integrity for several months. In contrast, within the crude reaction mixture of allicin, sinigrin and myrosinase, alligrin shows greater reactivity, as evidenced by HPLC monitoring, which reveals its rearrangement into secondary sulfur-containing products. This reflects the highly reactive chemical environment created by the interaction between glucosinolate-derived intermediates and organosulfur species.

The analytical and preparative HPLC chromatograms of the reaction mixture revealed several additional peaks beyond the major product alligrin revealing of possible rearrangement products formed under the reaction conditions. Seven of these secondary compounds were successfully isolated and purified using preparative HPLC under optimised chromatographic parameters.

Due to the limited yield of each isolated compound which was less than one milligram, comprehensive structural characterisation was challenging. Only two compounds were obtained in sufficient quantity for structural elucidation by ^{1}H-NMR spectroscopy, with LC-MS analysis to confirm their molecular formula, molecular weights, and fragmentation behaviour. The remaining five compounds were recovered in quantities sufficient only for LC-MS analysis. Two were successfully isolated as pure compounds, while the final three co-eluted as mixture due to their closely overlapping retention times and insufficient quantities to achieve complete chromatographic separation. Nevertheless, the molecular formula and exact masses derived from each fragment ion were interpreted to propose putative structures, based on the established reactivity pathways of allicin and the sinigrin-derived aglycone intermediate (Figure 2.29).

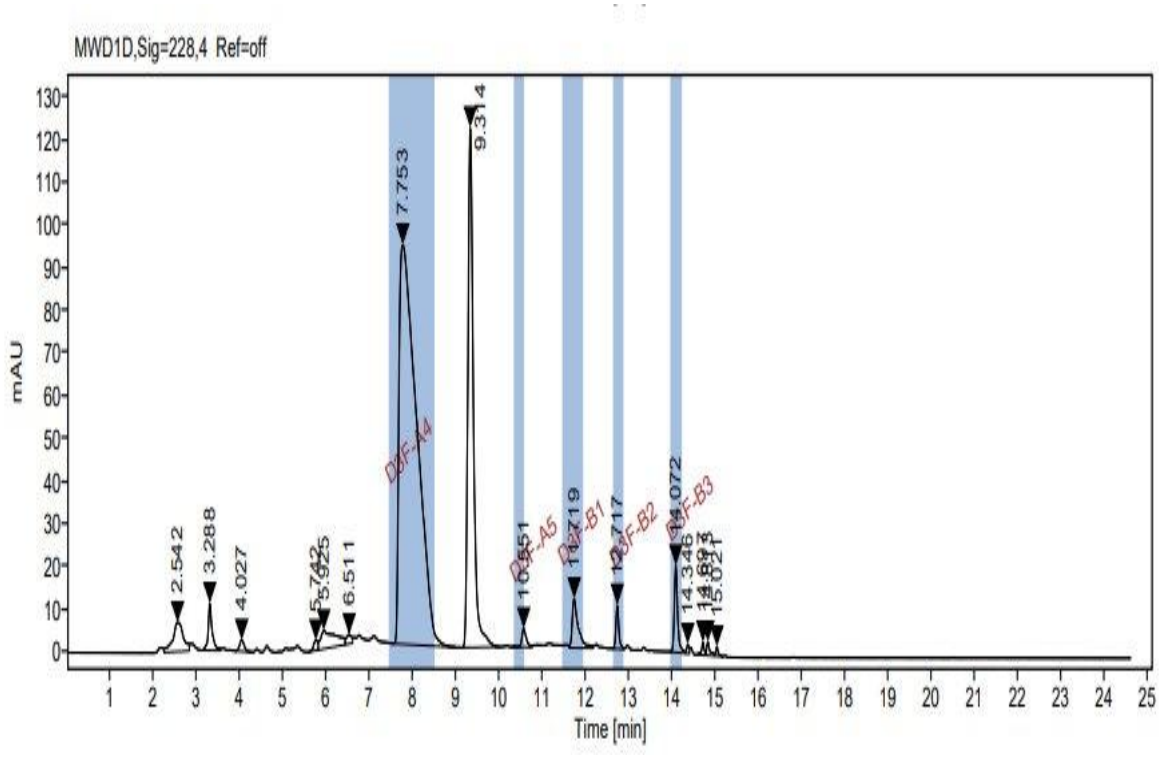

Figure 2.29: Prep-HPLC chromatogram of the sinigrin-allicin with myrosinase reaction mixture.

The first compound, eluting at a retention time of 10.5 minutes (Figure 2.29), was analysed exclusively by LC-MS.

The LC-ESI-MS2 spectrum of the purified compound **3** displayed a deprotonated molecular ion peak at m/z 299.9503 [M-H] $^-$, corresponding to the molecular formula $C_7H_{10}NO_4S_4^-$ (Figure 2.30). The isotopic pattern (including an M+2 peak at 17.6%) confirmed the presence of four sulfur atoms within the molecule. Fragment ions provided additional insight into the structure of compound **3** and fragmentation pattern. The ion at m/z 96.95 corresponds to a sulfate fragment $[HSO_4]^-$, while m/z 111.93 is attributed to a nitrogen-sulfur-oxygen fragment $[NH_2\text{-}O\text{-}SO_3]^-$, both characteristic of sulfonated and glucosinolate-related species. The fragment at m/z 136.95 corresponds to an allyl trisulfide anion $[CH_2{=}CH\text{-}CH_2\text{-}S\text{-}S\text{-}S]^-$, arising from cleavage of the S-C bond with retention of the allyl-trisulfide chain, indicating the presence of a trisulfide linkage within the molecule. The fragment at m/z 194.97 suggests partial cleavage of the S-S bond with retention of the sulfonate moiety, consistent with a sulfur-nitrogen-oxygen substructure. Higher-mass fragment ions, such as m/z 226.94 and m/z 258.91, correspond to losses of allyl or allyl-thiol fragments, confirming the presence of allyl-linked sulfur chains. Notably, fragments at m/z 95.95, m/z 194.96 and m/z 226.94 are shared with the fragmentation pattern of alligrin, suggesting a common structural origin and supporting the proposed structure of compound **3**.

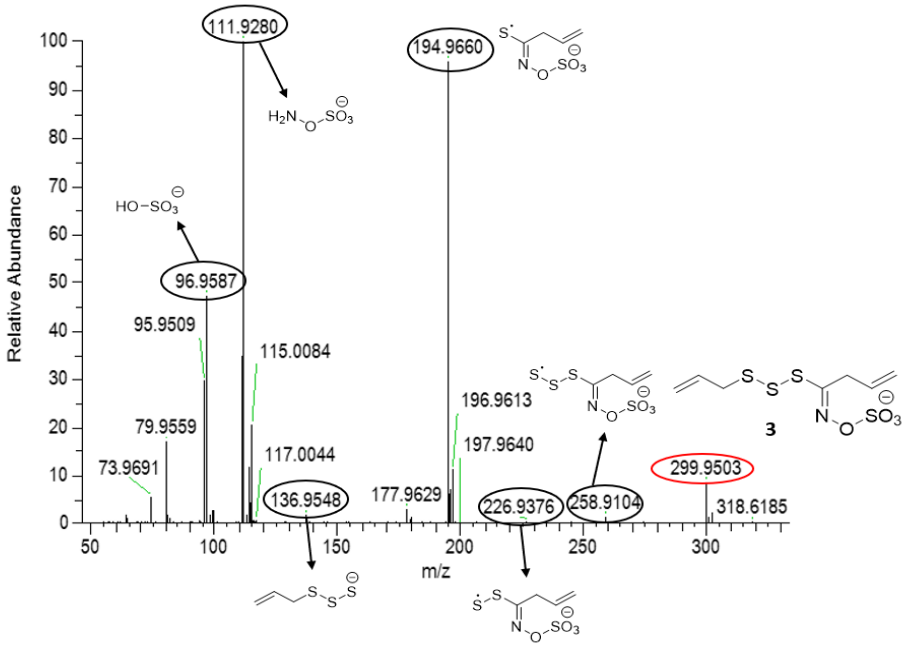

*Figure 2.30: LC-ESI-MS2 spectrum of the purified compound **3** ($C_7H_{10}NO_4S_4^-$).*

The plausible mechanism describes the self-rearrangement pathway of alligrin, leading to the formation of a trisulfide-linked product (Figure 2.31). pathway A, the reaction begins with alligrin existing in equilibrium, resulting in the formation of compound **1**, which reacts with another alligrin molecule, generating compound **2** that features a trisulfide (-S-S-S-) linkage and a sulfated thiohydroximate intermediate. Subsequent bond reorganization occurs as the sulfated thiohydroximate group attacks the allyl moiety in compound **2**, producing two major products, a compound **3** and compound **4**. Alternatively, pathway B proposes a concerted reaction mechanism, considered more likely although not yet proven, in which both alligrin molecules simultaneously interact through a single transition state, directly yielding compounds **3** and **4** without passing through compound **2** as an intermediate. Overall, this transformation exemplifies a typical sulfur-exchange rearrangement observed in organosulfur chemistry, driven by the intrinsic nucleophilicity and electrophilicity of sulfur atoms.

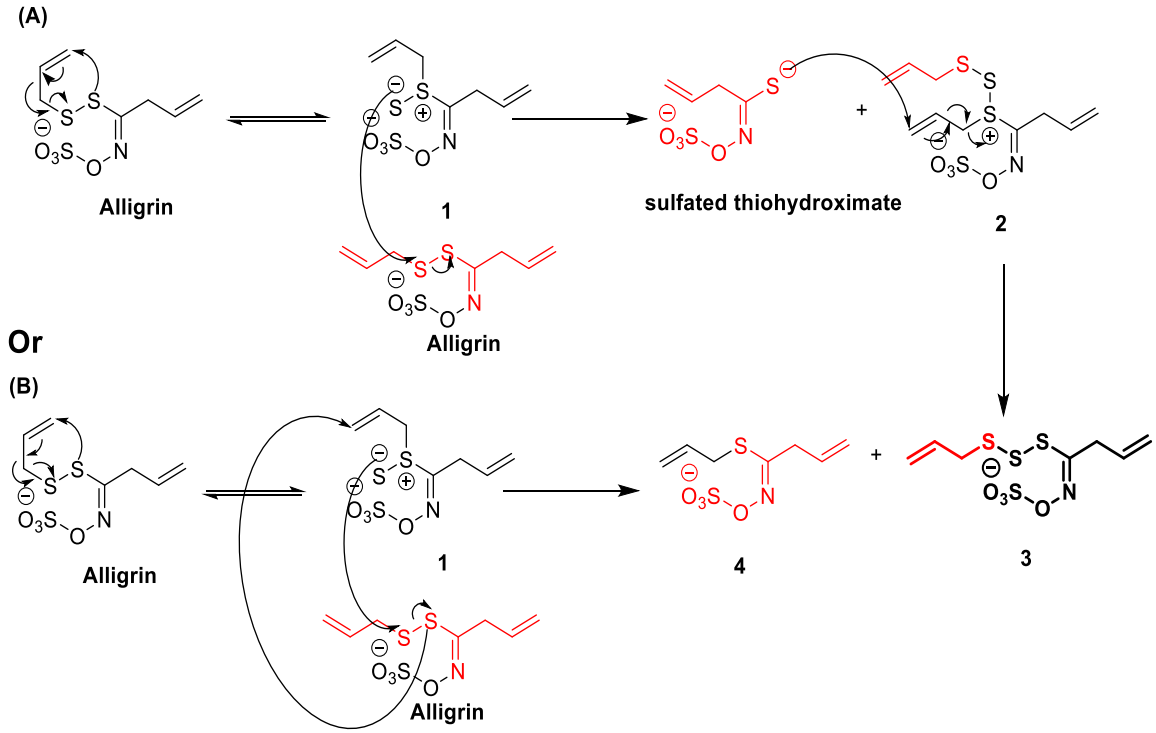

*Figure 2.31: Proposed plausible mechanism for the formation of compound **3**.*

The second compound, eluting at a retention time of 11.7 minutes (Figure 2.29), was recovered in sufficient quantity (approximately 1 mg) to permit full structural characterisation by both ^{1}H-NMR spectroscopy and LC-MS analysis.

The LC-ESI-MS2 spectrum of compound **9** displayed several diagnostic fragment ions that provide strong evidence for its structural composition and fragmentation behaviour (Figure 2.32). The precursor ion at *m/z* 339.98 $[M-H]^-$ corresponds to the molecular formula $C_{10}H_{14}NO_4S_4^-$, consistent with an extended sulfur containing system. Sequential fragmentation generated characteristic ions at *m/z* 298.94, 265.96, and 226.94, representing successive losses of an allyl group, allyl-thiol, and sulfur linked fragments, respectively confirming the presence of a polysulfide chain. Lower mass fragments at m/z 96.95 ($[HO\text{-}SO_3]^-$) and m/z 111.93 ($[H_2N\text{-}O\text{-}SO_3]^-$) are characteristic of sulfonated glucosinolate-derived moieties, while m/z 194.97 corresponds to a sulfur-nitrogen-oxygen species. The presence of fragments at m/z 194.97 and 111.93 in common with compound **3** further supports the proposed rearrangement mechanism leading to compound **9**.

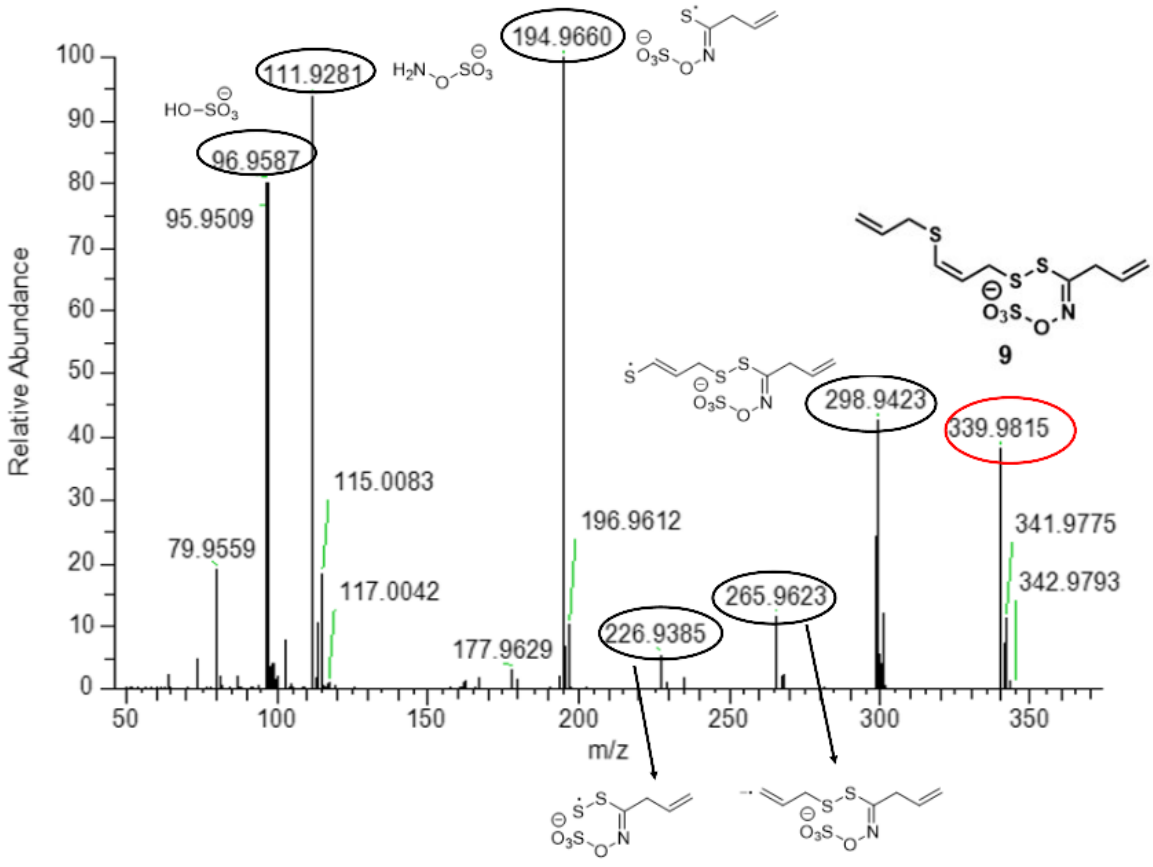

*Figure 2.32:MS2-LCMS spectrum of compound **9** ($C_{10}H_{14}NO_4S_4^-$).*

The proposed mechanism for the formation of compound **9** is directly inspired by the well-established ajoene formation pathway (Figure 2.34). Ajoene forms through the reaction of two allicin whereby one allicin molecule generates allyl sulfenic acid (CH_2=CH-CH_2-SOH) upon S-S bond cleavage (Figure 2.33). These reactive intermediate attacks the electrophilic sulfur of the second allicin molecule, forming a sulfonium-type intermediate (compound **5**) that subsequently undergoes dehydration and rearrangement, establishing a new vinyl C=C bond between the sulfur chains (compound **6**). Compound **6** then reacts with a second molecule of allyl sulfenic acid, which attacks the electrophilic sulfur centre, followed by loss of a proton and rearrangement to yield ajoene as a mixture of (E)- and (Z)-isomers [208].

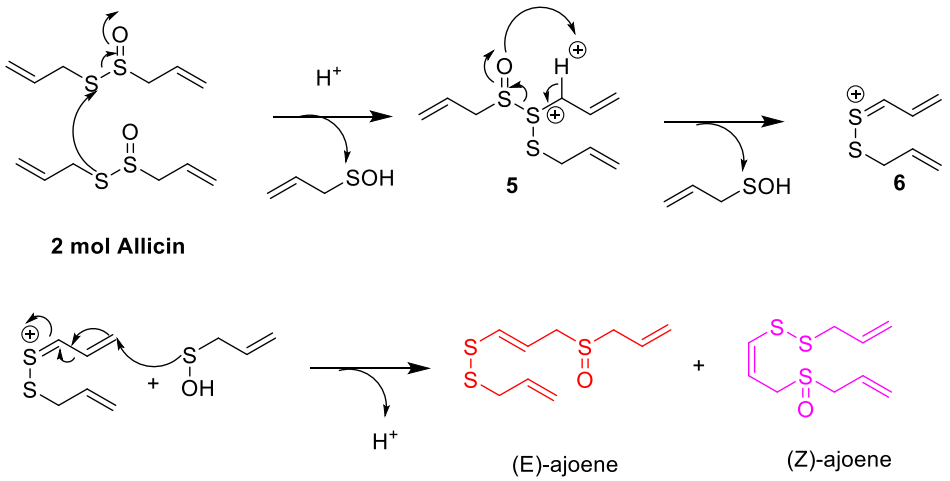

Figure 2.33: Mechanism formation of Ajoene from allicin transformation.

In close analogy to this pathway, the formation of compound **9** (Figure 2.34) proceeds through a mechanistically equivalent sequence, wherein the reactive sulfur centre of free allicin attacks the electrophilic sulfur atom of alliigrin, or alternatively through the reaction of two allicin equivalents, generating compound **5**, a mixed sulfonium-type intermediate directly analogous to that formed during ajoene synthesis. Subsequent proton transfer and elimination of allyl sulfenic acid yields compound **6**, a reactive allyl disulfide intermediate equivalent to the vinyl disulfide cation in the ajoene pathway.

Next, the negatively charged alliigrin existing in equilibrium (compound **1**) undergoes nucleophilic attack on the allyl moiety of compound **6**, generating compound **7**. This intermediate subsequently reacts with allyl sulfide, whereby nucleophilic attack occurs at the sulfur atom adjacent to the allyl moiety, yielding compound **8** along with diallyl disulfide as a

side product. Finally, intramolecular sulfur reorganisation within compound **8** drives further rearrangement, resulting in the formation of compound **9**.

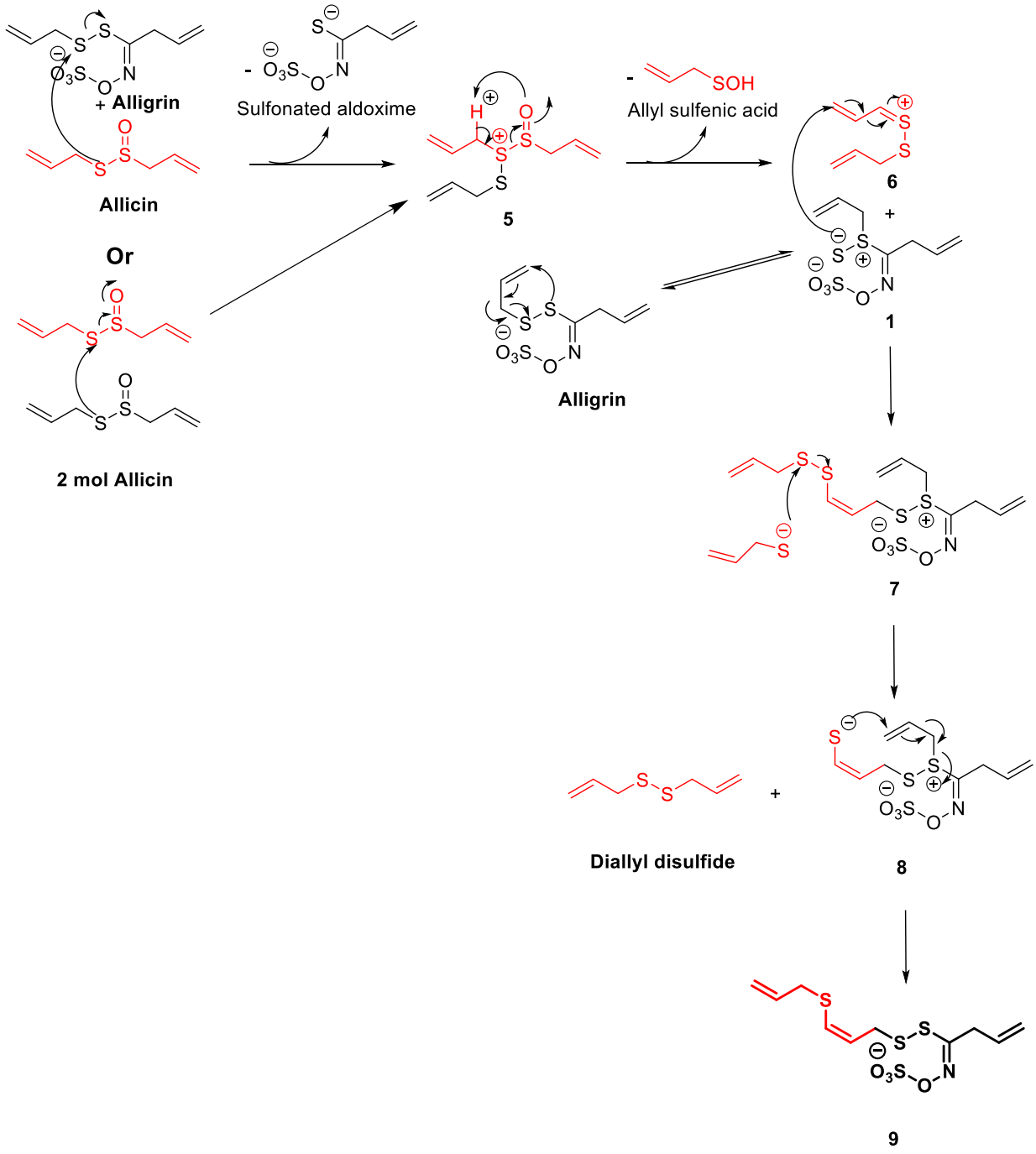

*Figure 2.34: Proposed mechanistic pathway for the formation of compound **9**.*

The ^{1}H NMR spectrum of compound 9 (Figure 2.35) displayed a set of characteristic resonances consistent with a structure containing multiple allylic environments. The signal at δ 6.40 (d, *J* = 9.3 Hz, 1H) was assigned to the vinylic proton H4, adjacent to sulfur. A vicinal coupling constant of 9.3 Hz falls within the range typical of *cis* alkene protons (*J* ≈ 6-12 Hz) and well below that expected for a *trans* arrangement (*J* ≈ 12-18 Hz). The internal S-CH=CH- double bond was therefore assigned the *Z* (*cis*) configuration. This value closely matches the coupling constant reported for the corresponding vinylic proton of (*Z*)-ajoene [209], which supports the involvement of a *Z*-ajoene-like intermediate in the reaction with alligrin. The multiplets at δ 5.98 (ddq, *J* = 16.3, 11.0, 5.5 Hz, 1H) and 5.91-5.75 (m, 2H) were attributed to additional vinylic protons within the conjugated allyl moieties, confirming the retention of multiple unsaturated bonds following conjugation. The signals at δ 5.21 (m, 4H) were assigned to terminal methylene protons (=CH_2) of the allyl chains, indicating that both the allicin- and alligrin-derived allyl groups remained structurally intact. In the aliphatic region, the multiplet at δ 3.74 (dd, *J* = 13.9, 7.2 Hz, 2H) was assigned to methylene protons adjacent to a quaternary carbon, whilst signals at δ 3.41 (d, *J* = 7.4 Hz, 2H) and 3.37 (d, *J* = 5.9 Hz, 2H) were attributed to methylene protons adjacent to sulfur atoms (CH_2-S).

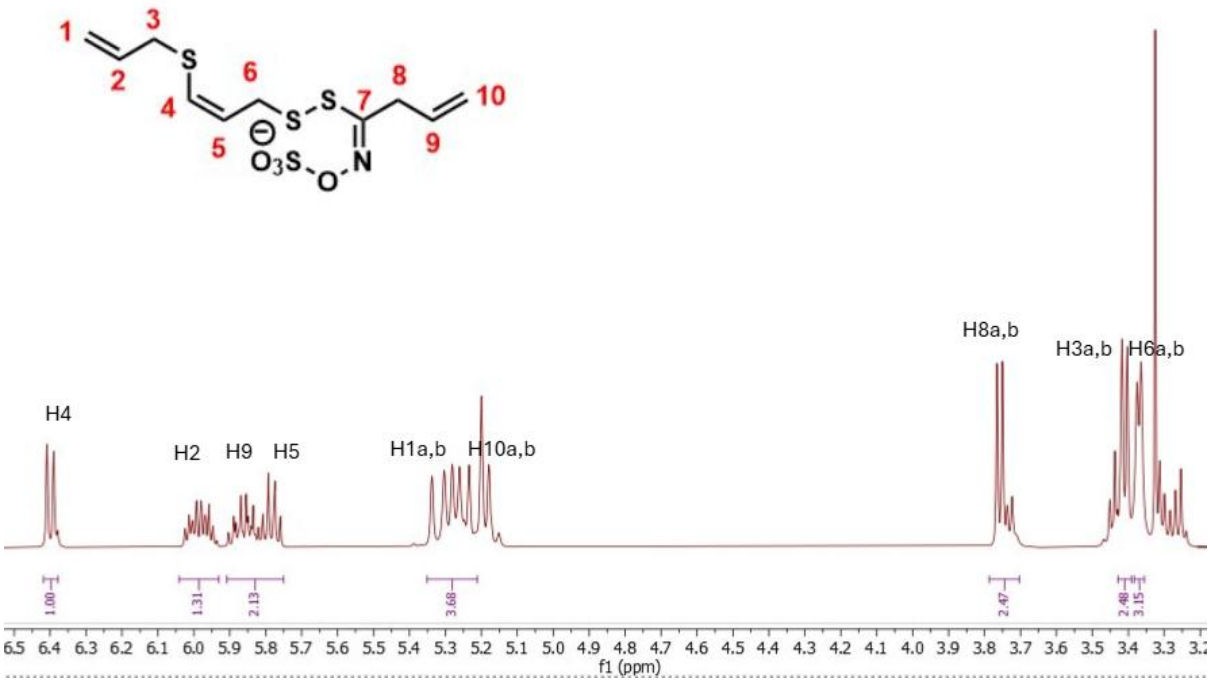

Figure 2.35: ^{1}H NMR (500 MHz, D_2O) of compound **9**.

The LC-ESI-MS2 spectrum of compound **10** revealed a different fragmentation pattern characteristic of extended sulfur structure (Figure 2.36). The precursor ion at *m/z* 371.95 [M-H] $^-$ corresponds to the molecular formula $C_{10}H_{14}NO_4S_5^-$, consistent with a structure containing five sulfur atoms. The ion at *m/z* 292.14 corresponds to a desulfated derivative of compound **10**, indicating loss of the sulfate group during fragmentation, while the peak at *m/z* 356.91 represents the loss of one oxygen atom from the sulfate moiety, suggesting sequential sulfate cleavage. The fragment ions at *m/z* 96.95 ($[HSO_4]^-$) and *m/z* 226.94 are diagnostic of sulfate and sulfur-nitrogen-oxygen fragments, respectively, and were also observed in the fragmentation pattern of alligrin, confirming a conserved core structure. Similarly, ions at *m/z* 194.97 and 111.93 were common to compounds **3** and **9**, supporting a shared sulfur rearrangement mechanism (Figure 2.30, 2.32). Together, these data confirm that compound **10** retains the fundamental sulfur-nitrogen-oxygen skeleton of alligrin while incorporating an additional sulfur atom, leading to a higher-order polysulfide structure.

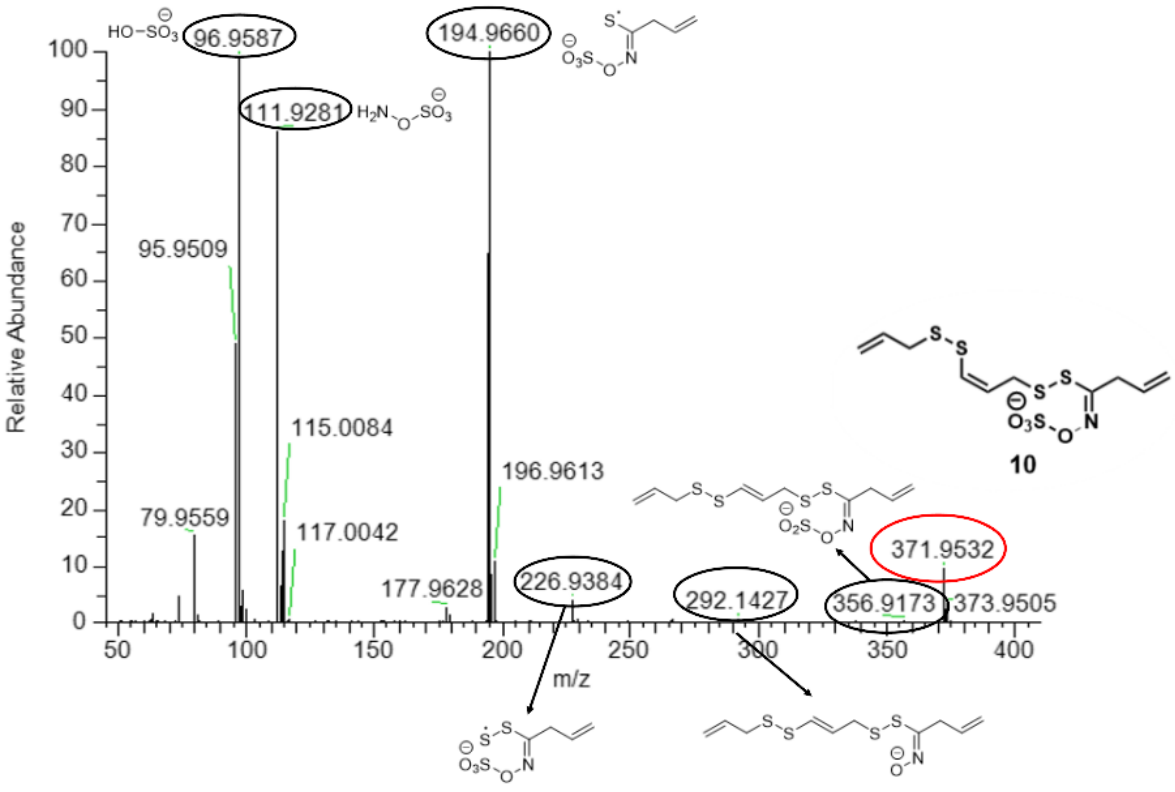

*Figure 2.36: MS2-LC-MS spectrum of compound **10** ($C_{10}H_{14}NO_4S_5^-$).*

The proposed mechanism for compound **10** (Figure 2.37) follows a similar sulfur-exchange and rearrangement pathway to that described for compound **9**, originating from the interaction between alligrin and allicin or two molecules of allicin (Figure 2.34). After the formation of compound **7**, the reaction proceeds through an additional sulfur-sulfur interaction involving allyl sulfide. In this step, the sulfur atom of allyl sulfide attacks the allyl moiety attached to the sulfur atom adjacent to the C-N-O-SO_3^- group, leading to the generation of compound **10** and diallyl sulfide as a by-product.

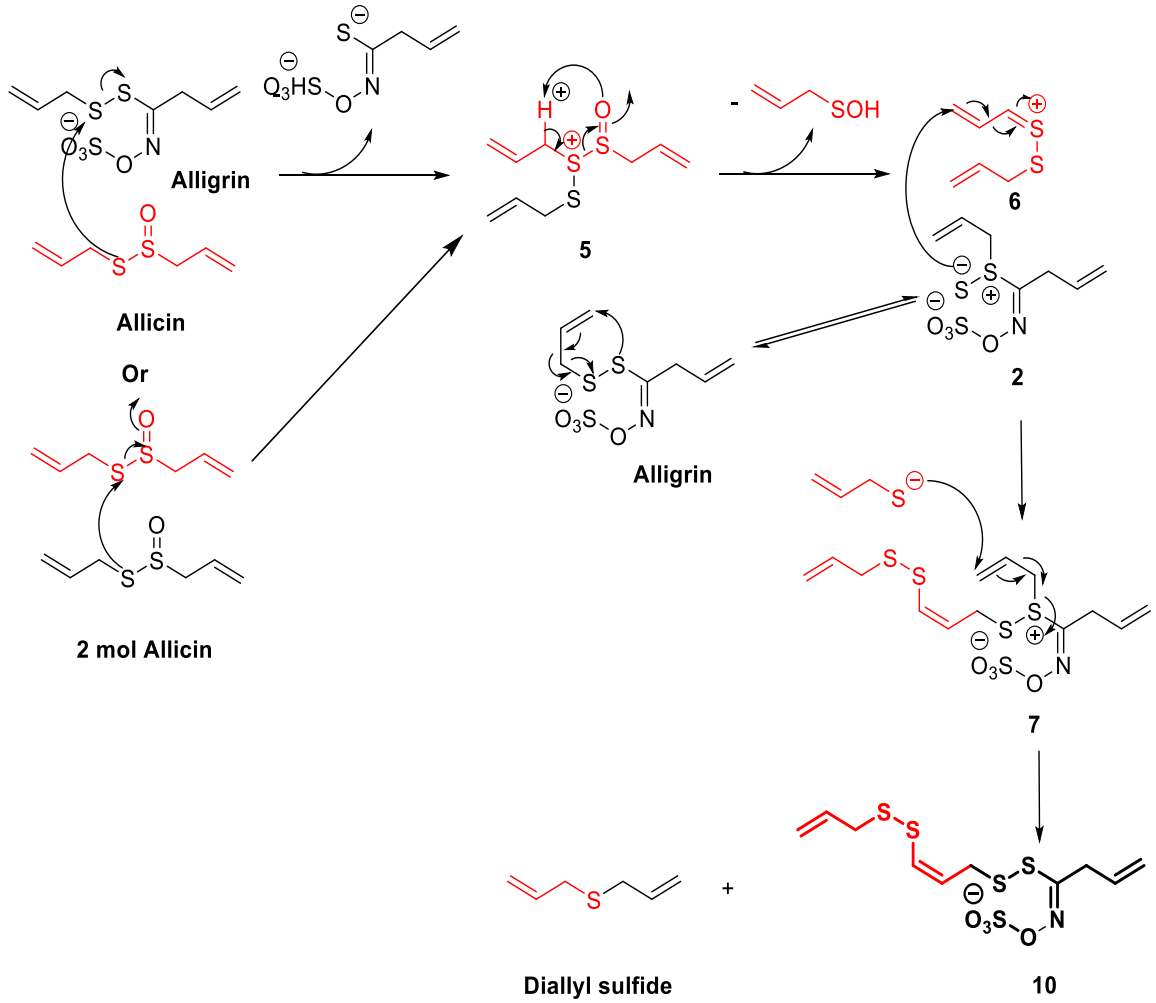

*Figure 2.37: Proposed mechanism for the formation of compound **10**.*

The ^{1}H NMR spectrum of compound **10** (Figure 2.38) displayed characteristic resonances consistent with a structure containing multiple allylic environments. The signal at δ 6.73 (dd, *J* = 9.4, 1.0 Hz, 1H) was assigned to the vinylic proton H4, attached to the carbon bearing the disulfide sulfur (=CH-S-S). The vicinal coupling constant of 9.4 Hz falls within the range typical of *cis* alkene protons (*J* ≈ 6-12 Hz), as for compound 9. Signals at δ 5.99-5.80 (m, 3H) were attributed to vinylic protons within the conjugated allyl moieties, confirming retention of multiple unsaturated bonds following conjugation, whilst those at δ 5.56-5.45 (m, 2H) and 5.28-5.19 (m, 2H) were assigned to terminal methylene protons (=CH_2), indicating that both allicin- and alligrin-derived allyl groups remained structurally intact. In the aliphatic region, multiplets at δ 3.86-3.71 (m, 2H), 3.63-3.55 (m, 2H), and 3.48-3.42 (m, 2H) were attributed to methylene protons adjacent to both a quaternary carbon and sulfur atoms (CH_2-S).

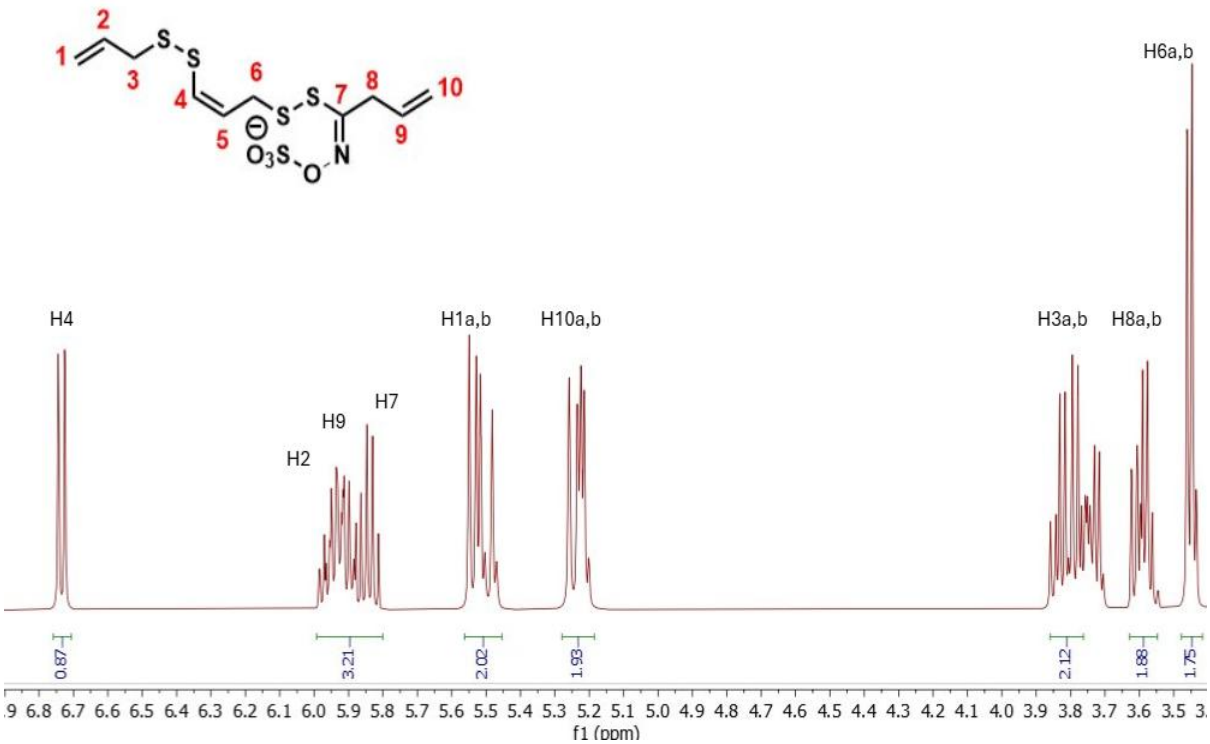

*Figure 2.38: ^{1}H NMR spectrum (500 MHz, D_2O) of compound **10**.*

The fourth compound, eluting at a retention time of 14 minutes (Figure 2.29), was analysed exclusively by LC-MS. The LC-ESI-MS² spectrum of compound **13** displayed several diagnostic fragment ions providing strong evidence for its structural composition and fragmentation behaviour (Figure 2.39). The precursor ion at m/z 411.9845 $[M-H]^-$ corresponds to the molecular formula $C_{13}H_{18}NO_4S_5$, consistent with an extended sulfer containing system and the sulfonated oxime moiety. Sequential fragmentation generated characteristic ions at m/z 337.9652 and 265.9630, representing losses of allyl-containing sulfur fragments. The remaining fragment ions at m/z 226.9383, 196.9610, 194.9658, 111.9280, and 96.9586 are consistently observed across compounds **3**, **9**, and **10** strongly supporting a shared structural origin throughout fragmentation.

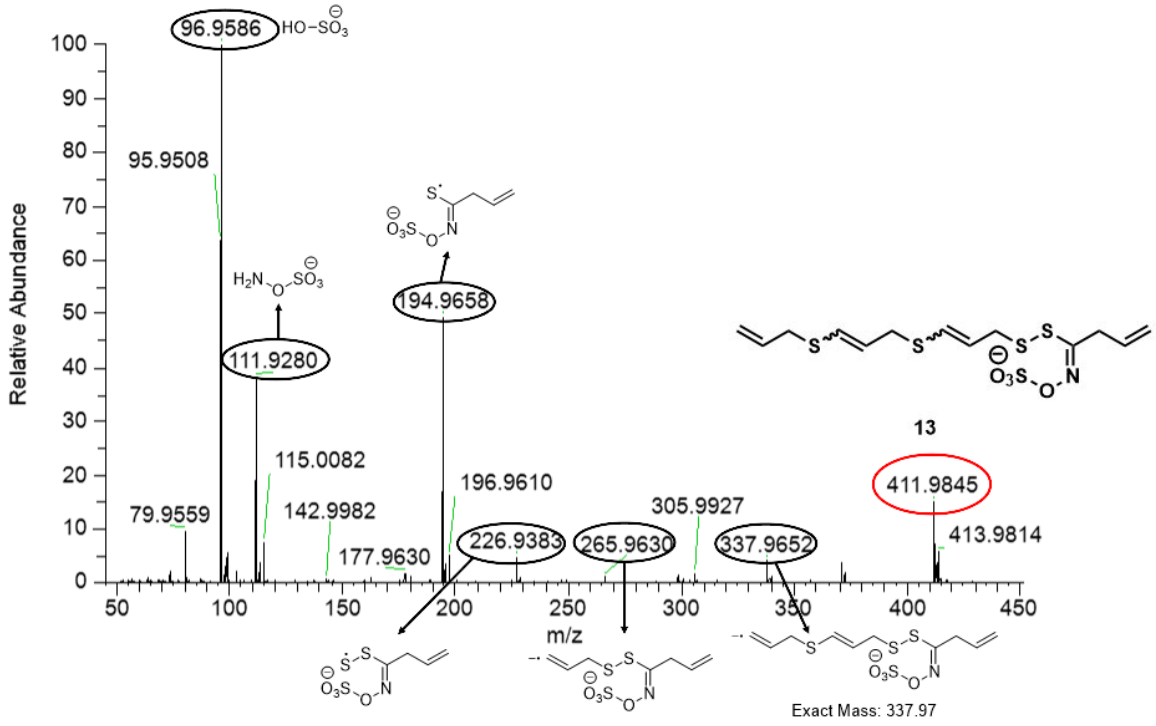

*Figure 2.39: LC-ESI-MS² spectrum of compound **13** ($C_{13}H_{18}O_4NS_5$).*

The plausible proposed mechanism for compound **13** (Figure 2.40) formation is directly inspired by the mechanism established for compound **9**, following an identical pathway through compounds **5** to **8** at which point the mechanism differs. The negatively charged sulfur centre of compound **8** attacks the allyl bond of compound **6** generating compound **11,** wherein the allyl thiol attacks the terminal sulfur atom of compound **11**, forming compound **12** with diallyl disulfide released as a by-product. After which the sulfur atom of compound **12** attacks the allyl moiety adjacent to the sulfur atom next to the C=N-O-SO_3^- group, this triggers intramolecular sulfur reorganisation, finally yielding compound **13**.

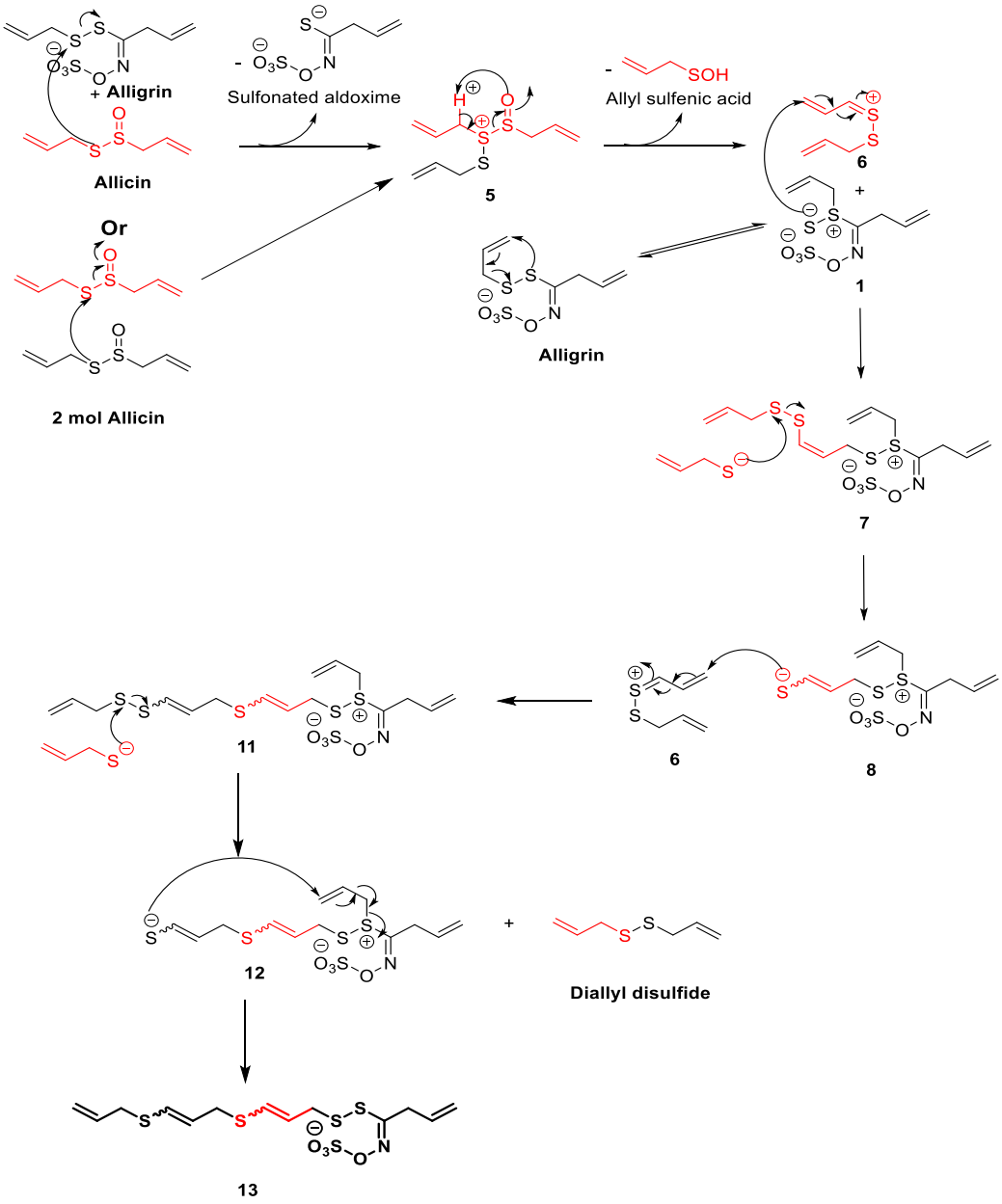

*Figure 2.40: Proposed mechanism for the formation of compound **13**.*

Three additional compounds, eluting at retention times of 14.3, 14.6, and 15.0 minutes (Figure 2.29), co-eluted as a mixture due to their closely overlapping retention times and insufficient abundance for individual isolation, and were therefore characterised exclusively by LC-MS analysis.

The fifth compound, eluting at a retention time of 14.3 minutes (Figure 2.29). The LC-ESI-MS² spectrum of compound **14** displayed diagnostic fragment ions providing evidence for its structural composition and fragmentation behaviour (Figure 2.41). The precursor ion at m/z 414.0009 [M-H] ⁻ corresponds to the molecular formula $C_{13}H_{20}O_4NS_5^-$. All fragment ions at m/z 226.9385, 194.9658, 111.9280, and 96.9587 are consistently observed across compounds **3**, **9**, **10**, and **13**.

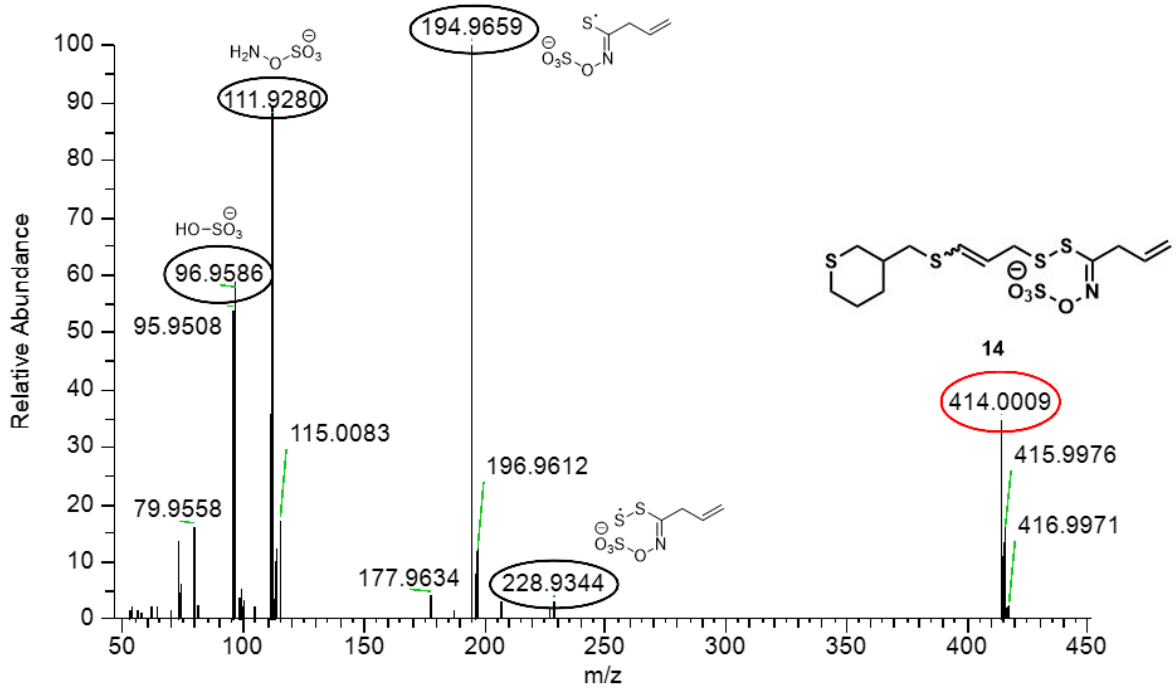

*Figure 2.41:LC-ESI-MS² spectrum of compound **14** ($C_{13}H_{20}O_4NS_5$).*

The proposed mechanism for compound **14** (Figure 2.42) shares the initial steps of compound **9** through intermediates **5** to **9**, in the presence of thioacrolein, a reactive intermediate generated from allicin decomposition. From this point, the terminal alkene of the thioacrolein intermediate attacks the terminal allyl moiety of compound **9** via an intramolecular thia-Michael addition, driving ring closure to form a saturated six-membered thiane ring, yielding compound **14**. This mechanistic proposal is further supported by the analogous cyclisation pathway and LC-ESI-MS² fragmentation pattern proposed for compound **17**, discussed afterward. The mechanism proposed here and in the alternative proposed mechanism are tentative and should not be considered definitive in the absence of further spectroscopic evidence.

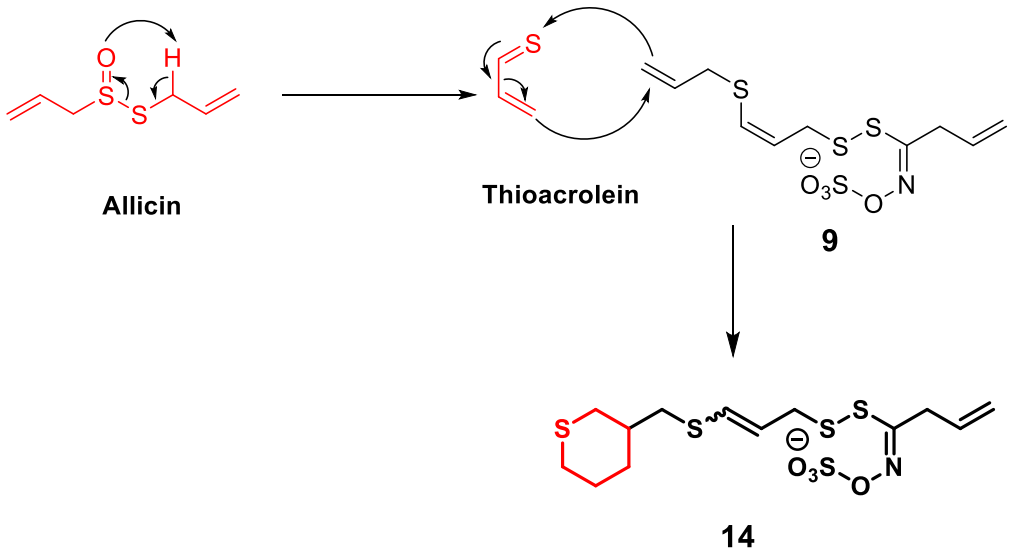

*Figure 2.42: Proposed mechanism for the formation of compound **14**.*

The alternative mechanism for compound **14** (Figure 2.43) formation follows an identical pathway to compound **9** through intermediates **5** to **9**. Beyond this point, the negatively charged sulfur centre of the allyl sulfide acts as a nucleophile, attacking the terminal alkene of the adjacent allyl moiety via nucleophilic addition, driving bond reorganisation and saturation of the double bond, ultimately yielding compound **14** featuring a saturated carbon chain in place of the terminal allyl group. The LC-ESI-MS² molecular ion at m/z 414.0009 [M-H] ⁻ is consistent with the proposed structure, supporting the presence of an extended polysulfide chain (Figure 2.44).

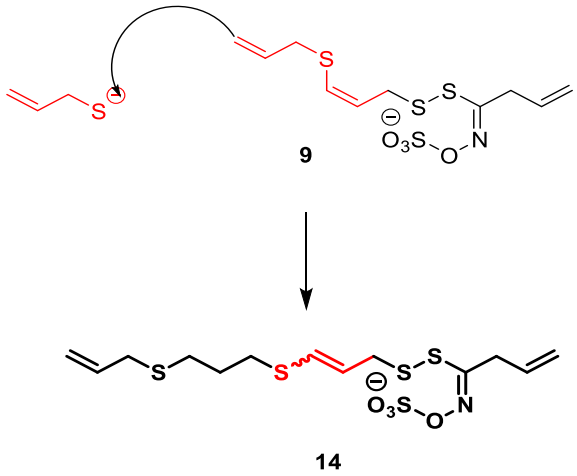

*Figure 2.43: Alternative proposed mechanism for the formation of compound **14**.*

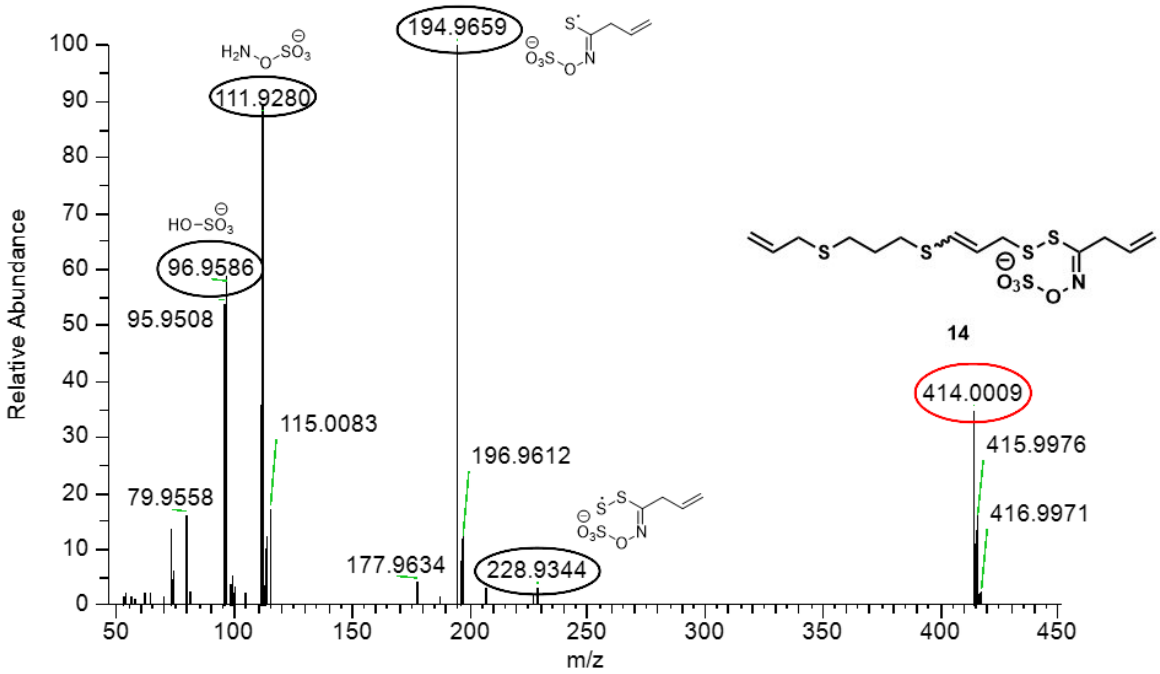

*Figure 2.44: LC-ESI-MS² spectrum of compound **14** ($C_{13}H_{20}O_4NS_5$).*

The sixth compound, eluting at a retention time of 14.6 minutes (Figure 2.29). The LC-ESI-MS² spectrum of compound **15** displayed precursor ion at m/z 443.9568 [M-H] ⁻ corresponds to the molecular formula $C_{13}H_{18}NO_4S_6^-$ (Figure 2.45). The fragment ion at m/z 402.9172 represents the loss of an allyl fragment, while the remaining fragment ions at m/z 337.9656, 274.0214, 226.9385, 194.9658, 111.9280, and 96.9587 are consistently observed across compounds **3**, **9**, **10** and **13**, strongly supporting a shared structural origin throughout fragmentation.

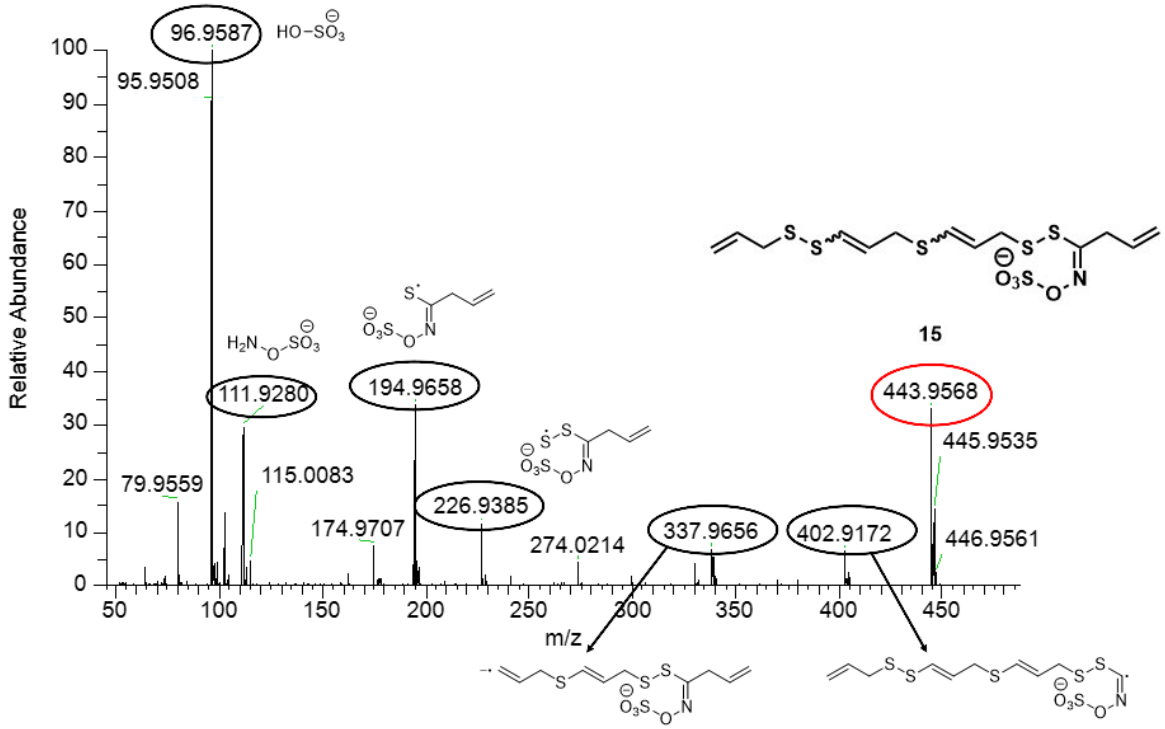

*Figure 2.45: LC-ESI-MS² spectrum of compound **15** ($C_{13}H_{18}NO_4S_6$).*

The mechanism for compound **15** (Figure 2.46) formation follows an identical pathway to compound **13** through intermediates **5** to **8**, at which point the negatively charged sulfur centre of compound **8** attacks the allyl bond of compound **6** forming compound **11**, after which the allyl sulfide attacks the allyl moiety adjacent to the sulfur atom next to the C=N-O-SO_3^- group, triggering intramolecular sulfur reorganisation to yield compound **16**.

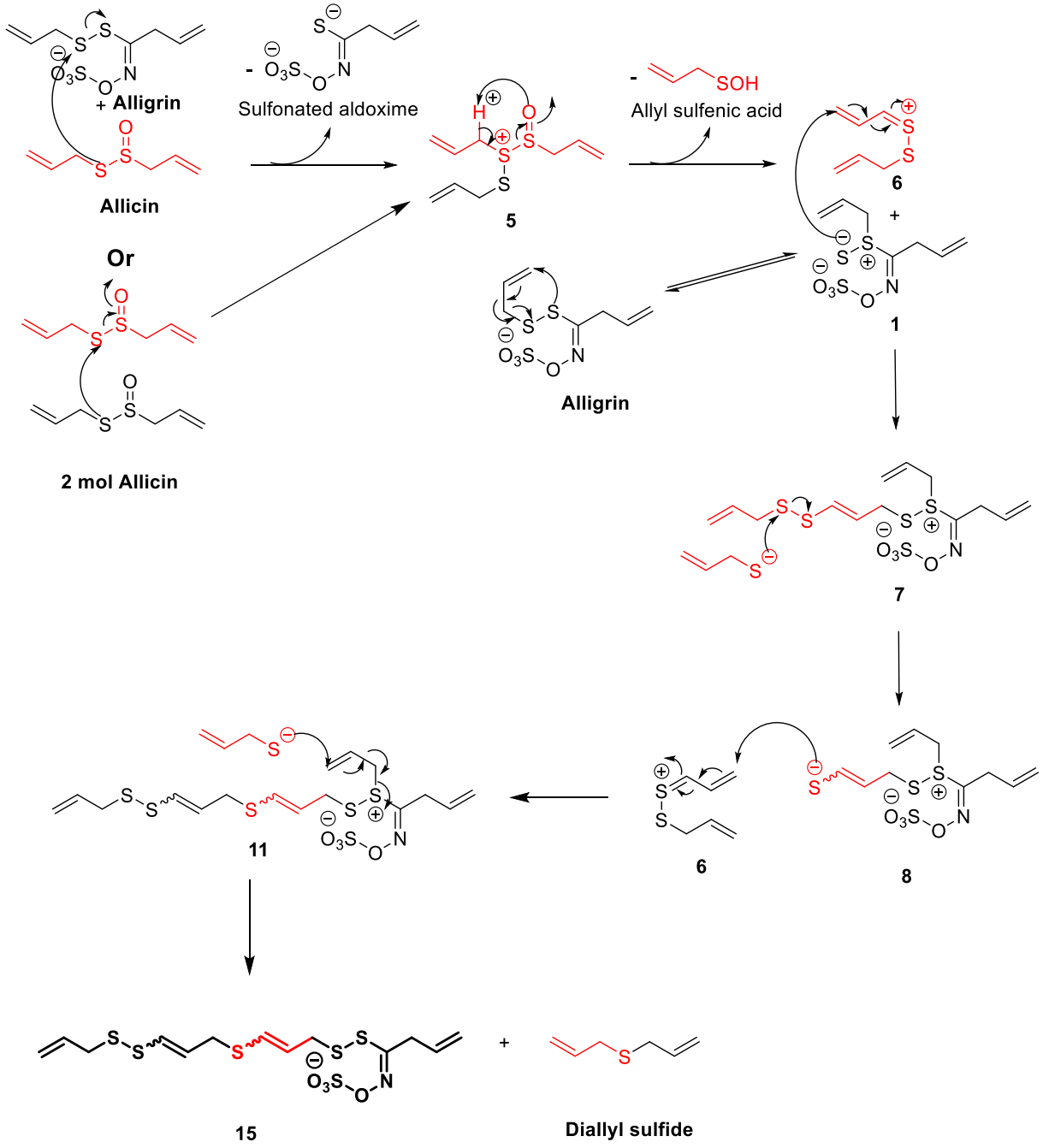

*Figure 2.46: Proposed mechanism for the formation of compound **15**.*

The seventh compound, eluting at a retention time of 15.0 minutes (Figure 2.29), was characterised exclusively by LC-MS analysis. The LC-ESI-MS² spectrum of compound **16** displayed several diagnostic fragment ions (Figure 2.47). The precursor ion at m/z 517.9761 $[M-H]^-$ corresponds to the molecular formula $C_{16}H_{24}NO_4S_7^-$. The fragment ion at m/z 476.9371 represents the loss of an allyl fragment from the precursor ion, while sequential fragmentation at m/z 403.9256 confirms further loss of the thiane-CH_2-S ring fragment from the chain end. The remaining fragment ions at m/z 226.9385, 194.9658, 111.9280 and 96.9587 are consistently observed across compounds **3**, **9**, **10**, **13** and **15**.

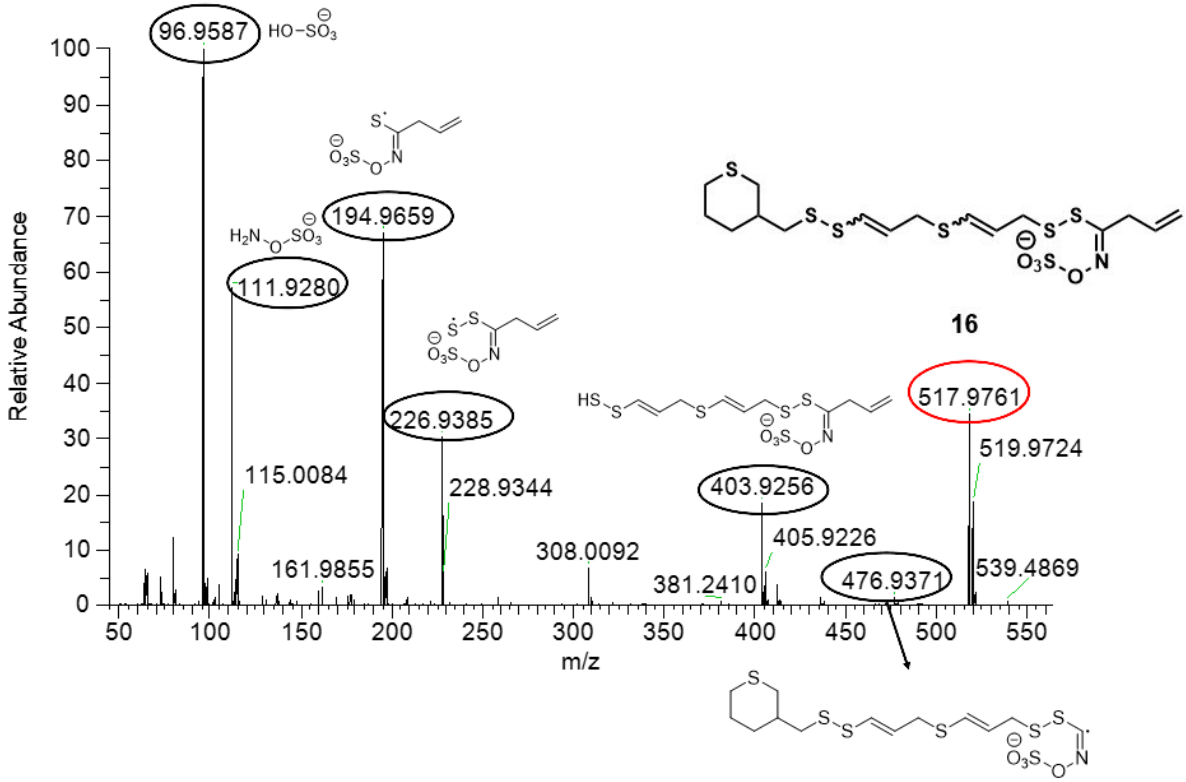

*Figure 2.47: LC-ESI-MS² spectrum of compound **16** ($C_{16}H_{24}NO_4S_7$).*

The proposed mechanism for compound **16** (Figure 2.48) shares the initial steps of compound **15** formation (Figure 2.46), in the presence of thioacrolein, a reactive intermediate generated from allicin decomposition. From this point onwards, the terminal alkene of the thioacrolein intermediate attacks the terminal allyl moiety of compound **15** via an intramolecular thia-Michael addition, driving ring closure to form a saturated six-membered thiane ring, yielding compound **16** (same as in compound 14 (Figure 2.42)).

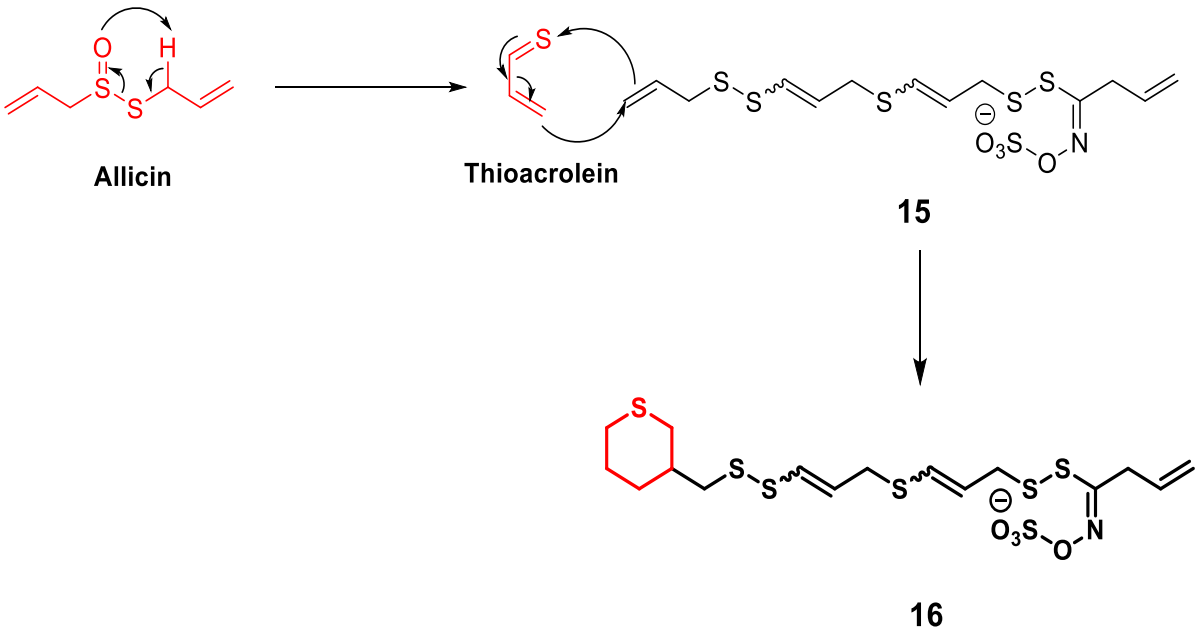

*Figure 2.48: Proposed mechanism for the formation of compound **16**.*

Although a tentative structure incorporating a sulfur-rich allylic chain was proposed, the precise sulfur connectivity and regiochemistry could not be fully established from MS data alone. Full structural confirmation would require complementary techniques such as NMR spectroscopy or X-ray crystallographic analysis, which were beyond the scope of the present study.

The alternative proposed mechanism for compound **16** (Figure 2.49) also shares the initial steps of compound **15** formation. Beyond this point, an analogous pathway to the alternative mechanism described for compound **14** was followed, ultimately yielding compound **16** where the negatively charged sulfur atom of the allyl sulfide acts as a nucleophile, attacking the terminal alkene of the allyl moiety of compound **15**. The LC-ESI-MS² molecular ion at *m/z* 517.9761, alongside fragment ions at *m/z* 476.9371 and 403.9256, is consistent with the proposed structure, supporting the presence of an extended polysulfide chain (Figure 2.50).

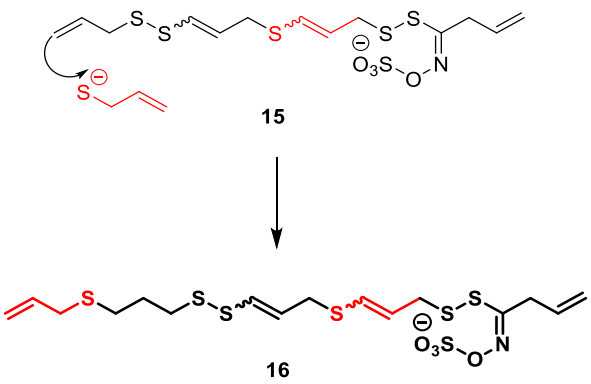

*Figure 2.49: Proposed mechanism for the formation of compound **16**.*

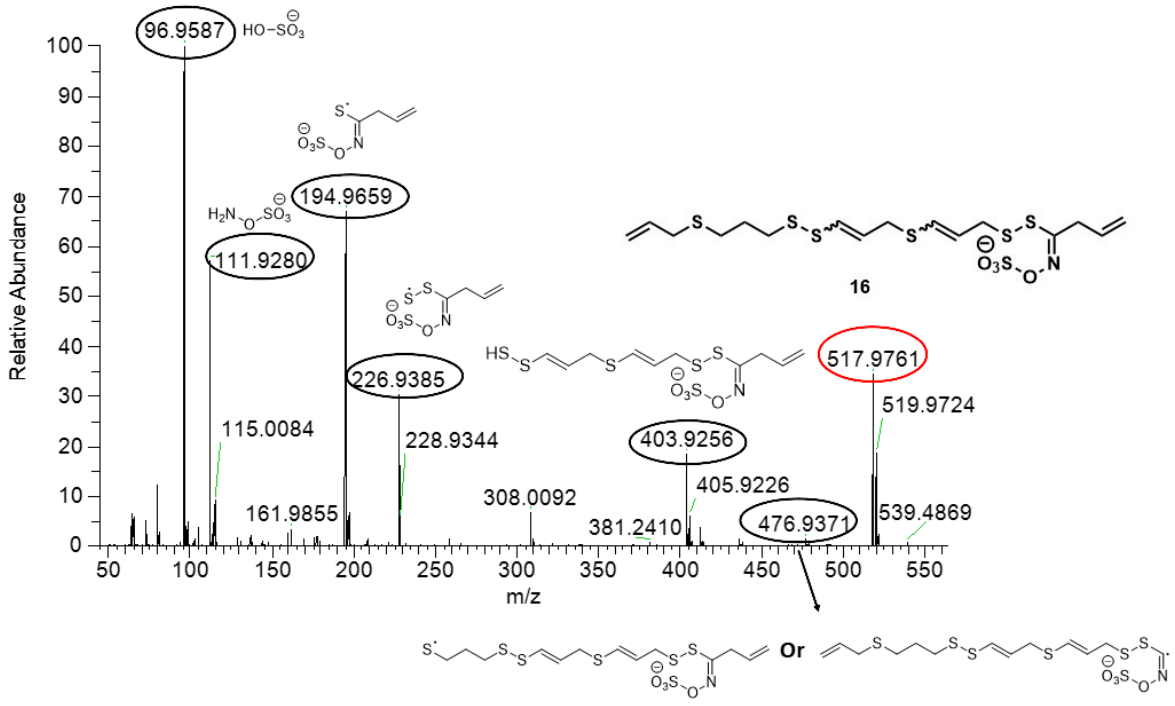

*Figure 2.50: LC-ESI-MS² spectrum of compound **16** ($C_{16}H_{24}NO_4S_7$).*

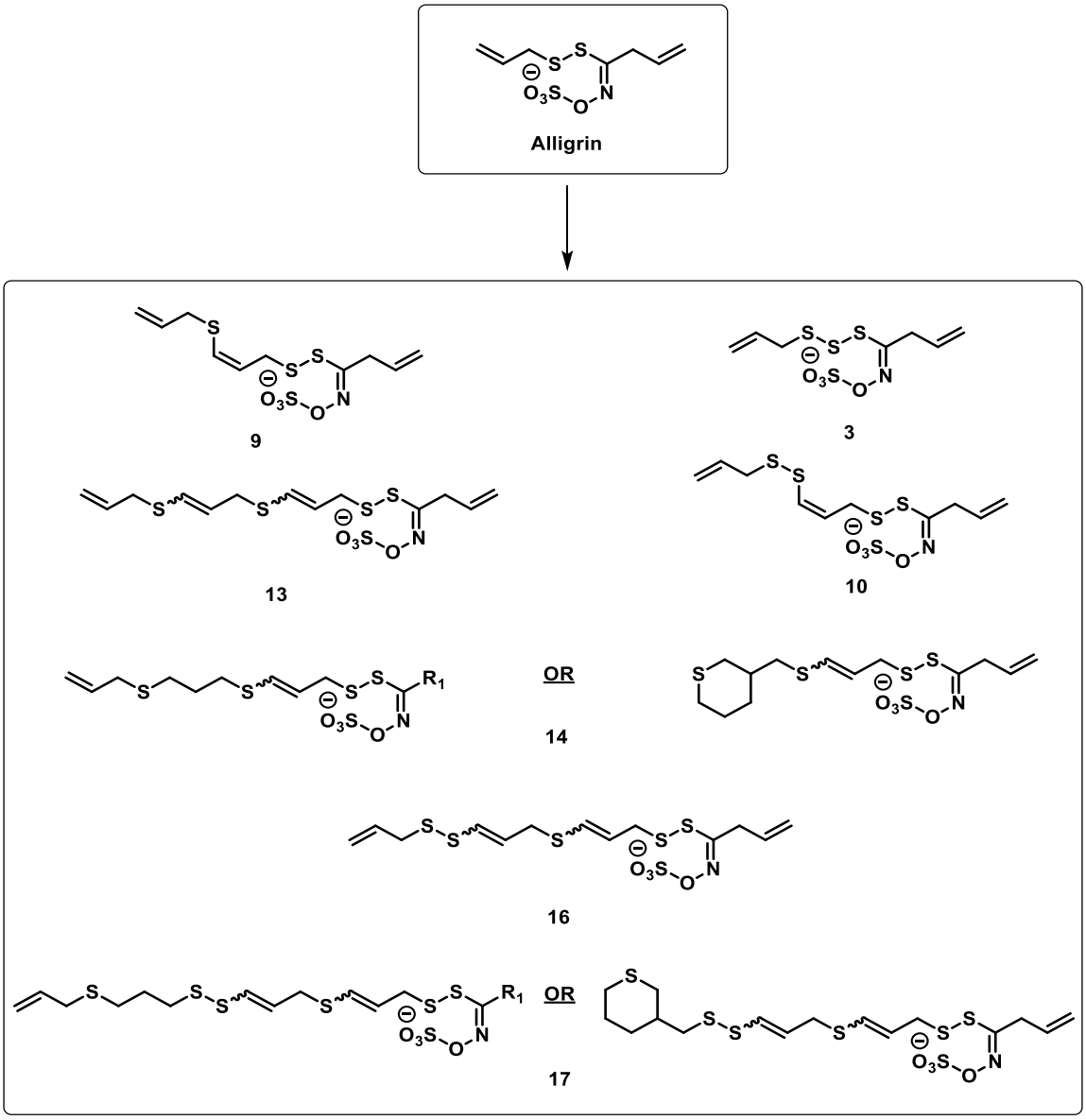

Figure 2.51: Structural overview of alligrin and its secondary rearrangement products.

2.1.6 Experimental validation of alligrin rearrangement pathways

To further validate the proposed mechanistic pathways of alligrin rearrangement, a series of experiments were conducted under controlled conditions. To investigate the formation mechanisms of compounds **9**, **10**, **13**, **14**, **15** and **16**, alligrin was co-incubated with allicin at room temperature for 3 hours and at 80 °C for 15, 30, and 60 minutes. Control experiments, in which allicin was incubated alone under identical conditions, were performed to confirm that the observed products arose specifically from the interaction between alligrin and allicin rather than from allicin decomposition alone, thereby validating the proposed cross-reactivity mechanism. In a parallel set of experiments, pure alligrin was incubated at 80 °C for the same time intervals to examine its self-rearrangement pathway and confirm the independent formation of compound **3** in the absence of allicin.

Each reaction was monitored using the optimized HPLC method (Section 2.1.4.1.1) to detect product formation over time. The retention times of the resulting peaks were compared with those observed in the original sinigrin-allicin and myrosinase reaction mixture to verify whether the same compounds were formed. Matching retention profiles confirmed that the new products were identical to those previously detected in the mixture. To further validate these findings, all samples were analysed by LC-MS, which confirmed their molecular weights and demonstrated full structural consistency with the compounds isolated earlier.

The results revealed that heating pure alligrin at 80 °C induce intramolecular sulfur-sulfur exchange, leading to a self-rearrangement process and forming compound **3** (more data in section 2.1.7 and LC-MS data in appendix), with no evidence of compounds **9**, **10**, **13**, **14**, **15**, or **16**. Whereas, co-incubation of alligrin with allicin at both room temperature and 80 °C promotes intermolecular sulfur exchange reactions, yielding the more complex rearrangement products **9, 10** and **13** (Figure 2.52, 2.53, and 2.54) while compounds **14**, **15** and **16** may also form under these conditions but remain below the detectable limit of the analytical method used. Additional peaks observed in the chromatograms are attributed to decomposition products of allicin which are commonly generated during thermal or prolonged incubation of allicin under aqueous conditions.

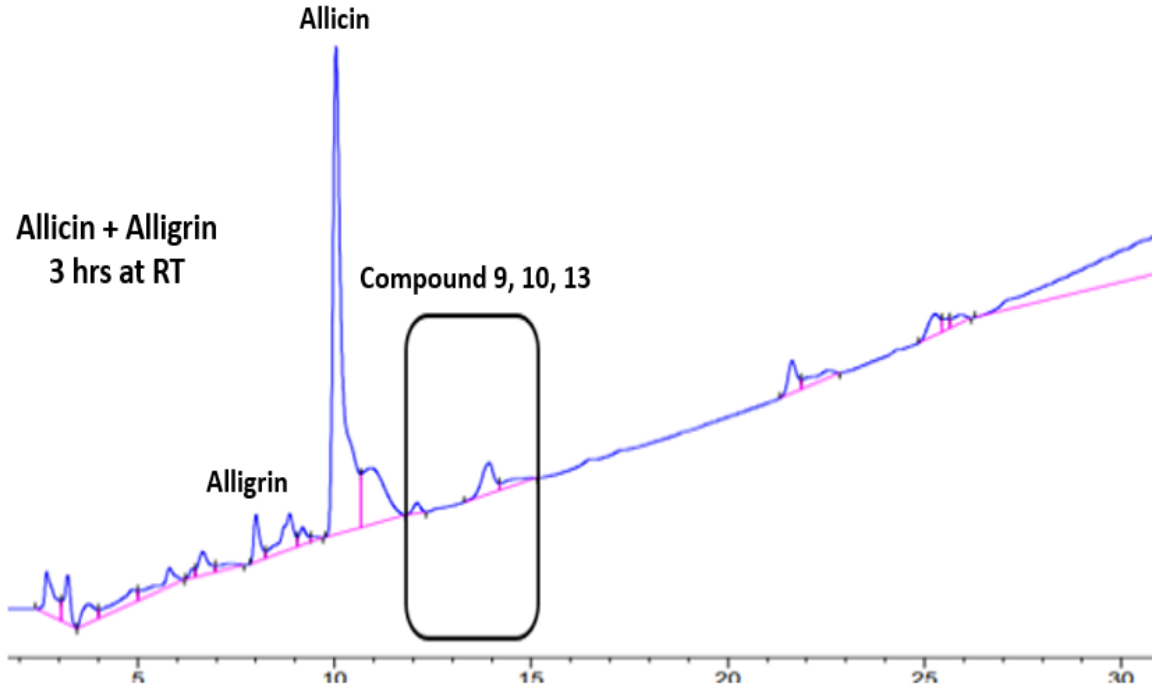

Figure 2.52: HPLC chromatogram of alligrin incubated with allicin at room temperature for 3 hours.

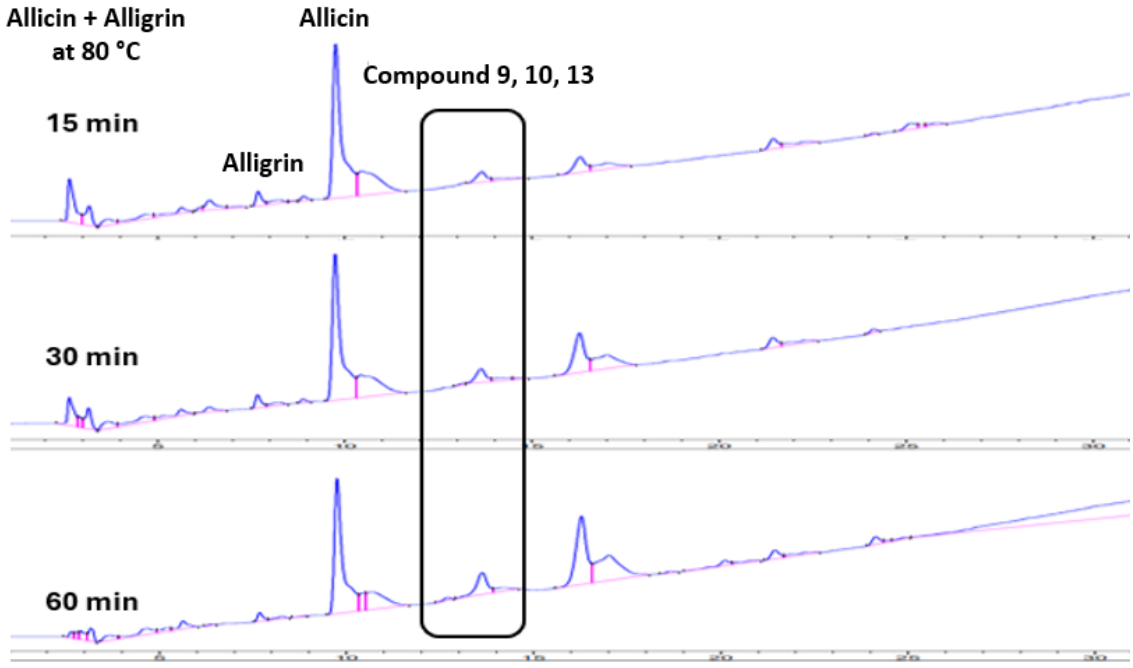

Figure 2.53:HPLC chromatograms of alligrin incubated with allicin at 80 °C for 15, 30, and 60 minutes.

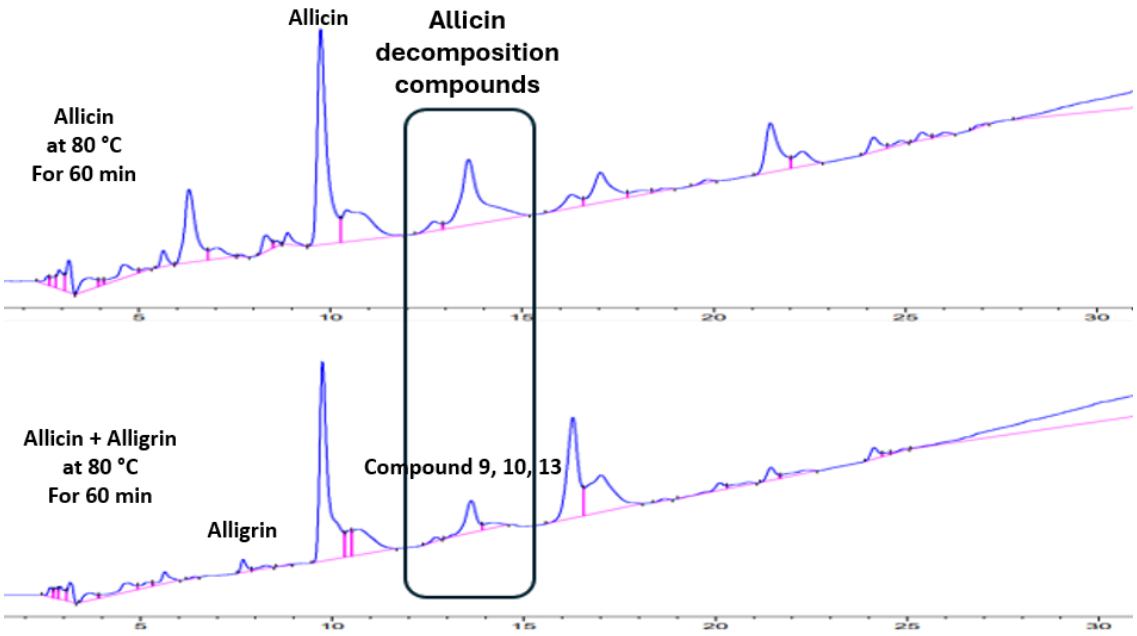

Figure 2.54:HPLC chromatograms comparing allicin alone and allicin co-incubated with alligrin at 80 °C for 60 minutes.

After confirming the rearrangement mechanisms of alligrin, the next step was to examine its thermal behaviour under cooking-like conditions. This experiment aimed to assess how temperature affects alligrin's stability, structural changes, and potential formation of new sulfur derivatives relevant to dietary and biological contexts.

2.1.7 Thermal treatment of alligrin to mimic cooking process

The combination of cruciferous vegetables such as broccoli, mustard, or cabbage with garlic is common in everyday cooking, a practice that may facilitate the formation of alligrin. Given the natural reactivity of sulfur-containing natural products and their susceptibility to structural transformation upon heating, a series of controlled thermal experiments were conducted to investigate the stability and degradation behaviour of alligrin under conditions mimicking realistic cooking temperatures. The resulting temperature-dependent transformation pathways, supported by both HPLC and LC-MS analyses, are illustrated in the reaction schemes below, with full LC-MS data provided in the appendix.

In this study, at moderate temperatures (50-100 °C), alligrin partially rearranged to yield compound **3**, previously identified as a self-rearrangement product, providing further evidence supporting the proposed mechanism of intermolecular sulfur exchange (Figure 2.55-

2.56). This finding suggests that mild heating promotes controlled molecular rearrangement without extensive decomposition, preserving the core organosulfur structure of alligrin.

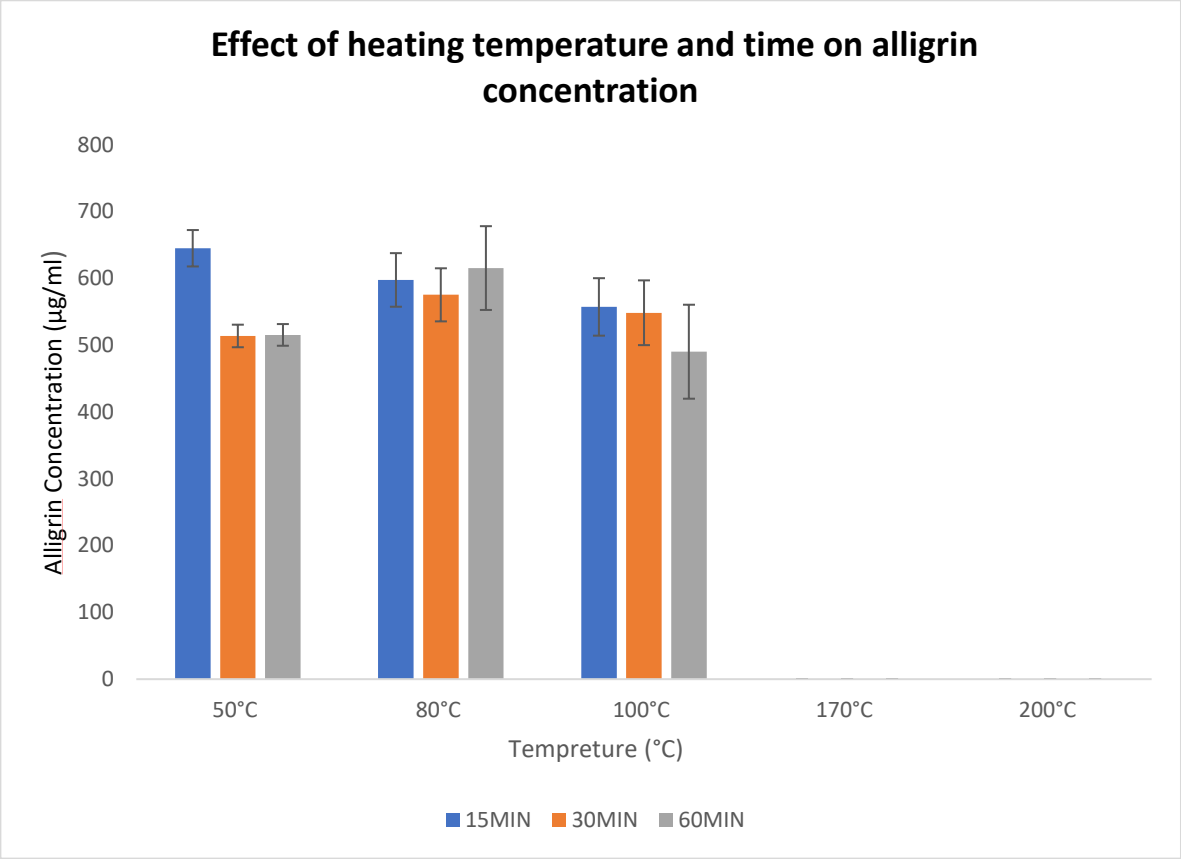

Figure 2.55: Thermal stability profile of alligrin at different temperatures." Values are mean ± SD, n = 3"

In contrast, at higher temperatures (170-200 °C), alligrin showed complete thermal degradation. LC-MS analysis showed the formation of oxidised sulfur-containing products, which were putatively assigned as allyl thiosulfate ($C_3H_5O_3S_2$, *m/z* 152.96) and allyl dithiosulfate ($C_3H_5O_3S_3$, *m/z* 184.93) on the basis of their accurate masses and fragmentation patterns (Figure 2.56). The ion tentatively assigned as allyl thiosulfate gave fragment ions at *m/z* 80.96 ($[HSO_3]^-$), *m/z* 111.92 ($[S\text{-}SO_3]^-$), and *m/z* 73.01 ($[C_3H_5S]^-$), consistent with a sulfonate-thiosulfate system. Similarly, the ion putatively assigned as allyl dithiosulfate gave fragments at *m/z* 143.90 ($[S\text{-}S\text{-}SO_3]^-$), *m/z* 112.94 ($[HS\text{-}SO_3]^-$), and *m/z* 79.95 ($[SO_3]^-$) (LC-MS data in appendix). These assignments are based on mass spectrometric data alone. Confirmation would require comparison with authentic standards or further spectroscopic characterisation such as NMR. Interestingly, related compounds such as sodium 2-propenyl

thiosulfate have also been reported in garlic extracts heated in hot water [210], which supports the proposed assignments

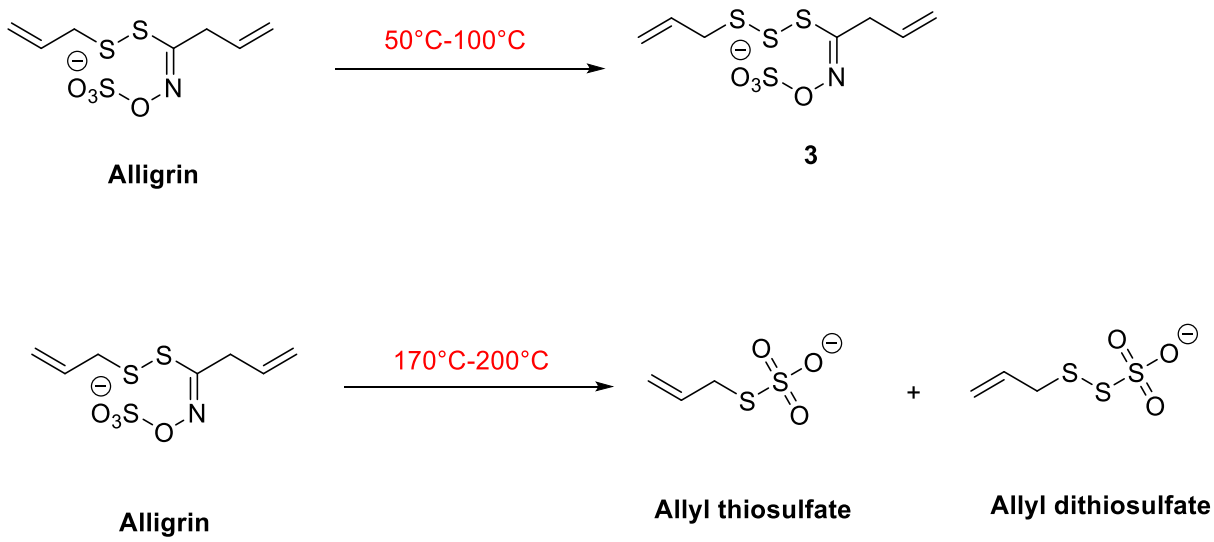

Figure 2.56: Proposed thermal degradation products of alligrin at 50-100 °C and 170-200 °C.

These findings suggest that milder cooking methods, such as boiling or steaming, may preserve most of alligrin's structure and activity, whereas frying or roasting at high temperatures can lead to its breakdown and a loss of its bioactive potential.

2.1.8 Studying myrosinase catalytic hydrolysis of glucoraphanin in presence of allicin

The next stage in these studies involved applying the previously described novel reaction to another glucosinolate specifically glucoraphanin which derived from broccoli. Investigating how glucoraphanin reacts with allicin under similar conditions can produce novel compound might be more potent than alligrin.

2.1.8.1 HPLC analysis of glucoraphanin activation by myrosinase in phosphate buffer

Using the same method applied to sinigrin in Section 2.1.2.3, glucoraphanin was incubated with myrosinase in phosphate buffer and analysed by HPLC. The chromatogram (Figure 2.57) showed a dominant peak at a retention time of 7.2 min, confirming successful myrosinase-catalysed hydrolysis of glucoraphanin and production of sulforaphane as the principal product [211]. This validates that myrosinase remained fully active towards glucoraphanin under the

assay conditions, providing the basis for subsequent investigation of its hydrolysis in the presence of allicin.

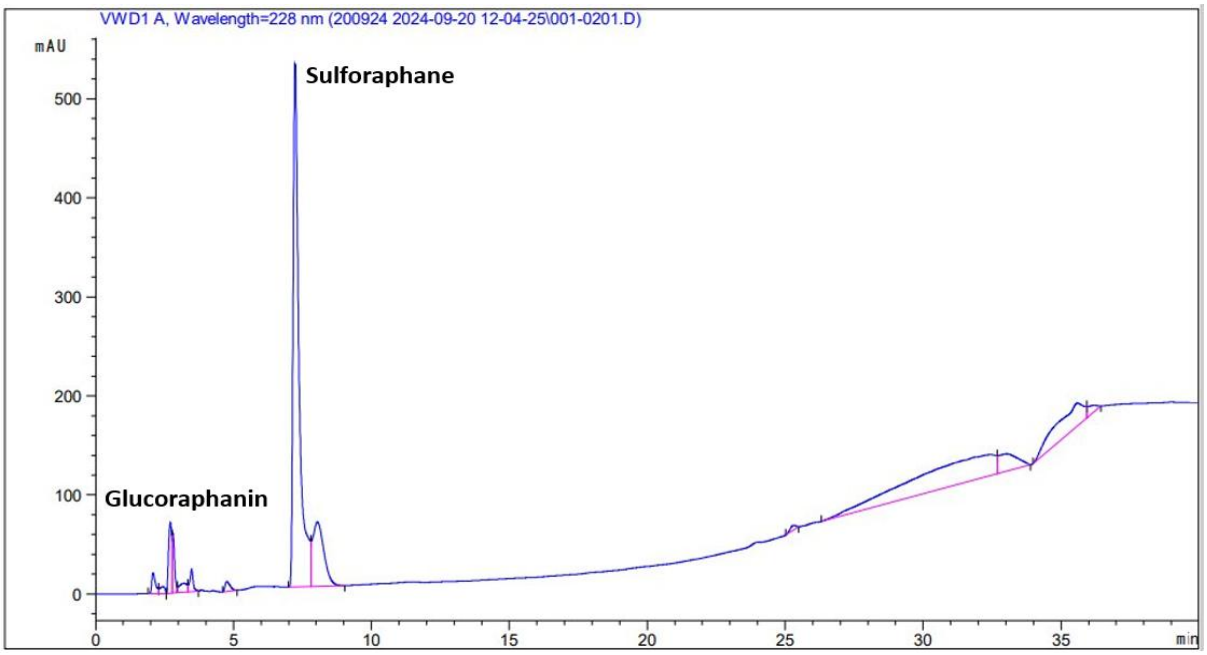

Figure 2.57: Analytical HPLC chromatograms of sulforaphane obtained by hydrolysis of glucoraphanin via myrosinase at retention time 7.2 min.

2.1.9 Myrosinase catalytic hydrolysis of glucoraphanin in presence of garlic organosulfur compounds

2.1.9.1 Enzymatic reaction in acetonitrile (MeCN)/phosphate buffer

To investigate the interaction between garlic-derived organosulfur compound (allicin) and the hydrolysis intermediate of glucoraphanin, the same optimized experimental conditions established for the sinigrin-allicin reaction were applied and monitored by ^{1}H-NMR (section 2.1.4.2) (Figure 2.58-2.59).

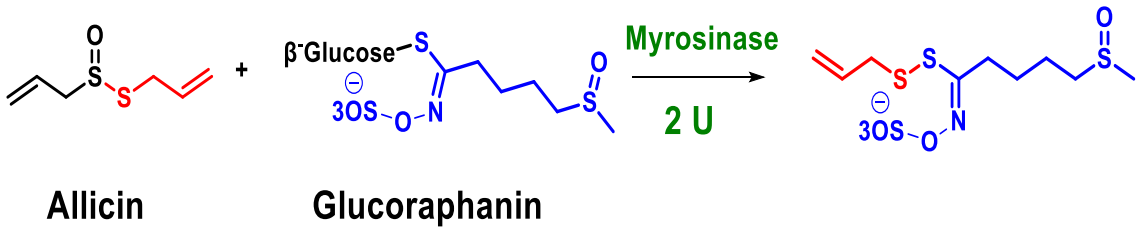

Figure 2.58: Reaction scheme showing the enzymatic interaction between allicin and glucoraphanin in the presence of 2 U of myrosinase using 25% (v/v) acetonitrile in phosphate buffer (pH 6) as solvent. The reaction yields a novel sulfur-containing compound formed through coupling of the allicin-derived allyl sulfide moiety with the glucosinolate aglycone intermediate.

The ^{1}H-NMR spectrum (500 MHz, D_2O) of the myrosinase-catalysed reaction between glucoraphanin and allicin (Figure 2.59) revealed new signals at δ 5.4 ppm and δ 3.6 ppm, consistent with the formation of a novel compound. These resonances are attributed to the interaction between the reactive aglucone intermediate generated upon myrosinase-catalysed hydrolysis of glucoraphanin and allicin. The resulting product, [(Z)-[5-(methylsulfinyl)-1-(prop-2-en-1-yldisulfanyl) pentylidene] amino] sulfate. was designated **alliphanin** a name derived from *alli-* (allicin) and *-phanin* (glucoraphanin) following the nomenclature established for alligrin.

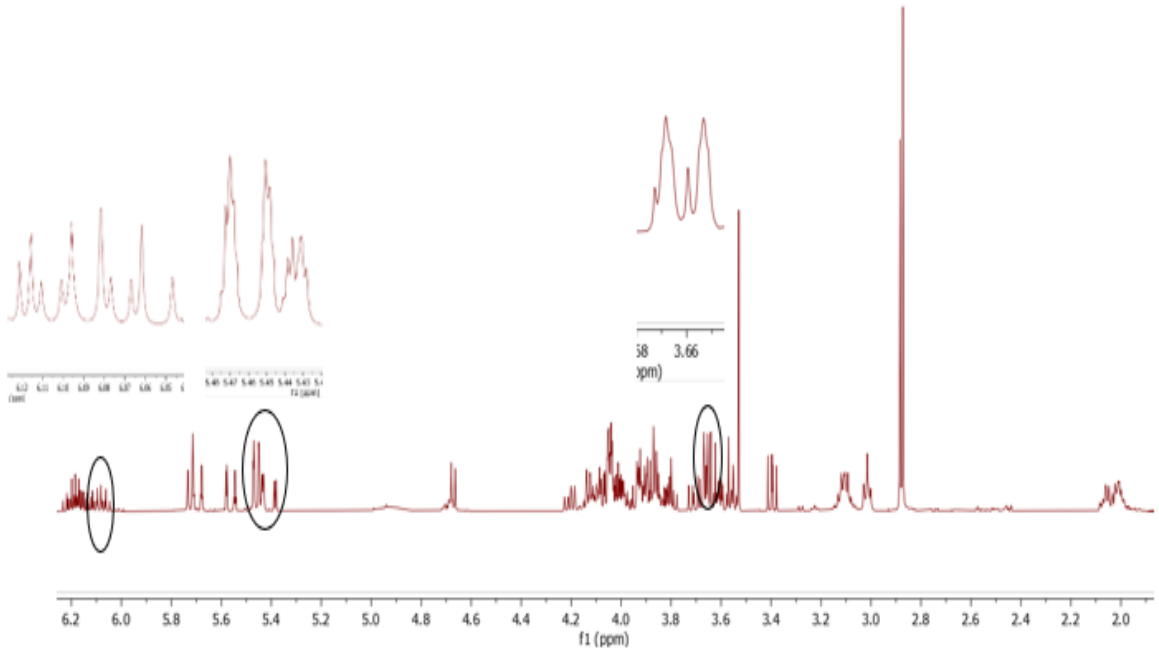

Figure 2.59: ^{1}H-NMR spectra (500 MHz, D_2O) of enzyme catalytic mixture reaction of glucoraphanin and allicin with myrosinase.

2.1.10 Isolation, purification, and elucidation of alliphanin by analytical methods

Following the optimisation of the reaction between the glucoraphanin hydrolysis intermediate and allicin, the same procedure used for the sinigrin-allicin system was applied to isolate and characterise the resulting products.

2.1.10.1 High-performance liquid chromatography (HPLC)

The analytical HPLC chromatogram of the glucoraphanin-allicin reaction mixture demonstrated clear separation of all major components under the same optimised chromatographic conditions. Glucoraphanin eluted at a retention time of 2.9 minutes, followed by the newly formed compound alliphanin at 4.6 minutes. Sulforaphane, the primary enzymatic hydrolysis product of glucoraphanin, appeared at 7.2 minutes, while allicin was detected at 9.9 minutes (Figure 2.60).

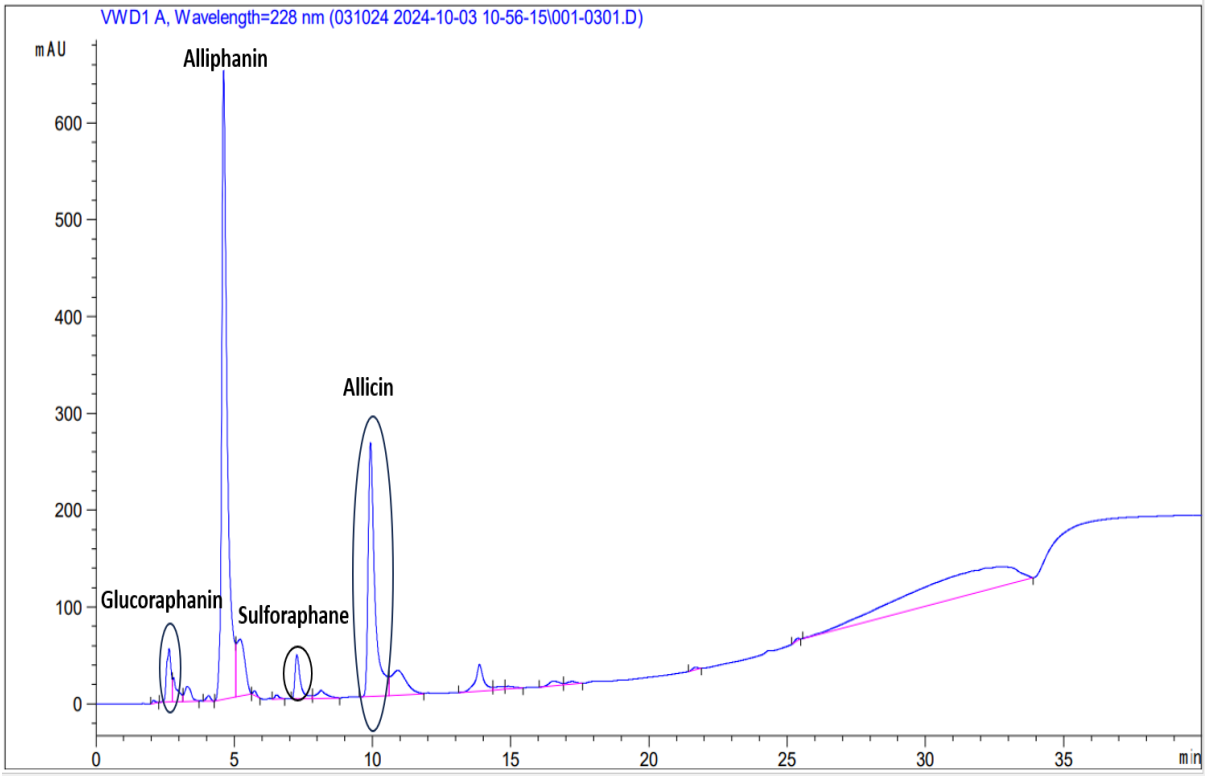

Figure 2.60: HPLC chromatogram of the allicin, glucoraphanin and myrosinase reaction mixture.

2.1.10.2 Preparative high-performance liquid chromatography (Prep-HPLC)

The preparative HPLC protocol previously optimised for the sinigrin-allicin system (Section 2.1.4.2) was applied directly to isolate alliphanin from the glucoraphanin-allicin reaction mixture. Using an injection volume of 750 µL, alliphanin eluted at a retention time of 4.2

minutes with complete baseline separation from all neighbouring peaks (Figure 2.61), confirming successful isolation of the target compound yielding 1mg.

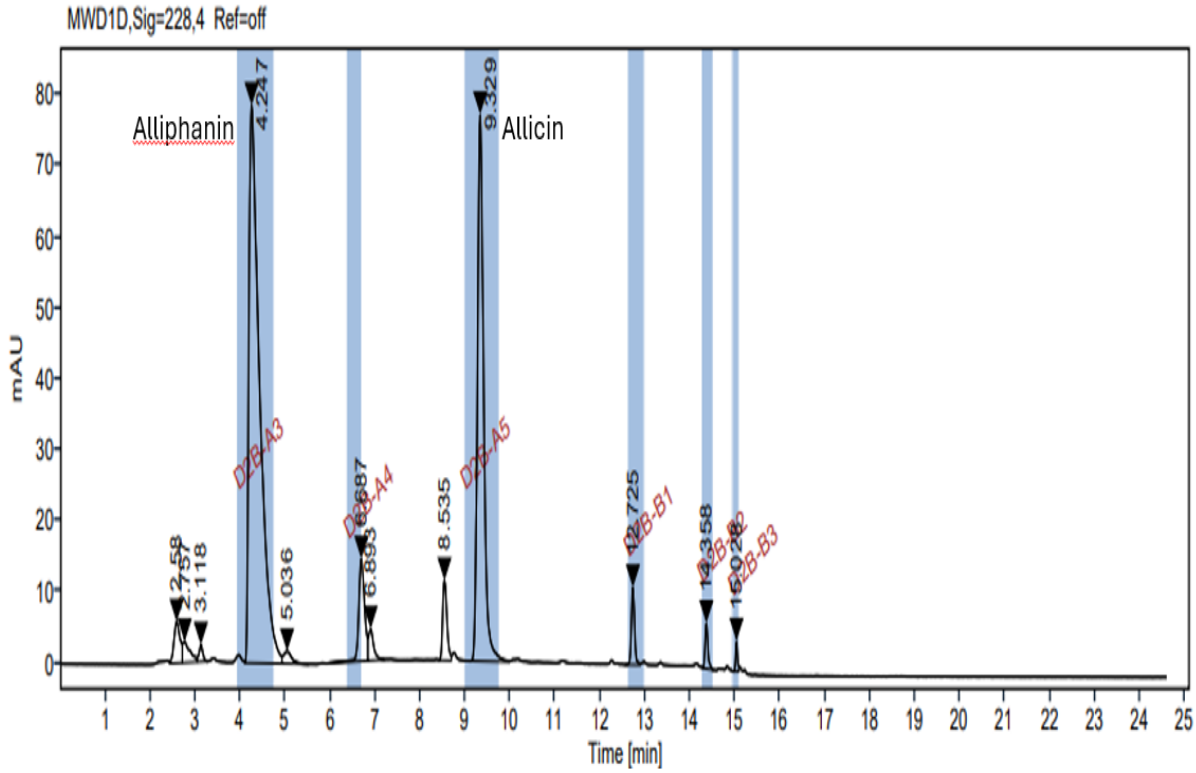

Figure 2.61: Preparative reversed-phase HPLC chromatogram of the reaction mixture showing the separation of alliphanin and its rearrangement products. The alliphanin fraction was collected between 4.2 and 5.0 minutes using the same optimized preparative HPLC conditions previously established for the sinigrin-allicin reaction.

2.1.11Structure elucidation of alliphanin

2.1.11.1 1D-Nuclear magnetic Resonance (1D-NMR)

The ^{1}H NMR spectrum of prep-HPLC purified alliphanin showed characteristic signals consistent with the proposed sulfur-linked structure (Figure 2.62). The vinylic proton signal appeared as a doublet of doublet of triplets at δ 5.89 ppm (ddt, J = 17.4, 10.0, 7.5 Hz, 1H), while the terminal methylene protons of the allyl group resonated as a multiplet between δ 5.28-5.20 (m, 2H), confirming the presence of an intact allyl moiety from allicin. The methylene protons adjacent to sulfur were observed at δ 3.46 (dt, J = 7.5, 0.9 Hz, 2H), characteristic of deshielding caused by S-CH_2 coupling. Additional multiplets at δ 3.01-2.90 (m, 2H) and δ 2.87-2.82 (m, 2H) correspond to methylene protons located near the sulfoxide and disulfide linkages, respectively, while a singlet at δ 2.71 (s, 3H) was assigned to the methyl

group attached to the sulfinyl sulfur. The aliphatic multiplet at δ 1.88-1.79 (m, 4H) was attributed to methylene protons within the extended aliphatic chain. Together, these spectral features confirm the coexistence of allylic, sulfide, and sulfinyl environments, providing strong evidence for the formation of a sulfur-bridged hybrid structure consistent with the proposed alliphanin structure.

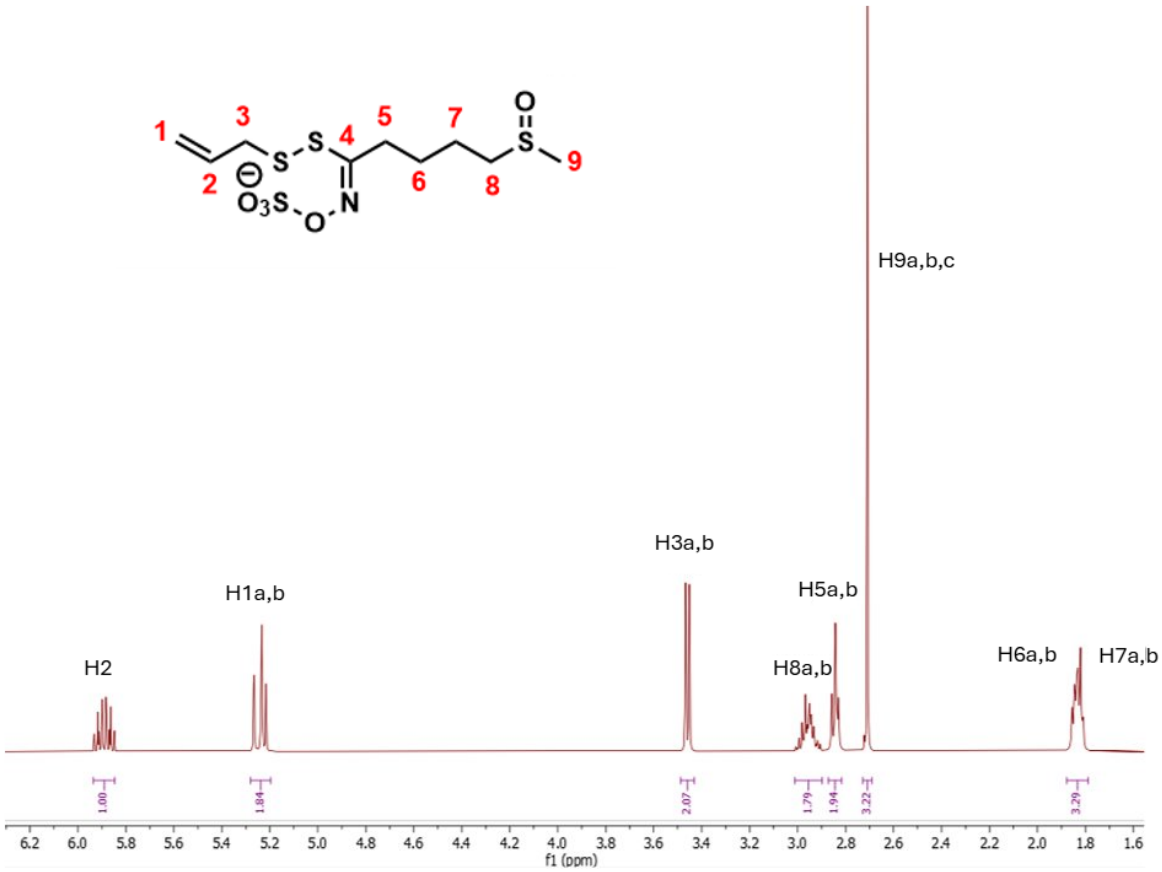

Figure 2.62 :¹H-NMR spectrum (500 MHz, D_2O) of alliphanin.

The ^{1}H-^{1}H COSY spectrum of alliphanin (Figure 2.63) confirmed the connectivity of proton pairs within the proposed structure. Cross-peaks observed at δ 5.8, and δ 5.2 ppm confirm the allyl system derived from the allicin moiety, whilst correlations in the δ 1.8-2.9 ppm region confirm the sequential CH_2-CH_2 connectivity of the aliphatic chain derived from the glucoraphanin aglucone. The COSY data are fully consistent with the proposed structure of alliphanin, supporting the structural assignment made based on ^{1}H-NMR and confirming the integrity of the novel compound following preparative isolation.

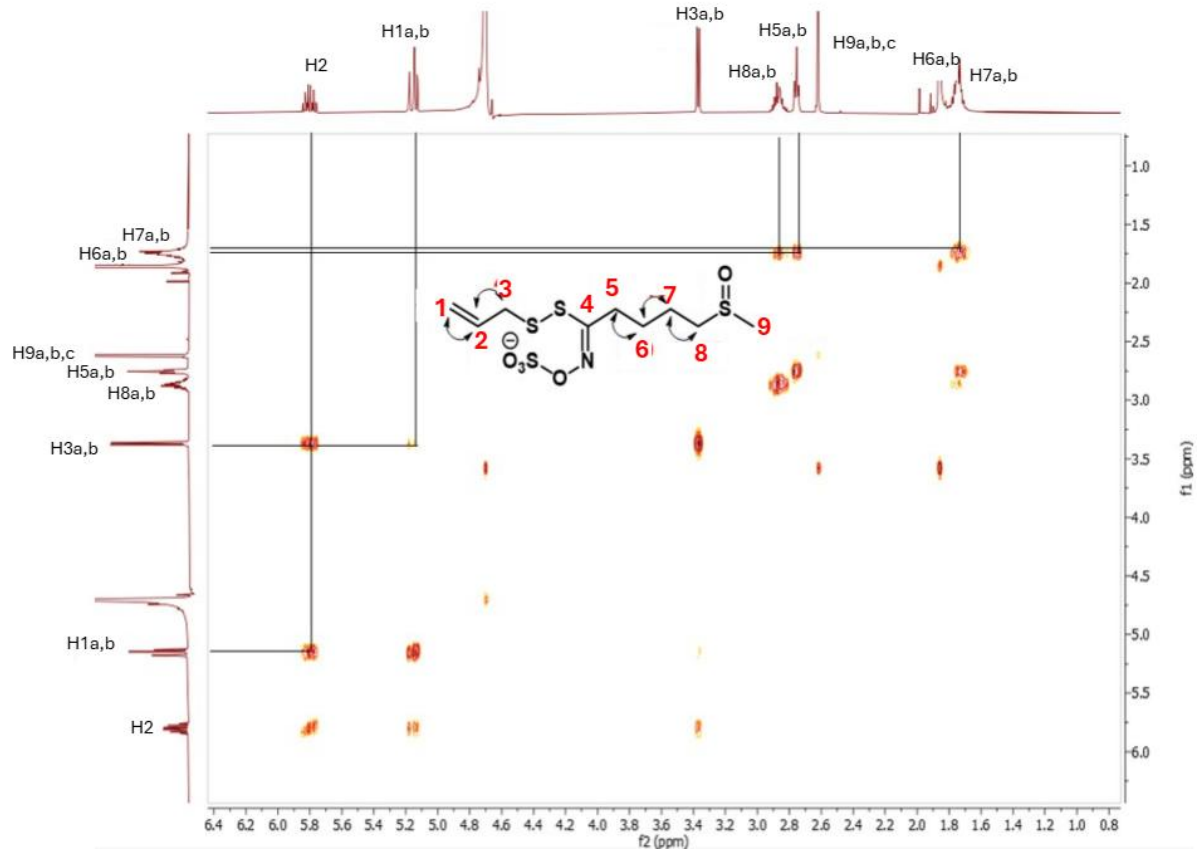

Figure 2.63: COSY-NMR spectrum (500 MHz, D_2O) of alliphanin

The ^{13}C NMR spectrum of alliphanin exhibited characteristic carbon signals consistent with the proposed sulfur-bridged structure (Figure 2.64). The downfield signal at δ 180.65 ppm was attributed to a quaternary carbon attached to sulfur and oxygen within the sulfated thiohydroximate moiety. Signals observed at δ 131.58, and δ 120.03 ppm were assigned to the vinylic carbons of the allyl group, verifying that the double bond remained intact after conjugation.

In the aliphatic region, peaks at δ 52.10, 42.29, and 36.33 ppm correspond to methylene and the methyl group carbons adjacent to sulfur atoms (CH_2-S=O, CH_2-S and S=O-CH_3), reflecting the deshielding effects characteristic of sulfur substitution. The remaining resonances at δ 30.35, 25.47 and 21.08 ppm were assigned to aliphatic methylene carbons further removed from the sulfur centres, representing the extended alkyl chain of the molecule.

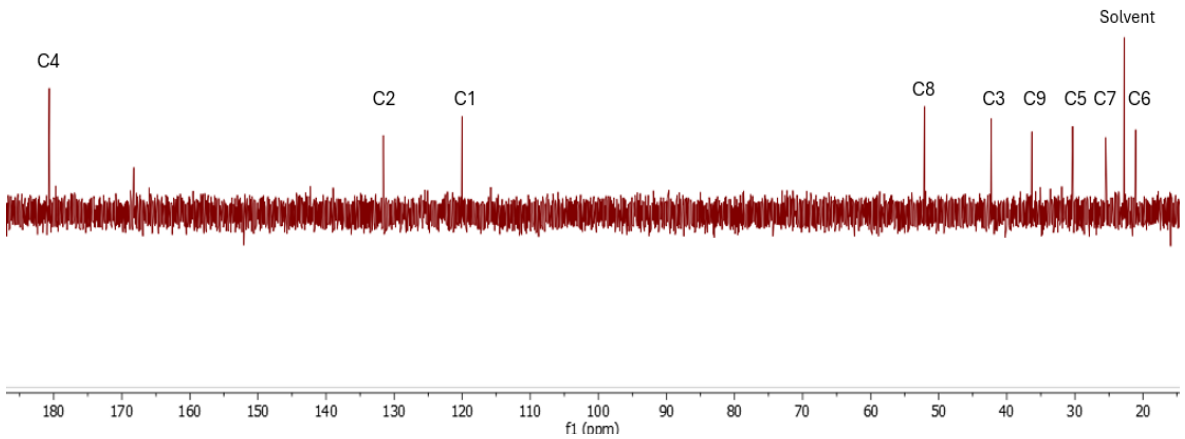

Figure 2.64: ^{13}C-NMR spectrum (126 MHz, D_2O) of alliphanin.

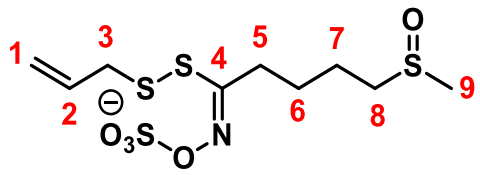

Figure 2.65: Chemical structure of alliphanin with atom numbering; green = proton (^1H) assignments, red = carbon (^{13}C) assignments.

Table 2.6: ^1H, ^{13}C and COSY- NMR data of alliphanin measured at 500 MHZ in D_2O.

	^{1}H NMR	COSY	^{13}C NMR
Position	**δ H (J in Hz)**	J_{HH}	**δ C (Hz)**
1 -CH_2	5.28-5.20 (m, 2H) ppm	H-1a, b and H2	120 ppm
2 -CH	5.88 ppm (ddt, J=17.4, 10.0, 7.5 Hz, 1H) ppm	H-2 and H-1a, b H-2 and H-3a, b	131 ppm
3 -CH_2	3.43 (dt,7.5, 0.9 Hz, 2H) ppm	H-3a, b and H-2	42.2 ppm
4	-	-	180.65 ppm
5 -CH_2	2.87-2.82 (m, 2H) ppm	H-5a, b and H-6a, b	30.1 ppm
6,7 -CH_2	1.88-1.79 (m,4H) ppm	H-6a, b and H-7a, b	21, 25.4 ppm
8 -CH_2	3.01-2.90 (2H) ppm	H-7a, b and H-8a, b	52.1 ppm
9 -CH_3	2.71 (S, 3H) ppm	-	36.3 ppm

2.1.12Liquid chromatography-mass spectrometry (LC-MS)

The negative ion mode of LC-HR-ESI-MS showed a prominent molecular ion peak at m/z 345.989 $[M-H]^-$, which aligns with the calculated theoretical value for the molecular formula $C_9H_{16}NO_5S_4$ (calculated: 345.989 Da), confirming the proposed molecular composition of alliphanin (Figure 2.66).

Fragmentation analysis further supported this assignment. The dominant fragment at m/z 95.95 ($[HSO_4]^-$) with 100% relative abundance corresponds to a sulfate ion, characteristic of sulfonated glucosinolate derivatives. Additional diagnostic ions included m/z 240.95, corresponding to cleavage within the sulfoxide side chain while retaining the sulfonate moiety, and m/z 304.95, which reflects the partial loss of an allyl group. Collectively, these spectral features provide strong evidence for the proposed structure of alliphanin as a sulfur-rich conjugate formed through the interaction of allicin and glucoraphanin hydrolysis intermediates.

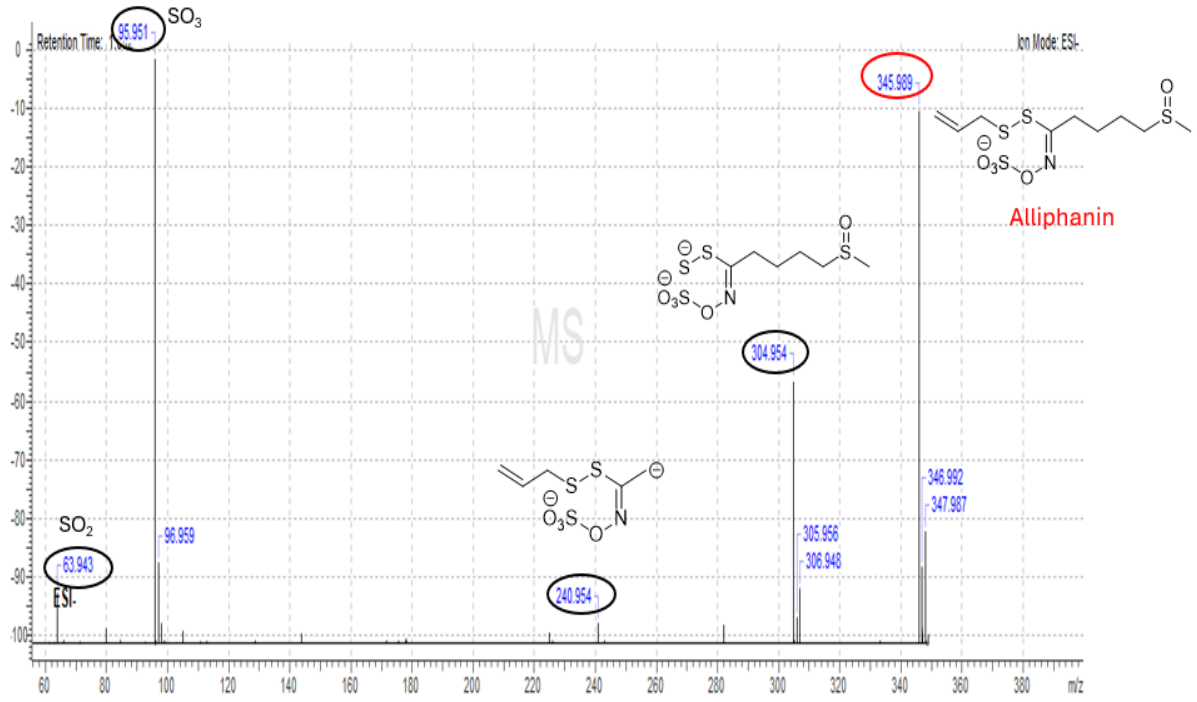

Figure 2.66: LC-ESI-MS² spectrum of alliphanin.

2.1.13Stability profile of alliphanin

Similar to alligrin, purified alliphanin shows good stability at -20 °C but undergoes gradual structural transformation when stored within the crude reaction mixture, suggesting a natural capacity for further rearrangement under these conditions. HPLC and LC-MS studies confirmed the formation of multiple rearrangement products derived from alliphanin, consistent with the reactivity characteristic of sulfur-rich organosulfur compounds (Figure 2.67).

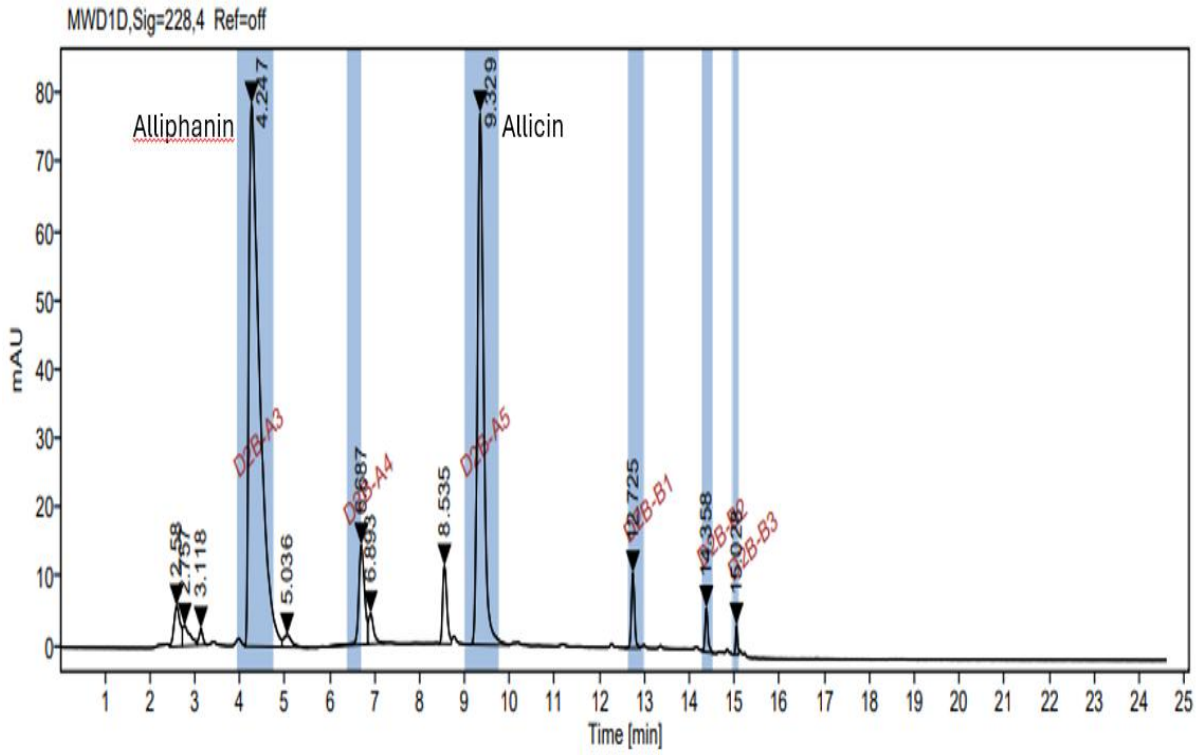

Figure 2.67: Prep-HPLC chromatogram of the glucoraphanin-allicin with myrosinase reaction mixture.

The first peak, eluting at a retention time of 6.3 minutes (Figure 2.67), was collected in a small quantity (less than 1 mg) sufficient for LC-MS analysis to confirm its structural features.

The LC-ESI-MS² spectrum of the purified compound **19** showed a deprotonated molecular ion peak at *m/z* 377.9639 [M-H] ⁻, consistent with the molecular formula $C_9H_{16}NO_5S_5^-$ (Figure 2.68). The isotopic pattern, featuring an M+2 peak around 22%, confirmed the presence of multiple sulfur atoms within the molecule. Fragmentation analysis revealed several key ions supporting the proposed structure of the alliphanin rearrangement product (compound **19**). Characteristic sulfate-related fragments were detected at *m/z* 95.95 ($[HSO_4]^-$) and *m/z*

111.93 ([NH_2-O-SO_3] $^-$), both typical of sulfonated glucosinolate derivatives. The fragment at m/z 257.96 corresponds to the loss of the sulfinyl-containing chain. The fragment at *m/z* 272.98 suggested partial S-S bond cleavage while retaining the sulfonyl functionality, whereas *m/z* 336.92 indicated the loss of an allyl moiety. Notably, the sulfur-rich fragments at *m/z* 95.95 and 111.93 were also present in the fragmentation spectrum of alliphanin, suggesting a common structural origin. Collectively, these findings strongly support the proposed structure of compound **19** as a rearranged sulfur-containing derivative of alliphanin.

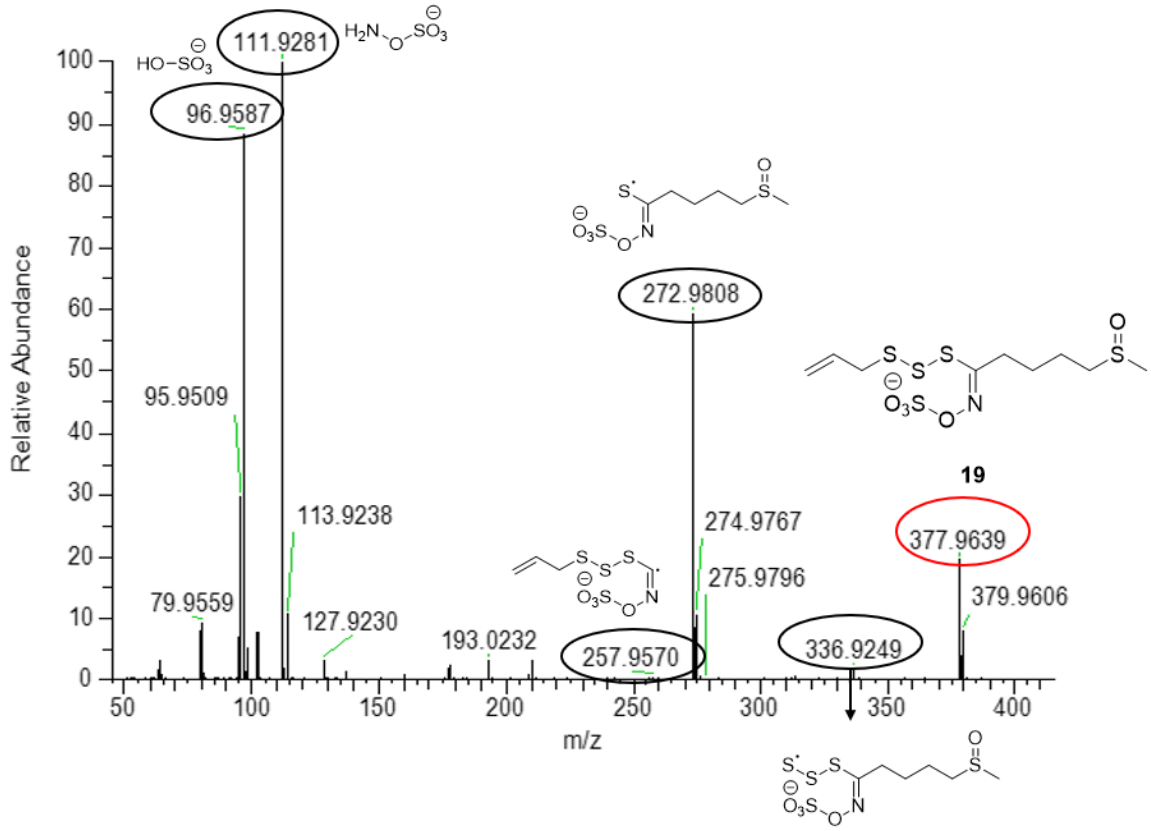

*Figure 2.68: LC-ESI-MS² spectrum of the purified compound **19**.*

The proposed mechanism for the formation of compound **19** (Figure 2.69) closely parallels the mechanism proposed for compound **3** (section 2.1.6), suggesting a shared sulfur-exchange pathway between these structurally analogous organosulfur systems (Figure 2.31).

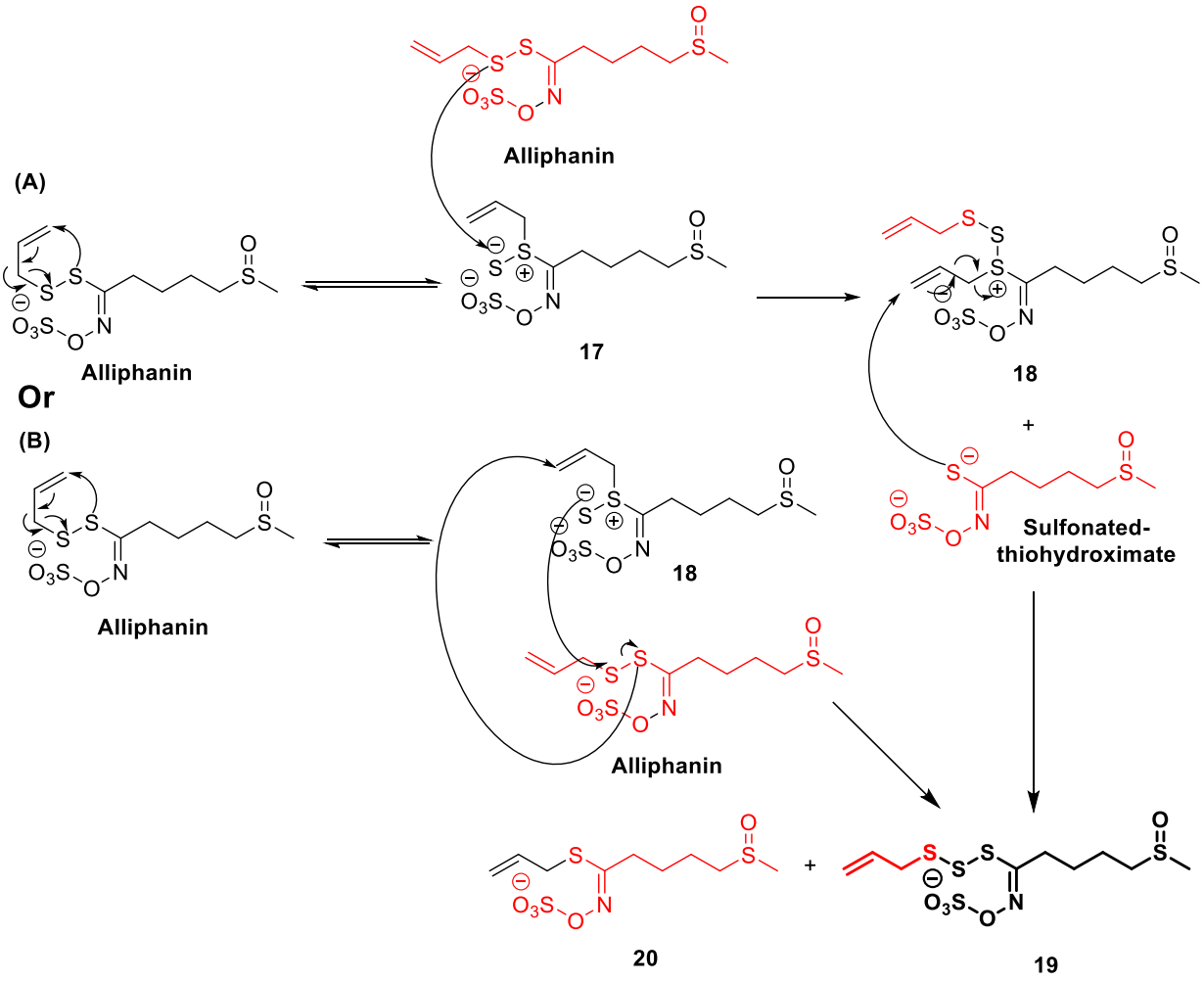

*Figure 2.69: Proposed plausible mechanism for the formation of compound **19**.*

The second peak, eluting at a retention time of 12.7 minutes (Figure 2.67). The LC-ESI-MS² spectrum of compound **21** showed a molecular ion at m/z 417.9958 [M-H] ⁻, consistent with the molecular formula $C_{12}H_{20}NO_5S_5$, indicative of a complex multi-sulfer atoms structure (Figure 2.70). Fragmentation analysis revealed several diagnostic ions that support this structure. The peaks at m/z 95.95 and 111.93 correspond to the same characteristic fragments observed in compound **19**, confirming a shared sulfur-nitrogen-oxygen core structure. The fragment at m/z 272.98 represents cleavage within the sulfur chain while retaining the sulfonyl side chain and sulfate group, whereas ions at m/z 343.97 and 376.95 indicate sequential losses of thio-allyl and allyl group, characteristic of extended sulfur linkages. Collectively, these findings confirm that compound **21** ($C_{12}H_{20}NO_5S_5$) results from the oxidative rearrangement of alliphanin, yielding a derivative featuring an ajoene-like chain.

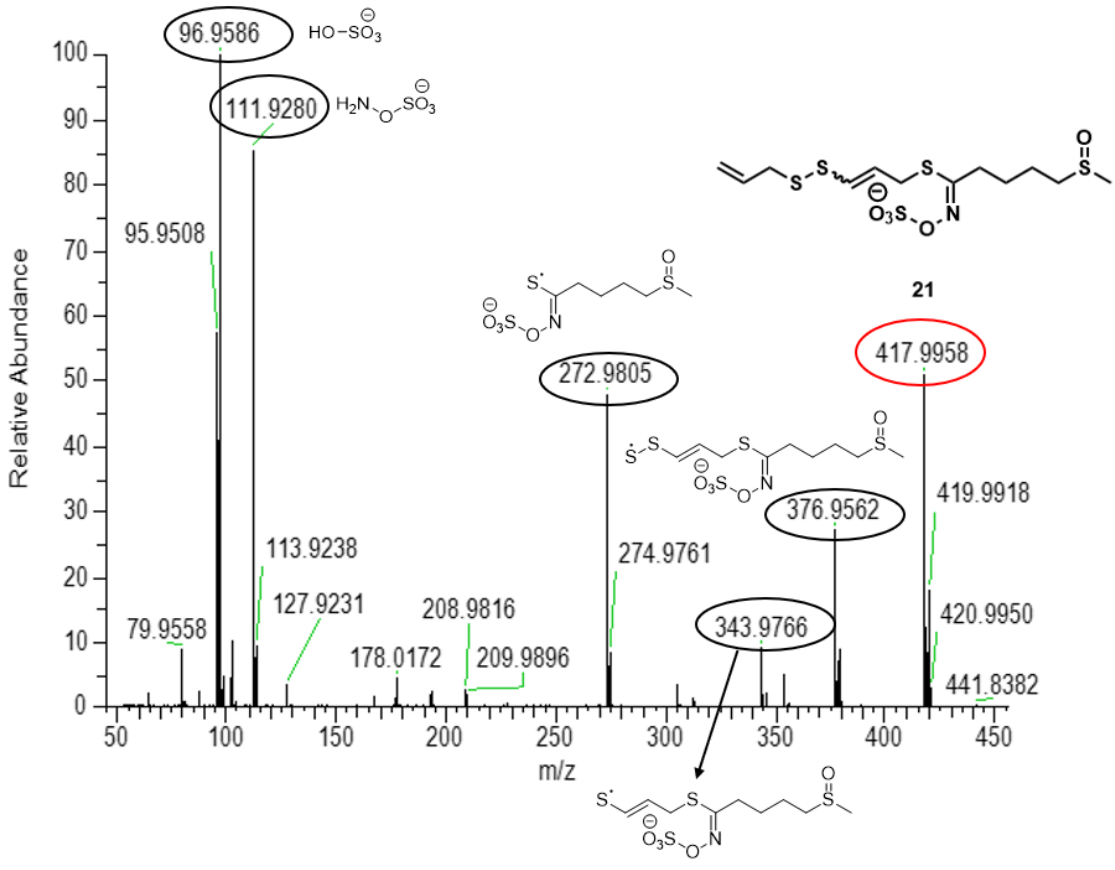

*Figure 2.70: LC-ESI-MS² spectrum of compound **21**.*

The proposed mechanism illustrates the formation of compound **21** through a sulfur exchange and rearrangement process initiated by the interaction between alliphanin and free allicin (Figure 2.71). The reaction begins with the sulfur atom of alliphanin (or allicin) attacking the sulfur atom of allicin, generating sulfonated-thiohydroximate and compound **5**. In compound **5**, proton transfer and subsequent elimination of allyl sulfenic acid (allyl-SOH) produce compound **6**, a reactive allyl disulfide compound that rearranges into an ajoene-like structure. In the following step, sulfonated-thiohydroximate undergoes sulfur-sulfur exchange with compound **6**, resulting in the formation of compound **21**, which features a multi-sulfer atoms compound similar to the characteristic structural motif of ajoene.

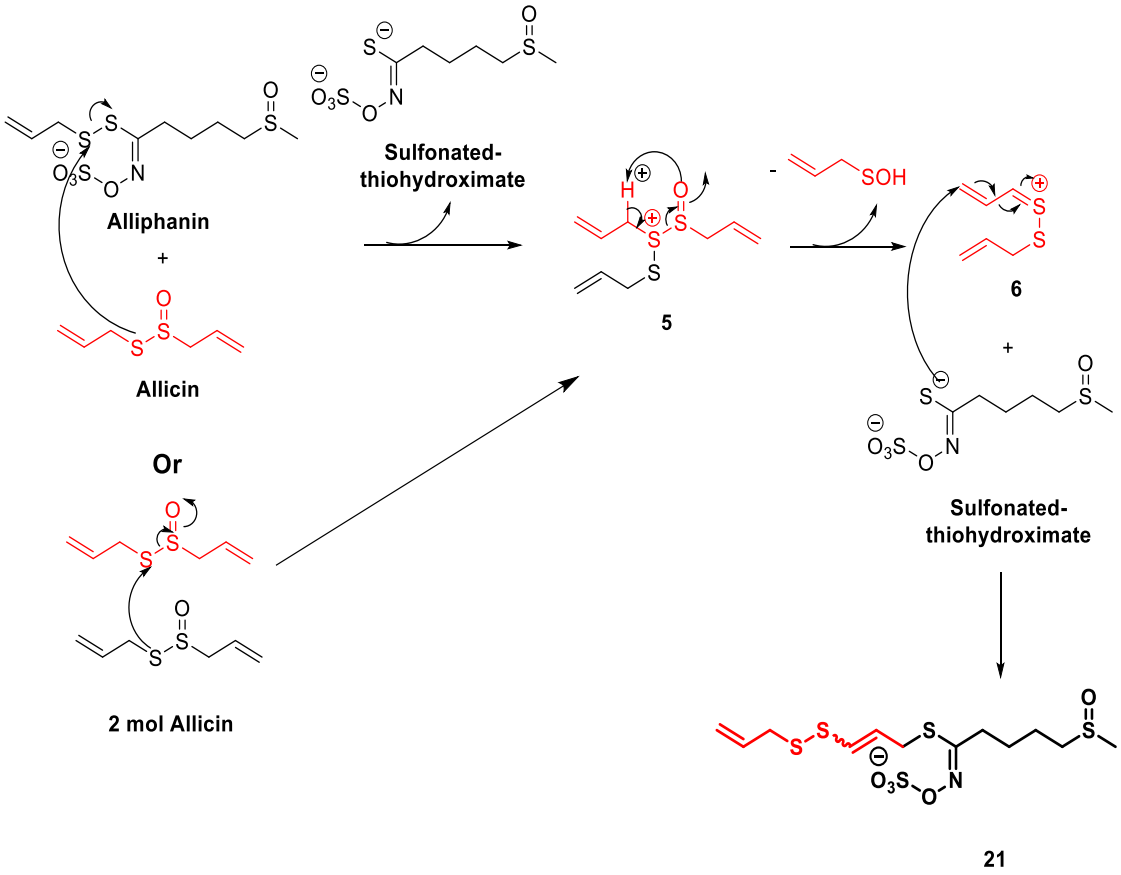

*Figure 2.71: Proposed mechanism for the formation of compound **21**.*

The third peak, eluting at a retention time of 14.3 minutes (Figure 2.67), was collected in a small quantity that was sufficient for LC-MS analysis to determine its molecular composition.

The LC-ESI-MS² spectrum of compound **23** displayed a molecular ion peak at *m/z* 449.97 [M-H] ⁻, consistent with the molecular formula $C_{12}H_{20}NO_5S_6^-$, confirming a structure containing six sulfer atoms (Figure 2.72). The isotopic distribution further supported the presence of multiple sulfur atoms. Fragmentation analysis revealed a key ion at m/z 385.97, corresponding to the loss of the sulfoxide group from the molecular ion. The fragment at m/z 304.95 corresponds to the further loss of an ajoene-like fragment, while the ion at m/z 272.98 indicates further sulfur cleavage with retention of both sulfoxide and sulfonate moieties, characteristic of extended sulfur chain rearrangement.

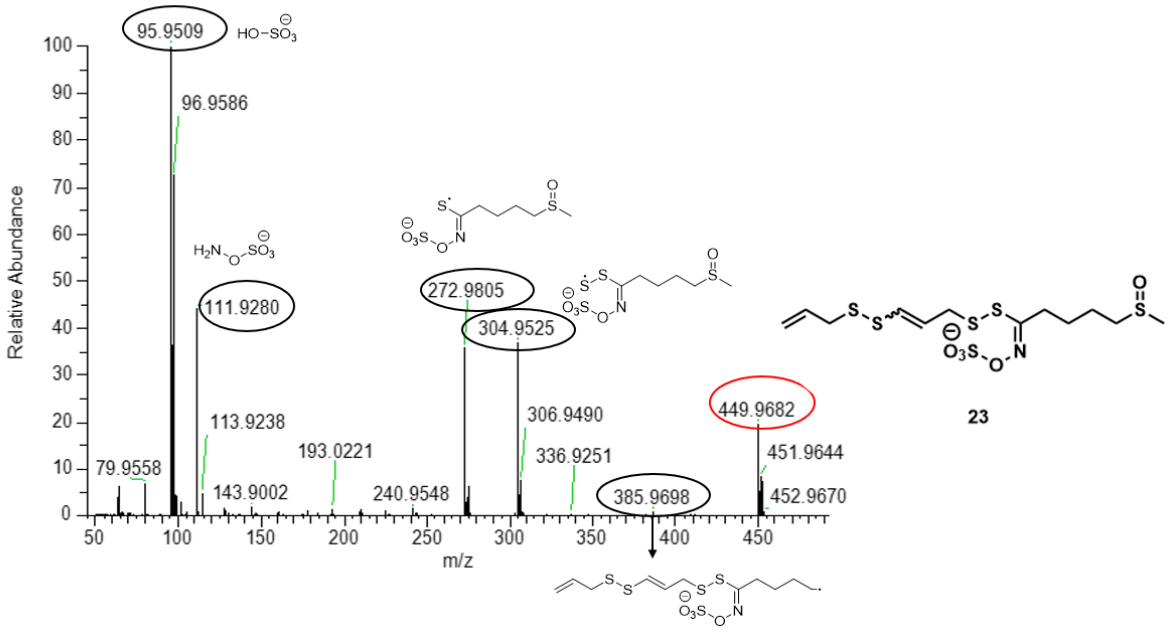

*Figure 2.72: LC-ESI-MS² spectrum of compound **23**.*

The proposed mechanism outlines the formation of compound **23** through a multi-step sulfur exchange and rearrangement process initiated by the interaction between alliphanin and allicin (Figure 2.73). The reaction begins when the sulfur atom of alliphanin (or allicin) attacks the sulfur centre of allicin, generating compound **5**. Subsequent proton transfer and elimination of allyl sulfoxide (allyl-SOH) lead to the formation of compound **6**.

In the subsequent step, compound **6** undergoes a sulfur-sulfur exchange with compound **17** forming compound **22**. Further reaction with allyl sulfide results in the generation of compound **23**, characterized by an extended six sulfer atoms that closely resembles the backbone of ajoene derivatives and diallyl sulfide as by product.

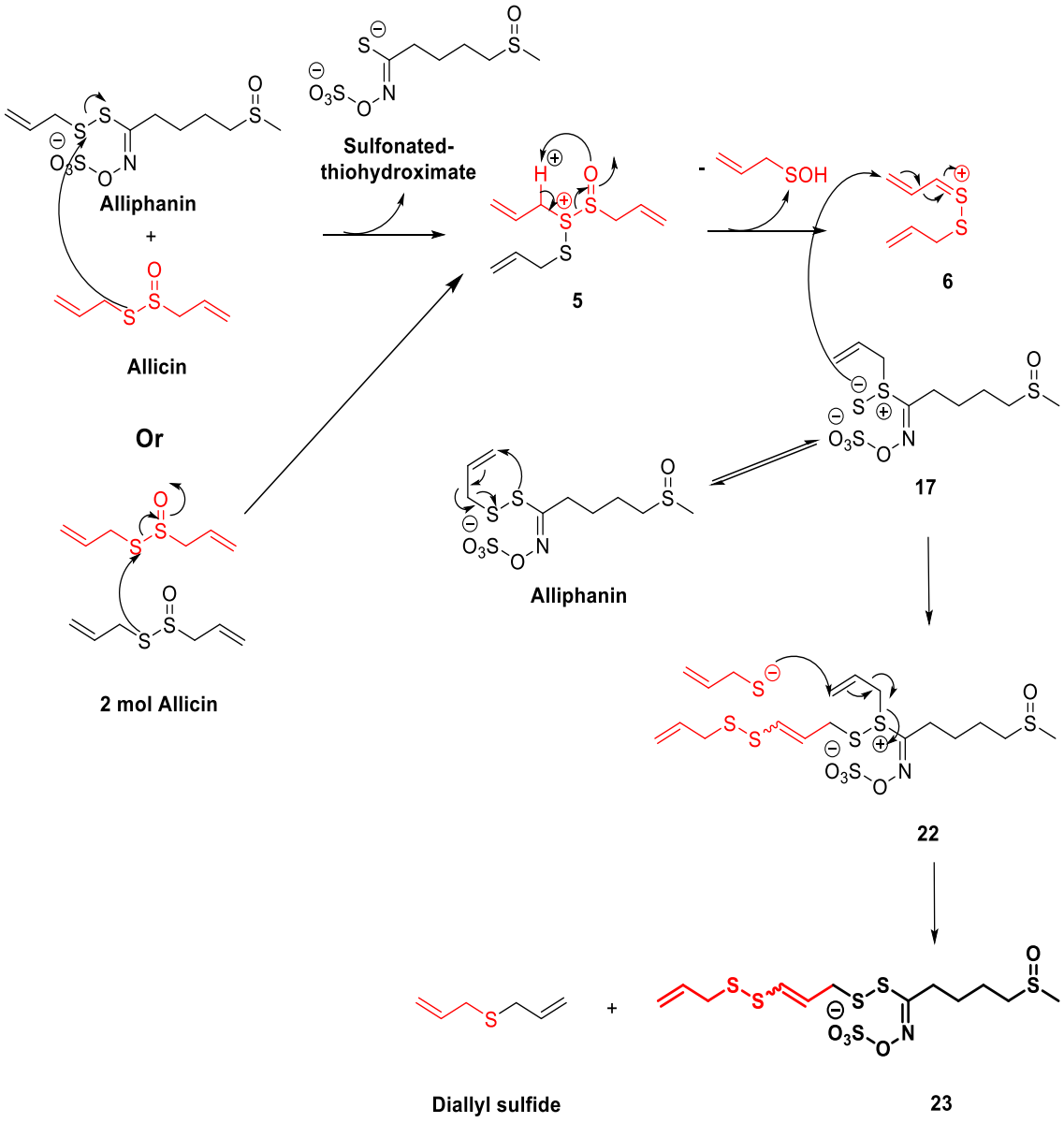

*Figure 2.73: Proposed plausible mechanism for the formation of compound **23**.*

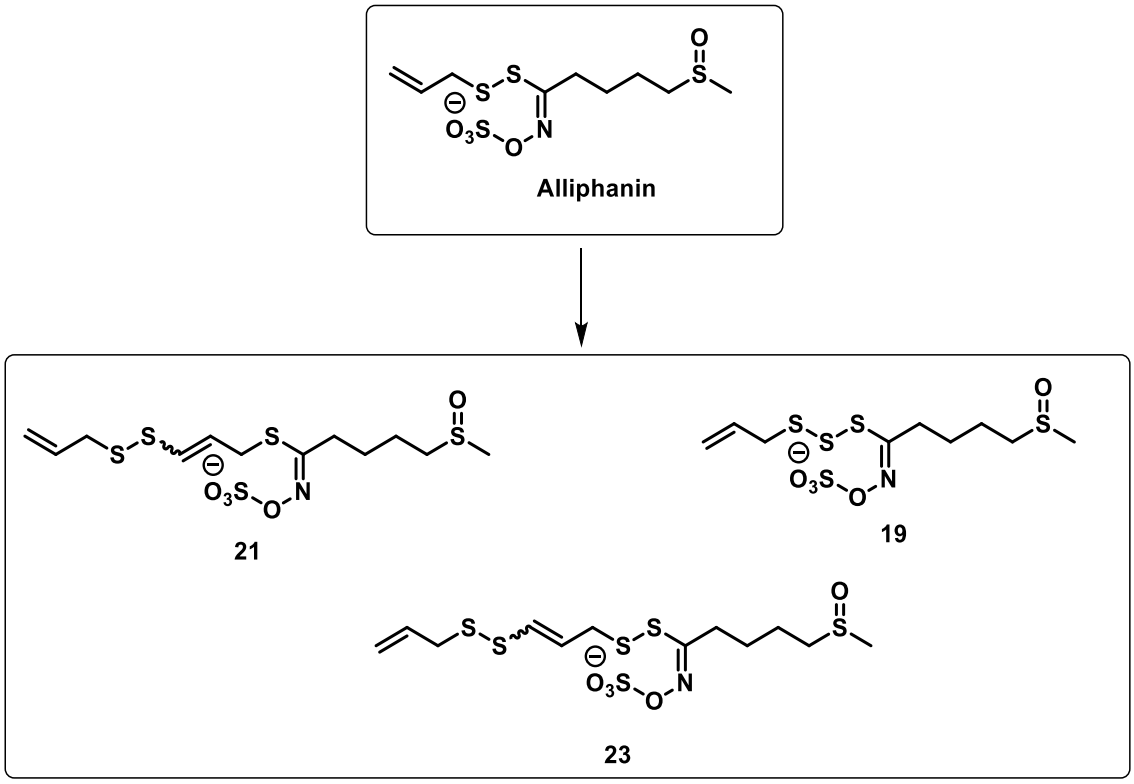

Figure 2.74: Structural overview of alliphanin and its secondary rearrangement products.

2.1.14Summary and conclusion

This chapter presented a comprehensive investigation into the thiol reactivity of hydrolysis intermediates derived from glucosinolates and their interaction with the garlic-derived organosulfur compound allicin. It explored for the first time how sulfur-containing molecules from two different plant families *Allium* (garlic) and *Brassicaceae* (mustard, broccoli), can chemically interact to form completely novel compounds. This study addressed a significant gap in natural product chemistry, as previous studies had only explored the independent bioactivities of glucosinolate and allicin derived compounds, with no previous work had looked at whether their sulfur metabolites could directly react with each other.

The investigation began by elucidating the structural and reactivity profiles of individual reactants. Sinigrin and glucoraphanin were chosen as model glucosinolates from mustard and broccoli and were enzymatically hydrolysed by myrosinase to generate thiol-reactive aglycone intermediates.

Under the optimized conditions, the enzymatic hydrolysis of glucosinolates in the presence of allicin yielded previously unreported sulfur-containing compounds. When sinigrin was used

as the substrate, the reaction produced a novel molecule named alligrin, whereas glucoraphanin gave rise to a closely related compound was formed, which was identified as alliphanin.

The discovery of these compounds represents a new chemical class of organosulfur natural products, expanding the structural and mechanistic diversity of plant sulfur chemistry. The structural validation of alligrin through single-crystal X-ray diffraction provided clear evidence of the disulfide bridge linking the two plant-derived fragments and highlighted the presence of a sulfate moiety capable of influencing solubility, redox potential, and biological interactions.

Beyond their initial formation, both alligrin and alliphanin demonstrated sulfur reactivity, undergoing further rearrangement to yield a series of higher-order polysulfide derivatives containing four, five, six, and seven sulfur atoms. Mechanistic studies revealed that these transformations proceed via intermolecular self-rearrangement pathway through sulfur exchange, and cross-reactivity with residual allicin pathway, collectively generating a diverse array of complex polysulfide structures.

Thermal stability experiments mimicking cooking conditions revealed that alligrin undergoes partial decomposition to compound 3 observed at 50-100 °C, preserving structural integrity under mild cooking conditions such as boiling or steaming. At higher temperatures (≥170 °C), representative of frying or roasting, significant decomposition occurred yielding oxidised sulfur species including allyl thiosulfate and allyl dithiosulfate. These results suggest that culinary preparation methods could strongly influence the bioavailability and functional activity of such sulfur conjugates in food systems.

The findings of this chapter provide strong evidence that metabolites from *Allium* and *Brassicaceae* plants can chemically interact to form new sulfur-linked natural products through enzyme-mediated thiol-sulfur coupling. These results broaden our understanding of sulfur-based phytochemistry and open new avenues for the discovery of multifunctional natural products with potential antimicrobial, antioxidant, and anticancer activities. The next chapter will investigate whether these compounds can also be generated directly from crude mixtures of glucosinolate-producing plants and crushed garlic, enabling the use of alligrin and alliphanin as reference standards for HPLC analysis of natural plant preparations.

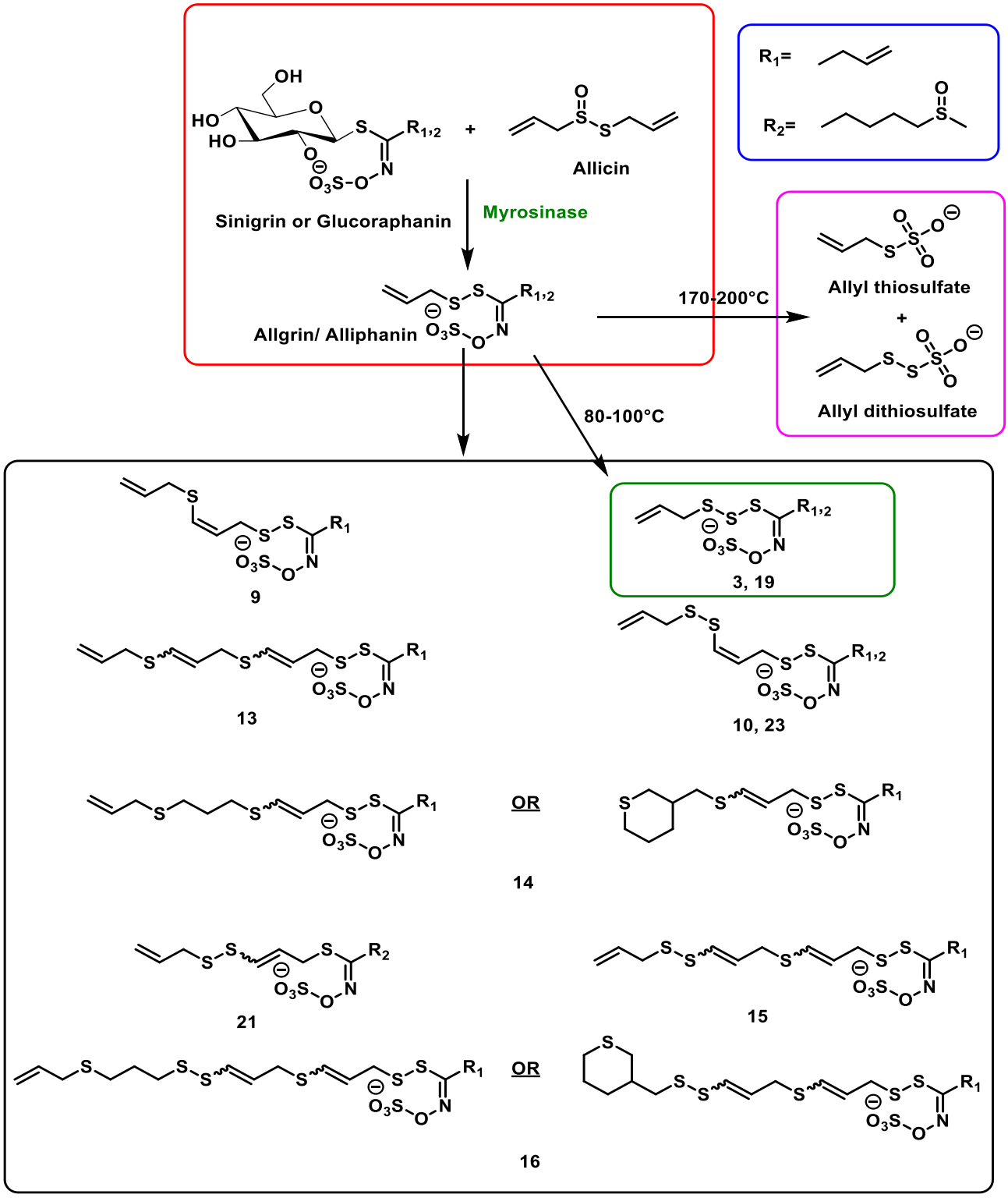

Figure 2.75: Summary of all compounds identified in this chapter.

3 Investigation of Alligrin and Alliphanin Formation in Crude Plants Mixtures

3.1 Introduction

In the previous chapter, the controlled enzymatic interaction between allicin and glucosinolates hydrolysis intermediates was shown to generate two novel sulfur-linked conjugates, alligrin and alliphanin.

The next question was whether these conjugates could also form naturally, outside the controlled model system. Many cooking practices involve combining garlic with glucosinolate-rich vegetables or spices such as mustard seeds and broccoli which contain endogenous myrosinase capable of activating glucosinolates. At the same time, alliinase in garlic rapidly generates allicin when the cloves are crushed. This creates a realistic biochemical environment in which reactive sulfur species from both plant families may interact.

Therefore, the reasoning of this chapter is to investigate whether sulfur-sulfur coupling reactions similar to those observed in vitro also occur in crude plants mixtures (in vivo), reflecting real-world food preparation and natural plant-plant interactions.

3.2 Aims of this chapter

The aim of this chapter is therefore to detect, identify, and confirm the formation of alligrin and alliphanin in crude mixtures of garlic with mustard seed powder or broccoli, using the HPLC method established in Chapter 2 alongside LC-MS analysis.

3.3 Analytical identification of individual plant extracts and mixture of two plants extract

3.3.1 Analytical identification of allicin from crude garlic extract

The crude extract of aqueous freshly crushed garlic was analysed by HPLC to confirm the presence of allicin prior to evaluating its reactivity with glucosinolate-rich plant materials. This step was essential to establish the allicin profile within garlic alone, serving as a reference

chromatographic fingerprint against which the reaction mixtures with mustard seed and broccoli could be confidently assessed.

The HPLC chromatogram of crude garlic extract recorded 30 minutes after crushing (Figure 3.1) revealed a clear and well-resolved allicin peak at a retention time of 9.9 minutes, fully consistent with that established for synthesised allicin in Chapter 2, confirming its identity under the same chromatographic conditions. The prominent peak intensity reflects both the natural abundance of allicin immediately following garlic crushing and the high sensitivity of detection at 228 nm, the wavelength at which thiosulfinates strongly absorb.

Quantification using the established calibration curve (Figure 3.2), following correction for all dilution factors, yielded an allicin content of 4.21 mg/g (25.95 µmol/g) of fresh garlic clove, in close agreement with previously reported values of 2.5-5.0 mg/g fresh weight [49, 212], confirming the validity of the extraction protocol and the reliability of the HPLC quantification method employed throughout this study.

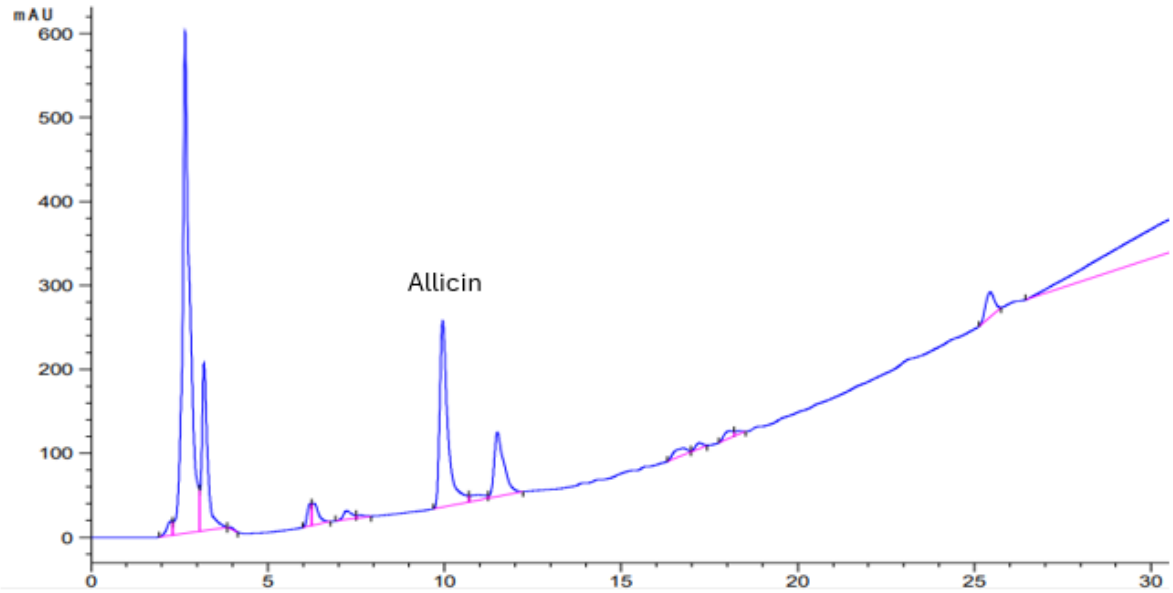

Figure 3.1: HPLC chromatogram of aqueous crude garlic extract 30 min after crushing.

3.3.1.1 Monitoring the formation, concentration and stability of allicin in fresh garlic

The formation and stability of allicin in aqueous freshly crushed garlic were monitored over a 60-minutes period using HPLC. Allicin levels increased progressively during the first 35-40 minutes, reaching a maximum before showing a slight decline toward 60 minutes (Figure

3.2a). This graph reflects the rapid but temporary nature of allicin biosynthesis catalysed by alliinase upon mechanical disruption of garlic tissue. The initial rise corresponds to active conversion of alliin to allicin, whereas the subsequent decrease is consistent with allicin's well-documented chemical instability as it readily undergoes degradation or conversion into secondary sulfur compounds such as polysulfides over time[49, 213]. These observations align with previously reported allicin kinetics, which show maximum peak formation within the first 30-40 minutes after homogenisation[213]. Importantly, identifying this maximum formation window is essential for the present study, as it establishes the optimal time point at which freshly generated allicin should be mixed with mustard seeds powder or broccoli to maximise the formation of the novel sulfur compounds alligrin and alliphanin.

A calibration curve was generated using serial dilutions of purified synthetic allicin demonstrating excellent linearity (R^2 = 0.9994) across the analytical range (Figure 3.2b), confirming a reliable relationship between concentration and HPLC peak area. This calibration was used to quantify allicin in freshly homogenised garlic crude extracts with concentrations monitored over a 60-minute period. As shown in Figure 3.2a, allicin levels ranged from approximately 3.38 -4.53 mg/g throughout the experiment. During the first 10-15 minutes, minor fluctuations were observed, consistent with the initial activation of alliinase and rapid conversion of alliin following tissue disruption. Allicin concentrations reached maximum values of approximately 4.21-4.53 mg/g between 30 and 35 minutes consistent with previously reported values in the literature [212].

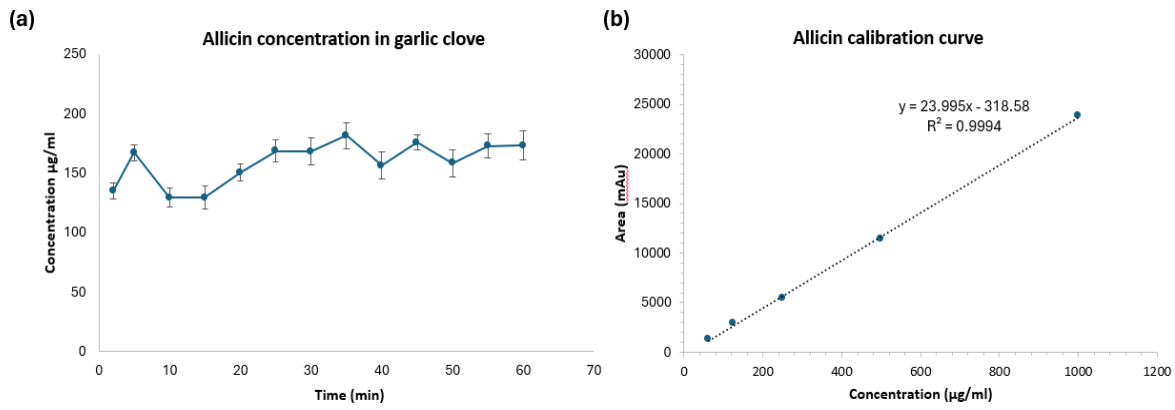

Figure 3.2: (a) Time-course analysis of allicin formation and stability in aqueous freshly crushed garlic over 60 minutes. "All measurements were performed in triplicate (n=3)". (b) Allicin calibration graph.

Once allicin formation in freshly crushed garlic was confirmed, the next step was to analyse mustard seeds powder as the second plant system. These seeds provide the aglycone intermediate required for the next mixing experiment, where combining garlic with mustard seed powder resulted in the formation of alligrin.

3.3.2 Analytical identification of the aglycone intermediate in crude mustard seeds powder extract

In this study, Colman's Original Mustard Powder a commercial preparation consistingof white mustard (*Sinapis alba*) and brown mustard (*Brassica juncea*) seeds powder was used as the glucosinolate source. The exact ratio of the two seed varieties is not publicly released by the manufacturer. However, both glucosinolates sinalbin and sinigrin are expected to be present in the extract.

Upon aqueous extraction endogenous myrosinase is activated and initiates rapid hydrolysis of sinigrin from *B. juncea* to yield AITC under neutral pH conditions. The resulting HPLC chromatogram (Figure 3.3) reveals a clear sinigrin peak at approximately 2.9 minutes and a well-resolved sinalbin peak at approximately 5 minutes. The delayed retention of sinalbin reflects its aromatic p-hydroxybenzyl side chain which confers greater hydrophobicity and stronger interaction with the reverse-phase stationary phase relative to the more polar sinigrin. The dominant sinalbin peak is consistent with literature reports that sinalbin levels in *S. alba* are generally higher than sinigrin levels in *B. juncea* [214].

Despite sinalbin being present in greater abundance, a prominent AITC peak at 14 minutes confirms that sinigrin was selectively and near-complete hydrolysis (≈99.97%) within 15 minutes, while sinalbin remained largely unhydrolyzed. This observation is primarily attributed to *B. juncea* myrosinase exhibiting substantially higher catalytic activity (2.75 units/mL) than that of *S. alba* (0.63 units/mL), alongside greater substrate affinity for sinigrin as its endogenous glucosinolate.

Although sinalbin may absorb at the selected detection wavelength (228 nm) [215], its hydrolysis product p-hydroxybenzyl isothiocyanate was not detected under the current HPLC conditions. Furthermore, the slower hydrolysis kinetics of sinalbin attributable to the lower myrosinase activity in *S. alba* relative to *B. juncea*, likely account for the absence of p-

hydroxybenzyl isothiocyanate in the chromatogram in contrast to the prominently detected AITC peak. Therefore, the analysis was focused on sinigrin activation and AITC formation as the reactive intermediate necessary for alligrin production in the garlic-mustard mixture experiments.

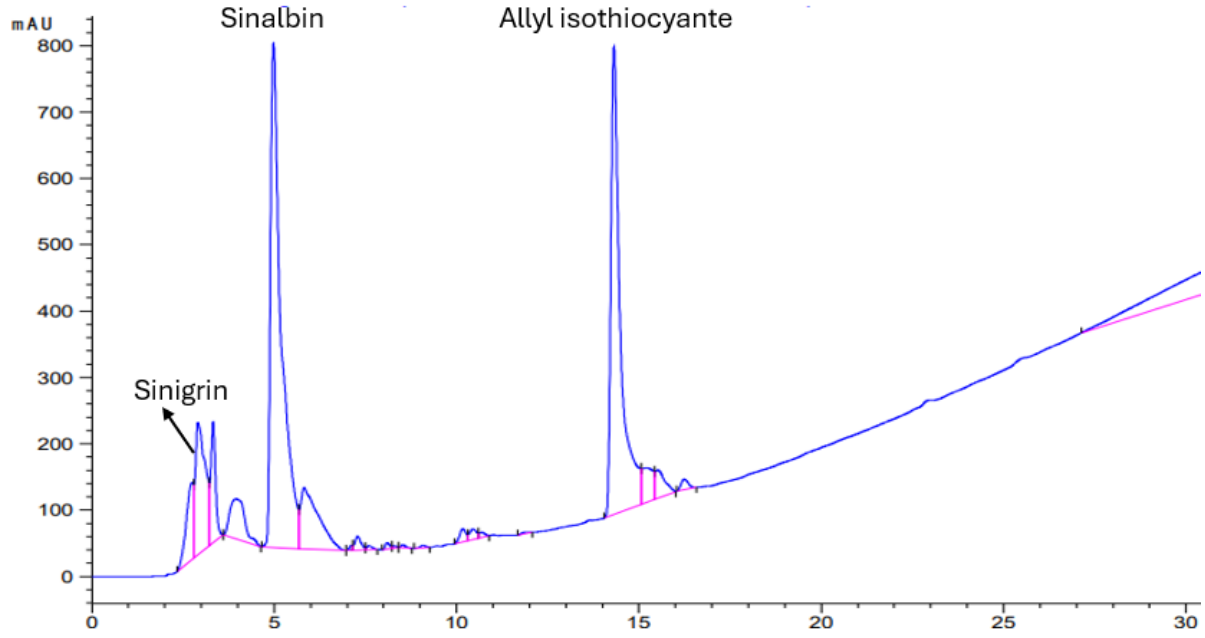

Figure 3.3: HPLC chromatogram of aqueous crude mustard seeds powder extract after 15 min.

3.3.2.1 Monitoring the formation, concentration, and stability of allyl isothiocyanate in mustard seeds powder

The calibration curves for both sinigrin and AITC standard were generated using series of standard solutions analysed under the same HPLC conditions applied to the mustard seed powder extract, yielding linear relationships between concentration and peak area (sinigrin $y = 9101.3x + 10103$, $R^2 = 0.9956$, AITC $y = 5.3041x + 1388.9$, $R^2 = 0.9559$), providing a reliable basis for quantification of both compounds (Figure 3.4b, d).

The concentration of sinigrin in mustard seeds powder decreased rapidly from approximately 0.038 mg/g (0.106 µmol/g) at 2 minutes to a stable level of approximately 0.032 mg/g (0.089 µmol/g) beyond 10 minutes (Figure 3.4a), reflecting near-complete hydrolysis by endogenous myrosinase. These values are notably lower than the typically reported sinigrin content of 11-16 mg/g dry weight in B. juncea seeds [215], suggesting that the majority of sinigrin had

already undergone enzymatic conversion prior to the earliest measurement, consistent with the rapid onset of myrosinase activity upon aqueous extraction[168].

Concurrently, AITC reached its highest concentration of approximately 42.82 mg/g (431.88 µmol/g) at 2 minutes, stabilising at approximately 38.76 mg/g (391.11 µmol/g) beyond 10 minutes (Figure 3.4c), with the inverse relationship between sinigrin depletion and AITC formation directly confirming efficient myrosinase-catalysed hydrolysis under the extraction conditions employed. The elevated AITC yields observed relative to those reported for pure B. juncea preparations (2-17 mg/g) [216] may be attributed to the synergistic contribution of myrosinase enzymes from both S. alba and B. juncea present in Colman's Original Mustard Powder, collectively enhancing the hydrolytic conversion of sinigrin beyond levels achievable by either species independently. Additionally, differences in extraction conditions, particle size, and water-to-powder ratio may further contribute to the elevated yields, and these values should therefore be interpreted as indicative of relative release kinetics rather than absolute AITC content.

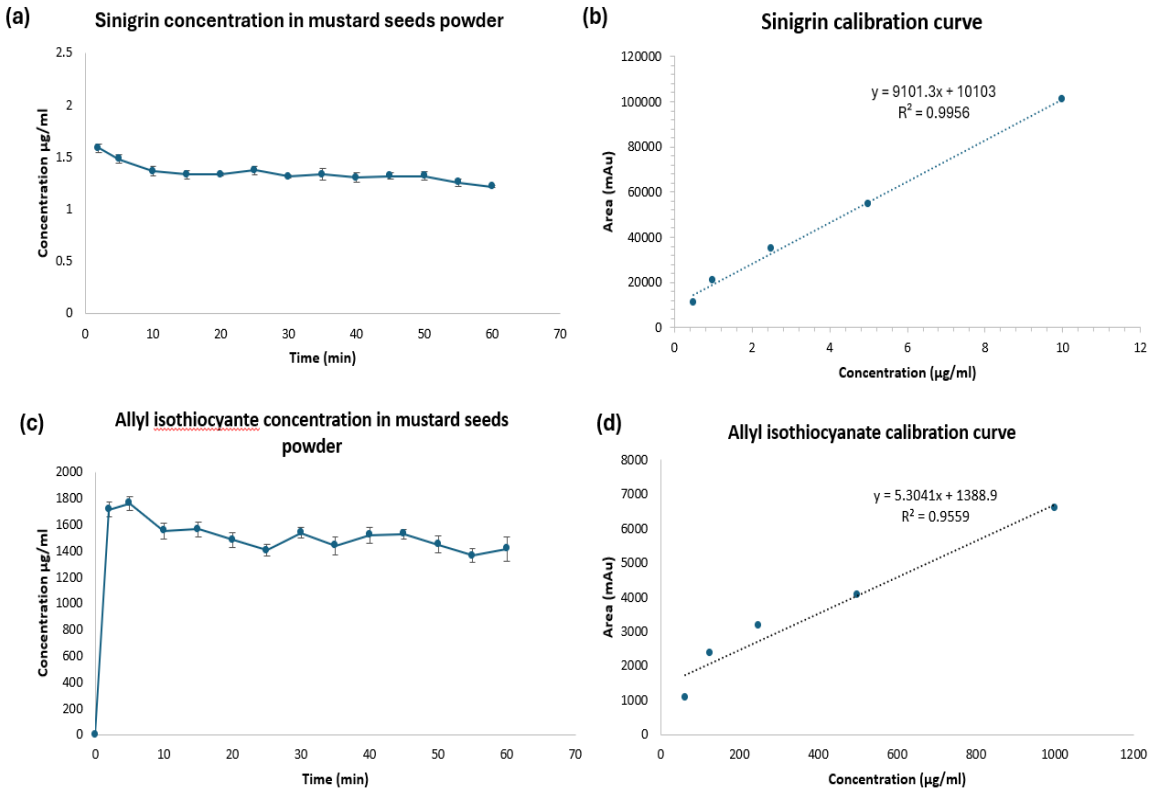

Figure 3.4: (a) Time-course analysis of sinigrin hydrolysis and (c) allyl isothiocyanate (AITC) formation from mustard seed powder over 60 minutes, with corresponding calibration curves for (b) sinigrin and (d) AITC used for quantification.

These findings highlight the importance of immediate sample analysis following preparation, as the 2 minutes timepoint represents the optimal window for maximising reactive intermediate availability. Having confirmed the presence and quantification of allicin and the sinigrin-derived aglycone intermediate as the two reactive sulfur precursors, formation and quantification of alligrin in the combined garlic-mustard seeds powder mixture was subsequently investigated.

3.3.3 Analysis of the garlic-mustard seeds powder mixture for alligrin production

To investigate the reactivity of intermediates generated upon combining garlic and mustard seed powder, the aqueous extract of freshly crushed garlic was first allowed to stand for 30 minutes, a timepoint at which allicin concentration reaches its near-maximum level. An equivalent amount of mustard seed powder was then added, and the mixture was completely homogenised and incubated for 15 minutes, corresponding to the timepoint at which AITC reaches its maximum concentration. HPLC analysis of the crude garlic-mustard mixture revealed a new peak at a retention time of 7.8 minutes (Figure 3.5), identical to that of the authenticated alligrin standard and absent in either plant extract alone, confirming alligrin formation upon interaction of allicin with the sinigrin aglycone intermediate.

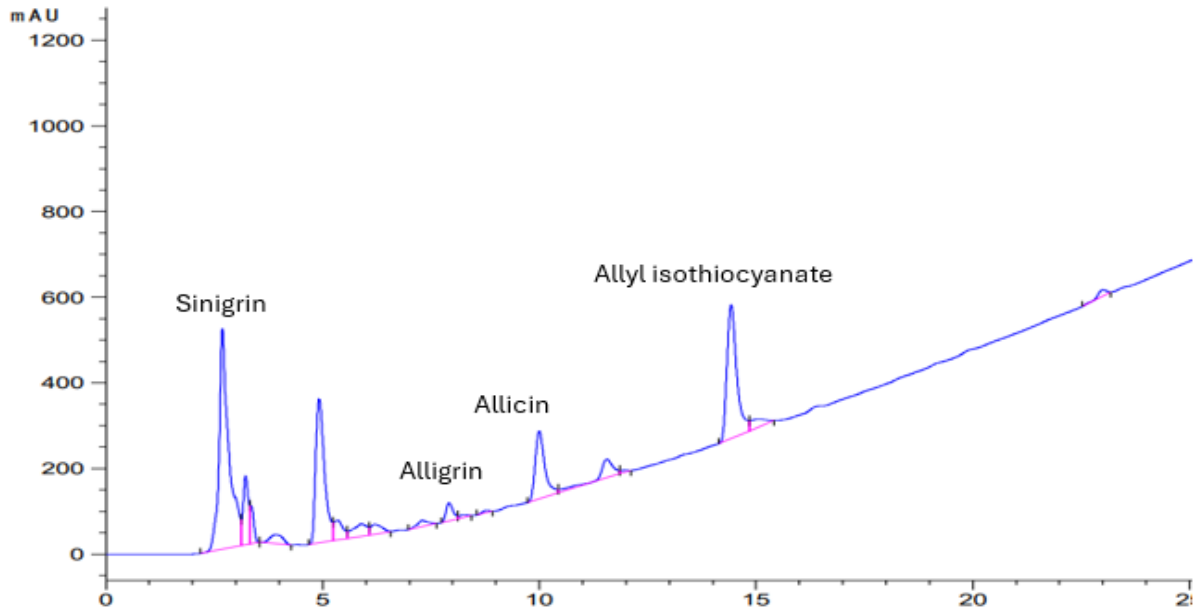

Figure 3.5: HPLC chromatogram of the garlic- mustard seeds powder mixture showing the formation of alligrin.

To confirm its identity a spiking experiment was performed by adding the purified alligrin to the reaction mixture of garlic and mustard seeds powder sample (Figure 3.6). The resulting chromatographic analysis showed a clear increase in the area under the 7.8-minute peak, verifying that this peak corresponds to the same compound previously isolated and characterised. This result provides strong evidence that the novel compound is consistently formed during the interaction of allicin with sinigrin hydrolysis products in both purified systems and crude plant material under food preparation-like conditions.

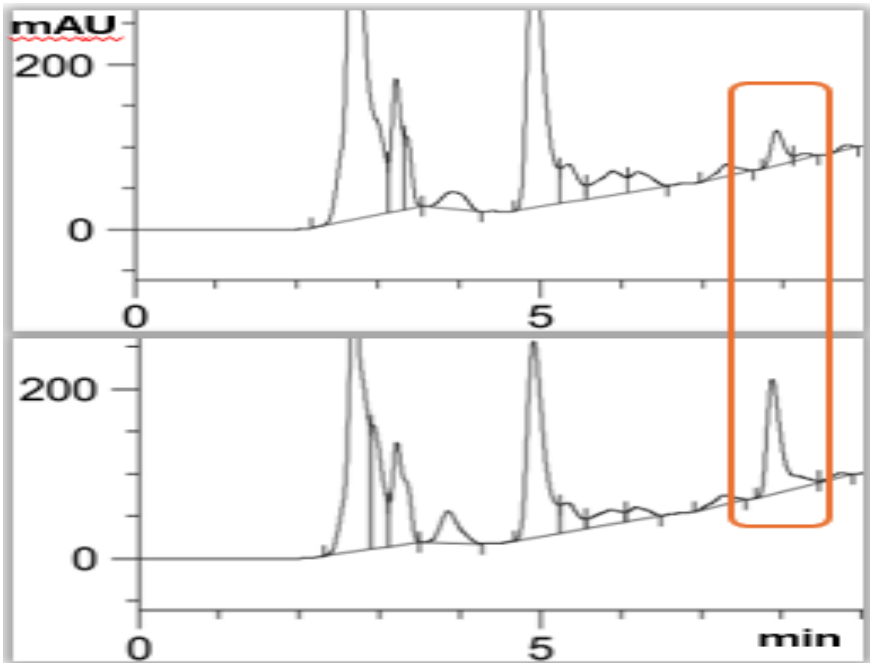

Figure 3.6: Comparison of the garlic- mustard seeds powder mixture before (top) and after (bottom) spiking with purified alligrin. The highlighted peak increases in intensity in the spiked sample, confirming its identity as alligrin.

Further confirmation of alligrin formation was obtained through LC-MS analysis of the garlic-mustard seeds powder mixture extract. The chromatographic peak assigned to alligrin was subjected to mass spectrometric detection and exhibited a molecular ion consistent with the expected mass of alligrin. The observed *m/z* value, together with the characteristic fragmentation pattern detected in negative electrospray ionisation (ESI^-) mode, provides strong evidence for the successful formation of alligrin within the crude garlic-mustard extract (Figure 3.7).

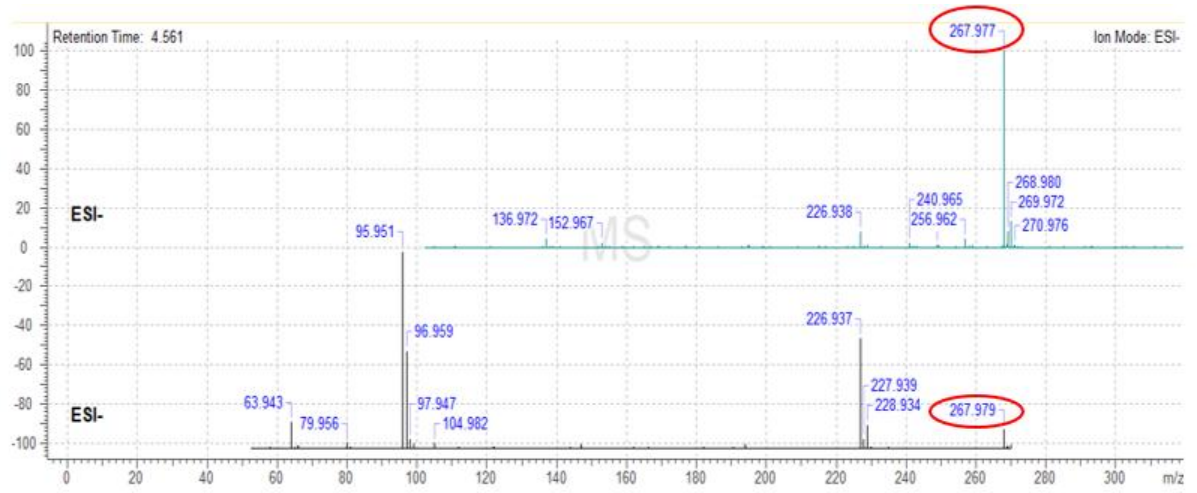

Figure 3.7: LC-MS confirmation of alligrin formation in mustard seed powder extract.

3.3.3.1 Quantitative assessment of alligrin formation and stability

The calibration curve of pure alligrin (Figure 3.8) showed excellent linearity between analyte concentration and HPLC peak area, described by the equation $y = 4.4749x - 132.33$ with an R^2 value of 0.9995. This high degree of linearity confirms consistent detector response and validates the HPLC method for quantitative determination of alligrin in crude plant extract.

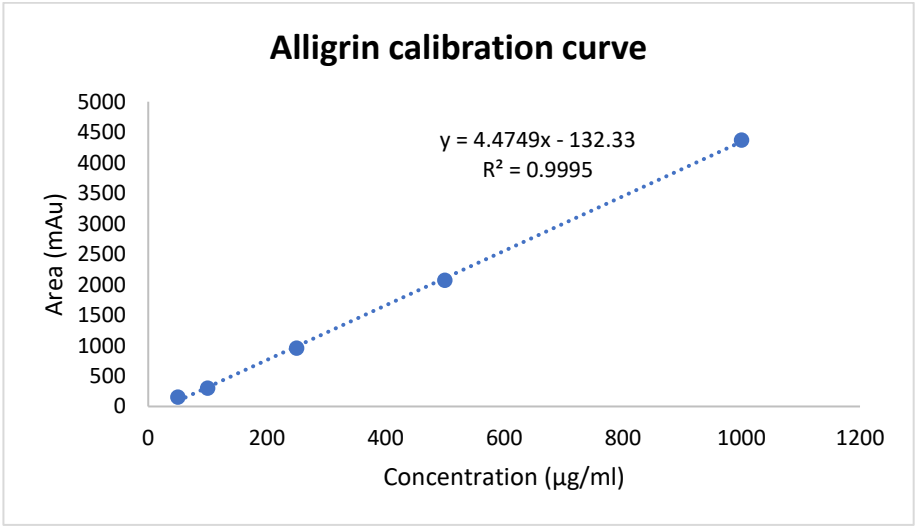

Figure 3.8: Calibration curve for alligrin showing the linear relationship between concentration and HPLC peak area.

Quantitative HPLC analysis of the crude garlic-mustard mixture was conducted following an optimised preparation protocol (section 3.3.3). Using validated calibration curves for sinigrin ($R^2 = 0.9956$), AITC ($R^2 = 0.9559$) (Figure 3.4), allicin ($R^2 = 0.9994$) (Figure 3.2), and alligrin ($R^2 = 0.9995$) (Figure 3.8).

Sinigrin was nearly completely hydrolysed in both the pure mustard extract (0.033 mg/g, 0.0919 µmol/g) and the mixture with garlic (0.0331 mg/g, 0.0919 µmol/g), confirming efficient myrosinase-catalysed hydrolysis during mixing, with ≈99.97% of sinigrin consumed (Table 3.1). AITC was produced *in situ* from sinigrin hydrolysis, reaching (39.06 mg/g, 393.94 µmol/g) in the pure mustard extract at t=15, and decreased to (19.77 mg/g, 199.40 µmol/g) in the mixture with garlic, representing a consumption of (19.29 mg/g, 194.55 µmol/g) (≈49.38%), attributable to volatilisation, degradation, and participation in alligrin formation.

Allicin decreased from (4.20 mg/g, 25.88 µmol/g) in the pure garlic extract at t=15 to (1.896 mg/g, 11.68 µmol/g) in the mixture, indicating a consumption of (2.304 mg/g, 14.20 µmol/g) (≈54.86%). Alligrin was successfully quantified at (2.20 mg/g, 8.20 µmol/g) in the crude mixture, absent in either plant extract alone, confirming its formation through the interaction of allicin and the sinigrin-derived AITC intermediate. Alligrin represented ≈1.36% of the total mixture consumed (602.70 µmol/g), with allicin acting as the limiting reagent in its formation.

Of the total reactive pool, nearly half of the available sinigrin hydrolysis intermediate (≈49.38%) was consumed, while a slightly higher proportion of allicin (≈54.86%) was used up in this reaction, suggesting allicin was somewhat more reactive under these conditions. Only a small fraction (≈1.36%) of the total consumed mixture was ultimately converted to form alligrin, reflecting an overall low formation efficiency. The remaining allicin was probably lost to competing degradation pathways such as diallyl polysulfide formation, ajoene-type rearrangements, or reaction with alligrin to produce its rearrangement products below the limit of detection. The considerable loss of sinigrin hydrolysis intermediate is attributed to its inherent volatility, conversion to AITC, or tendency to undergo hydrolysis and degradation under aqueous conditions.

Table 3.1: Quantitative analysis of key compounds in crude garlic-mustard mixture.

Compound	Plant extract before mixing (µmol/g)		Plant extract after mixing (µmol/g)	Consumed after mixing (µmol/g)	Consumed percentage %
	t=0	t=15	t=15	t=15	t=15
Sinigrin	394.046	0.106	0.0919	393.95	≈99.97%
AITC	0	393.94	199.40	194.55	≈49.38%
Allicin	0	25.88	11.68	14.2	≈54.86%
Alligrin	0	0	8.20	8.20	≈1.36%

Following confirmation of alligrin formation under the established garlic-mustard conditions, further optimisation focused on enhancing the yield of sinigrin aglycone intermediates.

3.3.4 Optimising sinigrin hydrolysis for enhanced alligrin formation

To optimise alligrin production in the garlic-mustard system, experiments were carried out to evaluate whether supplementing the crude mustard seed powder with exogenous myrosinase could enhance sinigrin hydrolysis and thereby increase AITC availability. Since alligrin formation is directly dependent on the sinigrin aglycone intermediate, improving the rate and extent of enzymatic hydrolysis was considered a key strategy for maximising alligrin yield under the established reaction conditions.

3.3.4.1 Influence of external myrosinase on sinigrin degradation and allyl isothiocyanate production from mustard seeds powder

Allyl isothiocyanate release from mustard seeds powder was monitored over 60 minutes with and without exogenous myrosinase supplementation (Figure 3.9a, b). Although external myrosinase caused a slightly faster initial reduction of sinigrin, the overall AITC profiles for both treatments were similar and reaching maximum concentration within 5-10 minutes before stabilising and gradually declining. These results indicate that the endogenous

myrosinase activity in mustard seeds powder is sufficient to drive efficient sinigrin hydrolysis, and that exogenous enzyme supplementation offers no practical benefit for enhancing AITC availability or alligrin yield.

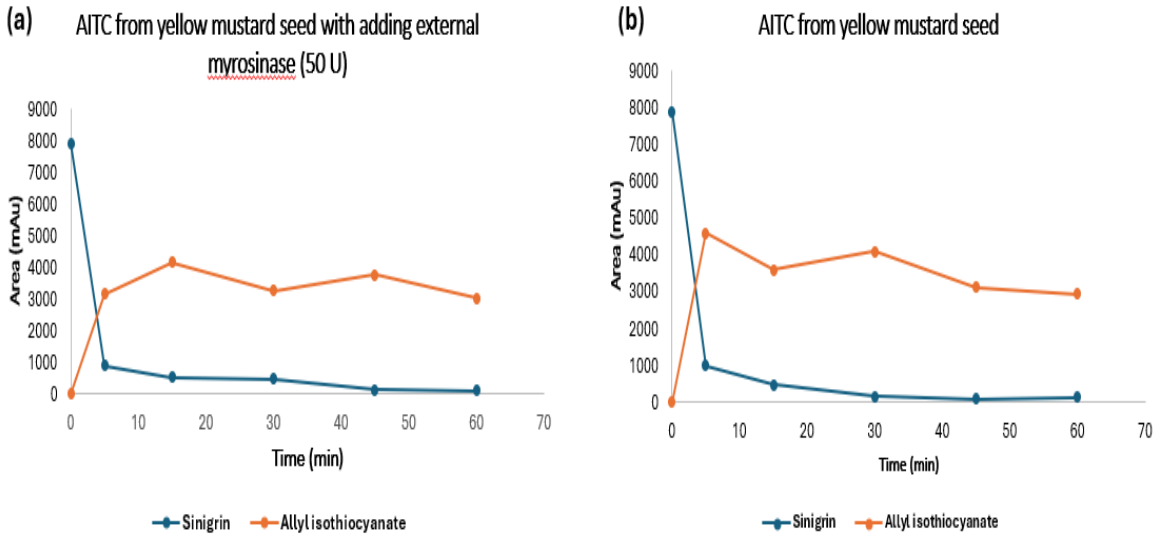

Figure 3.9: Time-course analysis of sinigrin and allyl isothiocyanate (AITC) formation from yellow mustard seed powder (a) in the presence and (b)absence of exogenously added myrosinase enzyme.

Given that increasing myrosinase activity did not enhance alligrin yield, following optimisation focused on improving alligrin recovery through concentration of the crude plant mixture extract as an alternative strategy. This approach aimed to increase detectable alligrin levels without altering the underlying enzymatic reactions.

3.3.4.2 Effect of sample concentration on alligrin recovery

To investigate whether sample concentration could improve alligrin recovery, the crude garlic-mustard extract was concentrated overnight using a Genevac centrifugal evaporator prior to HPLC analysis. However, chromatographic analysis of the concentrated sample revealed a complete loss of the alligrin peak (Figure 3.10). Indicating that alligrin is highly unstable within the crude plant mixture and susceptible to rapid degradation during prolonged solvent removal, likely due to its reactive and volatile nature under these conditions.

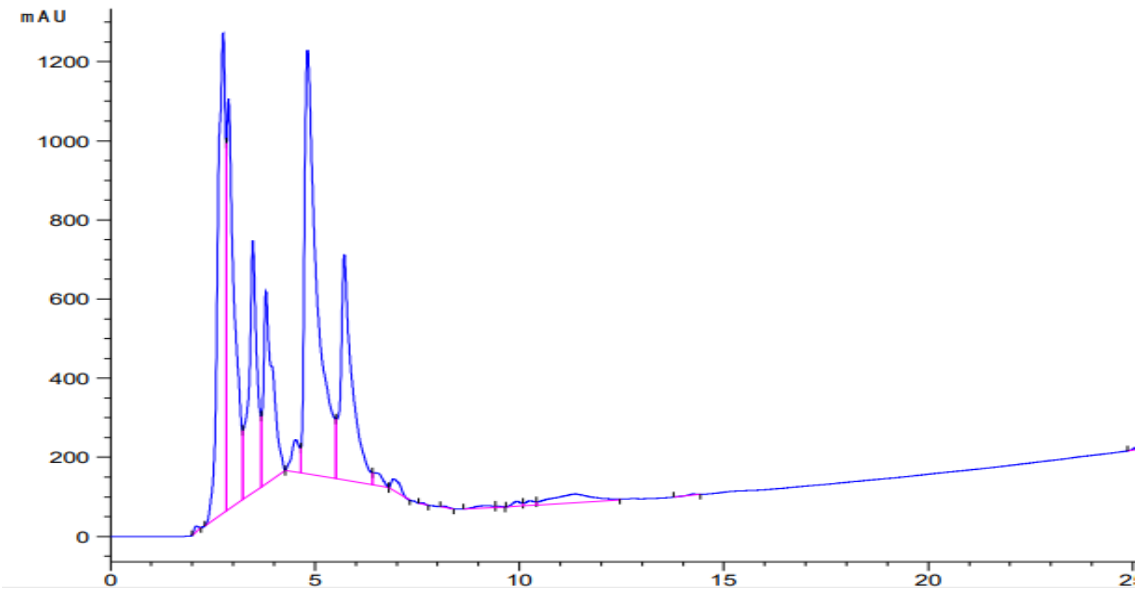

Figure 3.10: Effect of sample concentration on alligrin formation.

These findings demonstrate that prolonged solvent evaporation is not a suitable strategy for improving alligrin recovery from crude plant extracts, further highlighting the need for rapid sample analysis and minimal handling when working with reactive sulfur-containing conjugates. The relatively low alligrin formation efficiency (≈1.36%), combined with substantial unreacted fractions of both the sinigrin hydrolysis intermediate (≈50.62% remaining) and allicin (≈45.14% remaining), clearly indicates that there is considerable room for improvement. Given that allicin was the limiting reagent in this reaction (14.20 µmol/g versus 194.55 µmol/g of sinigrin hydrolysis intermediate), simply increasing the garlic-to-mustard ratio would likely be the most straightforward way to increase alligrin yield. Adjusting the pH using acidic agents such as vinegar could also help stabilise both substrates and reduce losses through competing hydrolysis and degradation, while better control of

temperature and incubation time would help retain the sinigrin hydrolysis intermediate long enough to participate in alligrin formation. However, these parameters were not pursued in this thesis due to time limitations and are recommended as priorities for future work.

3.3.5 Analytical identification of the aglycone intermediate in crude broccoli extract

Fresh broccoli was selected as the glucosinolate source due to its high glucoraphanin content, which upon aqueous homogenisation undergoes rapid myrosinase-catalysed hydrolysis to generate an unstable aglycone intermediate that rearranges to form sulforaphane. Prior to the garlic-broccoli interaction experiments, the aqueous crude broccoli extract was analysed using the same HPLC method. The chromatogram (Figure 3.11) revealed a major glucoraphanin peak at 2.6 minutes alongside a relatively small sulforaphane peak at 7.2 minutes, indicating that myrosinase-catalysed hydrolysis of glucoraphanin was only partially complete under the applied extraction conditions, consistent with the lower endogenous myrosinase activity of broccoli relative to mustard seed powder.

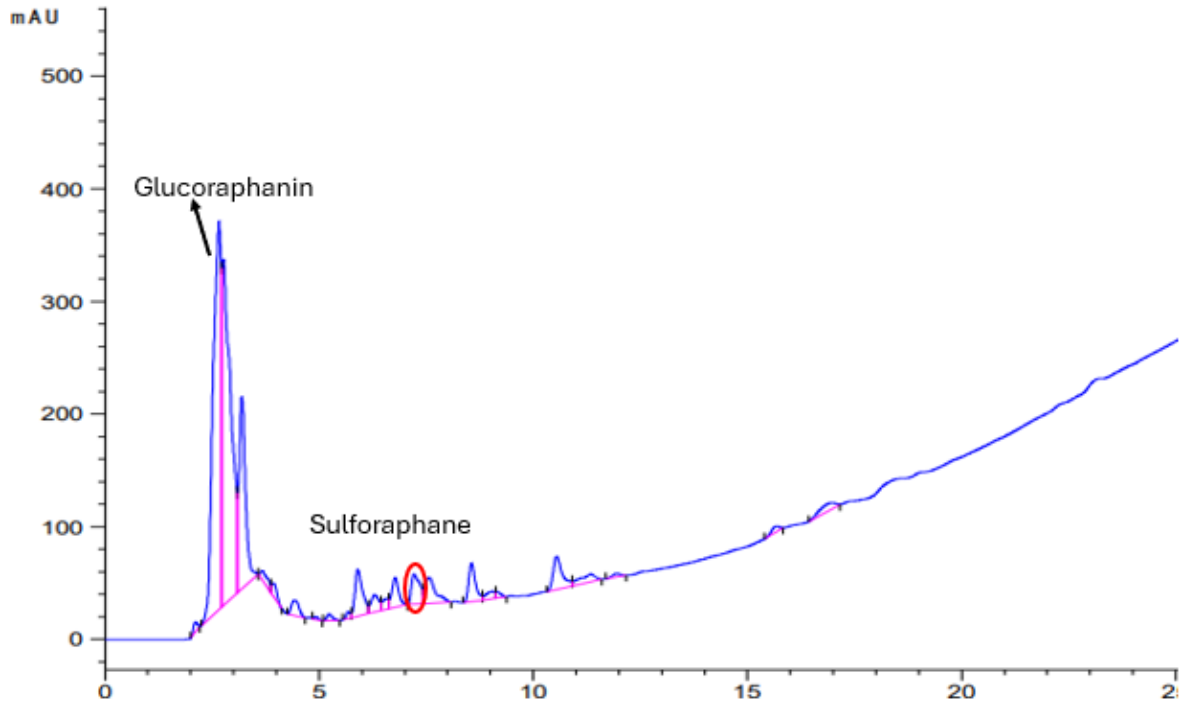

Figure 3.11: HPLC chromatogram of crude aqueous broccoli extract.

3.3.5.1 Monitoring the formation, concentration, and stability of sulforaphane in broccoli crude extract

The hydrolysis of glucoraphanin and formation of sulforaphane were monitored in crude broccoli extract over 60 minutes by HPLC (Figure 3.12). Glucoraphanin concentration remained relatively stable throughout the 60-minute period, ranging approximately between 240 and 300 µg/mL with minor fluctuations, suggesting that glucoraphanin was not substantially depleted under the experimental conditions (Figure 3.12a). At the same time, sulforaphane reached its maximum concentration within 5-10 minutes before gradually declining, reflecting its well-known chemical instability and susceptibility to oxidation under aqueous conditions (Figure 3.12c), consistent with previously reported sulforaphane degradation profiles [217]. Calibration curves for glucoraphanin ($y = 12.238x + 1154.7$, $R^2 = 0.9998$) and sulforaphane ($y = 2.0695x + 20.712$, $R^2 = 1.0000$) demonstrated excellent linearity, confirming the reliability of the method for quantification of both compounds in crude broccoli extract (Figure 3.12b, d).

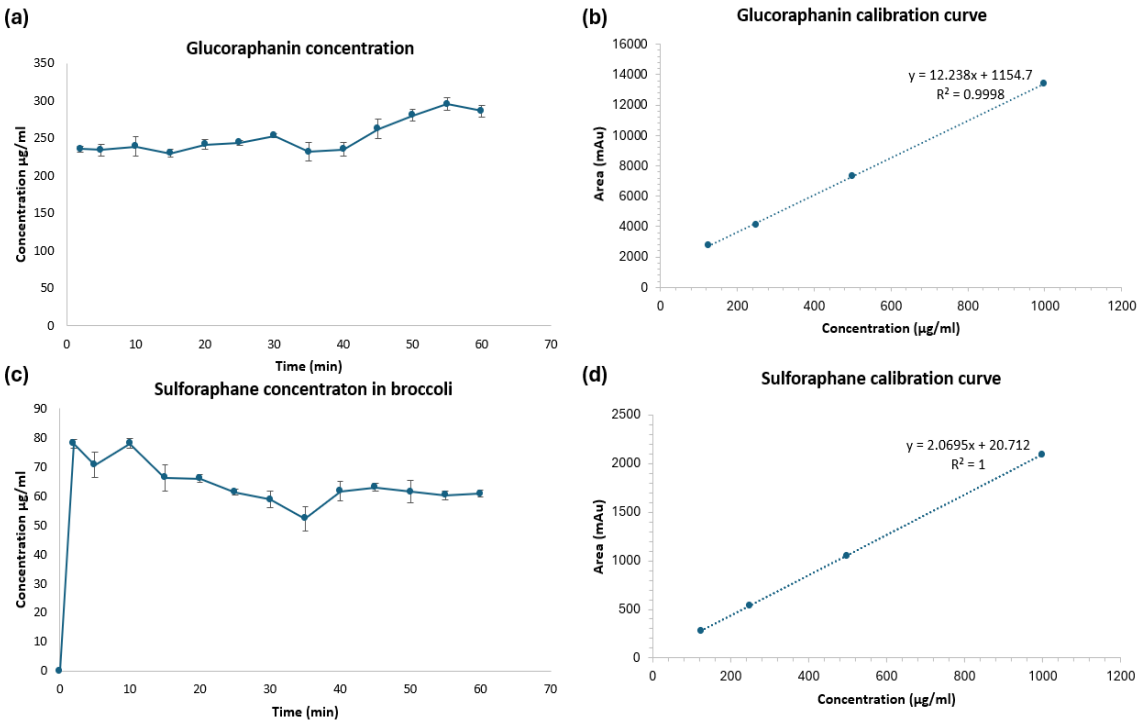

Figure 3.12: (a) Time-course analysis of glucoraphanin hydrolysis and (c) sulforaphane formation in broccoli extract over 60 minutes, with corresponding calibration curves for (b) glucoraphanin and (d) sulforaphane used for quantification.

The initial glucoraphanin concentration was recorded at the earliest measurable timepoint as 7.79 mg/g (17.87 µmol/g). a value notably higher than previously reported ranges of 0.047-1.295 mg/g fresh weight [218], which may be related to the specific broccoli variety used or differences in extraction efficiency. The persistently high glucoraphanin levels throughout the 60-minute monitoring period further confirm incomplete hydrolysis, consistent with the relatively low endogenous myrosinase activity in broccoli.

By 10 minutes, glucoraphanin had declined to 5.97 mg/g (13.69 µmol/g), alongside sulforaphane formation at 1.95 mg/g (11.00 µmol/g). consistent with the reported sulforaphane range of 1.89-3.7 mg/g across different varieties and preparation methods[219]. Notably, the sulforaphane accumulation (11.00 µmol/g) considerably exceeded the glucoraphanin consumption (4.18 µmol/g), confirming that hydrolysis had already initiated prior to the first recorded timepoint, likely during the initial extraction and sample preparation steps.

3.3.6 Analysis of the garlic-broccoli mixture for alliphanin production

HPLC analysis of the crude garlic-broccoli mixture (Figure 3.13) revealed characteristic peaks corresponding to glucoraphanin, allicin, and sulforaphane at their expected retention times. However, no quantifiable alliphanin peak was detected, with only a trace signal of 24.83 mAU observed at its expected retention time falling below the reliable quantification range of the established calibration curve ($y = 3.3984x + 4422.2$, $R^2 = 0.984$, Figure 3.14).

This limited yield of alliphanin is likely attributable to insufficient myrosinase-catalysed glucoraphanin hydrolysis under the applied extraction conditions as reflected by only trace sulforaphane formation (Figure 3.11). Suggesting that endogenous myrosinase activity was inadequate to generate sufficient aglycone intermediate for alliphanin formation. This contrasts with the mustard seed system, where myrosinase activity was sufficient to drive near complete sinigrin hydrolysis and facilitate alligrin formation. Importantly, LC-MS analysis (Figure 3.15) of the same garlic-broccoli mixture confirmed the presence of alliphanin at its expected molecular ion and providing qualitative evidence of its formation despite concentrations falling below the limit of quantification.

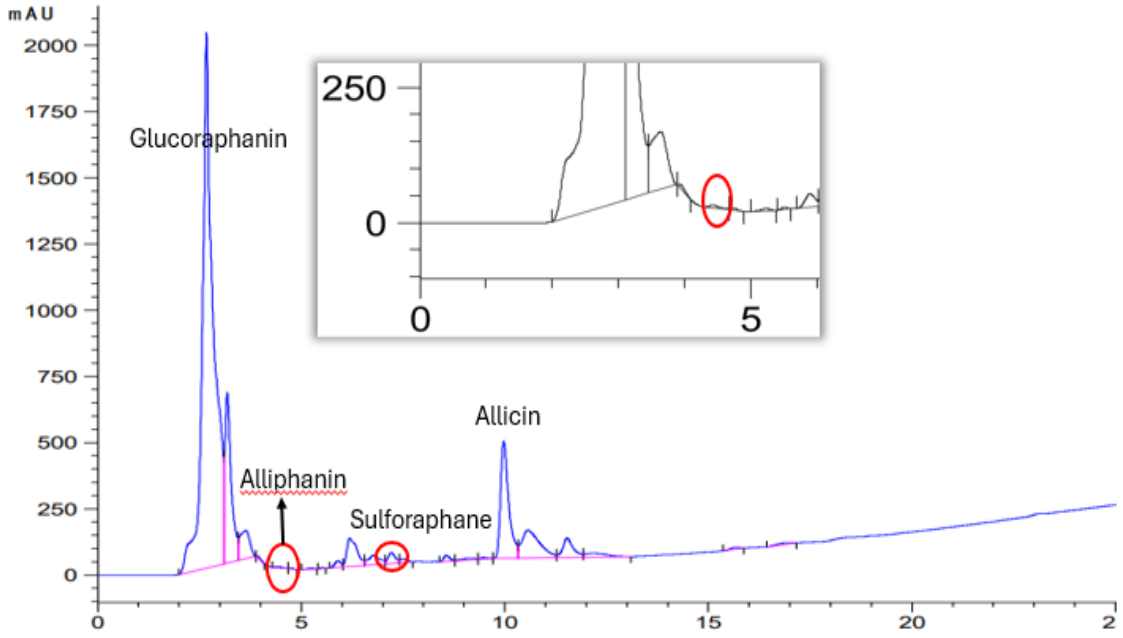

Figure 3.13: HPLC chromatogram of the crude garlic-broccoli mixture showing characteristic peaks for glucoraphanin, allicin, and sulforaphane, with a trace signal at the expected alliphanin retention time below the reliable quantification limit.

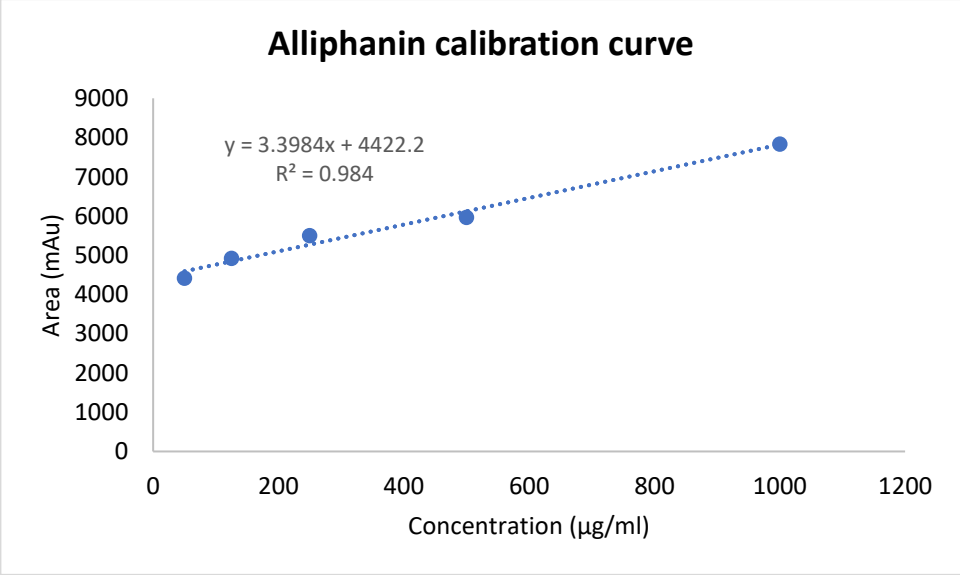

Figure 3.14: Alliphanin calibration curve showing the linear relationship between alliphanin concentration and HPLC peak area, with the regression equation (y = 3.3984x + 4422.2) and an R^2 value of 0.984.

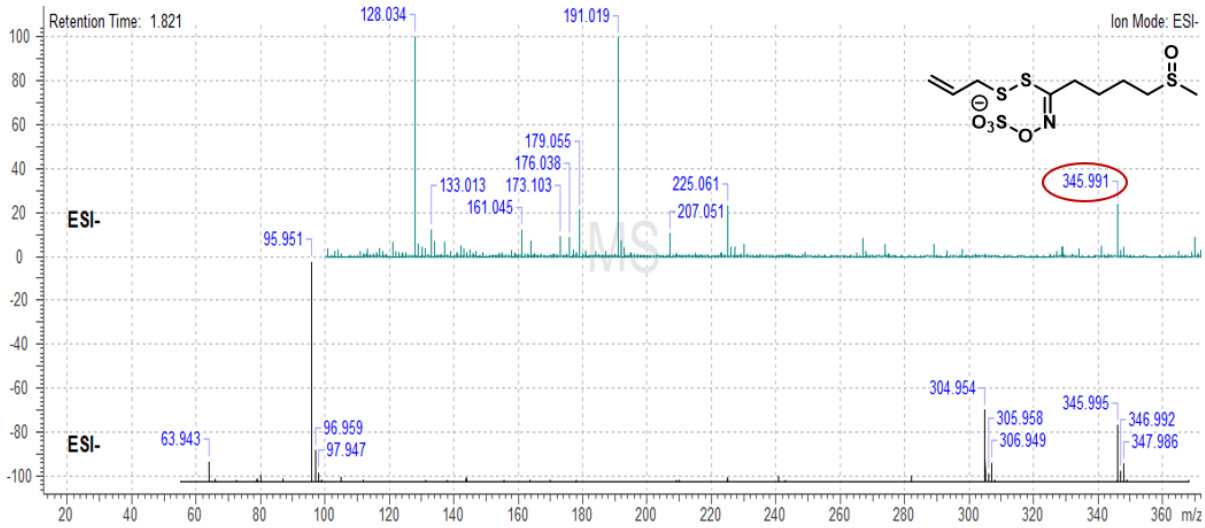

Figure 3.15: LC-MS confirmation of alliphanin in broccoli and garlic crude mixture.

3.4 Summary and conclusion

This chapter investigated whether the novel sulfur compounds alligrin and alliphanin, previously generated under controlled model conditions (in chapter 2), could also form within crude plants mixture. By systematically analysing garlic, mustard seeds powder, broccoli and their mixtures, this study demonstrated that the enzymatic environments of intact plant tissues are sufficient to drive the formation of these novel organosulfur compounds.

Freshly crushed garlic was confirmed as a reliable source of allicin, with time-course analysis establishing an optimal formation window within the first 30-40 minutes following tissue disruption. Mustard seeds powder and broccoli provided active glucosinolate-myrosinase systems, generating allyl isothiocyanate from sinigrin and sulforaphane from glucoraphanin, respectively. Alligrin formation in the garlic-mustard mixture was confirmed by HPLC retention time matching, spiking experiments, and LC-MS analysis, yielding a quantifiable concentration of 2.2 mg/g crude mixture. In contrast, alliphanin was barely detected in the crude garlic-broccoli mixture, falling below the reliable limit of quantification, consistent with lower effective myrosinase activity and reduced aglycone intermediate availability in broccoli compared with mustard seed powder.

Attempts to optimise detection by concentrating crude extracts using Genevac evaporation were unsuccessful for both mixtures. In each case, concentration led to loss of the alligrin or alliphanin peak, demonstrating that these compounds are unstable within mixture plants

extract, despite being relatively stable when analysed as purified compounds. These findings demonstrate that reactive sulfur-linked conjugates are particularly susceptible to degradation during solvent evaporation in mixture plants extract. Overall, this chapter provides strong evidence that allicin-glucosinolate conjugation reactions occur naturally under relevant food-like preparation conditions, while highlighting the importance of precise timing, minimal sample handling, and rapid analysis when working with highly reactive sulfur species.

4 Novel Sulfur Metabolites Arising from Garlic-Brassica Interactions: Antibacterial Activity and Mechanistic Insights

4.1 Aim of this chapter

The aim of this chapter was to explore the antimicrobial activity of alligrin and alliphanin both as purified compounds and as natural byproducts produced during the preparation of garlic-mustard/broccoli combinations. This chapter also provides an initial exploration of the mechanisms behind the antibacterial effects of these novel sulfur metabolites.

4.2 Antibacterial activity of crude plant extracts and mixed plants extract systems

Activity was assessed against *Staphylococcus aureus*, MRSA, *Escherichia coli*, and *Pseudomonas aeruginosa*. Organisms that have acquired significant resistance to conventional β-lactam antibiotics, which act through inhibition of penicillin-binding proteins (PBPs) involved in cell wall biosynthesis. This study therefore investigated plant-derived sulfur compounds as a mechanistically different alternative, targeting intracellular thiol-dependent pathways specifically glutathione and thiol-containing enzymes to overcome established antibiotic resistance.

The antibacterial activity of aqueous crude plant extracts and their binary combinations was initially evaluated using the disc diffusion assay as a preliminary screening approach prior to the investigation of purified compounds. Ampicillin and ciprofloxacin were included as positive reference controls to validate assay performance and evaluate the potency of plant-derived extracts relative to established clinical antibiotics.

Disc diffusion screening revealed a different antibacterial profile across the individual plant extracts and their combinations (Table 4.1, 4.2). Garlic aqueous extract demonstrated activity against Gram-positive organisms producing inhibition zones of 18 mm against both *Staphylococcus aureus* and MRSA, and reduced activity against *Escherichia coli* (13 mm), with no inhibition detected against *Pseudomonas aeruginosa*. These results are consistent with previously reported inhibition zones for aqueous garlic extracts against *S. aureus* (15-20 mm) [220], MRSA (16-24 mm)[221], and *E. coli* (10-14 mm) [220], and confirm the documented

absence of activity against *P. aeruginosa* [82]. The selectivity towards Gram-positive reflects the well-established mechanism of allicin, which irreversibly inhibits thiol-dependent enzymes through covalent modification of active-site cysteine residues through S-thio-allylation [49]. The moderate activity is likely associated with allicin instability under aqueous conditions [49], while the lack of activity against *P. aeruginosa* is consistent with the intrinsic resistance of this organism, mediated by outer membrane impermeability and the MexAB-OprM efflux system [49, 220].

Mustard seeds powder and broccoli extracts showed no measurable inhibition against any of the bacterial strains tested. Although glucosinolate-rich Brassica species are well established as precursors of antimicrobial isothiocyanates including allyl isothiocyanate (AITC) from mustard and sulforaphane from broccoli bioactivity is critically dependent on effective myrosinase-mediated hydrolysis and adequate compound stability [184]. The absence of activity in these extracts is consistent with reports demonstrating that AITC and sulforaphane exhibit poor aqueous solubility and rapid degradation under neutral pH conditions, limiting their accumulation to inhibitory concentrations in buffered systems [222]. Similar findings have been reported by Dufour *et al.* [184] and Luciano *et al.* [222], who observed negligible antibacterial activity in aqueous Brassica extracts unless isothiocyanate stability was enhanced through pH adjustment or encapsulation.

Interestingly, mixture extract of garlic with either mustard seeds or broccoli resulted in an enhancement of antibacterial activity compared to individual extract tested alone (Table 16-17). Both mixed extract systems produced larger inhibition zones against *S. aureus* (21-23 mm) and MRSA (25 mm) than garlic extract alone (18 mm) and demonstrated increased inhibition of *E. coli* (16 mm compared with 13 mm), whilst activity against *P. aeruginosa* remained undetectable across all preparations. significantly, clinical antibiotics produced larger inhibition zones compared with all tested plant extracts, including garlic, mustard seeds powder, broccoli and their combined mixtures reflecting their superior antimicrobial potency.

This enhancement indicates that the potentiation of antibacterial activity in the mixed systems cannot be assigned to simple additive effects but instead suggests a synergistic interaction between the two extract components. This synergy most plausibly raised from reactions between garlic-derived allicin and aglycon intermediates generated when Brassica

tissue is disrupted. These reactions produced novel hybrid organosulfur species (alligrin and alliphanin) with properties different from either parent compound, potentially offering enhanced membrane permeability and broader enzyme inhibition, together explaining the superior antibacterial activity observed in the combined extracts systems against susceptible bacterial strains.

Table 4.1: Representative agar diffusion plates showing the antibacterial activity of crude plant extracts and mixed extract systems against Gram-positive and Gram-negative bacterial strains using the disc diffusion assay. Note: ***Mixture 1*** *is garlic mixed with mustard seeds powder while* ***mixture 2*** *is garlic with broccoli. Discs labelled* ***Y*** *represent the aqueous mustard seeds extract alone, and* ***B*** *represent the aqueous broccoli extract alone. Sterile water was used as the negative control, and ampicillin served as the positive control.*

	Gram-positive bacteria		**Gram-negative bacteria**	
	Staphylococcus aureus (SA)	Methicillin-resistant *Staphylococcus aureus* (MRSA)	*Escherichia coli (E.C)*	*P. aeruginosa (P.A)*
Garlic	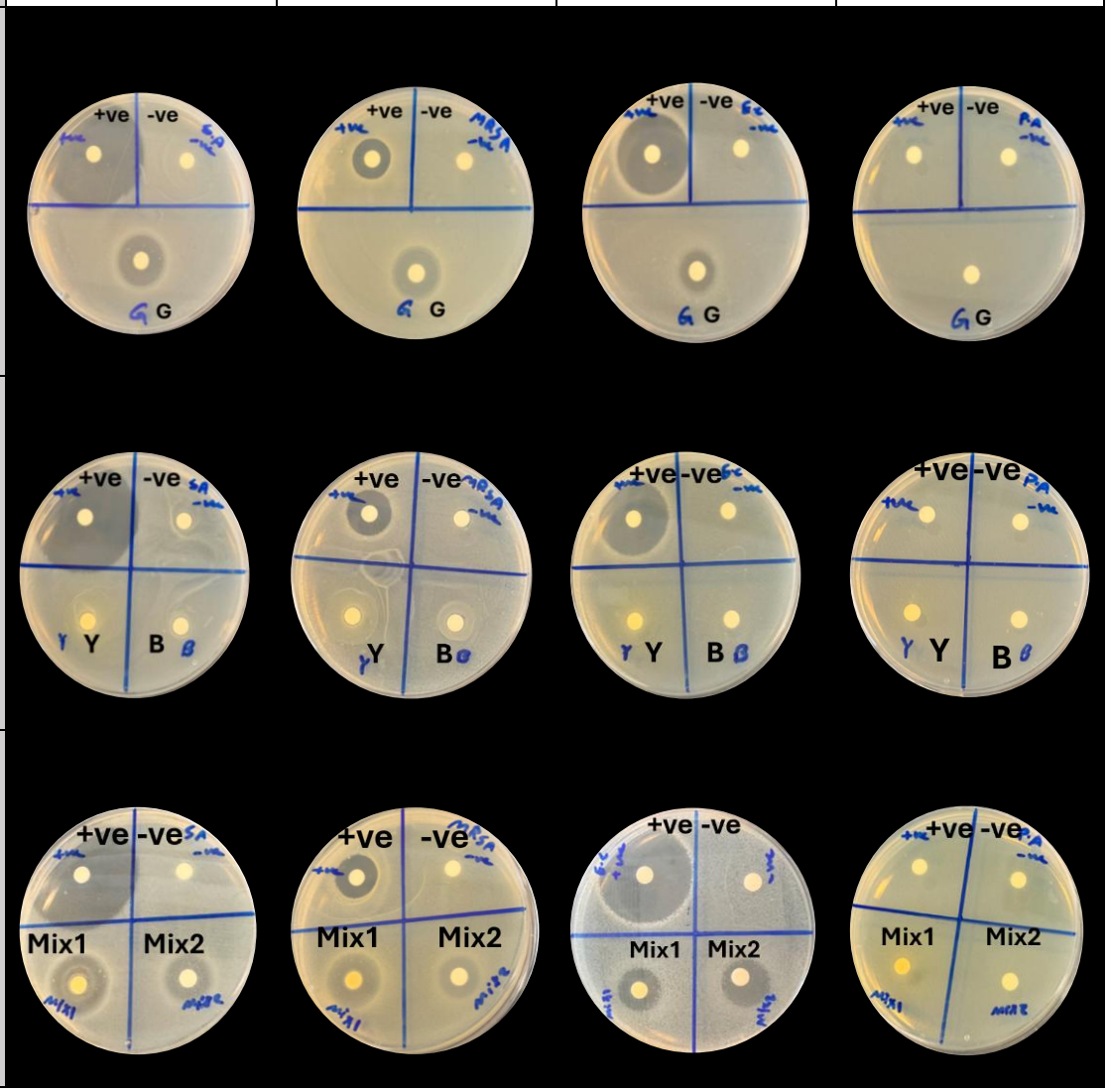			
Mustard seeds powder(Y)-Broccoli(B)				
Mixture 1 and Mixture 2				

Table 4.2: Antibacterial activity of crude plant extracts and mixed extract systems expressed as inhibition zone diameters (mm). Ampicillin and ciprofloxacin were used as positive controls.

Samples	Bacteria inhibitory zone (mm)			
	SA	MRSA	E. C	P. A
Garlic	18	18	13	0
Mustard seeds powder (Y)	0	0	0	0
Broccoli (B)	0	0	0	0
Mixture 1 (Garlic+ Mustard seeds powder)	21	25	16	0
Mixture 2 (Garlic+ Broccoli)	23	25	16	0

4.3 Antibacterial activity of alligrin compared with allicin and sinigrin

To elucidate the impact of structural hybridisation on antibacterial activity, alligrin was evaluated alongside its parent structural components allicin and sinigrin. Antibacterial activity was assessed against a Gram-positive strain (MRSA) and a Gram-negative strain (*Escherichia coli*) using the disc diffusion assay at equimolar concentrations, with ampicillin included as a positive reference control to validate assay performance and confirm strain susceptibility (Table 4.3).

Alligrin showed selective antibacterial activity against MRSA, producing concentration-dependent inhibition zones of 11 mm at 53.4 mmol and 15 mm at 106.7 mmol, whilst no activity was detected against *E. coli* at either concentration tested. Sinigrin similarly produced no measurable inhibition against either bacterial strain, consistent with the well-documented lack of antibacterial activity of intact glucosinolates prior to enzymatic hydrolysis [123]. In contrast, allicin demonstrated broader-spectrum activity, inhibiting both MRSA and *E. coli*. At

equivalent molar concentrations, allicin produced larger inhibition zones against MRSA than alligrin (16 mm versus 11 mm at 53.4 mM; 33 mm versus 15 mm at 106.7 mm), indicating that allicin is more potent antibacterial agent than alligrin (Table 4.4). This superior activity consistent with previously reported findings on the mechanism of allicin, through the highly electrophilic thiosulfinate moiety readily penetrates bacterial membranes and irreversibly inactivates thiol-dependent enzymes in both Gram-positive and Gram-negative organisms [49]. Despite alligrin and allicin produced measurable inhibition zones, these remained less potent than synthetic antimicrobial agents.

The lower potency of alligrin relative to allicin suggests that incorporation of the sinigrin-derived moiety into the hybrid structure restricts the ability of the thio-allyl motif from allicin to react with bacterial thiol targets. The presence of the sulfated group (SO_3^-) within the sinigrin-derived moiety increases both the molecular size and polarity of alligrin, likely reducing its ability to penetrate the hydrophobic outer membrane of Gram-negative bacteria and limiting access of the thio-allyl motif to active-site cysteine residues. Nevertheless, the activity against MRSA indicates that the hybrid core structure preserves sufficient electrophilicity to react with thiol-containing targets in Gram-positive organisms, requiring further investigation of its mechanism of action and structure-activity relationships.

*Table 4.3: Comparative antibacterial activity of alligrin, allicin, and sinigrin against methicillin-resistant Staphylococcus aureus (MRSA) and Escherichia coli (E.C) determined by the disc diffusion assay. Agar plates were divided into four quadrants to allow direct within-plate comparison. For **alligrin**, discs labelled **2** correspond to 2.6 µmol and **1** to 5.3 µmol. For **allicin**, discs labelled **A5** correspond to 2.6 µmol and **A15** to 5.3 µmol. For **sinigrin**, discs labelled **S20** correspond to 2.6 µmol and **S50** to 5.3 µmol. 70% methanol was used as the negative control, and **ampicillin** was included as the positive control.*

	Gram-positive bacteria	**Gram-negative bacteria**
	Methicillin-resistant *Staphylococcus aureus* (MRSA)	*Escherichia coli* (*E.C*)
Alligrin	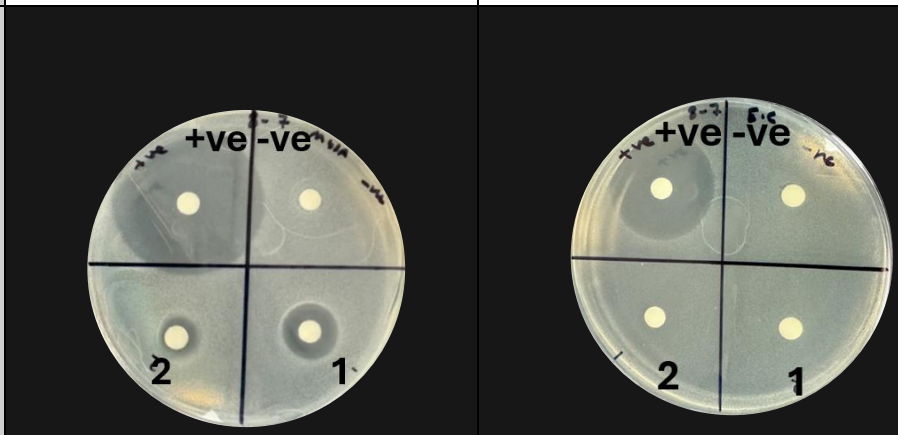	
Allicin		
Sinigrin	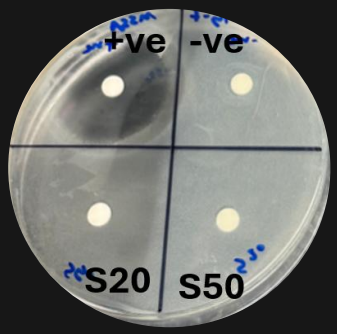	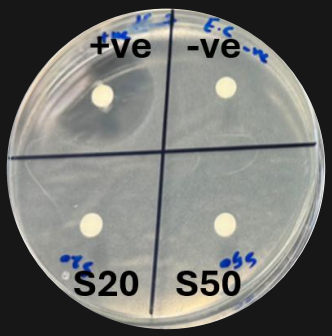

Table 4.4: Bacterial inhibition zone diameters (mm) produced by alligrin, allicin, and sinigrin. Inhibition zones against (MSSA; Gram-positive) and (E. coli; Gram-negative) measured using the disc diffusion assay.

Samples	Samples concentration		Bacteria inhibitory zone (mm)	
	µg/disc	µmol/disc	MRSA (Gram +ve)	E.C (Gram -ve)
Ampicillin	60	0.172	40	30
Alligrin	715	2.6	11	0
	1435	5.3	15	0
Allicin	430	2.6	16	19
	865	5.3	33	26
Sinigrin	950	2.6	0	0
	1915	5.3	0	0

As alligrin shows an antibacterial profile different from both allicin and sinigrin, further structural investigation is required to identify the functional elements responsible for its biological activity. The sulfate group (SO_3^-) incorporated from the sinigrin-derived moiety represents a key structural modification that influences the charge, reactivity, and membrane interactions of alligrin, likely modulating its antibacterial potency. To investigate the influence of this sulfate group to biological activity, the effect of enzymatic desulfation on the antibacterial activity of alligrin was investigated, providing further insight into the structure-activity relationships controlling the bioactivity of this hybrid organosulfur compound.

4.4 Desulfation of alligrin and structure-activity relationship analysis

Structural modification of bioactive compounds represents a well-established strategy for defining structure-activity relationships and identifying functional groups critical for biological activity. Within the glucosinolate family, sulfation of the thiohydroximate moiety is a defining structural feature that strongly influences molecular polarity, aqueous stability, enzymatic recognition, and membrane permeability [135]. Therefore, enzymatic desulfation has been widely used in glucosinolate research as a tool to assess the impact of the sulfate group to biological function and compound reactivity [135].

The structure of alligrin contains a sulfate-bearing thiohydroximate motif linked to the thio-allyl motif of allicin (Figure 4.1). The presence of the sulfate group (SO_3^-), which carries a permanent negative charge tending reduces membrane permeability, slowing passive diffusion across bacterial membranes and limiting access to intracellular thiol-dependent targets. This may explain the reduced antibacterial potency of alligrin relative to allicin.

Sulfation is known to influence the electrophilicity and thiol-reactivity of organosulfur compounds. Removing the sulfate group would be expected to modify the charge distribution and reactivity of alligrin, potentially affecting both its antibacterial potency and spectrum of activity. To investigate this, sulfatase-mediated desulfation was carried out to produce desulfo-alligrin (Figure 4.1), and its antibacterial activity was compared with that of alligrin under identical assay conditions.

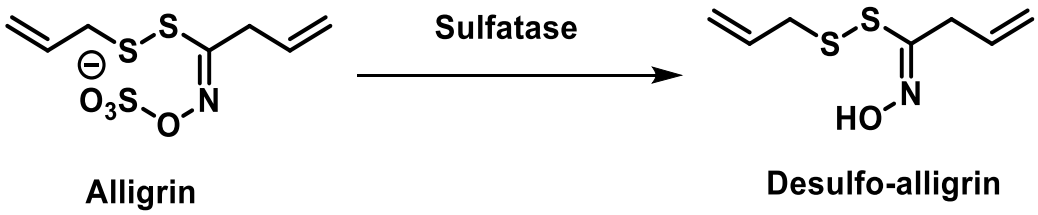

Figure 4.1: Enzymatic desulfation of alligrin to desulfo-alligrin by sulfatase.

4.4.1 Enzymatic desulfation of alligrin for structure-activity relationship analysis

The sulfatase-mediated desulfation was performed to generate desulfo-alligrin following the desulfation protocol (see Section 7.2.10.2). Successful desulfation was confirmed by HPLC analysis (Section 7.2.3.1), which revealed an obvious shift in retention time from 7.6 min for alligrin to 15.5 min for desulfo-alligrin (Figure 4.2), indicating a significant reduction in molecular polarity upon removal of the negatively charged sulfate group. The increased retention of desulfo-alligrin on the stationary phase is consistent with its greater hydrophobicity relative to the parent compound, confirming complete enzymatic conversion before the antibacterial evaluation.

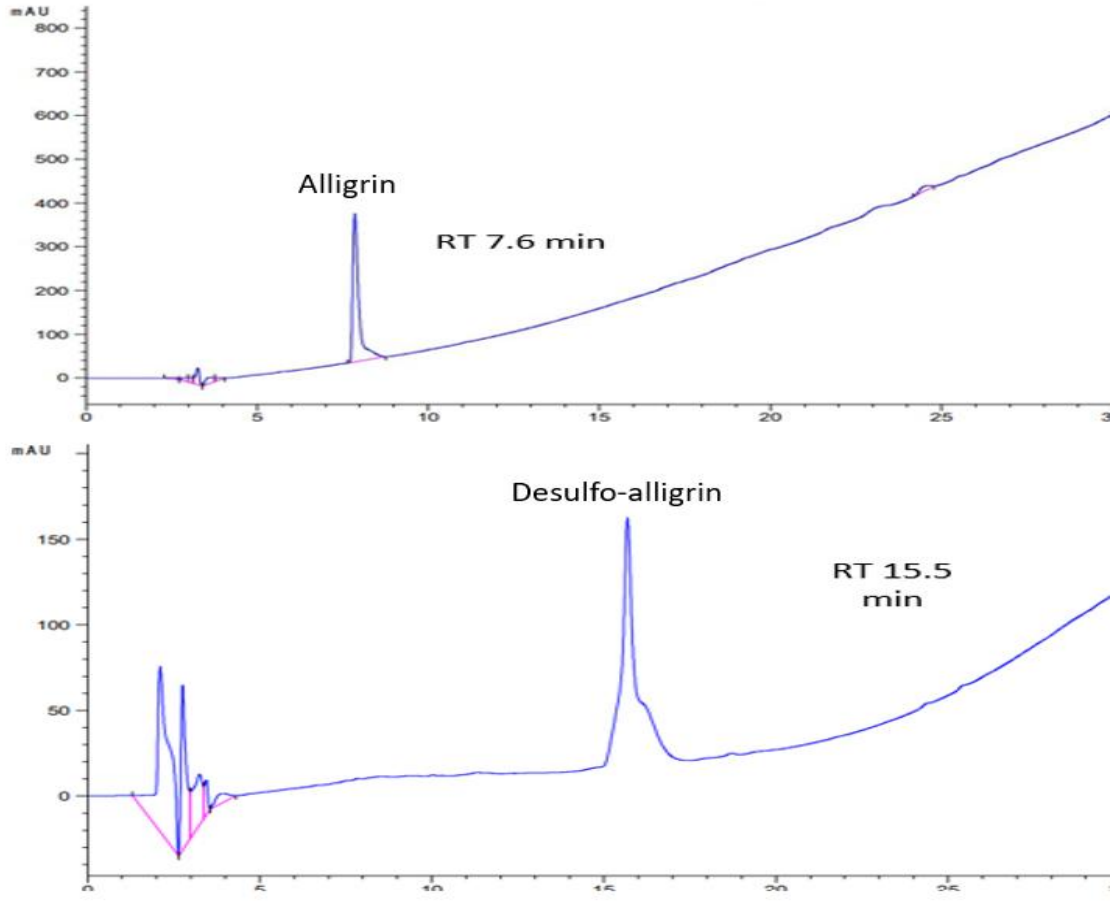

*Figure 4.2: HPLC chromatograms of alligrin and desulfo-alligrin. Alligrin eluted at **RT 7.6 min**, while desulfo-alligrin eluted later at **RT 15.5 min**.*

Successful desulfation of alligrin was further confirmed by ^{1}H NMR spectroscopy, which revealed changes in chemical shift values across the vinyl and allylic regions of the spectrum, consistent with alterations in the electronic environment following removal of the sulfate group (Figure 4.3).

In the vinyl region (5.0-6.0 ppm), desulfo-alligrin exhibited terminal alkene protons (H1,2 and H9,10) at δ 5.08-5.18, 5.74-5.83 and 5.83-5.93 ppm with minimal chemical shift differences compared with alligrin reflecting their greater distance from where the structural modification occurred. Protons H6,7 and H9,10 showed a measurable downfield shift relative to alligrin, consistent with their closer position to the desulfation site where removal of the electron-withdrawing SO_3^- group alters local electron density. The retention of all vinyl signals confirms allyl moiety integrity and selective sulfatase activity on the sulfate group. Together, the observed chemical shift changes are chemically consistent with the transition from a sulfated to a free sulfated group form, providing structural validation of successful desulfation (see LC-MS data in appendix).

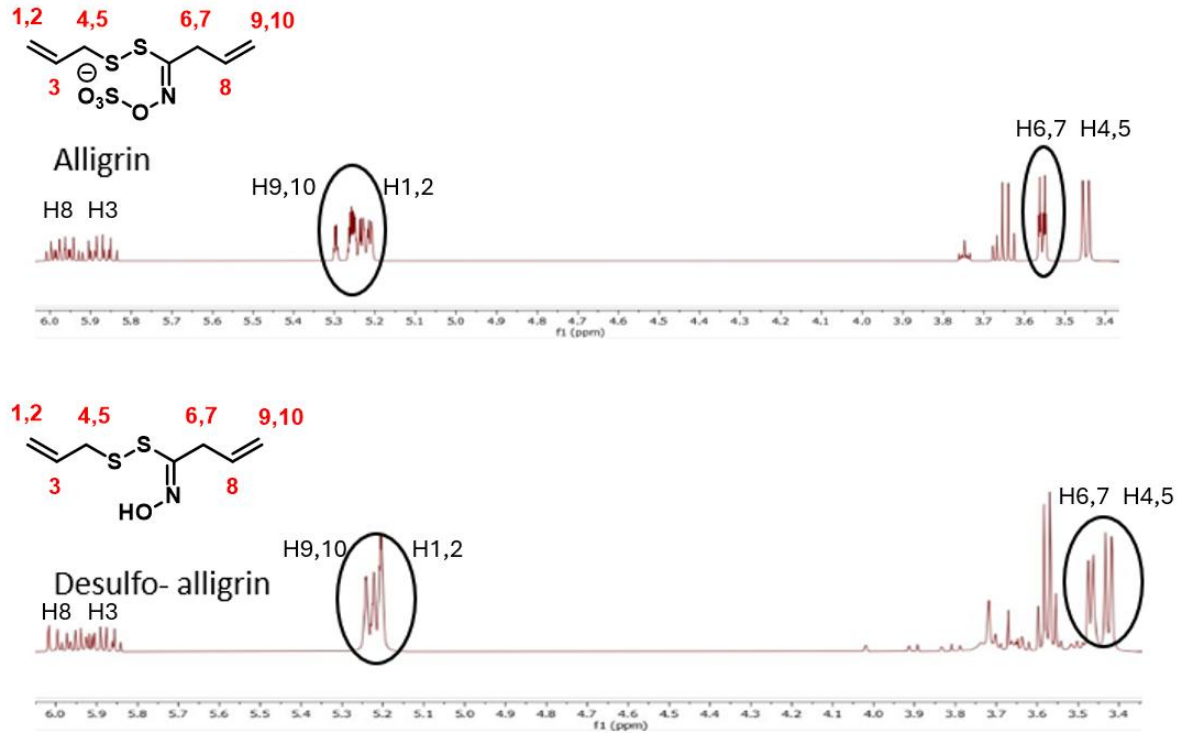

Figure 4.3: ^{1}H NMR spectra of alligrin and desulfo-alligrin.

Following desulfation of alligrin, the antibacterial activity of the resulting desulfo-alligrin was evaluated against the same bacterial group under identical assay conditions, enabling a direct assessment of the contribution of the sulfate moiety to antibacterial potency.

4.4.2 Effect of desulfation on the antibacterial activity of alligrin

Alligrin exhibited dose-dependent antibacterial activity against Gram-positive bacteria, producing inhibition zones (37 mm) against *Staphylococcus aureus* and (25 mm) against MRSA at the higher concentration. Moderate activity was also observed against *Escherichia coli* (17 mm), while no inhibition was detected against *Pseudomonas aeruginosa*. These findings indicate that alligrin shows significant antimicrobial potency against Gram-positive pathogens, including antibiotic-resistant strains. In contrast, the desulfated alligrin showed no detectable antibacterial activity at either concentration tested, suggesting that the sulfate -containing functional groups present in the parent compound are critical for biological activity (Tables 4.5, 4.6).

Table 4.5: Comparative antibacterial activity of alligrin and desulfo-alligrin at high concentration against Gram-positive and Gram-negative bacteria. Note The upper quadrants contain alligrin (A1, 10.6 µmol; A2, 5.6 µmol), while the lower quadrants contain desulfo-alligrin (D1, 10.6 µmol; D2, 5.6 µmol).

	Gram-positive bacteria		**Gram-negative bacteria**	
	Staphylococcus aureus (SA)	methicillin-resistant *Staphylococcus aureus* (MRSA)	*Escherichia coli (E.C)*	*P. aeruginosa* (P.A)
Alligrin and Desulfo-alligrin	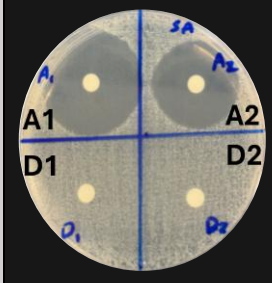	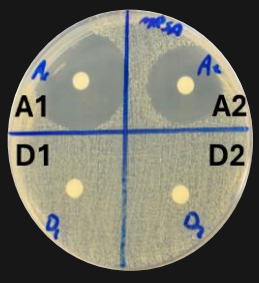	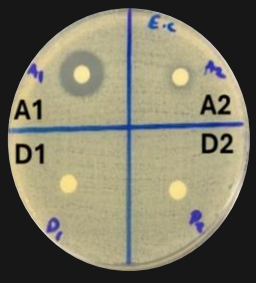	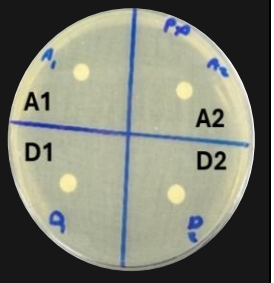

Table 4.6: Bacterial inhibition zone diameters (mm) of alligrin and desulfo-alligrin at the same molar concentrations. Alligrin showed antibacterial activity against Gram-positive bacteria, whereas desulfo-alligrin was inactive against all tested strains, indicating the essential role of the sulfate group in antibacterial activity.

Samples	Samples concentration		Bacteria inhibitory zone (mm)			
	µg/disc	µmol/disc	SA	MRSA	E. C	P. A
Ampicillin	60	0.172	45	20	27	0
Ciprofloxacin	30	0.0905	26	25	36	36
Alligrin	2850	10.6	37	25	17	0
	1435	5.3	30	20	0	0
Desulo-alligrin	2000	10.6	0	0	0	0
	1000	5.3	0	0	0	0

Although desulfation led to a loss of antibacterial activity at concentrations where alligrin remained active, it was unclear whether this reflected a complete loss of bioactivity or simply a reduction in potency. To address this, desulfo-alligrin was tested at higher concentrations to determine whether any antibacterial activity could be recovered and to further understand the contribution of the sulfate group to alligrin's antibacterial activity.

4.4.3 Antibacterial activity of desulfo-alligrin at high concentrations

Initial comparison of alligrin and desulfo-alligrin at equivalent concentrations of approximately 100 mmol and 200 mmol revealed a clear difference in antibacterial activity. Based on the loss of desulfo-alligrin activity, the concentration was increased to assess whether antibacterial effects could be recovered at a higher dose (Table 4.7). At 400 mmol, desulfo-alligrin produced weak but detectable inhibition zones against all tested organisms

including S. aureus (8 mm), MRSA (13 mm), E. coli (17 mm), and P. aeruginosa (10 mm) (Table 4.8). While this concentration is higher than typical antimicrobial testing ranges, it was used specifically to detect residual bioactivity following desulfation rather than to assess therapeutic potential. Interestingly, activity was recovered against Gram-negative organisms at this concentration, suggesting that removal of the SO_3^- group improves outer membrane penetration due to the reduction in molecular polarity. The fact that such a high concentration was needed to produce only weak inhibition clearly demonstrates that the sulfate group is essential to the potency of alligrin.

*Table 4.7: Antibacterial activity of desulfo-alligrin against Gram-positive and Gram-negative bacteria. The disc diffusion assay showing the antibacterial activity of desulfo-alligrin against Gram-positive (*Staphylococcus aureus *and MRSA) and Gram-negative (*Escherichia coli *and* P. aeruginosa*) bacterial strains at high molar concentration. Plates were divided into quadrants to allow direct within-plate comparison. Label "1" corresponds to desulfo-alligrin at 21.13 µmol, while label "2" corresponds to desulfo-alligrin at 10.6 µmol.*

	Gram-positive bacteria		**Gram-negative bacteria**	
	Staphylococcus aureus *(SA)*	methicillin-resistant *Staphylococcus aureus* (MRSA)	*Escherichia coli* *(E.C)*	*P. aeruginosa* *(P.A)*
Desulso-alligrin	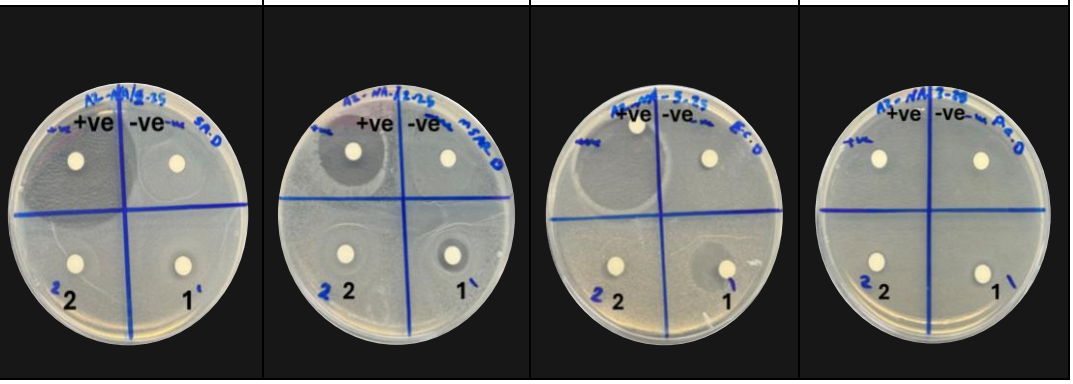			

Table 4.8: Antibacterial activity of desulfo-alligrin at increasing molar concentrations. Bacterial inhibition zone diameters (mm) produced by desulfo-alligrin against Staphylococcus aureus *(SA), methicillin-resistant* S. aureus *(MRSA),* Escherichia coli *(E.C), and* Pseudomonas aeruginosa *(P.A) determined using the disc diffusion assay.*

Samples concentration		**Bacteria inhibitory zone (mm)**			
µg/disc	**µmol/disc**	**SA**	**MRSA**	**E. C**	**P. A**
4000	21.13	8	13	17	10
2000	10.6	0	0	0	0

This finding suggests that the antibacterial activity of alligrin is driven by its sulfate -containing groups rather than the core molecular structure alone. Accordingly, a thiol-mediated mechanism of action is proposed to explain the observed antibacterial behaviour of alligrin.

4.5 Proposed mechanism of action of alligrin

The biological activity of sulfur-containing phytochemicals commonly through interactions with cellular thiols, leading to modulation of redox balance, enzyme function, and cellular signalling pathways [199]. Compounds such as allicin and isothiocyanates are well known to react with low-molecular-weight thiols (e.g., glutathione, cysteine, and protein thiols), forming reversible or irreversible sulfur adducts that disrupt essential cellular processes in microbial cells [184, 199]. The sulfur-rich structure of alligrin suggests that its antibacterial activity through a similar thiol-dependent mechanism.

The chemical structure of alligrin contains electrophilic sulfur and a sulfated thiohydroximate motif, indicating a strong potential to participate in thiol exchange reactions within bacterial cells. As illustrated in the proposed mechanism (Figure 4.4). The primary pathway involves nucleophilic attack by intracellular glutathione on the sulfur centre of alligrin, resulting in the formation of S-allylmercaptoglutathione, followed by the release of a sulfonated aldoxime

intermediate. This unstable intermediate may undergo further rearrangement to generate allyl isothiocyanate (AITC), a known electrophilic antimicrobial species. Subsequent interaction of AITC with cellular thiols can lead to the formation of S-(N-allylthiocarbamoyl) glutathione (Figure 4.4).

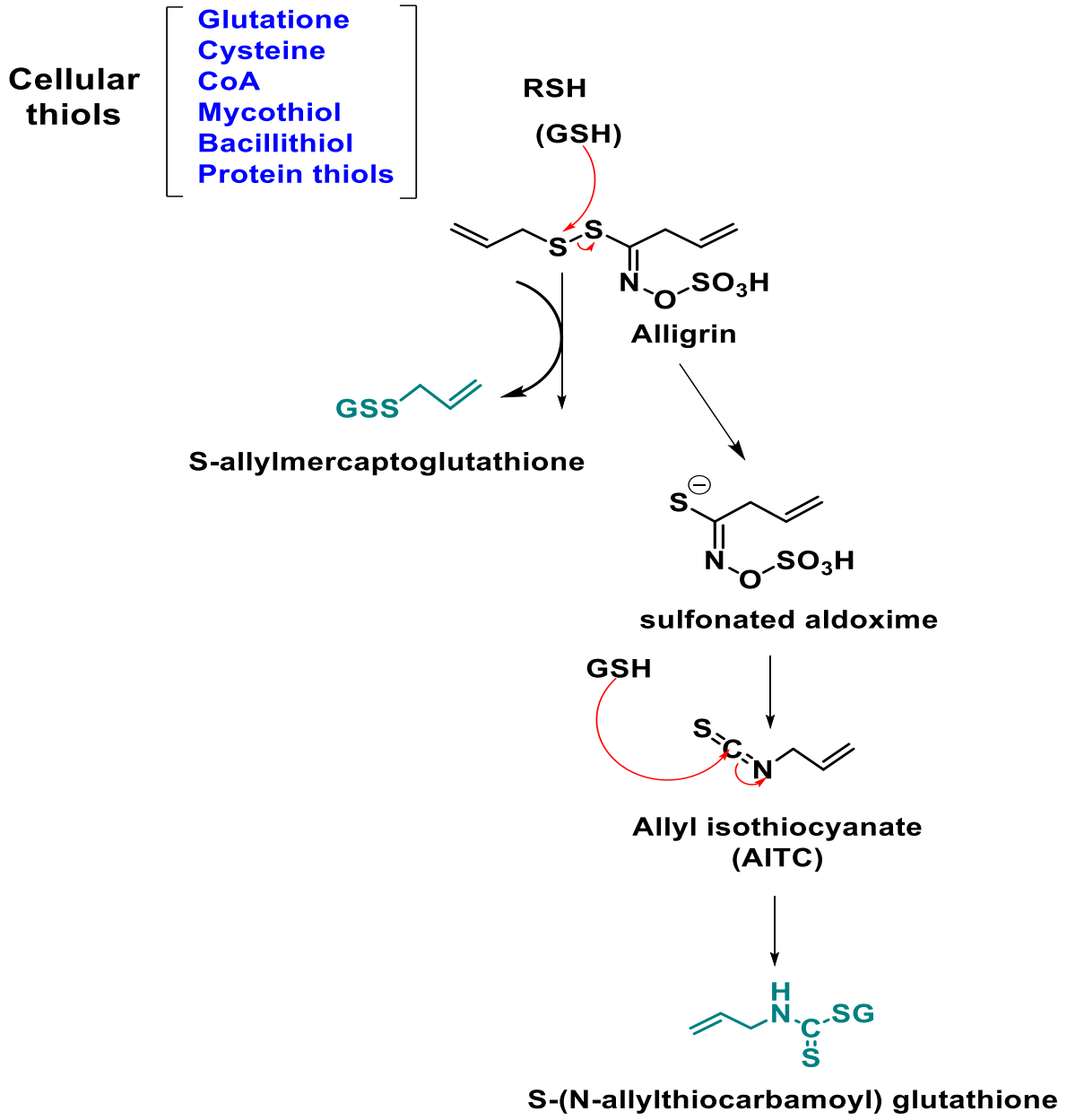

Figure 4.4:Proposed thiol-dependent mechanism of alligrin activity.

Together, these two pathways would deplete cellular thiols, disrupt redox homeostasis, and impair essential enzymatic functions, producing an antibacterial effect greater than either pathway could achieve alone.

4.6 Preliminary evaluation of thiol reactivity of alligrin and desulfo-alligrin with glutathione

To obtain experimental support for the proposed thiol-dependent mechanism of action of alligrin, its chemical reactivity toward glutathione was investigated. Glutathione represents the major low-molecular-weight thiol in biological systems, playing a central role in redox regulation, thiol exchange, and detoxification of electrophilic compounds [223]. Given the electrophilic character of the thio-allyl group in alligrin, direct interaction with glutathione would be expected if its antibacterial activity is mediated through thiol-reactive mechanisms.

Alligrin (1.50 mg/mL, 5.58 mmol) was incubated with freshly prepared glutathione (1.70 mg/mL, 5.53 mmol) at equimolar concentration, falling within the reported physiological range of intracellular glutathione (1-10 mmol) [223], for 30 minutes at room temperature and monitored by HPLC and LC-MS. The result showed complete disappearance of the alligrin peak following incubation, accompanied by the appearance of new early eluting peaks consistent with the formation of highly polar reaction products (Figure 4.5).

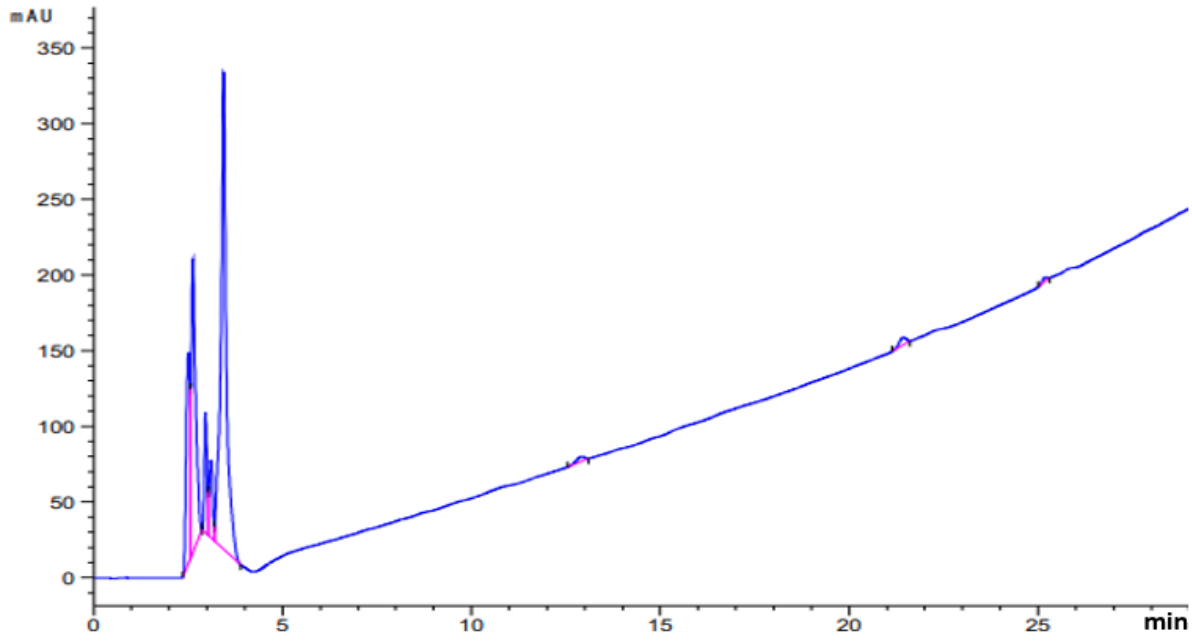

Figure 4.5:HPLC chromatogram of alligrin after incubation with glutathione.

LC-MS analysis of the incubation mixture identified two sulfur-conjugated products, providing direct evidence that alligrin undergoes thiol-mediated transformation through two concurrent reaction pathways (Figures 4.7, 4.8), consistent with the proposed mechanism illustrated in Figure 4.4. The first pathway yielded S-allylmercaptoglutathione (SAMG), detected at m/z 378.08 $[M-H]^-$ ($C_{13}H_{21}N_3O_6S_2$), alongside a sulfonated aldoxime intermediate (Figures 4.4, 4.6, 4.7). The second pathway produced S-(N-allylthiocarbamoyl) glutathione, detected at m/z 405.09 $[M-H]^-$ ($C_{14}H_{22}N_4O_6S_2$) (Figures 4.4, 4.8, 4.9).

These findings demonstrate that glutathione reacts with alligrin through both direct thio-allyl conjugation and secondary isothiocyanate trapping pathways. Both can depleting cellular thiol pools and disrupting redox homeostasis, a mechanism analogous to the well-established thiol-reactivity of allicin [224].

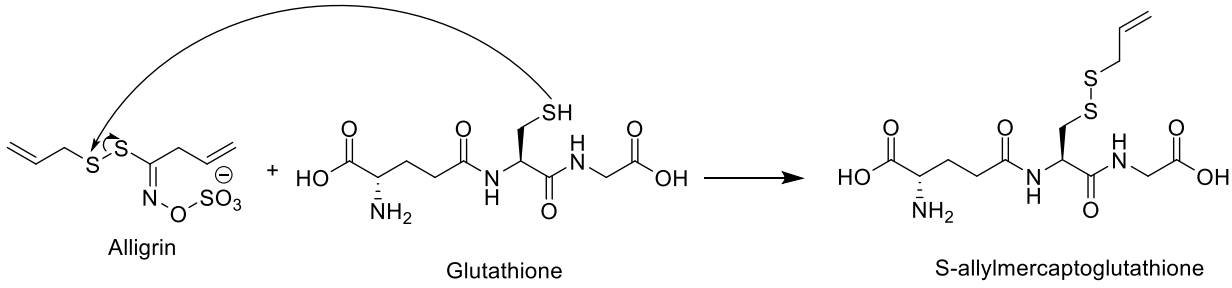

Figure 4.6: Proposed mechanism of the reactivity of alligrin with glutathione.



Figure 4.7: LC-MS spectrum of the alligrin-glutathione incubation mixture showing formation of S-allylmercaptoglutathione.

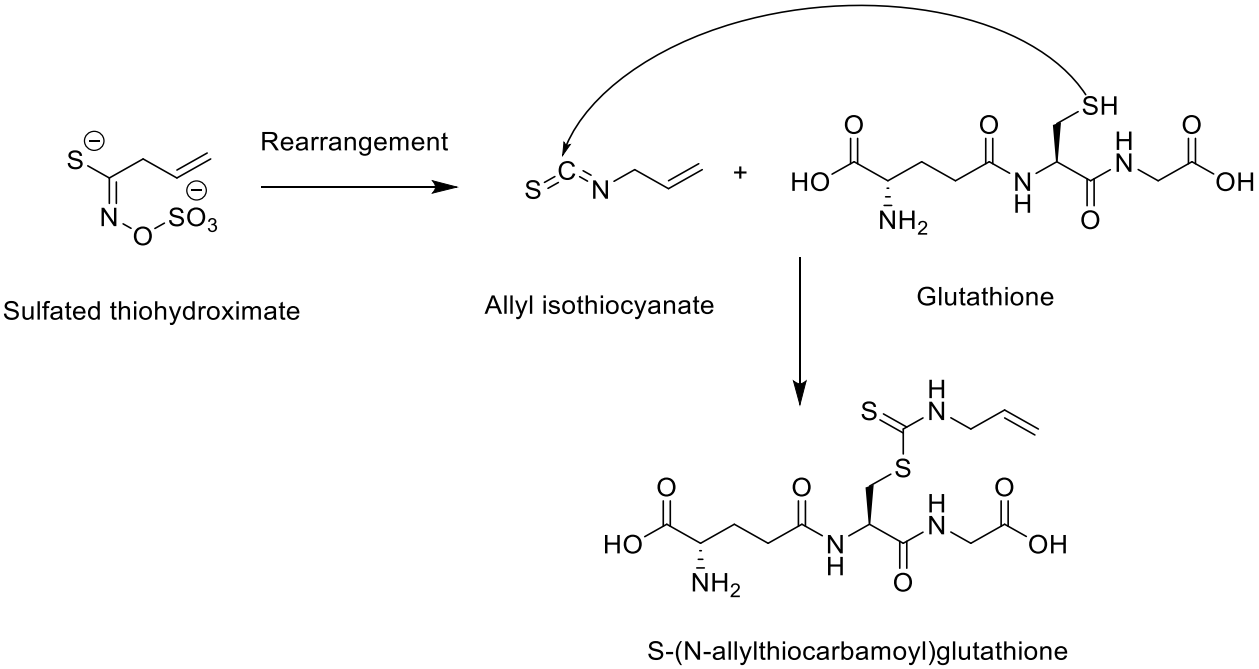

Figure 4.8: Proposed mechanism of the reactivity of alligrin with glutathione.

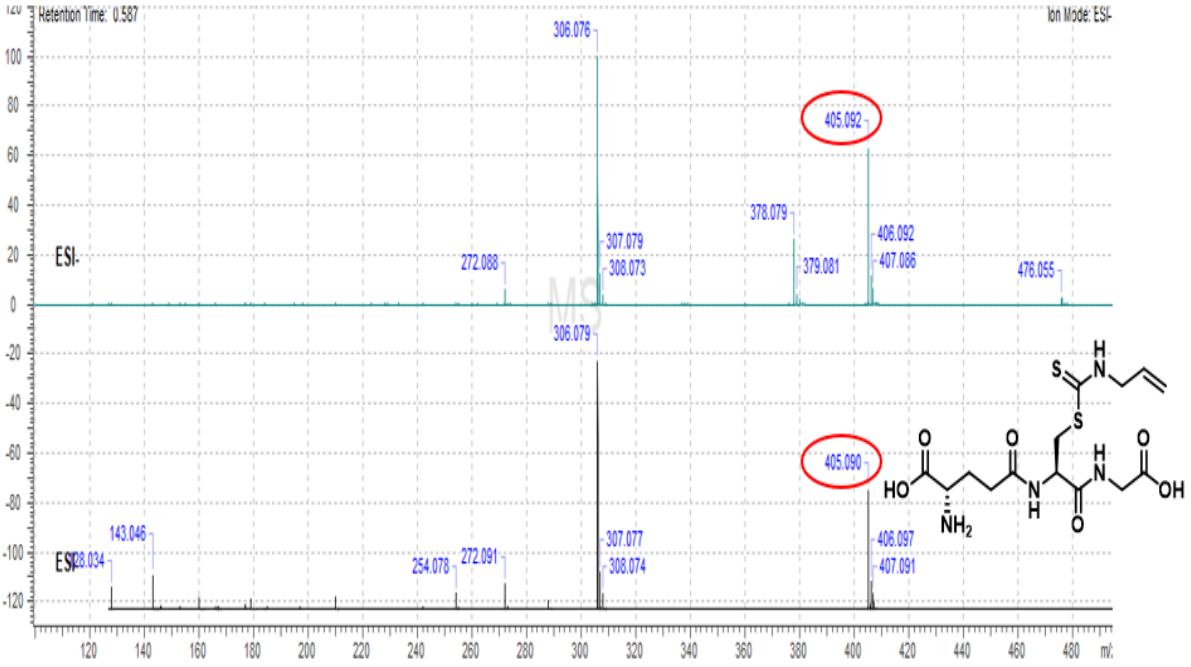

Figure 4.9: LC-MS spectrum of the alligrin-glutathione incubation mixture showing formation of a S-(N-allylthiocarbamoyl) glutathione.

To further investigate the role of the sulfate group in thiol reactivity, the same experiment was performed with desulfo-alligrin (1.04 mg/mL, 5.50 mmol) under identical conditions. LC-MS analysis confirmed the formation of S-allylmercaptoglutathione but not S-(N-allylthiocarbamoyl) glutathione. The absence of the latter product is consistent with the requirement for a sulfate leaving group in the rearrangement of the sulfonated aldoxime intermediate to generate allyl isothiocyanate (AITC), a step that cannot occur in desulfo-alligrin (Figures 4.10, 4.11).

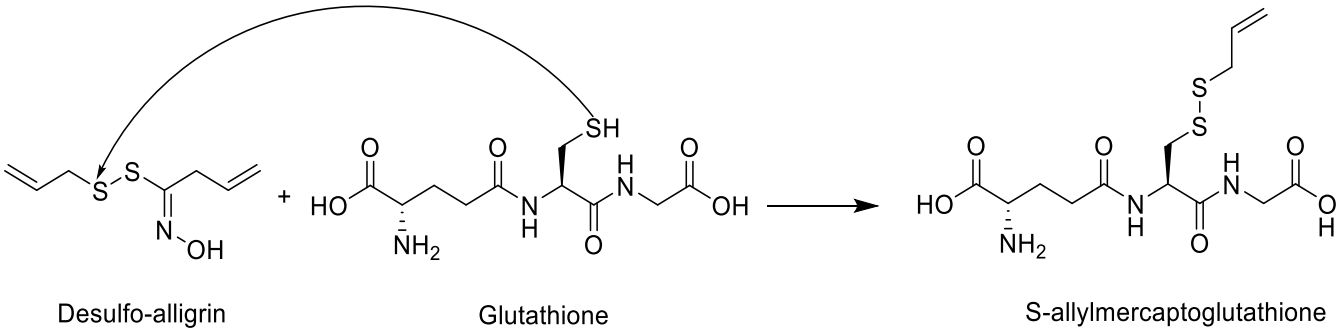

Figure 4.10: Proposed mechanism of the reactivity of desulfo-alligrin with glutathione.

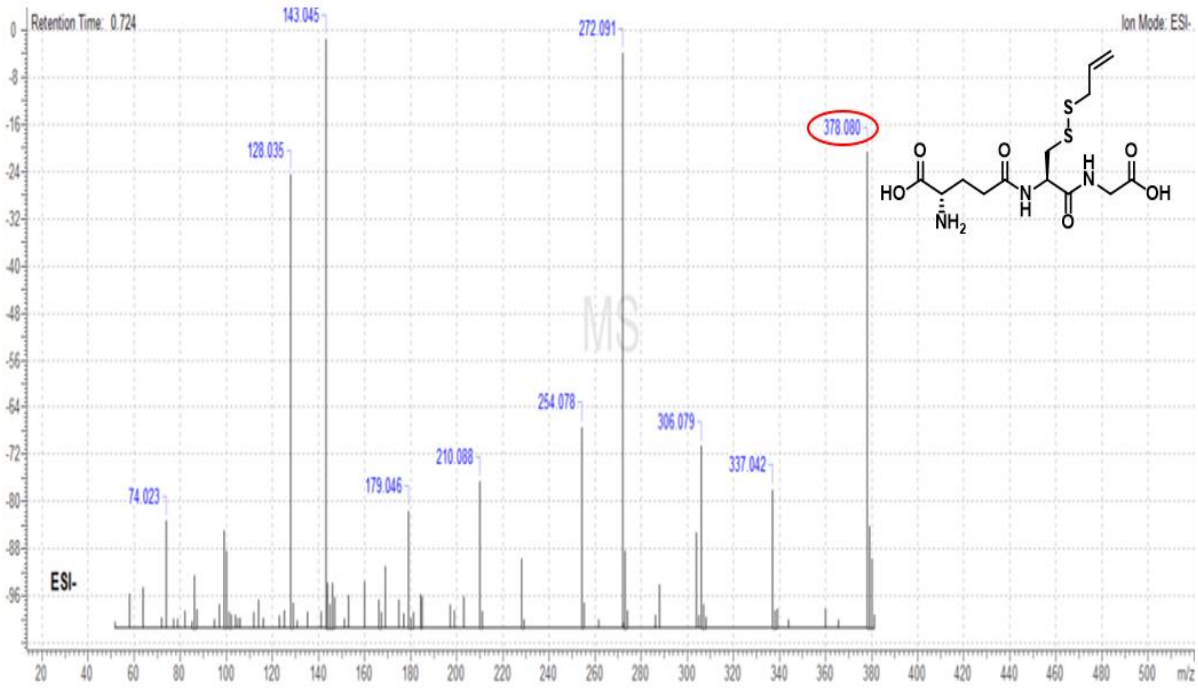

Figure 4.11: LC-MS spectrum of the desulfo-alligrin-glutathione incubation mixture showing formation of S-allylmercaptoglutathione.

4.7 Summary and conclusion

This chapter investigated the antibacterial activity arising from chemical interactions between garlic- and glucosinolate-derived sulfur metabolites. Initial screening of crude aqueous plant extracts showed that garlic exhibited moderate activity against the tested organisms, while mustard seed powder and broccoli extracts were inactive under the conditions used. Significantly, mixing garlic with glucosinolate-containing plant enhanced antibacterial activity against Gram-positive bacteria and Escherichia coli, suggesting that novel sulfur-conjugated compounds formed through garlic-glucosinolate interactions are responsible for the observed enhancement.

Building on these findings, purified sulfur-containing compounds were evaluated to establish structure-activity relationships. Alligrin exhibited selective activity against Gram-positive bacteria, including methicillin-resistant Staphylococcus aureus, though with reduced potency and a narrower spectrum than allicin. Sinigrin showed no antibacterial activity under any of the conditions tested.

Enzymatic desulfation of alligrin resulted in a loss of antibacterial activity, confirming that the sulfate group plays a critical role in mediating potency. Although weak activity was detected for desulfo-alligrin at higher concentrations, this finding demonstrates that sulfation is essential to the biological activity of alligrin and responsible for its structure-activity relationship.

Mechanistic investigations supported a thiol-dependent mode of action. Incubation of alligrin with glutathione led to rapid disappearance of the parent compound and formation of sulfur-containing conjugates, as confirmed by HPLC and LC-MS analysis. Identification of S-allylmercaptoglutathione and S-(N-allylthiocarbamoyl) glutathione provided direct chemical evidence for thiol-sulfur exchange and secondary transformation pathways. Overall, this chapter demonstrate that the biological activity of plant-derived sulfur metabolites can be modulated through structural conjugation, offering new insight into their chemical reprogramming.

5 Alligrin: Crystal Structure, Stereochemical Analysis, and Comparative Study of a Novel Natural Product

5.1 Introduction and aim

X-ray crystallography is the most powerful tool available for proving the structure of novel natural products. Unlike NMR, infrared, and mass spectrometry, which can suggest but never definitively prove a molecular structure. Single-crystal X-ray diffraction alone provides a direct determination of all atomic positions in three-dimensional space, yielding precise bond lengths, bond angles, torsion angles and resolving stereochemical questions that are inaccessible by any other routine analytical method.

This chapter reports the single-crystal X-ray diffraction study of alligrin crystals of which were obtained during its chromatographic purification as described in Chapter 2. Alligrin is characterised by the novel heteroatomic chain C-S-S-C-C=N-O-SO_3^-, in which the thio-allyl fragment from allicin is covalently combined with the sulfonated oxime fragment from sinigrin through a new disulfide bridge, a connectivity motif previously unreported in any natural product.

The aim of this chapter is to determine the crystal structure and absolute stereochemistry of alligrin by single-crystal X-ray diffraction, and to compare its disulfide geometry and bonding parameters with those of disulfide-containing proteins and the parent compound sinigrin, using PyMOL as a molecular visualisation tool to analyse and compare the three-dimensional structures of these compounds.

5.2 Crystal structure determination of alligrin by single-crystal x-ray diffraction

Single-crystal X-ray diffraction analysis of alligrin reveals a molecular structure defined by the continuous heteroatomic chain C-S-S-C-C=N-O-SO_3^-, in which two chemically different structural fragments are united through a new disulfide bridge into a single covalent structure. The first fragment, derived from allicin, contains the thio-allyl fragment C1-C2-C3-S8, in which the terminal allyl group is connected through the carbon to the disulfide (Figure

5.1). The second fragment, derived from sinigrin, contains the fragment S9-C7=N1-O11-S10(=O12) (=O13) (=O14), in which the oxime carbon C7 bears the *Z*-configured C7=N1 double bond connected through O11 to the sulfonate group, completing the sinigrin-derived sulfonated oxime arm. In addition, C7 bonded to the allyl group including C4, C5 and C6, making it the central branching point that connects the oxime, sulfonate and allyl substituents within this fragment. The two main fragments are covalently connected at the S8-S9 disulfide bridge, which closes the full C-S-S-C-C=N-O-SO_3^- heteroatomic chain and indicates the specific point of chemical union between the allicin and sinigrin precursor fragments.

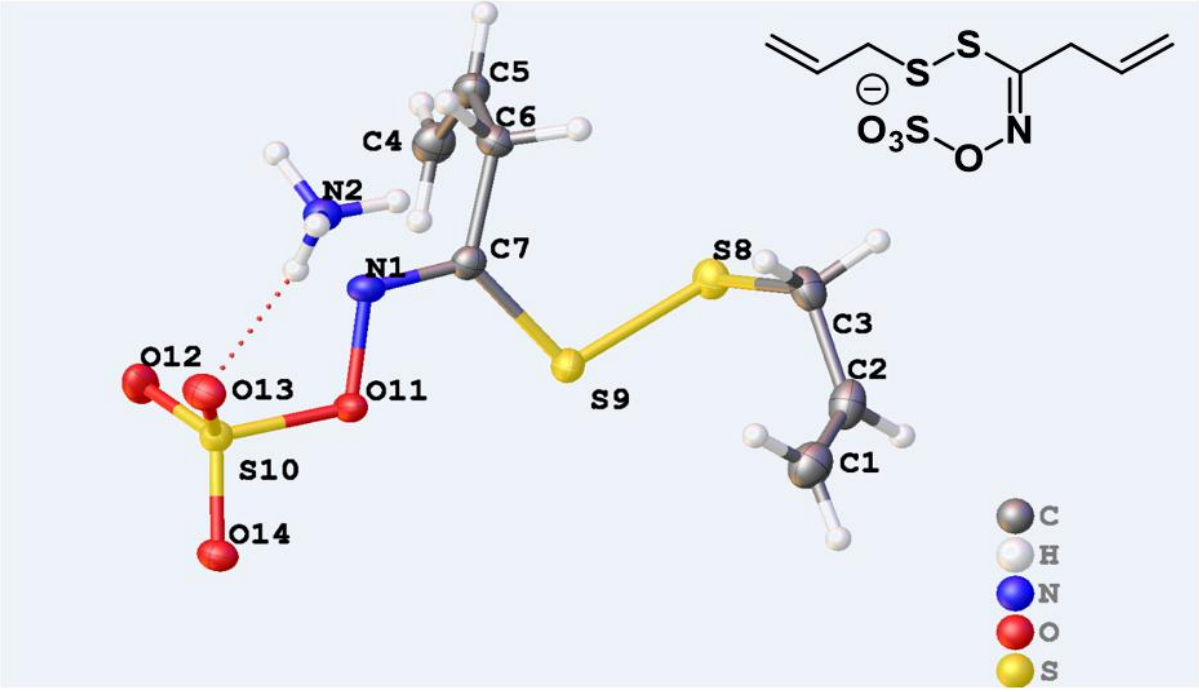

Figure 5.1: Crystal structure of alligrin determined by single-crystal X-ray diffraction, revealing the unusual disulfide bridge S8-S9 that covalently connects the allylthio fragment of allicin with the sulfonated oxime fragment of sinigrin.

A structurally significant finding from the SXRD analysis is the clear identification of the sulfonate group S10(=O12) (=O13) (=O14), retained intact from the sinigrin precursor and directly connected through O11 to the oxime nitrogen N1. This sulfonyloxy moiety introduces significant ionic character to the molecule, expected influencing its solubility and biological properties. Its presence is further reflected in the solid-state conformation, the N-H donors at N2 (introduced from the ammonium acetate crystallisation medium) form intramolecular hydrogen bonds with the sulfonate oxygen acceptor O13, visualised as red dashed contacts in Figure 5.1, playing a critical role in stabilising the molecular conformation of the alligrin.

The geometry of the disulfide linkage is fully consistent with established values for organic disulfides, both adjacent C-S bond lengths measure to 1.8 Å and the central S-S bond measures 2.0 Å (Figure 5.2), confirming the covalent integrity of the new C-S-S-C bridge. The C-S-S-C dihedral angle of 97.3° across S8-S9 (Figure 5.2) is consistent with the typical gauche conformation observed in disulfide bonds, which arises from sulfur lone-pair repulsion and is expected to influence the molecule's thiol-exchange reactivity and biological activity. The presence of multiple sulfur atoms in different oxidation states such as a disulfide in the C-S-S-C bridge and a sulfonate in the -O-SO_3^- group gives alligrin the potential to interact with biological thiols through redox reactions, which is consistent with the known antimicrobial and antioxidant activities of organosulfur compounds from both the Alliaceae and Brassicaceae families.

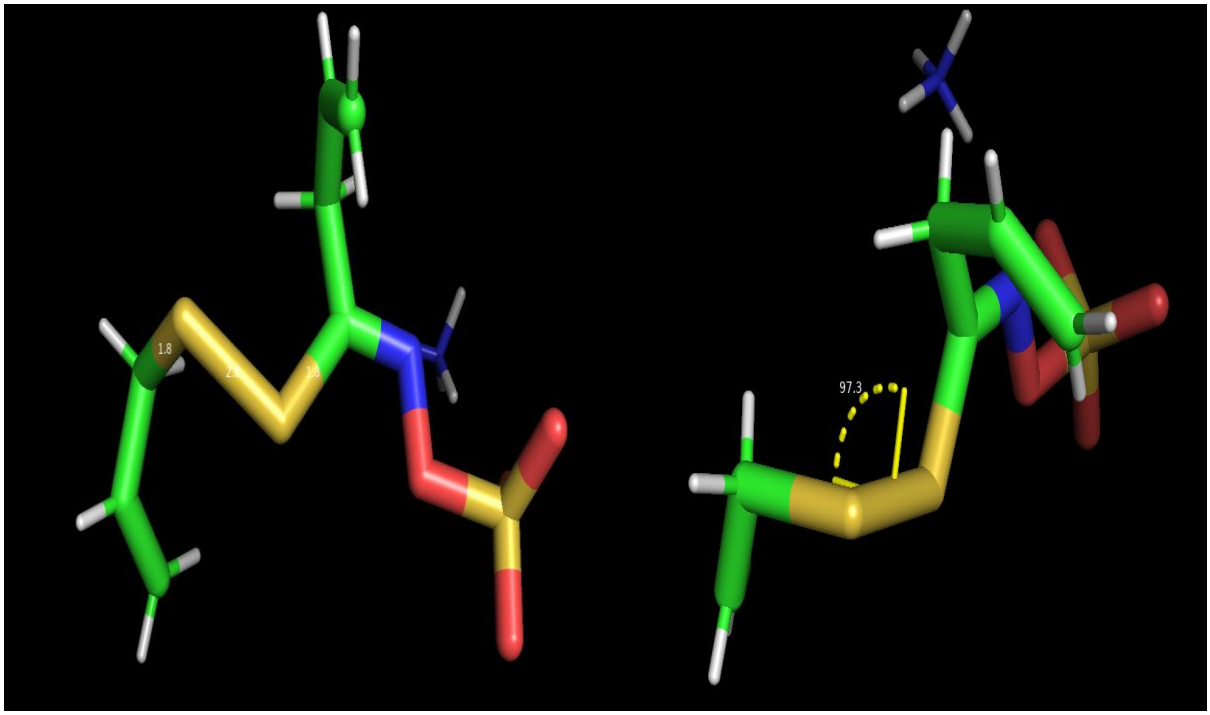

Figure 5.2: Crystal structure of alligrin showing (left) the disulfide bridge bond lengths (C-S = 1.8 Å, S-S = 2.0 Å) and (right) the C-S-S-C dihedral angle of 97.3°, confirming the characteristic gauche geometry of the disulfide linkage.

To the best of our knowledge, alligrin represents the first crystallographically characterised natural compound in which an allicin motif is directly conjugated with a sinigrin motif making this structure of considerable significance both to natural product chemistry and to the wider understanding of organosulfur reactivity at the chemical interface of these two plant families.

5.3 The disulfide bond: formation, electronic structure, and dihedral angle geometry

The disulfide bond (S-S bond) is one of the most chemically and structurally significant covalent linkages in chemistry and biochemistry. Formed by the oxidative coupling of two thiol (-SH) groups, disulfide bonds are characterised by a rich conformational range defined by a set of dihedral (torsion) angles along the C-S-S-C linkage. Understanding these angles is fundamental to predicting molecular geometry, reactivity, and three-dimensional fold stability and function [225]. The disulfide bond is formed by the two-electron oxidative coupling of two thiol groups, a reaction that can be represented as 2 R-SH → R-S-S-R + $2H^+$ + $2e^-$[226]. The resulting S-S bond has a characteristic length of approximately 2.04-2.05 Å, slightly longer than the adjacent C-S bonds (1.82 Å), a difference that reflects the interaction between the lone pairs on the two adjacent sulfur atoms and the consequent weakening of the S-S bond relative to a purely covalent two-centre interaction.

The three-dimensional geometry of a disulfide linkage R-S-S-R is fully described by five sequential dihedral angles along the C-S-S-C backbone, as summarised in Table 5.1 [225, 227]. Of these, the central C-S-S-C torsion angle χ_3 (Cβ-Sγ-Sγ'-Cβ') often called the "disulfide dihedral" is the most structurally and chemically significant, as it explains the handedness of the disulfide bridge and directly controls the stereochemical relationship between the two adjacent carbon-bearing arms.

Table 5.1:Dihedral angles describing the geometry of a disulfide linkage[227].

Angle	Atoms involved	Description
χ_1 (chi1)	N-Cα-Cβ-S	Side-chain torsion from backbone
χ_2 (chi2)	Cα-Cβ-Sγ-Sγ'	Torsion about the Cβ-Sγ bond
χ_3 (chi3)	Cβ-Sγ-Sγ'-Cβ'	The central **C-S-S-C dihedral**
χ_2' (chi2')	Sγ-Sγ'-Cβ'-Cα'	Mirror torsion about Cβ'-Sγ'
χ_1' (chi1')	Sγ'-Cβ'-Cα'-N'	Side-chain torsion from backbone

Quantum mechanical calculations and crystallographic studies consistently show that disulfide bonds strongly prefer gauche geometries, with χ_3 values clustering near ±90°, rather than the trans arrangement at 180°. Two energetically preferred geometries are observed, a right-handed conformation at approximately +90°, which is the most common in both small molecules and proteins, and a left-handed conformation at approximately -90°, which is less frequent but well characterised. This gauche preference arises from two electronic effects, lone-pair repulsion between the two sulfur atoms is greatest in planar configurations and minimised at 90°, while stabilising hyper-conjugative interactions between the sulfur lone pairs and the adjacent S-C antibonding orbitals are maximised at the gauche geometry [228]. This preference is well illustrated by dimethyl disulfide (CH_3-S-S-CH_3), the simplest organic disulfide, in which the C-S-S-C dihedral angle is approximately 85° in both the gas phase and the crystal structure[229], providing a useful reference for evaluating more complex disulfide geometries such as that of alligrin.

5.3.1 Disulfide bonds in proteins: The cystine and glutathione comparison with alligrin

In proteins, disulfide bonds form between the thiol groups of two cysteine yielding cystine, a covalently linked amino acid pair. Cystine is the predominant disulfide-containing unit found in proteins and is an essential determinant of protein folding, stability, and biological function [230]. Beyond structural proteins, disulfide bonds are equally critical in small biological molecules such as glutathione, the most abundant low-molecular-weight thiol in cells forms the disulfide-bridged dimer glutathione disulfide (GSSG) upon oxidation (Figure 5.3), a reaction that plays a key role in cellular redox homeostasis and antioxidant defence[231].

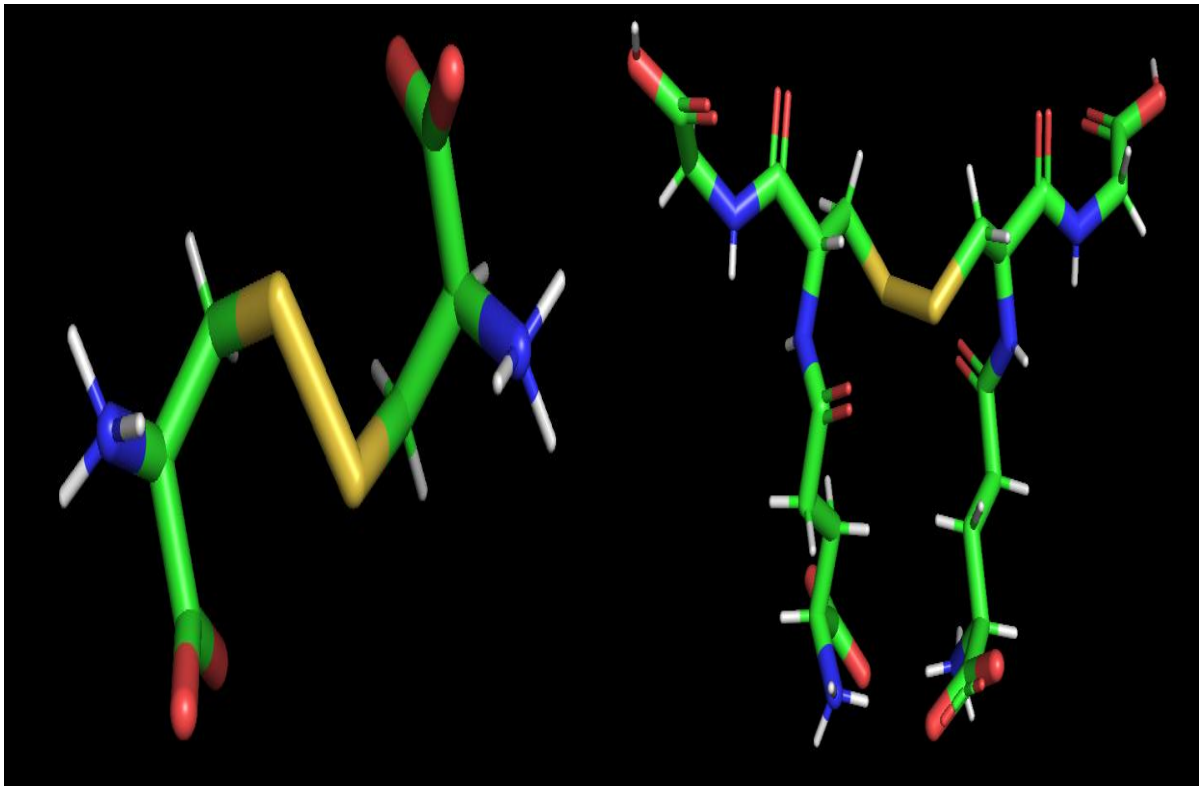

Figure 5.3: Three-dimensional crystal structure of L-cystine (left) and glutathione disulfide (GSSG) (right) showing the C-S-S-C disulfide bridge.

The crystal structure of L-cystine (Figure 5.4) reveals the characteristic geometric features of the biological disulfide bond. The adjacent C-S bond lengths measure 1.8 Å on each side of the disulfide bridge and the central S-S bond measures 2.0 Å, values in close agreement with those observed in alligrin (C-S = 1.8 Å, S-S = 2.0 Å), demonstrating that the fundamental bond metric parameters of the disulfide linkage are conserved across both biological and natural product systems. The dihedral angle analysis of L-cystine reveals a C-S-S-C torsion (χ_3) of 73.7°, adjacent by two equivalent C-C-S-S torsions of 81.6°, confirming the characteristic right-handed gauche geometry.

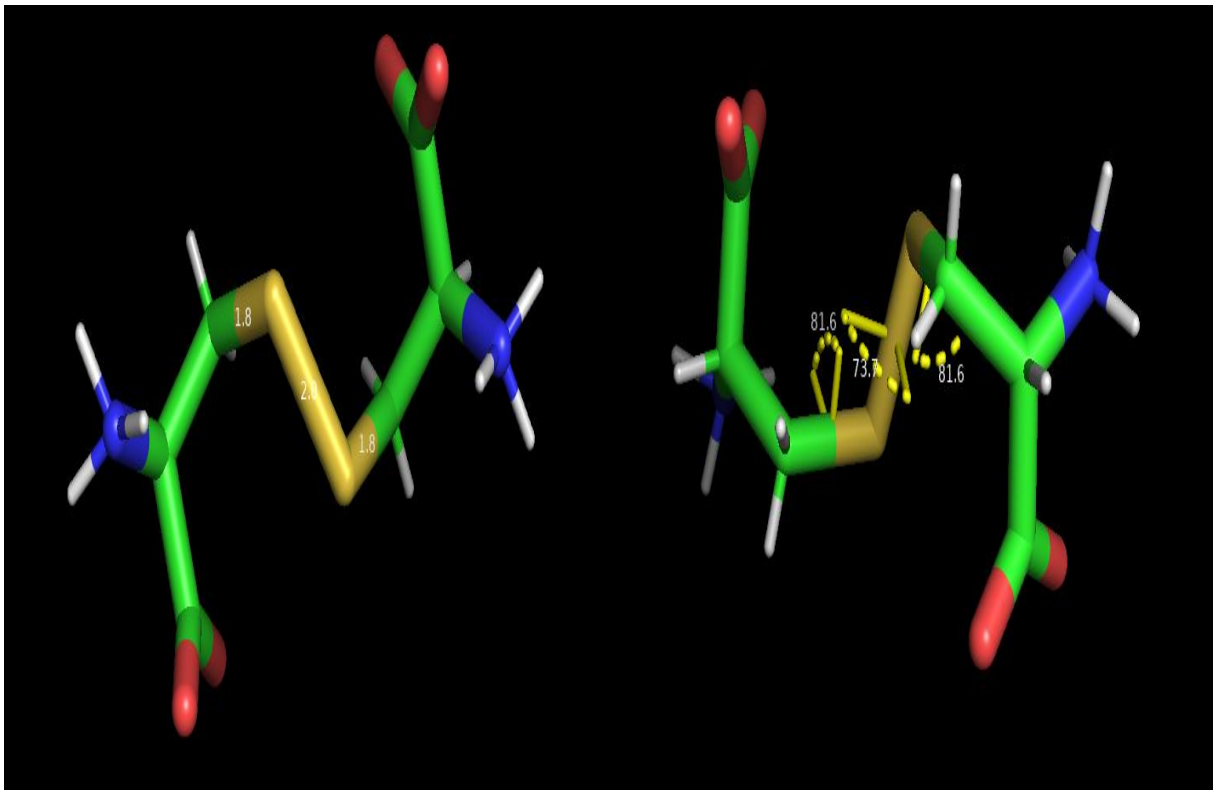

Figure 5.4: Bond length measurements (left) and dihedral angle (right) analysis of the L-cystine disulfide bridge.

Similarly, the crystal structure of glutathione disulfide (GSSG, Figure 5.5) reveals a symmetric dimeric structure in which two glutathione tripeptide arms, each bearing the γ-glutamyl, cysteinyl, and glycyl residues are covalently united through a central disulfide bridge. The disulfide bond in GSSG shows a C-S-S-C torsion angle of -97.6°, confirming the left-handed (*M*) gauche geometry, with adjacent C-S bond lengths of 1.8 Å and a central S-S bond of 2.0 Å (Figure 5.5, right) consistent with the disulfide geometry of alligrin, despite arising within a structurally different molecular environment.

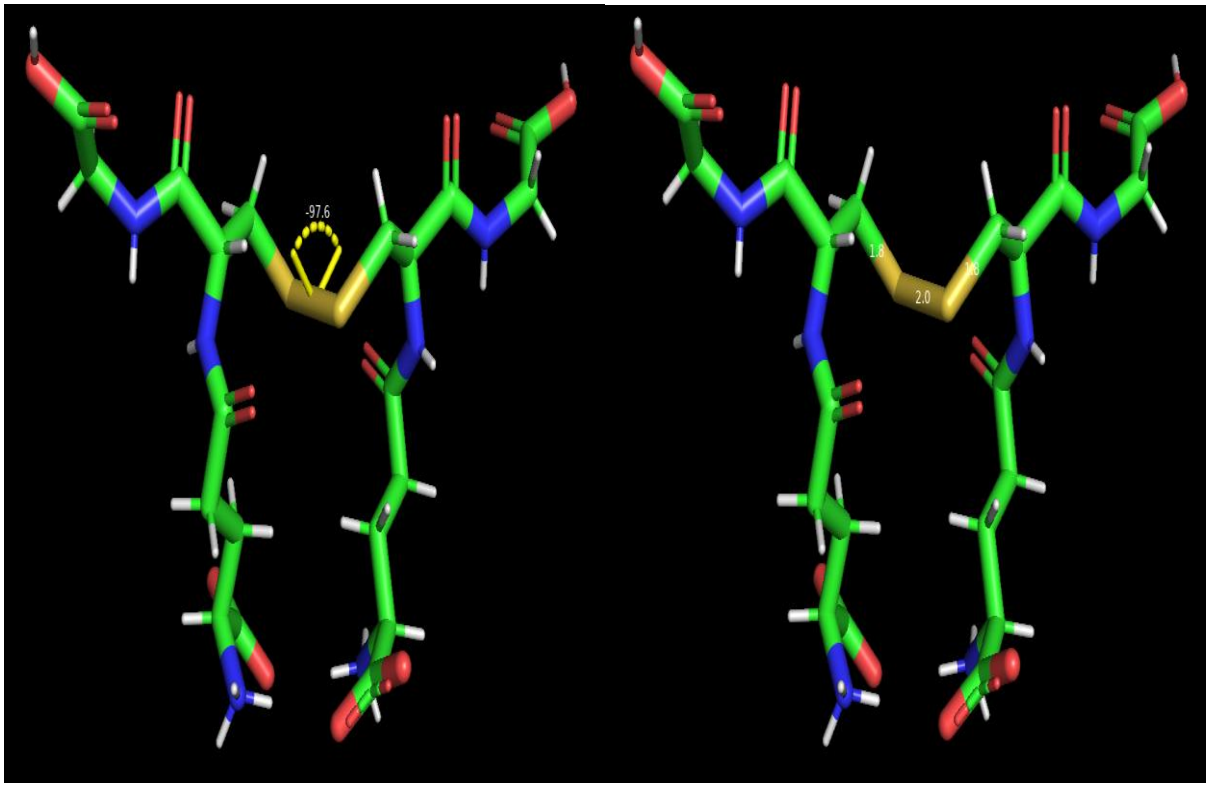

Figure 5.5: Bond length measurements (left) and dihedral angle (right) analysis of glutathione disulfide (GSSG).

Overall, the χ_3 dihedral angle in crystallographically characterised protein disulfides shows a strongly bimodal distribution centred near +87° (right-handed) and −83° (left-handed), consistent with the gauche preference observed in both L-cystine and GSSG. Approximately 97% of all protein disulfides exhibits gauche χ_3 values.

5.4 Crystallographic comparison of the C-S-S-C-N=O connectivity in alligrin and synthetic disulfide compound

A search of the SciFinder chemical database for compounds containing the C-S-S-C-N=O connectivity, the essential heteroatomic chain of alligrin, revealed no naturally occurring compound sharing this motif, further confirming the unique nature of alligrin as a natural product. The closest structural previously reported was a synthetic compound, designated compound 8b, reported by Yang et al., in which a novel disulfide bridge is intentionally introduced into the backbone of an aminoxy peptide by replacing conventional cysteine side-chain disulfides with sulfur atoms incorporated directly into the amide groups. Compound 8b thus represents the only crystallographically characterised molecule in the chemical literature in which a C-S-S-C unit is connected to a nitrogen- oxygen bearing fragment in a way geometrically analogous to the C-S-S-C-N=O chain of alligrin, making it the most instructive available comparator for evaluating the disulfide geometry and conformational behaviour of the novel natural product.

In compound 8b, the C-S-S-C dihedral angle measures -105.1°, indicating a left-handed orientation of the disulfide with the two adjacent C-S bonds in an almost perpendicular arrangement (Figure 5.6). In alligrin the equivalent torsion measures +97.3°, a right-handed gauche conformation of comparable value but opposite handedness. The near-equal absolute values -105.1° and 97.3° both fall within the 85°-105° range universally characteristic of organic disulfides, confirming that despite their entirely different chemical origins, the two compounds share the same fundamental gauche disulfide geometry arising from sulfur lone-pair interaction [232].

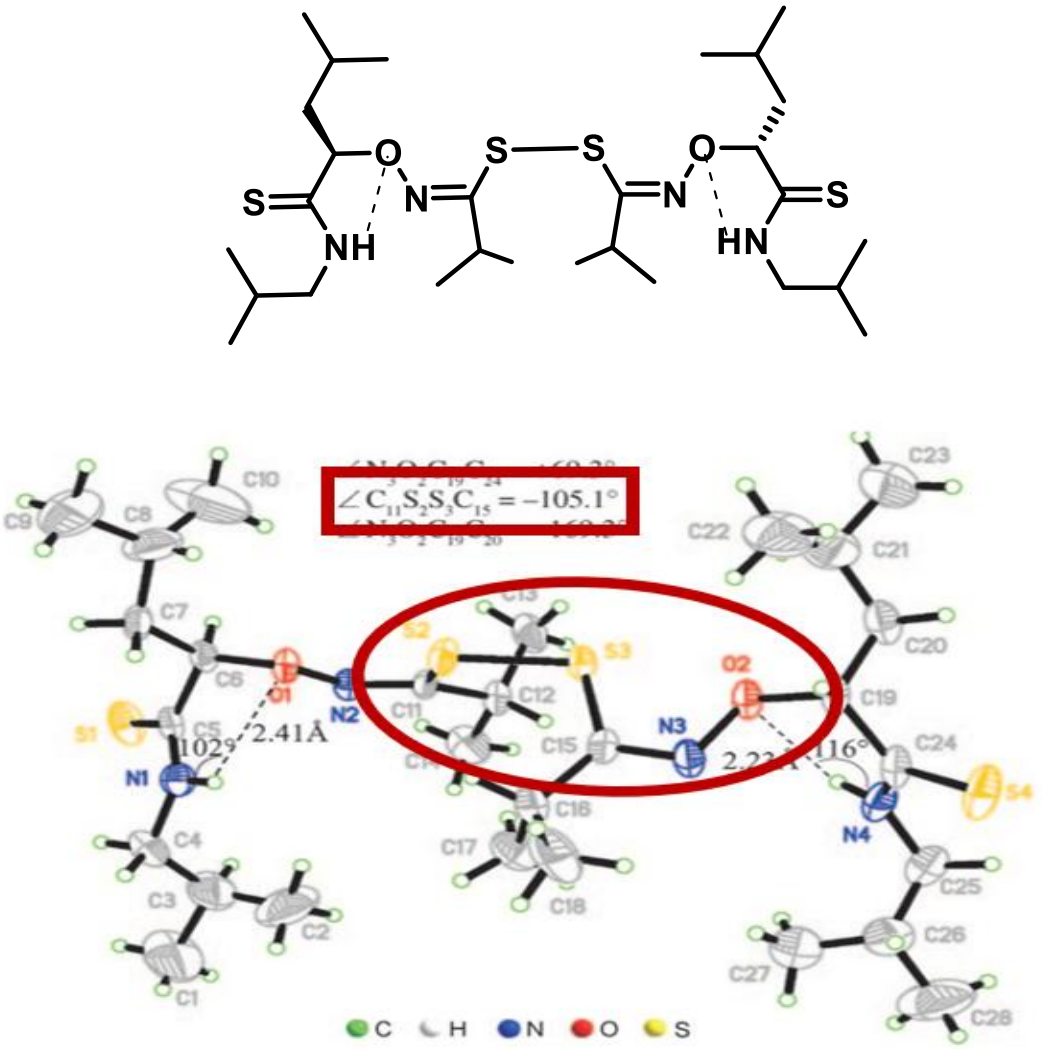

Figure 5.6: the crystal structure of synthetic backbone disulfide compound 8b determined by single-crystal X-ray diffraction.

A second important parallel is the structural novelty of the disulfide linkage in each case. In compound 8b the disulfide is notable because it is formed in the peptide backbone rather than between cysteine side chains, representing a new type of backbone crosslink previously unreported in natural peptide chemistry. In alligrin the disulfide is equally unprecedented in a different sense, it bridges the organosulfur framework of allicin to the thiohydroximate carbon of sinigrin, creating the first naturally occurring C-S-S-C-C=N-O-SO_3^- connectivity ever characterised crystallographically.

Table 5.2: Crystallographic comparison of the C-S-S-C-N=O connectivity in alligrin and synthetic backbone disulfide compound 8b.

Feature	Alligrin	Compound 8b
C-S-S-C torsion	+97.3° (*P*, right-handed)	−105.1° (*M*, left-handed)
Disulfide type	Natural product inter-fragment bridge	Synthetic backbone crosslink
Chemical novelty	First natural C-S-S-C-C=N-O-SO_3^-	First backbone disulfide in peptide

Table 5.3: Summarises the disulfide bond geometric parameters of alligrin alongside those of L-cystine, glutathione disulfide (GSSG), and compound 8b, allowing a direct comparison of S-S bond lengths, C-S bond lengths, χ_3 dihedral angles, and handedness across these structurally distinct compounds.

Compound	S-S (Å)	C-S (Å)	χ_3 (°)	Handedness
L-Cystine	2.0	1.8	+73.7	*P* (right-handed)
Glutathione disulfide (GSSG)	2.0	1.8	−97.6	*M* (left-handed)
Alligrin	2.0	1.8	+97.3	*P* (right-handed)
Compound 8b	2.04	1.82	−105.1	*M* (left-handed)

5.5 Implications of disulfide geometry for the biological activity of alligrin

The crystallographic comparison of the disulfide geometry of alligrin with those of L-cystine, glutathione disulfide, and synthetic compound 8b carries significant implications for the potential biological activity of the novel natural product.

The most direct biological implication of the disulfide bond in alligrin is its potential reactivity towards cellular thiols, particularly glutathione (GSH) and cysteine in proteins. Allicin, one of the two precursor molecules of alligrin, its antimicrobial and antifungal activities are widely reported through this mechanism. Its thiosulfinate S-S bond undergoes rapid sulfur-exchange reactions with cellular thiols, forming mixed disulfides that inhibit thiol-dependent enzymes and disrupt redox homeostasis [49, 233]. Although the disulfide bond of alligrin differs chemically from the thiosulfinate motif of allicin, it retains the ability to undergo thiol-disulfide exchange reactions under physiological conditions (chapter 4 section 4.5- 4.6), suggesting that alligrin may share some of the biological thiol-targeting activity of its allicin precursor. The right-handed gauche geometry of the alligrin disulfide (χ_3 = +97.3°) places the two molecular arms the thio-allyl fragment and the sulfonated oxime fragment in a specific three-dimensional orientation that will influencing the accessibility of the S-S bond and thereby modulating the rate and selectivity of thiol exchange reactions in a biological environment.

The handedness of the disulfide bridge right-handed (*P*) in alligrin and L-cystine, left-handed (*M*) in GSSG and compound 8b is a stereochemical property with direct implications for molecular recognition by biological receptors and enzymes. Enzymes that process disulfide bonds, including thioredoxin, glutaredoxin, and protein disulfide isomerase, have evolved active sites that are stereo-complementary to the specific disulfide geometries they encounter in their natural substrates [231]. The right-handed disulfide geometry of alligrin (+97.3°) is the same handedness as the predominant protein cystine disulfide (+87°), raising the possibility that alligrin could interact productively with the same enzymatic machinery that processes protein disulfides potentially acting as a competitive substrate, inhibitor, or redox modulator in cellular thiol-disulfide exchange pathways.

5.6 Crystal structure of sinigrin and comparative analysis with the novel compound alligrin

5.6.1 The crystal structure of sinigrin

The molecular structure of sinigrin contains three distinct structural fragments connected into a single anionic molecule. The first fragment is the β-D-glucopyranose ring in the $^4C_1$ chair conformation, in which all hydroxyl groups in equatorial positions, giving the ring maximum stability. The anomeric centre at C-1 carries the thioglycoside linkage in the β (equatorial) configuration, which is characteristic of all glucosinolates. The second fragment is the sulfonated oxime group, in which the central carbon carries a C=N double bond, with the thioglycoside carbon on one side and the N-O-SO_3^- group on the other. The third fragment is the allyl side chain -CH_2-CH=CH_2 attached directly to the central carbon of the oxime and providing the 2-propenyl group characteristic of sinigrin specifically (Figure 5.7).

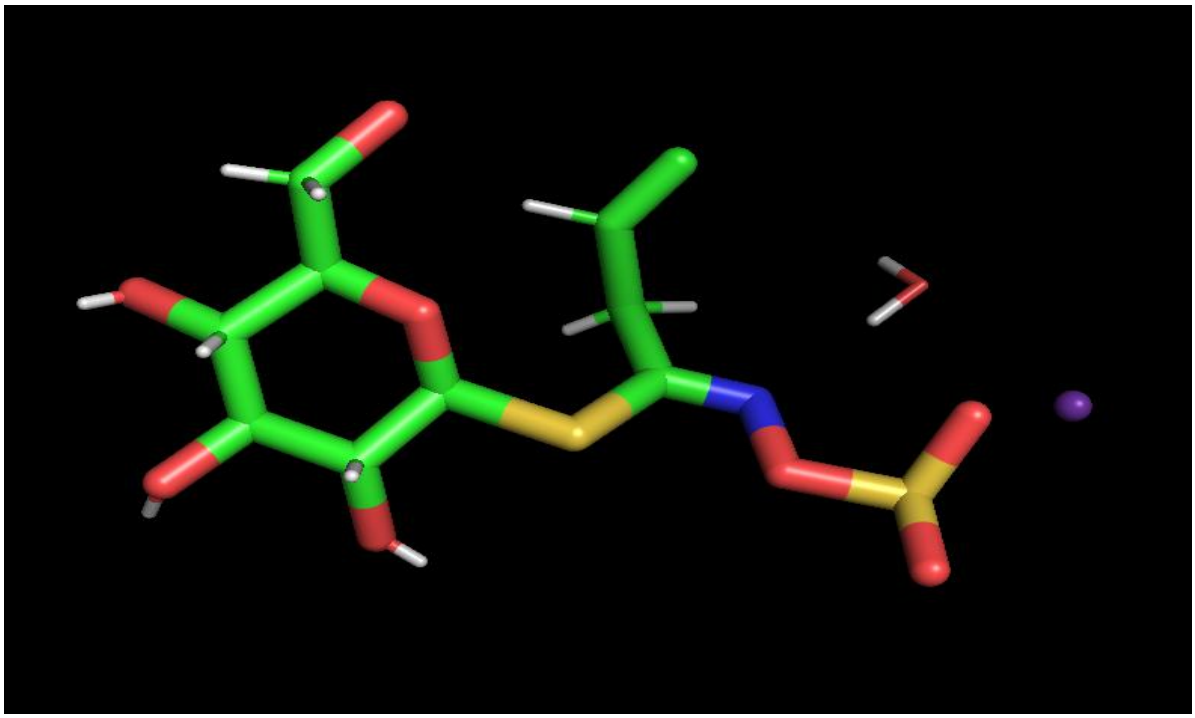

Figure 5.7: Crystal structure of sinigrin showing the three principal structural domains: the β-D-glucopyranose ring in the $^4C_1$ chair conformation (left), the sulfonated oxime aglucone connected through the thioglycoside bond (centre), and the sulfonate group (right).

5.6.2 Comparative crystal structure analysis: Sinigrin versus Alligrin

A direct comparison of the bond lengths in the crystal structures of sinigrin and alligrin shows that the sinigrin-derived fragment is well preserved in alligrin, while clear differences are observed in the regions that have undergone chemical transformation.

The terminal C=C double bond measures 1.2 Å in sinigrin and 1.3 Å in alligrin, the slight elongation in alligrin may reflect a weak interaction between the alkene and the neighbouring C-S bond, though both values are within the normal range for terminal alkenes. The allylic C-C single bond and the internal C-C bond connecting the allyl arm to the oxime carbon both measure 1.5 Å in each structure, confirming that the allyl region is unchanged across the two compounds and is unaffected by the chemical transformation (Figure 5.8).

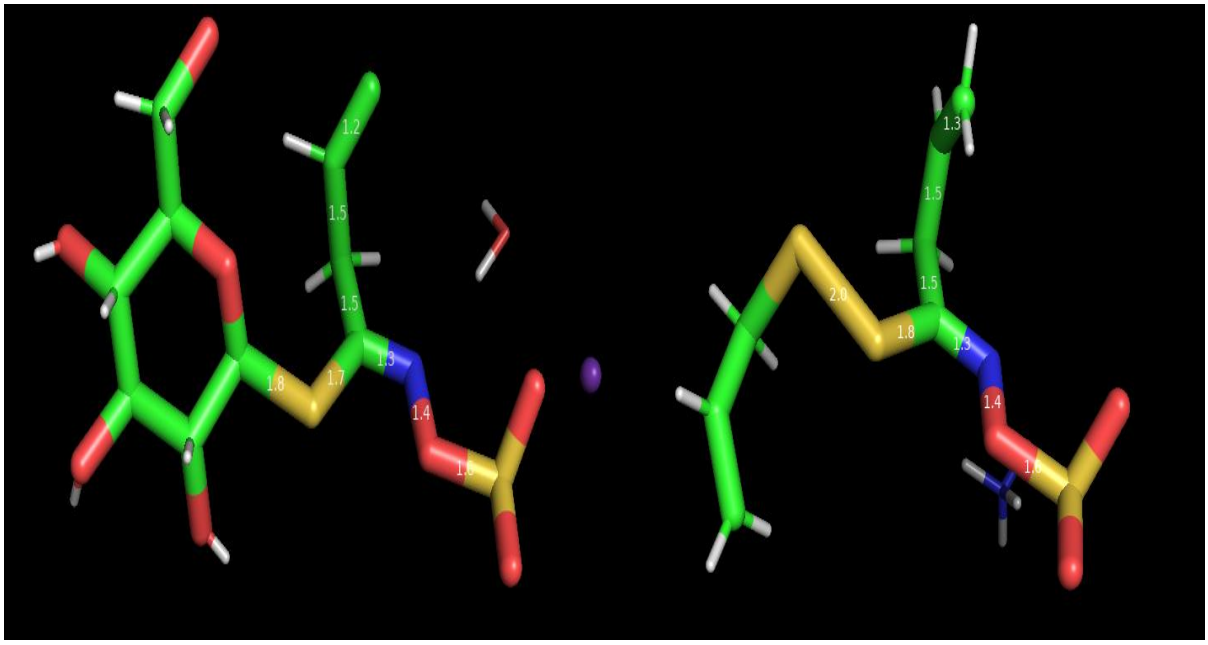

Figure 5.8: Bond length comparison between sinigrin (left) and alligrin (right), determined by single-crystal X-ray diffraction.

Notably, both sinigrin and alligrin retain the Z configuration at the C=N bond despite the structural transformation from glucosinolate to disulfide product. This confirms that the reaction proceeds with full retention of configuration at the C=N bond, and that the replacement of the thioglucose group with the new disulfide bridge does not affect the oxime geometry. The C=N bond length of 1.3 Å and the N-O distance of 1.4 Å are identical in both structures, further confirming that the oxime-sulfonate electronic fragment is transferred

intact from sinigrin into alligrin without alteration of bond order, electronic character, or stereochemical configuration.

The C-S bond lengths are closely comparable across both structures, measuring 1.8 Å in alligrin and 1.7 Å in sinigrin, confirming that the sulfur-carbon connectivity at the oxime carbon is well preserved. The most significant structural difference between the two compounds is the replacement of the β-D-glucopyranose ring in sinigrin, which represents most of the molecular volume and provides four hydroxyl hydrogen-bond donors, with the C-S-S-C disulfide bridge in alligrin (C-S = 1.8 Å, S-S = 2.0 Å). This substitution eliminates all hydroxyl-based hydrogen bonding and replaces the rigid glucopyranose ring with a flexible disulfide unit, representing the only new structural feature introduced by the chemical transformation (Figure 5.8).

Table 5.4: summary of comparative bond lengths of sinigrin and alligrin.

Bond	Sinigrin (Å)	Alligrin (Å)
C=C terminal alkene	1.2	1.3
C-C allylic (sp^3-sp^2)	1.5	1.5
C-C internal (sp^3-sp^2)	1.5	1.5
C-S (thioglycoside/disulfide)	1.8	1.8
C-S (oxime side)	1.7	1.8
S-S disulfide	absent	2.0
C=N oxime	1.3	1.3
N-O	1.4	1.4
S-O (sulfonate)	1.6	1.6

5.6.3 Dihedral angle comparison: alligrin vs sinigrin

Dihedral angle analysis reveals key structural differences between alligrin and sinigrin. The most notable contrast is at the central sulfur-containing linkage, where the C-S-S-C dihedral angle in alligrin measures 97.3°, characteristic of the gauche conformation seen in organic disulfides, separating the thio-allyl arm from the oxime-sulfonate group at nearly a right angle. In sinigrin, no disulfide bond exists, instead the corresponding C-S-C-C torsion across the thio-glycoside linkage measures only 6.8°, reflecting the geometric constraints imposed by the glucopyranose ring. The contrast between 97.3° in alligrin and 6.8° in sinigrin therefore reflects entirely different bonding environments rather than a simple quantitative difference (Figure 5.9).

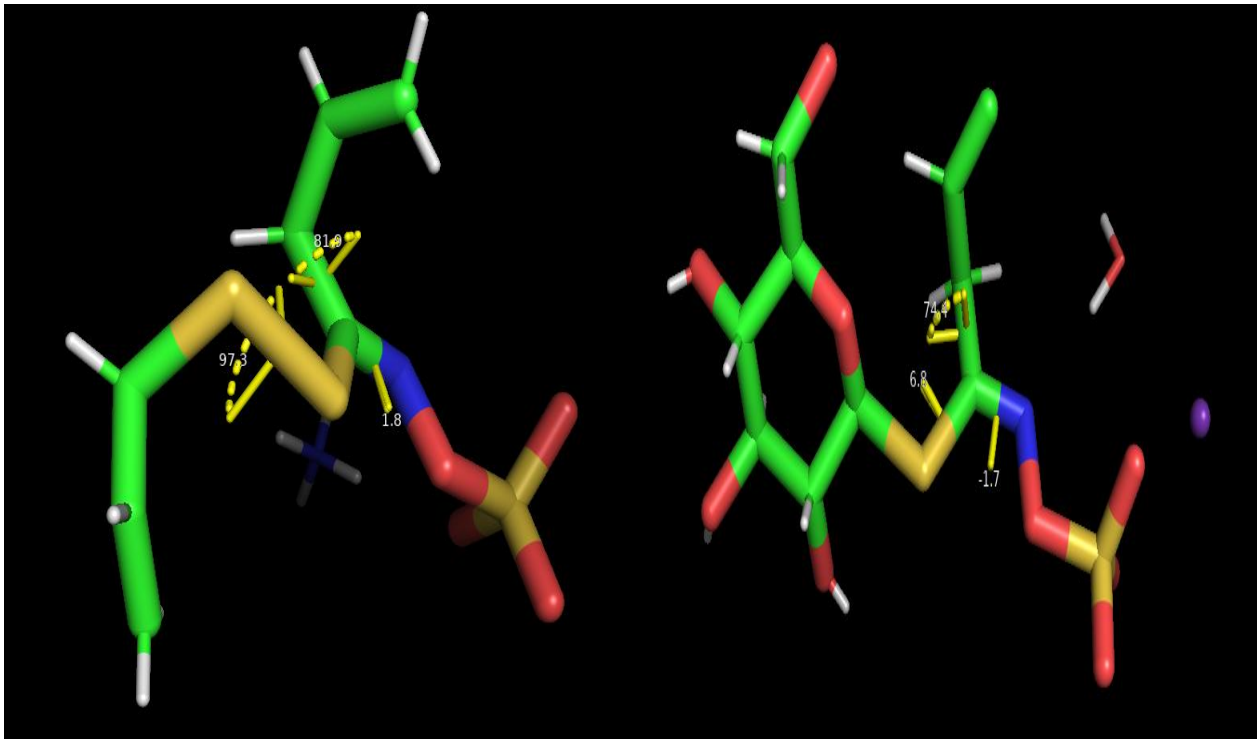

Figure 5.9: Dihedral angle comparison between alligrin (left) and sinigrin (right), determined by single-crystal X-ray diffraction.

The S-C-C-C torsion angle, describing the orientation of the allyl chain relative to the sulfur centre, measures 81.9° in alligrin and 74.4° in sinigrin. Both values fall within the gauche range, indicating that the allyl chain shows a similar orientation in both compounds. The small difference of approximately 7° suggests that changing the sulfur bonding environment from a thioether in sinigrin to a disulfide in alligrin has only a minor effect on the allyl chain geometry.

The S-C-N=O dihedral angle directly reflects the E/Z configuration at the C=N bond. In both sinigrin (-1.7°) and alligrin (+1.8°), this angle is near-zero, confirming oxime planarity and the Z configuration in both compounds, and providing crystallographic proof that the Z geometry is fully retained upon transformation from sinigrin to alligrin.

Table 5.5: Comparison of key torsion angles in alligrin and sinigrin.

Torsion angle	Alligrin (°)	Sinigrin (°)
S-C-C-C	81.9	74.4
S-C-N=O	1.8	-1.7

5.7 Summary and conclusion

This chapter has reported the first crystallographic characterisation of alligrin, a novel organosulfur natural product arising from the sulfur reactivity between allicin and sinigrin, and has presented a comprehensive structural analysis of its unprecedented C-S-S-C-C=N-O-SO_3^- connectivity determined by single-crystal X-ray diffraction, the only technique capable of providing definitive atomic-level proof of such an unusual and previously unreported heteroatomic chain.

The crystal structure of alligrin confirms that the thio-allyl fragment of allicin and the sulfonated oxime fragment of sinigrin are covalently linked through a new disulfide bridge, with C-S bond lengths of 1.8 Å and a central S-S bond of 2.0 Å. The disulfide exhibits the characteristic right-handed gauche conformation with a C-S-S-C torsion angle of 97.3°, consistent with the gauche preference of organic disulfides. The molecular conformation is further stabilised in the solid state by intramolecular N-H···O hydrogen bonds between the N2 donors and the sulfonate oxygen acceptors.

The disulfide geometry of alligrin falls within the gauche window established by L-cystine (χ_3 = +73.7°), glutathione disulfide (χ_3 = -97.6°), and compound 8b (χ_3 = -105.1°), confirming that the unique chemical environment of alligrin does not alter the fundamental disulfide

geometry. Comparison with compound 8b, the only crystallographically characterised compound sharing the C-S-S-C-N=O connectivity, shows that both compounds exhibit gauche disulfide geometry of comparable magnitude but opposite handedness, with alligrin being right-handed (P) and compound 8b left-handed (M).

The right-handed gauche geometry of the alligrin disulfide (+97.3°) closely mirrors that of L-cystine (+73.7°), suggesting that alligrin may interact with thiol-processing enzymes such as thioredoxin, glutaredoxin, and protein disulfide isomerase. Combined with the retention of the intact sinigrin-derived sulfonated oxime group, alligrin represents a dual-reactive hybrid molecule in which the thiol-targeting disulfide and the electrophilic oxime are united within a single structure, offering a potentially novel mode of biological activity absent in either precursor.

The bond-by-bond comparison confirms that the transformation from sinigrin to alligrin is structurally precise. The entire oxime-sulfonate framework is transferred intact, with both compounds retaining the Z configuration at the C=N centre, confirmed by near-zero S-C-N=O torsion values of -1.7° in sinigrin and +1.8° in alligrin. The only major structural change is the replacement of the glucopyranose ring and thioglycoside C-S bond with the new C-S-S-C disulfide bridge. Alligrin is therefore best understood as a structurally precise hybrid in which the bond metrics, electronic character, and Z stereochemistry of the sinigrin-derived framework are fully conserved.

Taken together, the results presented in this chapter provide the first crystallographic evidence that direct inter-family sulfur-exchange chemistry between Alliaceae and Brassicaceae metabolites can generate a structurally unprecedented hybrid natural product. This finding expands the known scope of organosulfur natural product chemistry and highlights the chemical interface between two of the most biologically significant sulfur-rich plant families as a rich and largely unexplored source of novel bioactive molecular structures worthy of further synthetic, biological, and pharmacological investigation.

6 General Conclusion

The aim of this thesis was to investigate whether the reactive sulfur metabolites generated by two edible plant families such as the Alliaceae (garlic) and the Brassicaceae (cruciferous vegetables) could chemically interact to generate novel organosulfur natural products. Four specific objectives were outlined at the beginning of this work to address this aim.

The first objective was to investigate the thiol reactivity of allicin with reactive intermediates generated during glucosinolate hydrolysis by myrosinase, and to determine whether these interactions lead to the formation of novel sulfur-containing conjugated compounds, including their subsequent chemical rearrangements and structural characterisation. The second objective was to detect, identify and confirm the formation of these novel compounds in crude mixed plants extract produced from combinations of garlic and glucosinolate-containing plants. The third objective was to assess the antibacterial activity of the newly formed compounds and the crude plants mixture extract, to evaluate their potential as enhanced or synergistic antimicrobial agents.

The results presented in **chapter 2** directly address the first objective, demonstrating the formation and structural elucidation of alligrin and alliphanin as the first members of a new class of organosulfur natural products. **Chapter 3** addresses the second objective, reporting the confirmed formation of alligrin and alliphanin in crude garlic-mustard and garlic-broccoli mixtures under conditions reflecting real-world food preparation. **Chapter 4** addresses the third objective, proving the antibacterial activity of alligrin against clinically relevant Gram-positive pathogens including MRSA and providing initial mechanistic evidence for a thiol-dependent mode of action. **Chapter 5** addresses the fourth objective, presenting the first crystallographic characterisation of alligrin, the comprehensive comparison of its disulfide geometry with L-cystine, glutathione disulfide and synthetic compound called 8b, and the bond-by-bond structural analysis with sinigrin, collectively establishing how the unique C-S-S-C-C=N-O-SO_3^- connectivity of alligrin.

6.1 Discovery and structural elucidation of novel organosulfur hybrid compounds

As reported in **Chapter 2**, the main achievement of this work is the discovery, isolation and full structural characterisation of two previously unreported organosulfur natural products. Alligrin arising from the interaction of allicin with sinigrin hydrolysis intermediate, and alliphanin arising from the analogous reaction with glucoraphanin hydrolysis intermediate.

Both alligrin and alliphanin were isolated by preparative HPLC and subjected to comprehensive structural characterisation using 1D and 2D NMR spectroscopy (COSY, HSQC, HMBC), high-resolution LC-MS and in the case of alligrin, clear confirmation by single-crystal X-ray diffraction. The crystallographic analysis definitively established that the thio-allyl fragment of allicin and the sulfonated oxime fragment of sinigrin are connected through a disulfide bridge forming the unusual connectivity C-S-S-C-C=N-O-SO_3^-, this connectivity had not previously been reported in any naturally occurring compound.

6.2 Reaction mechanism and chemical characterisation

Beyond the primary structure of alligrin and alliphanin, both compounds showed further sulfur reactivity undergoing multi-sulfur rearrangements through thiol-disulfide exchange. LC-MS^2 fragmentation analysis revealed multi-sulfur compound generated either through self-rearrangement or through reactivity with residual allicin. These results expand the known reactivity profile of these novel molecules and suggest that their fate in biological systems may involve a sequence of sulfur exchange reactions with endogenous thiols (Figure 119).

Stability studies provided further mechanistic insights. Alligrin was shown to be partially stable between 50-100°C, while at higher temperatures (170-200°C), it completely degraded into oxidised sulfur compounds including allyl thiosulfate and allyl di-thiosulfate. These observations suggest that moderate cooking methods such as boiling and steaming could

preserve the novel multi-sulfur compounds, while high-temperature treatments such as frying or roasting would lead to their degradation.

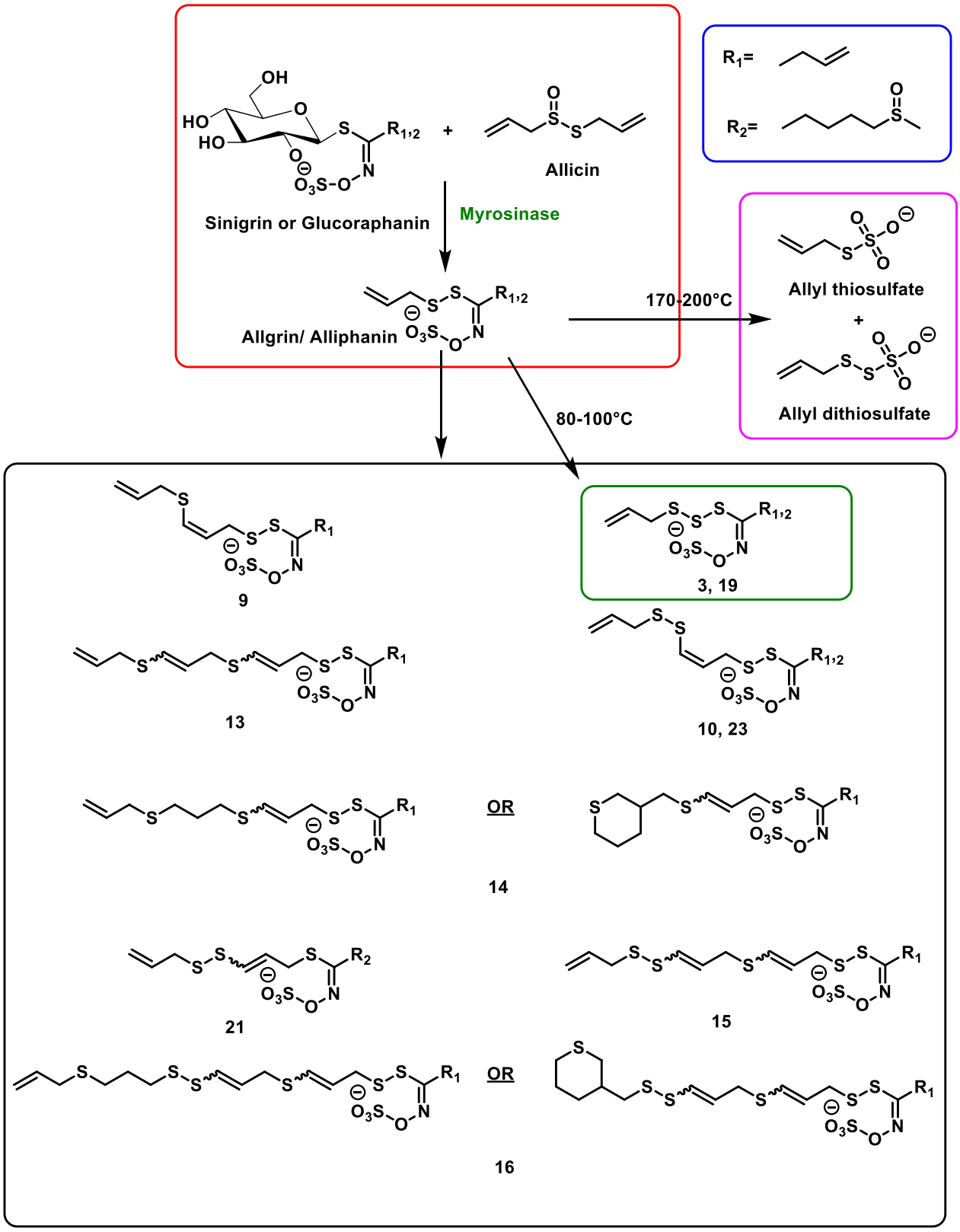

Figure 6.1: Summary of all novel organosulfur natural products identified and characterised in this work.

6.3 Formation of novel compounds in crude plants mixture

A **Chapter 3** confirmed that alligrin forms when freshly crushed garlic is mixed with mustard seed powder, confirmed by HPLC retention time matching, spiking experiments and LC-MS, demonstrating that this sulfur reactivity chemistry can occur during everyday culinary preparation. Alliphanin formation in the garlic-broccoli mixture was below the limit of detection under the conditions used. Remarkably, while both compounds showed stability as purified standards, they demonstrated rapid degradation in plant mixture reactions and during solvent evaporation.

6.4 Antibacterial activity and structure-activity relationships

Chapter 4 verified that combining garlic with glucosinolate-containing plants enhanced antibacterial activity against Gram-positive bacteria and Escherichia coli compared with garlic extract alone, suggesting novel sulfur compounds as the driving force behind this enhancement. Direct comparison of purified alligrin with allicin and sinigrin established clear structure-activity relationships. Sinigrin was entirely inactive against all tested strains, allicin displayed broad-spectrum activity against both Gram-positive and Gram-negative bacteria, while alligrin exhibited selective activity against Gram-positive bacteria including MRSA. This selectivity profile exhibits that structural hybridisation generates a compound with novel biological properties.

The critical role of the sulfate group was established through enzymatic desulfation experiments, whereby its removal resulted in complete loss of antibacterial activity. However, non-selective effects observed at approximately fourfold higher concentrations, demonstrating that sulfation is necessary for full antimicrobial potency. Mechanistic investigations further support a thiol-dependent mode of action, whereby glutathione incubation led to complete disappearance of alligrin and formation of S-allylmercaptoglutathione and a sulfonated aldoxime intermediate which may further react to release allyl isothiocyanate, with alligrin antimicrobial activity arising from these two pathways.

6.5 Crystallographic characterisation and structural significance of alligrin

The single-crystal X-ray diffraction analysis of alligrin, reported in **Chapter 5**, represents the definitive structural proof of this novel natural product and the most analytically comprehensive contribution of this thesis. The crystallographic data established all atomic positions in three-dimensional space with high accuracy, confirming the unique C-S-S-C-C=N-O-SO_3^- connectivity.

A comparison of the alligrin disulfide geometry with established reference compounds demonstrated that the unusual heteroatomic environment of this novel molecule leads to no alteration on the fundamental gauche preference of organic disulfides. Particularly, the right-handed gauche geometry of alligrin (+97.3°) closely mirrors the predominant dihedral angle in protein cystine disulfides (+87°), suggesting potential interaction with thiol cellular enzymes such as thioredoxin, glutaredoxin, and protein disulfide isomerase, providing a structural basis for its biological activity.

A comprehensive bond-by-bond comparison with the crystal structure of sinigrin revealed that the structural transformation from glucosinolate precursor to hybrid disulfide product is chemically precise. The entire oxime-sulfonate structure is transferred intact from sinigrin to alligrin, with the only major structural change being the replacement of the glucopyranose ring by the disulfide bridge, while the Z-configuration at the C=N centre is retained in both compounds.

6.6 Broader scientific significance

In natural product chemistry, this work establishes plant sulfur reactivity as a previously unreported pathway for generating structurally novel bioactive compounds, with broad implications for understanding chemical diversity in nature. In the context of antimicrobial resistance, alligrin targets bacterial thiol metabolism through a mechanism distinct from that of conventional antibiotics, suggesting a low propensity for cross-resistance with existing drugs. In food chemistry and nutritional science, the natural formation of alligrin in garlic-mustard seed mixtures under normal culinary conditions suggests that novel bioactive sulfur conjugates may already exist but undiscovered yet in commonly consumed food

combinations. The garlic and cruciferous vegetable metabolites act independently and opening new directions in food metabolomics.

6.7 Future directions

The results reported in this thesis open several clear avenues for future investigation. The following directions are considered most important for building upon the present findings.

6.7.1 Mechanistic studies of antibacterial activity

Although glutathione reactivity studies provided initial mechanistic evidence, the intracellular targets of alligrin in bacterial cells remain to be identified. Future work should employ proteomics methods such as activity-based protein profiling to map protein targets in living bacterial cells, as well transcriptomic analysis needs to identify which stress pathways are activated. The independent contribution of the sulfonated oxime moiety to biological activity also requires further investigation.

6.7.2 Exploration of other plant system combinations

Sinigrin and glucoraphanin were selected as model glucosinolates in this study, but the Brassicaceae family contains more than 130 structurally diverse glucosinolates. Systematic investigation of allicin reactivity with other glucosinolates, including indole and aromatic types such as glucobrassicin and gluconasturtiin, may yield a wider family of novel organosulfur hybrid natural products. Additionally, other thiol-reactive species produced by the Marasmiaceae family such as Shiitake Mushroom could be explored as alternative reaction partners with allicin or glucosinolate hydrolysis intermediates.

6.7.3 Investigation of alligrin formation under physiological and dietary conditions

The demonstration of alligrin formation in crude plant mixtures raises important questions about its fate in the gastrointestinal tract. Studies examining the stability of alligrin and alliphanin under simulated gastric and intestinal conditions are needed to assess bioavailability, and in vivo pharmacokinetic investigations in animal models to determine

whether these compounds reach systemic circulation following dietary intake. Metabolomic analysis of plasma and urine from subjects consuming garlic and cruciferous vegetables simultaneously could provide the first evidence that these novel conjugates are formed and absorbed under dietary conditions in humans.

6.7.4 Anticancer and antioxidant activity

Both allicin and glucosinolate hydrolysis products are well documented for anticancer and antioxidant activities mediated through thiol-dependent mechanisms. Alligrin, as a hybrid molecule combining electrophilic sulfur features from both classes represents a strong candidate for evaluation in cancer cell line models and oxidative stress assays. Its structural similarity to protein cystine disulfides further requires investigation of its potential to modulate the cellular redox.

7 Experimental Procedures and Analytical Methods

7.1 Materials

7.1.1 Chemicals and reagents

All solvents were of analytical or HPLC grade. Deuterated methanol (CD_3OD), deuterium oxide (D_2O), and deuterated dimethyl sulfoxide (DMSO-d_6) were used for NMR spectroscopic analyses. HPLC-grade acetonitrile (≥99.9%) was used for chromatographic separations.

Sinigrin hydrate (≥99.0%), myrosinase from *Sinapis alba* (white mustard) seeds, glucoraphanin, allyl isothiocyanate, sulforaphane, diallyl disulfide (≥98%), formic acid, Sulfatase type H-1 from *Helix pomatia (*≥10,000 units/g) and 4-nitrophenyl sulfate, (sulfatase substrate) were purchased from Sigma-Aldrich (UK). All reagents and chemicals were used as received without further purification.

7.1.2 Preparation of buffers

7.1.2.1 Potassium phosphate buffer (PPB)

Potassium phosphate buffer (0.1 M, pH 6.0) was prepared in accordance with the European Pharmacopoeia guidelines (Ph. Eur., 7th edition). Potassium dihydrogen phosphate (2.405 g) and dipotassium hydrogen phosphate (11.73 g) were dissolved in deionized water, and the final volume was adjusted to 1 L. The pH was confirmed to be 6.0 at room temperature using a calibrated pH meter.

For NMR experiments, deuterated phosphate buffer was obtained by three successive cycles of evaporation under reduced pressure and reconstitution in deuterium oxide (D_2O), effectively replacing exchangeable protons with deuterium prior to spectroscopic analysis.

7.1.2.2 Ammonium acetate buffer (NH_4OAc)

An ammonium acetate buffer (0.025 M, pH 6.0) was prepared by dissolving ammonium acetate (NH_4OAc, 1.927 g) in deionized water, with the final volume adjusted to 1 L. The pH was verified at 6.0 at room temperature using a calibrated pH meter prior to use. This buffer was used as the aqueous mobile phase in HPLC analysis.

7.1.3 Plant materials

Fresh garlic bulbs (*Allium sativum*) and broccoli (*Brassica oleracea* var. *italica*) were sourced from a local Tesco supermarket (Norwich, UK), while Colman's Original Mustard Powder was obtained from a local market. All plant materials were used fresh and processed immediately prior to enzymatic reactions.

7.2 Experimental procedure

Chapter 2

7.2.1 Synthesis of allicin

7.2.1.1 Performic acid pre-formation

H_2O_2 and formic acid were mixed in a ratio of 3:5 (0.75:1.25 mol= 750 µL: 1250 µL volumes) and incubated at room temperature for 90 min.

7.2.1.2 Synthesis of allicin using pre-formed performic acid

Diallyl disulfide (DADS, 0.5 g, 3.35 mmol, 98%) was dissolved in methanol (2.5 mL) and the resulting solution was stirred at 0°C for 5 minutes. A performic acid stock solution (2 mL, 7.34 mmol), prepared freshly was added dropwise to the reaction mixture under ice-bath cooling. The flask was subsequently removed from the ice bath, and the reaction mixture was allowed to warm to room temperature with continuous stirring for 15 minutes. The reaction was quenched by the addition of distilled water (25 mL). The resulting mixture was extracted three times with dichloromethane, and the combined organic layers were dried and concentrated under reduced pressure at RT to yield a clear, oily substance that smells like garlic [201]. Yield: 0.54 g, 3.327 mmol, 99.3 %.

7.2.2 Enzymatic reactions

7.2.2.1 Myrosinase catalytic hydrolysis of sinigrin/ glucoraphanin

All enzymatic reactions were conducted directly in NMR tubes. Enzymatic activity was defined as one unit (U) representing the amount of enzyme required to hydrolyse 1 µmol of sinigrin per minute at pH 6.5 and 37°C [200, 204].

Sinigrin/glucoraphanin hydrolysis was initiated by the addition of myrosinase (1 U) to a sinigrin/glucoraphanin solution (0.01 mM) in a total reaction volume of 800 µL. All reactions were conducted in deuterium potassium phosphate buffer (0.1 M, pH 6.0). The progression of enzymatic hydrolysis and the subsequent formation of sinigrin/glucoraphanin hydrolysis products were monitored by ^{1}H NMR spectroscopy at a single time point of 2 hours.

7.2.2.2 Myrosinase catalytic hydrolysis mixture of sinigrin/ glucoraphanin and allicin

7.2.2.2.1 Enzymatic reaction in dimethyl sulfoxide (DMSO)/phosphate buffer

7.2.2.2.1.1 Diallyl disulfide experiment:

A reaction mixture was prepared by dissolving 1.4 µL diallyl disulfide (DADS, 0.01 mM, 1.4mg) in DMSO-d_6 (250 µL) and subsequently combining the resulting solution with 5mg sinigrin (0.01 mM) dissolved in deuterated potassium phosphate buffer (0.1 M, pH 6.0, 750 µL), giving a total reaction volume of 1000 µL. The reaction was initiated by the addition of myrosinase (2 U) directly into the NMR tube, and the progression of the reaction was monitored by ^{1}H NMR spectroscopy at 3 hours.

7.2.2.2.1.2 Allicin experiment:

The same procedure was followed using 1.5 µL allicin (0.01 mM, 1.67mg) instead of DADS.

7.2.2.2.2 Enzymatic reaction in acetonitrile (MeCN)/phosphate buffer

A reaction mixture was prepared by dissolving 1.5 µL allicin (0.01 mM, 1.67mg) in acetonitrile (250 µL) and combining with 5mg sinigrin (0.01 mM) in deuterated potassium phosphate buffer (0.1 M, pH 6.0, 750 µL), giving a total volume of 1000 µL. Myrosinase (2 U) was added directly into the NMR tube to initiate the reaction, which was monitored by ^{1}H NMR spectroscopy at 3 hours.

7.2.2.3 Scale-up of the sinigrin-allicin reaction

Sinigrin (200 mg, 0.5 mmol) was dissolved in potassium phosphate buffer (30 mL, pH 6.0), and freshly prepared allicin (73 µL, 0.5 mmol) was dissolved in acetonitrile (10 mL). The two solutions were combined to give a total reaction volume of 40 mL, and the reaction was initiated by the addition of myrosinase (80 U). The mixture was allowed to react at room

temperature for 3 hours, after which the reaction mixture was subjected to preparative HPLC purification (section 7.2.3.2), with the target product eluting at a retention time of 7.6 min.

7.2.3 Chromatographic techniques

7.2.3.1 Analytical High-Performance Liquid Chromatography (HPLC)

All chromatographic analyses were performed on an Agilent Technologies 1100 Series HPLC system equipped with a binary pump, autosampler, and UV detector. The mobile phase consisted of ammonium acetate buffer (0.025 M, pH 6.0) containing 0.1% formic acid as solvent A and HPLC-grade acetonitrile as solvent B. UV detection was performed at 228 nm, with a fixed injection volume of 10 µL for all analyses. Prior to each chromatographic run, the column was washed with 100% acetonitrile for 12.5 minutes to remove residual contaminants, followed by equilibration with 25% (v/v) acetonitrile for a further 12.5 minutes.

An HPLC method was developed and optimised for the simultaneous separation and monitoring of glucosinolates, their hydrolysis products, and organosulfur compounds. Samples were analysed on a C18 reversed-phase column (Phenomenex Spherisorb, 5 µm, ODS2, 4.6 × 150 mm cartridge) at 30°C with a flow rate of 0.5 mL/min over a total run time of 40 minutes. Separation was achieved using a linear gradient elution program, start with 25% (v/v) aqueous acetonitrile at 0 minutes, increasing linearly to 100% (v/v) acetonitrile over 30 minutes, followed by an isocratic hold at 100% (v/v) acetonitrile for the remaining 10 minutes.

The developed method achieved satisfactory chromatographic separation of all target compounds within the 40-minute run time. The elution order reflected the increasing hydrophobicity of the compounds, consistent with the expected behaviour on a C18 reversed-phase stationary phase.

For the first reaction mixture, comprising sinigrin and allicin in the presence of myrosinase, the observed retention times were as follows: sinigrin at 2.9 min, alligrin at 7.6 min, allicin at 9.9 min, and allyl isothiocyanate (AITC) at 14.0 min.

For the second reaction mixture, comprising glucoraphanin and allicin in the presence of myrosinase, the observed retention times were as follows: glucoraphanin at 2.6 min, alliphanin at 4.6 min, sulforaphane at 7.2 min, and allicin at 9.9 min.

7.2.3.2 Preparative High-Performance Liquid Chromatography (Prep-HPLC)

Preparative chromatographic separation was performed by reversed-phase high-performance liquid chromatography (RP-HPLC) using an Agilent 1290 Prep LC system equipped with a Kinetex C18 column (5 µm, 100 Å, 150 × 21.2 mm). Prior to each run, the column was washed with 100% acetonitrile for 12.5 minutes to remove residual contaminants, followed by equilibration with 25% (v/v) acetonitrile for a further 12.5 minutes to ensure consistent retention behaviour.

The mobile phase consisted of ammonium acetate buffer (0.025 M, pH 6.0) containing 0.1% formic acid as solvent A and HPLC-grade acetonitrile as solvent B. Separation was carried out at a flow rate of 10.6 mL/min, and UV detection was performed at 228 nm. Crude samples were prepared at a concentration of 5 mg/mL in acetonitrile and potassium phosphate buffer (25:75, v/v, pH 6.0) prior to injection.

Method optimisation was performed with respect to both injection volume and gradient elution conditions. Injection volume was evaluated by testing loading volumes in the range of 200-1000 µL at a constant sample concentration of 5 mg/ml. An injection volume of 750 µL was selected for all subsequent preparative separations, as it provided the optimal balance between sample loading capacity and chromatographic resolution.

The gradient elution program is summarised in Table 7.1. The separation was initiated with a mobile phase composition of 75% solvent A and 25% solvent B (v/v) at a flow rate of 10.6 mL/min. A linear gradient was applied over 12 minutes, reaching 100% solvent B at 12.0 minutes, after which the flow rate was simultaneously increased to 20.0 mL/min. These conditions were maintained isocratically (100% acetonitrile) for a further 12.5 minutes, giving a total run time of 24.6 minutes to ensure complete elution of all retained compounds. The elution order of all target compounds was consistent with those observed by analytical HPLC (section 7.2.3.1).

Table 7.1: Gradient elution program used for preparative HPLC separation.

Time (min)	Aqueous phase (% v/v)	Acetonitrile (% v/v)	Flow rate (ml/min)
0	75	25	10.6
12	0	100	10.6
12.1	0	100	20
24.6	0	100	20

7.2.4 Spectroscopic analysis for structural elucidation

7.2.4.1 Nuclear Magnetic Resonance (NMR)

NMR spectra were acquired on a Bruker Avance III spectrometer operating at 500 MHz for ^{1}H and 125 MHz for ^{13}C nuclei. Chemical shifts (δ) are reported in parts per million (ppm) relative to the residual solvent signal, with typical ranges of 0-15 ppm for ^{1}H NMR and 0-220 ppm for ^{13}C NMR spectra. Coupling constants (J) are expressed in Hertz (Hz). ^{1}H and ^{13}C NMR spectra were routinely recorded using 32 and 2000 scans respectively, however, for rearrangement products obtained in limited quantities, the number of ^{1}H NMR scans was increased to 320 to enhance the signal. The number of scans was otherwise adjusted according to sample concentration and sensitivity requirements. Where required for clear structural elucidation, a full suite of two-dimensional NMR experiments was employed, including COSY, HSQC, and HMBC All spectra were processed and analysed using MestReNova software (version 14.1).

Allicin: Oily colourless. **^{1}H NMR** (500 MHz, methanol-d_4) δ 6.10-5.95 (m, 2H), 5.56 (d, *J* = 4.8 Hz, 1H), 5.56-5.49 (m, 1H), 5.41 (dddd, *J* = 16.9, 7.0, 2.6, 1.3 Hz, 1H), 5.34-5.27 (m, 1H), 4.06 (dt, *J* = 13.1, 6.3 Hz, 1H), 4.02-3.93 (m, 1H), 3.93-3.82 (m, 2H). **^{13}C NMR** (125 MHz, methanol-d_4): δ 132.1, 119.8, 63.2, 37.8 ppm.

Sinigrin: White crystal. **^{1}H NMR** (500 MHz, D_2O) δ 6.06 (dddd, *J* = 16.9, 10.2, 6.5, 5.4 Hz, 1H), 5.36 (dd, *J* = 17.2, 1.6 Hz, 1H), 5.32 (dd, *J* = 10.2, 1.5 Hz, 1H), 5.05 (d, *J* = 9.8 Hz, 1H), 3.91 (dd, *J* = 12.5, 2.1 Hz, 1H), 3.71 (dd, *J* = 12.5, 5.9 Hz, 1H), 3.61 - 3.56 (m, 1H), 3.56 - 3.53 (m, 1H), 3.53 - 3.51 (m, 1H), 3.50 (d, *J* = 3.7 Hz, 1H), 3.46 - 3.42 (m, 1H), 3.42 -3.37 (m, 1H). **^{13}C NMR** (126 MHz, D_2O) δ 162.98, 132.08, 118.40, 81.55, 80.00, 77.05, 71.94, 69.13, 60.64, 36.11 ppm. [234].

Allyl isothiocyanate (AITC): Light yellow. **^{1}H NMR** (500 MHz, methanol-d_4) δ 5.92 (dddt, J = 17.1, 9.9, 7.6, 4.9 Hz, 1H), 5.40-5.33 (m, 1H), 5.27 (dd, J = 9.3, 1.4 Hz, 1H), 4.20 (dt, J = 4.9, 1.8 Hz, 2H). **^{13}C NMR** (126 MHz, D_2O) δ 130.26, 117.65, 47.04 ppm.

Glucoraphanin: White powder. **The ^{1}H NMR** (500 MHz, D_2O) δ 5.18 (d, *J* = 9.8 Hz, 1H), 4.07 (dd, *J* = 12.6, 2.2 Hz, 1H), 3.88 (dd, *J* = 12.6, 6.1 Hz, 1H), 3.76 - 3.70 (m, 1H), 3.62 (ddd, *J* = 10.0, 8.9, 1.0 Hz, 2H), 3.17 - 3.08 (m, 2H), 2.99 (td, *J* = 7.1, 1.9 Hz, 2H), 2.89 (s, 3H), 2.12 - 1.96 (m, 2H). **The ^{13}C NMR** (126 MHz, D_2O) δ 161.60, 118.14, 80.78, 79.23, 76.23, 71.11, 68.33, 59.92, 51.29, 35.61, 30.73, 24.55, 20.44, 3.10, 2.07, 0.31, 0.20, -0.00, -0.25, -2.08, -3.11, -16.57 ppm.

Sulforaphane: Light yellow. **The ^{1}H NMR** (500 MHz, acetonitrile-d_3) δ 3.88 (m, 2H), 3.11 (m, 2H), 2.90 (s, 3H), 2.07 (m, 5H). **^{13}C NMR** (126 MHz, D_2O) δ 50.94, 43.43, 35.73, 27.09, 18.53 ppm [235, 236].

Alligrin: White crystal. **MS** (negative mode, *m/z*): 267.97. **^{1}H NMR** (500 MHz, D_2O) δ 5.96 (1H, m), 5.87 (1H, m), 5.26 (2H, m), 5.22 (2H, m), 3.56 (2H, dt, *J* = 6.12, 1.60 Hz), 3.45 (2H, dt, *J* = 7.39, 1.00 Hz). **The ^{13}C NMR** (125 MHz, D_2O) δ 167.57, 132.13, 131.69, 119.96, 118.30, 42.24, and 34.65 ppm.

Alliphanin: White powder**. MS** (negative mode, *m/z*): 354.98. The **^{1}H NMR** (500 MHz, D_2O) δ 5.89 (ddt, J = 17.4, 10.0, 7.5 Hz, 1H), 5.28-5.20 (m, 2H), 3.46 (dt, J = 7.5, 0.9 Hz, 2H), 3.01-

2.90 (m, 2H), 2.87-2.82 (m, 2H) δ 2.71 (s, 3H), 1.88-1.79 (m, 4H). **^{13}C NMR** (126 MHz, D_2O) δ 180.65, 131.58, 120.03, 52.10, 42.29, 36.33, 30.35, 25.47, 22.76, 21.08 ppm.

Compound 9: White powder**. MS** (negative mode, *m/z*): 339.98. **^{1}H NMR** (500 MHz, D_2O) δ 6.40 (d, *J* = 9.3 Hz, 1H), 5.98 (ddq, *J* = 16.3, 11.0, 5.5 Hz, 1H), 5.91 - 5.75 (m, 2H), 5.35 - 5.21 (m, 4H), 3.74 (dd, *J* = 13.9, 7.2 Hz, 2H), 3.41 (d, *J* = 7.4 Hz, 2H), 3.37 (d, *J* = 5.9 Hz, 2H) ppm.

Compound 11: White powder**. MS** (negative mode, *m/z*): 371.95. **^{1}H NMR** (500 MHz, D_2O) δ 6.73 (dd, *J* = 9.4, 1.0 Hz, 1H), 5.99 - 5.80 (m, 3H), 5.56 - 5.45 (m, 2H), 5.28 - 5.19 (m, 2H), 3.86 - 3.71 (m, 2H), 3.63 - 3.55 (m, 2H), 3.48 - 3.42 (m, 2H) ppm.

Desulfo-alligrin: White powder**. MS** (positive mood, *m/z*)**:** 190.036. **^{1}H NMR** (500 MHz, D_2O) δ 5.93 - 5.83 (m, 1H), 5.83 - 5.74 (m, 1H), 5.18 - 5.08 (m, 1H), 3.38 (dd, *J* = 6.1, 1.9 Hz, 1H), 3.34 (dd, *J* = 7.5, 1.0 Hz, 1H) ppm.

7.2.4.2 Liquid Chromatography-Mass Spectrometry (LC-MS)

LC-Q-Exactive-MS/MS data were obtained using a Thermo Scientific hybrid quadrupole-Orbitrap mass spectrometers coupled with UHPLC system. Samples were prepared at a final concentration of 0.5 mg/mL by dissolving crude mixture reaction extracts or purified compounds in in 15% (v/v) acetonitrile to maintain compatibility with the initial mobile phase conditions. All samples were filtered through a PTFE 0.2 µm syringe filter prior to analysis and transferred to 1.5 mL LC-MS vials (Fisher Scientific, UK).

Samples separations were performed using a Kinetex® XB-C18 column (2.6 µm, 100 Å, 50 × 2.1 mm) with a gradient elution program employing acetonitrile and an aqueous mobile phase of deionised water (containing 0.1% formic acid). The aqueous phase was used instead of ammonium acetate buffer (0.025 M, pH 6.0) to enhance ionisation efficiency. Analyses were carried out at a flow rate of 0.6 mL/min, with injection volumes ranging from 10 to 50 µL depending on sample quantity. The HPLC gradient conditions applied are summarised in Table 7.2.

Table 7.2: HPLC method used during LC-MS analysis.

Time (min)	H_2O (%)	Acetonitrile (%)
0	85	15
12	35	65
13.5	0	100
16.5	0	100
16.6	85	15
25	85	15

Mass spectrometric detection was performed using electrospray ionisation (ESI) operated in negative/positive ion mode over an m/z range of 50-1500. High-resolution accurate-mass spectrometry (HRAMS), together with tandem MS (MS/MS), was used to support molecular formula assignment and structural characterisation of the analytes. All acquired data were processed and analysed using Xcalibur software (Thermo Fisher Scientific) and ACD/Spectrus processor (version 2021.2.2, ACD/Labs).

7.2.4.3 X-ray crystallography

7.2.4.3.1 Crystallisation

A clear white plate-shaped crystal of alligrin was obtained by slow evaporation under a gentle stream of nitrogen gas at room temperature. The resulting crystals were examined under an optical microscope to assess their morphology and suitability for diffraction analysis.

7.2.4.3.2 Single Crystal X-ray Diffraction (SCXD)

Single-crystal X-ray diffraction analysis was carried out by Dr. Alexander Morritt at the School of Chemistry, Pharmacy and Pharmacology, University of East Anglia. Full details of the data collection, structure solution, and refinement protocols followed in this study are provided in the Appendix, as established by Dr. Alex.

7.2.5 Experimental validation of alligrin rearrangement pathways

To investigate the rearrangement pathways of alligrin, controlled incubation experiments were conducted using equimolar stock solutions of purified alligrin (5 mM, 1.345 mg/mL in deionised water) and allicin (5 mM, 0.811 mg/mL in acetonitrile, 0.73 µL) under defined thermal conditions. Reactions were carried out in sealed Eppendorf vials placed in a heating block and organised into three experimental sets: (i) co-incubation of alligrin with allicin, (ii) allicin-only controls, and (iii) alligrin-only incubations.

For co-incubation experiments, alligrin stock solution (125 µL) was combined with allicin stock solution (125 µL) in deionised water and acetonitrile, respectively, giving a total reaction volume of 500 µL. These mixtures were incubated either at room temperature for 3 hours or at 80°C for 15, 30, and 60 minutes. Allicin-only control samples were prepared by combining allicin stock solution (500 µL) with acetonitrile (500 µL) and incubated at 80°C for the same time intervals. For alligrin-only incubations, purified alligrin stock solution (500 µL) was combined with deionised water (500 µL) and incubated at room temperature for 3 hours and at 80°C for 15, 30, and 60 minutes to examine the temperature-dependent formation of compound **3**. At the end of each incubation period, reactions were quenched by the addition of 500 µL of 50% acetonitrile in deionised water (v/v) to prevent further thermal degradation, and the resulting solutions were transferred to HPLC vials prior to analysis.

Following each incubation period, samples were prepared for analysis by both HPLC and LC-MS. Products formation were monitored by HPLC using the optimised analytical method described in Section 7.2.3.1, and peak retention times were compared against those obtained from the original sinigrin-allicin-myrosinase reaction mixture to confirm the formation of identical products (compounds **3**, **9**, **10**, **13**, **14**, **16**, and **17**). Selected time-point samples were further analysed by LC-MS to confirm molecular weight and corroborate structural assignments with previously characterised compounds.

Compounds	Peak retention time in mixture reaction	Peak retention time in heating samples
3	10.5 min	10.8 min
9	11.7 min	12 min
11	12.7 min	13 min
13	14 min	14.3 min

7.2.6 Thermal treatment of alligrin

To evaluate the thermal stability of alligrin, a stock solution (5 mM, 1.3 mg/mL) was prepared in deionised water and distributed into separate Eppendorf vials. Samples were heated at 50, 80, and 100°C for defined time intervals of 15, 30, and 60 minutes. At each time point, a 250 µL sample was immediately quenched upon removal from the heat block by the addition of an equal volume of 50% (v/v) acetonitrile in deionised water to arrest further thermal degradation.

For high-temperature studies, a fresh alligrin stock solution was prepared and transferred to sealed Ace glass pressure tubes, which were heated in an oil bath at 170 and 200°C for the same time intervals. All samples were analysed by HPLC using the optimised analytical method (3) described in Section 7.2.3.1 to assess chemical stability and degradation profiles. Selected time-point samples were further analysed by LC-MS to confirm the molecular weight of degradation products.

Chapter 3

7.2.7 Plant preparations

7.2.7.1 Preparation of individual plant extracts

7.2.7.1.1 Preparation of allicin in fresh garlic extract

Fresh garlic cloves (10 g) were homogenised with potassium phosphate buffer (40 mL, 0.1 M, pH 6.0) for 1 minute using a kitchen blender. The resulting homogenate was allowed to stand at room temperature, and samples were collected at defined time points of 0, 2, 5, 10, 15, 20,

25, 30, 35, 40, 45, 50, 55, and 60 minutes. At each time point, a 1 g of the crude homogenate was quenched by the addition of 50% (v/v) acetonitrile in potassium phosphate buffer and the total volume adjusted to 5 mL in falcon tube. The resulting solution was transferred to an HPLC vial and analysed by HPLC using the optimised analytical method described in Section 7.2.3.1, with an injection volume of 10 µL.

7.2.7.1.2 Preparation of aglycon intermediate in mustard seeds powder/ broccoli

The procedure described above (section 7.2.7.1.1) was applied without modification to mustard seeds powder/ broccoli, use instead 10 g of mustard seeds powder/ broccoli for the fresh garlic cloves.

7.2.7.2 Preparation of mixed plants extract

7.2.7.2.1 Preparation mixture of garlic and mustard seeds powder

A mixture reaction experiment was conducted to investigate the chemical interaction between fresh garlic and mustard seed powder. Fresh garlic cloves (10 g) were homogenised with potassium phosphate buffer (40 mL, 0.1 M, pH 6.0) for 1 minute and allowed to stand at room temperature for 30 minutes to permit enzymatic conversion and formation of allicin. Subsequently, mustard seeds powder (10 g) was added to the garlic homogenate, and the combined mixture was blended for a further 1 minute to ensure uniform mixing. The reaction mixture was then allowed to stand for 15 minutes at room temperature.

For HPLC analysis, a 1 g of the crude homogenate was quenched by the addition of 50% (v/v) acetonitrile in potassium phosphate buffer and the total volume adjusted to 5 mL in a falcon tube. The resulting solution was transferred to an HPLC vial and analysed using the optimised analytical method described in Section 7.2.3.1, with an injection volume of 10 µL.

7.2.7.2.2 Preparation mixture of garlic and broccoli

The garlic-broccoli mixture was prepared following the same procedure described for the garlic-mustard system (Section 7.2.7.2.1), with broccoli substituted for mustard seeds powder.

7.2.7.3 Calculation of alligrin content in crude garlic-mustard mixture

Alligrin was quantified in the garlic-mustard mixture by external calibration under identical HPLC conditions using the optimised analytical method described in Section 7.2.3.1. A 1 g portion of the crude garlic-mustard mixture was prepared for analysis as described in Section 7.2.7.2.1.

The alligrin calibration curve was constructed by linear regression and described by the equation: y=4.4749x-132.33

Using the calibration curve, the concentration of alligrin in the extract was determined to be 133.91 µg/ml. The total amount of alligrin was subsequently calculated as:

133.91 µg/mL × 5.00 mL = 669.55 µg

Normalised to the mass of crude material (0.3 g):

669.55 µg ÷ 0.3 g = 2231.8 µg/g = **2.23 mg/g of crude material**

Converting to micromolar per gram:

2231.8 µg/g ÷ 268 g/mol × 1000 = **8.33 µmol/g of crude material**

7.2.8 Optimisation method of sinigrin hydrolysis for enhanced alligrin formation

To evaluate the effect of exogenous myrosinase on sinigrin hydrolysis, comparative incubation experiments were conducted using mustard seed powder in the presence and absence of added enzyme. Mustard seeds powder (2 g) was extracted with potassium phosphate buffer (20 mL, 0.1 M, pH 6.0) and homogenised for 1 minute to obtain a crude extract. For enzyme-supplemented reactions, myrosinase (50 U) was added to the crude extract prior to incubation, while control reactions were prepared under identical conditions without the addition of exogenous myrosinase. All reaction mixtures were subsequently incubated at room temperature, and samples were collected at defined time points of 0, 5, 15, 20, 30, 45, and 60 minutes.

At each time point, a 1 g portion of the crude reaction mixture was quenched by the addition of 50% (v/v) acetonitrile in potassium phosphate buffer and the total volume adjusted to 5

mL in a falcon tube. The resulting solution was transferred to an HPLC vial and analysed using the optimised analytical method described in Section 7.2.3.1, with an injection volume of 10 µL, to monitor sinigrin degradation and the formation of allyl isothiocyanate (AITC).

7.2.9 Effect of sample concentration on alligrin formation

To investigate the effect of sample concentration on alligrin formation, the garlic-mustard seed powder mixture was prepared as described in Section 7.2.7.2.1. Prior to HPLC sample preparation, the crude homogenate was immediately transferred to a Genevac centrifugal evaporator and dried overnight at room temperature under reduced pressure to yield a concentrated dry residue for subsequent analysis.

Chapter 4

7.2.10Enzymatic sulfatase assay

7.2.10.1 Reagent preparation

The desulfation of alligrin was carried out by adapting the sulfatase assay protocol published by Sigma-Aldrich, in which 4-nitrocatechol sulfate serves as the standard substrate. Alligrin was prepared at a concentration of 1 mg/mL in deionised water (as substrate). Sulfatase was freshly prepared at a concentration of 5 U/mL in ice-cold 5 M NaCl dissolved in ultrapure water to maintain enzymatic stability and activity.

7.2.10.2 General assay procedure

All sulfatase reactions were carried out in a total volume of 1.0 mL, containing 0.5 mL of sodium acetate buffer (100 mM, pH 5.5), 0.4 mL of substrate solution (alligrin; 1 mg/mL stock solution, (0.4 mL, 0.0014 mM)), and 0.1 mL of sulfatase solution (5 U). Reaction mixtures were incubated at 37 °C in a heating block for 30 min. Following incubation, all reaction mixtures were analysed by HPLC using the optimised analytical method described in Section 7.2.3.1 and by LC-MS to confirm enzymatic activity and the formation of desulfo-alligrin.

7.2.10.3 Solid-phase extraction (SPE) purification of desulfo-alligrin

Desulfo-alligrin was purified by solid-phase extraction (SPE) using strong anion exchange (Strata SAX, Phenomenex, 55 µm, 70 Å, 1000 mg/6 mL) and strong cation exchange (Strata SCX, Phenomenex, 55 µm, 70 Å, 1000 mg/6 mL) cartridges in sequential combination.

For SAX purification, the cartridge was conditioned with three column volumes (CV) of 0.5 M HCl, followed by three CV of Milli-Q water. The sample of desulfo-alligrin dissolved in 5 mL of Milli-Q water, was loaded onto the conditioned cartridge. The purified compound was subsequently eluted with three CV of Milli-Q water and collected for further processing. The resulting fraction was then subjected to SCX purification following the same conditioning, loading, and elution procedure as described for the SAX cartridge, to isolate complementary cationic fractions. The combined purified fractions were evaporated to dryness to afford desulfo-alligrin as a white residue (0.29 mg, 0.0015 mmol). The residue was analysed by HPLC using the optimised analytical method described in Section 7.2.3.1 and by ^{1}H NMR spectroscopy to assess purity and confirm structural identity.

7.2.11Biological evaluation

7.2.11.1 Maintenance of bacterial strains and growth conditions

A group of Gram-positive and Gram-negative bacterial strains, representing both antibiotic-susceptible and antibiotic-resistant phenotypes, was selected for antibacterial evaluation. The Gram-positive strains involved methicillin- *resistant Staphylococcus aureus* (MRSA 13373) and *S. aureus* (RN4220), while the Gram-negative strains included *Escherichia coli* (NCTC 10418) and *Pseudomonas aeruginosa* (NCTC 10662) as susceptible reference strains. Details of all bacterial strains, including their sources and resistance profiles, are summarised in Table 7.3.

Table 7.3: Gram-positive and negative bacterial strains used for antibacterial evaluation.

Strain	Source	Gram stain	Antibiotic resistance	Reference
***Staphylococcus aureus* RN4220**	Genetically modified, derived from clinical isolate.	Positive	MRSA	[237]
***methicillin resistant Staphylococcus aureus* MRSA 13373**	NCTC	Positive	MRSA	[238]
***Escherichia coli* 10418**	NCTC	Negative	MDR	NCTC
***Pseudomonas aeruginosa* 10662**	NCTC	Negative	Susceptible	NCTC

All bacterial strains were maintained on nutrient agar (Merck, UK) slants in bijoux vials and stored at 4°C for up to five months. Prior to biological assays, strains were sub-cultured onto fresh nutrient agar and incubated at 37°C for 24 hours to obtain actively growing cultures. All growth media and reagents were sterilised by autoclaving at 121°C for 20 minutes prior to use. All microbiological procedures were carried out under aseptic conditions within a laminar flow cabinet.

7.2.11.2 Inhibition zone determination (Disc Diffusion Assay)

The antibacterial activity of aqueous extracts of fresh garlic, fresh broccoli, mustard seed powder, garlic-mustard seed powder and garlic-broccoli was evaluated by the agar disc diffusion method. The purified compounds alligrin, allicin, sinigrin and desulfo-alligrin were tested in the same way. Nutrient agar was sterilised by autoclaving (121 °C, 15 min), poured into sterile (90 mm) Petri dishes (20 mL per plate) and allowed to solidify at room temperature.

Colonies from overnight cultures of methicillin-resistant *Staphylococcus aureus* (MRSA) 13373, *S. aureus* RN4220, *Escherichia coli* NCTC 10418 and *Pseudomonas aeruginosa* NCTC 10662 were suspended in sterile phosphate-buffered saline (PBS). Each suspension was standardised by turbidity., its optical density at 600 nm (OD_{600}) was measured in a

spectrophotometer against a sterile PBS blank and adjusted to 0.1 by adding PBS or more bacterial cells. This turbidity is approximately equivalent to a 0.5 McFarland standard, corresponding to roughly 1-1.5 × 10^8 colony-forming units (CFU) per mL. An aliquot of each standardised suspension (1 mL) was spread evenly over the agar surface, and the plates were allowed to dry at room temperature for 30 min.

The aqueous extracts and the compounds alligrin, sinigrin and desulfo-alligrin were prepared in sterile water, and allicin was prepared in methanol. Ampicillin and ciprofloxacin (30 µg per disc) were used as positive controls. Sterile (6 mm) paper discs were loaded with a total of 30 µL of each sample, applied as three successive 10 µL aliquots with 10 min drying between applications, in a laminar flow cabinet. The loaded discs were placed on the inoculated agar. Discs loaded with sterile water or methanol alone (vehicle) served as negative controls on each plate.

Plates were incubated at 37 °C for (18-24) h. Antibacterial activity was assessed by measuring the total diameter of the inhibition zone around each disc in millimetres using a ruler [239, 240]. Each assay was performed in triplicate, and results are expressed as mean ± SD.

7.2.11.3 Evaluation of alligrin/desulfoalligrin reactivity with glutathione

Alligrin (1.50 mg/mL, 5.58 mM) and desulfo-alligrin (1.04 mg/mL, 5.50 mM) were each incubated separately with freshly prepared glutathione solution (1.70 mg/mL, 5.53 mM) at equimolar concentrations in a total reaction volume of 1 mL for 30 minutes at room temperature. All solutions were prepared in deionized water immediately prior to use. Reactions were quenched with 50% acetonitrile in deionized water and analysed by HPLC and LC-M.

8 References

1. Murray, C.J.L., et al., *Global burden of bacterial antimicrobial resistance in 2019: a systematic analysis.* Lancet, 2022. **399**(10325): p. 629-655.
2. Wagenlehner, F.M.E. and F. Dittmar, *Re: Global Burden of Bacterial Antimicrobial Resistance in 2019: A Systematic Analysis.* European Urology, 2022. **82**(6): p. 658-658.
3. Kariyawasam, R.M., et al., *Antimicrobial resistance (AMR) in COVID-19 patients: a systematic review and meta-analysis (November 2019-June 2021).* Antimicrobial Resistance and Infection Control, 2022. **11**(1).
4. Grossman, M.K., et al., *Extensively Drug-Resistant Pseudomonas aeruginosa Outbreak Associated With Artificial Tears.* Clin Infect Dis, 2024. **79**(1): p. 6-14.
5. Schleifer, K.H., *Classification of and : Past, present and future.* Systematic and Applied Microbiology, 2009. **32**(8): p. 533-542.
6. Turner, N.A., et al., *Methicillin-resistant: an overview of basic and clinical research.* Nature Reviews Microbiology, 2019. **17**(4): p. 203-218.
7. Arias, C.A. and B.E. Murray, *The rise of the: beyond vancomycin resistance.* Nature Reviews Microbiology, 2012. **10**(4): p. 266-278.
8. Li, J., et al., *Streptococcus pneumoniae beta-lactam resistance: epidemiological trends, molecular drivers, and innovative control strategies in the post-pandemic era.* Clin Microbiol Rev, 2025. **38**(3): p. e0008225.
9. Khanal, B., et al., *Antimicrobial Resistant Streptococcus pneumoniae.* Journal of Nepal Medical Association, 2010. **49**(3): p. 220-224.
10. Tacconelli, E., et al., *Discovery, research, and development of new antibiotics: the WHO priority list of antibiotic-resistant bacteria and tuberculosis.* Lancet Infectious Diseases, 2018. **18**(3): p. 318-327.
11. Wyres, K.L. and K.E. Holt, *as a key trafficker of drug resistance genes from environmental to clinically important bacteria.* Current Opinion in Microbiology, 2018. **45**: p. 131-139.
12. Pang, Z., et al., *Antibiotic resistance: mechanisms and alternative therapeutic strategies.* Biotechnology Advances, 2019. **37**(1): p. 177-192.
13. Crump, J.A., et al., *Epidemiology, Clinical Presentation, Laboratory Diagnosis, Antimicrobial Resistance, and Antimicrobial Management of Invasive Infections.* Clinical Microbiology Reviews, 2015. **28**(4): p. 901-937.
14. Delcour, A.H., *Outer membrane permeability and antibiotic resistance.* Biochimica Et Biophysica Acta-Proteins and Proteomics, 2009. **1794**(5): p. 808-816.
15. Ude, J., et al., *Outer membrane permeability: Antimicrobials and diverse nutrients bypass porins in.* Proceedings of the National Academy of Sciences of the United States of America, 2021. **118**(31).

16. Malanovic, N. and K. Lohner, *Gram-positive bacterial cell envelopes: The impact on the activity of antimicrobial peptides.* Biochimica Et Biophysica Acta-Biomembranes, 2016. **1858**(5): p. 936-946.

17. Ho, C.S., et al., *Antimicrobial resistance: a concise update.* Lancet Microbe, 2025. **6**(1).

18. Belay, W.Y., et al., *Mechanism of antibacterial resistance, strategies and next-generation antimicrobials to contain antimicrobial resistance: a review.* Frontiers in Pharmacology, 2024. **15**.

19. Kumawat, M., et al., *Role of bacterial efflux pump proteins in antibiotic resistance across microbial species.* Microbial Pathogenesis, 2023. **181**.

20. Kim, J., et al., *Structural Insights into Transporter-Mediated Drug Resistance in Infectious Diseases.* Journal of Molecular Biology, 2021. **433**(16).

21. Nazir, A., et al., *The Global Challenge of Antimicrobial Resistance: Mechanisms, Case Studies, and Mitigation Approaches.* Health Science Reports, 2025. **8**(7).

22. Mohanty, H., S. Pachpute, and R.P. Yadav, *Mechanism of drug resistance in bacteria: efflux pump modulation for designing of new antibiotic enhancers.* Folia Microbiologica, 2021. **66**(5): p. 727-739.

23. Darby, E.M., et al., *Molecular mechanisms of antibiotic resistance revisited(vol 21, pg 280, 2023).* Nature Reviews Microbiology, 2024. **22**(4): p. 255-255.

24. Nordmann, P., L. Dortet, and L. Poirel, *Carbapenem resistance: here is the storm!* Trends in Molecular Medicine, 2012. **18**(5): p. 263-272.

25. Samreen, et al., *Environmental antimicrobial resistance and its drivers: a potential threat to public health.* Journal of Global Antimicrobial Resistance, 2021. **27**: p. 101-111.

26. Hollenbeck, B.L. and L.B. Rice, *Intrinsic and acquired resistance mechanisms in enterococcus.* Virulence, 2012. **3**(5): p. 421-433.

27. Wilson, D.N., *Ribosome-targeting antibiotics and mechanisms of bacterial resistance.* Nature Reviews Microbiology, 2014. **12**(1): p. 35-48.

28. Biswas, S., et al., *Biofilms: mechanisms, quorum sensing, antibiotic resistance and implications in the food industry.* Biologia, 2025. **80**(7): p. 1803-1821.

29. Gao, Q., et al., *Bacterial DNA methyltransferase: A key to the epigenetic world with lessons learned from proteobacteria.* Frontiers in Microbiology, 2023. **14**.

30. Kunnath, A.P., et al., *Bacterial Persister Cells and Development of Antibiotic Resistance in Chronic Infections: An Update.* British Journal of Biomedical Science, 2024. **81**.

31. Zhao, A.L., J.Z. Sun, and Y.P. Liu, *Understanding bacterial biofilms: From definition to treatment strategies.* Frontiers in Cellular and Infection Microbiology, 2023. **13**.

32. Uruén, C., et al., *Biofilms as Promoters of Bacterial Antibiotic Resistance and Tolerance.* Antibiotics-Basel, 2021. **10**(1).

33. Li, X. and J. Ju, *Intracellularly driven chemical modifications of antimicrobial secondary metabolites: Potent mechanisms of self-resistance.* Pharm Sci Adv, 2024. **2**: p. 100032.

34. Mora-Ochomogo, M. and C.T. Lohans, *β-Lactam antibiotic targets and resistance mechanisms: from covalent inhibitors to substrates.* Rsc Medicinal Chemistry, 2021. **12**(10): p. 1623-1639.

35. Nashwan, A.J., et al., *Antimicrobial Resistance: Stewardship and One Health in the Eastern Mediterranean Region.* Cureus Journal of Medical Science, 2024. **16**(4).

36. Fletcher-Miles, H., et al., *A scoping review to assess the impact of public education campaigns to affect behavior change pertaining to antimicrobial resistance.* American Journal of Infection Control, 2020. **48**(4): p. 433-442.

37. Buffie, C.G. and E.G. Pamer, *Microbiota-mediated colonization resistance against intestinal pathogens.* Nature Reviews Immunology, 2013. **13**(11): p. 790-801.

38. Oliveira, N.J.r., et al., *Antimicrobial peptides: structure, functions and translational applications.* Nature Reviews Microbiology, 2025. **23**(11): p. 687-700.

39. Newman, D.J. and G.M. Cragg, *Natural Products as Sources of New Drugs over the Nearly Four Decades from 01/1981 to 09/2019.* Journal of Natural Products, 2020. **83**(3): p. 770-803.

40. Koehn, F.E. and G.T. Carter, *The evolving role of natural products in drug discovery.* Nature Reviews Drug Discovery, 2005. **4**(3): p. 206-220.

41. Shen, B., *A New Golden Age of Natural Products Drug Discovery.* Cell, 2015. **163**(6): p. 1297-1300.

42. Wang, Y.X., et al., *New drug discovery and development from natural products: Advances and strategies.* Pharmacology & Therapeutics, 2024. **264**.

43. Dias, D.A., S. Urban, and U. Roessner, *A historical overview of natural products in drug discovery.* Metabolites, 2012. **2**(2): p. 303-36.

44. Cragg, G.M. and D.J. Newman, *Biodiversity: A continuing source of novel drug leads.* Pure and Applied Chemistry, 2005. **77**(1): p. 7-24.

45. Huang, X.Q. and N. Dudareva, *Plant specialized metabolism.* Current Biology, 2023. **33**(11): p. R473-R478.

46. Pichersky, E. and E. Lewinsohn, *Convergent Evolution in Plant Specialized Metabolism.* Annual Review of Plant Biology, Vol 62, 2011. **62**: p. 549-566.

47. Wu, M.X., T.R. Northen, and Y.Z. Ding, *Stressing the importance of plant specialized metabolites: omics-based approaches for discovering specialized metabolism in plant stress responses.* Frontiers in Plant Science, 2023. **14**.

48. Khameneh, B., et al., *Review on plant antimicrobials: a mechanistic viewpoint.* Antimicrobial Resistance and Infection Control, 2019. **8**.

49. Borlinghaus, J., et al., *Allicin: Chemistry and Biological Properties.* Molecules, 2014. **19**(8): p. 12591-12618.

50. Imenshahidi, M. and H. Hosseinzadeh, *Berberine and barberry: A clinical review.* Phytotherapy Research, 2019. **33**(3): p. 504-523.

51. Steinmann, J., et al., *Anti-infective properties of epigallocatechin-3-gallate (EGCG), a component of green tea.* British Journal of Pharmacology, 2013. **168**(5): p. 1059-1073.

52. Gupta, S.C., S. Patchva, and B.B. Aggarwal, *Therapeutic Roles of Curcumin: Lessons Learned from Clinical Trials.* Aaps Journal, 2013. **15**(1): p. 195-218.

53. Marchese, A., et al., *Antimicrobial activity of eugenol and essential oils containing eugenol: A mechanistic viewpoint.* Critical Reviews in Microbiology, 2017. **43**(6): p. 668-689.

54. Wahab, S., et al., *(Licorice): A Comprehensive Review on Its Phytochemistry, Biological Activities, Clinical Evidence and Toxicology.* Plants-Basel, 2021. **10**(12).

55. Periferakis, A.T., et al., *The Multifaceted Antimicrobial Profile of Piperine in Infectious Disease Management: Current Perspectives and Potential.* Pharmaceuticals, 2025. **18**(10).

56. Marchese, A., et al., *Antibacterial and antifungal activities of thymol: A brief review of the literature.* Food Chemistry, 2016. **210**: p. 402-414.

57. El-Saber Batiha, G., et al., *Chemical Constituents and Pharmacological Activities of Garlic (Allium sativum L.): A Review.* Nutrients, 2020. **12**(3).

58. Sönmez, I., Ü.H. Erol, and K. Sarpkaya, *Comprehensive morphological and biochemical characterization of garlic (L.) genotypes using multivariate analysis.* Bmc Plant Biology, 2025. **25**(1).

59. Dhall, R.K., et al., *History, evolution and domestication of garlic: a review.* Plant Systematics and Evolution, 2023. **309**(5).

60. Rivlin, R.S., *Historical perspective on the use of garlic.* Journal of Nutrition, 2001. **131**(3): p. 951s-954s.

61. Petrovska, B.B. and S. Cekovska, *Extracts from the history and medical properties of garlic.* Pharmacogn Rev, 2010. **4**(7): p. 106-10.

62. Shang, A., et al., *Bioactive Compounds and Biological Functions of Garlic (L.).* Foods, 2019. **8**(7).

63. Cavallito, C.J. and J.H. Bailey, *Allicin, the antibacterial principle of Allium sativum I Isolation, physical properties and antibacterial action.* Journal of the American Chemical Society, 1944. **66**: p. 1950-1951.

64. Khodavandi, A., et al., *Expression analysis of SIR2 and SAPs1-4 gene expression in Candida albicans treated with allicin compared to fluconazole.* Trop Biomed, 2011. **28**(3): p. 589-98.

65. Weber, N.D., et al., *In vitro virucidal effects of Allium sativum (garlic) extract and compounds.* Planta Med, 1992. **58**(5): p. 417-23.

66. Zhen, H., et al., *Experimental study on the action of allitridin against human cytomegalovirus in vitro: Inhibitory effects on immediate-early genes.* Antiviral Research, 2006. **72**(1): p. 68-74.

67. Gebhardt, R. and H. Beck, *Differential inhibitory effects of garlic-derived organosulfur compounds on cholesterol biosynthesis in primary rat hepatocyte cultures.* Lipids, 1996. **31**(12): p. 1269-76.

68. Agarwal, K.C., *Therapeutic actions of garlic constituents.* Medicinal Research Reviews, 1996. **16**(1): p. 111-124.

69. Fukao, T., et al., *The effects of allyl sulfides on the induction of phase II detoxification enzymes and liver injury by carbon tetrachloride.* Food Chem Toxicol, 2004. **42**(5): p. 743-9.

70. Rabinkov, A., et al., *The mode of action of allicin: trapping of radicals and interaction with thiol containing proteins.* Biochimica Et Biophysica Acta-General Subjects, 1998. **1379**(2): p. 233-244.

71. Seki, T., et al., *Anticancer effects of diallyl trisulfide derived from garlic.* Asia Pacific Journal of Clinical Nutrition, 2008. **17**: p. 249-252.

72. El-Saadony, M.T., et al., *Garlic bioactive substances and their therapeutic applications for improving human health: a comprehensive review.* Frontiers in Immunology, 2024. **15**.

73. Shimon, L.J., et al., *Two structures of alliinase from Alliium sativum L.: apo form and ternary complex with aminoacrylate reaction intermediate covalently bound to the PLP cofactor.* J Mol Biol, 2007. **366**(2): p. 611-25.

74. Focke, M., A. Feld, and H.K. Lichtenthaler, *Allicin, a Naturally-Occurring Antibiotic from Garlic, Specifically Inhibits Acetyl-Coa Synthetase.* Febs Letters, 1990. **261**(1): p. 106-108.

75. Leontiev, R., et al., *A Comparison of the Antibacterial and Antifungal Activities of Thiosulfinate Analogues of Allicin.* Scientific Reports, 2018. **8**.

76. Lawson, L.D. and Z.J. Wang, *Allicin and allicin-derived garlic compounds increase breath acetone through allyl methyl sulfide: Use in measuring allicin bloavailability.* Journal of Agricultural and Food Chemistry, 2005. **53**(6): p. 1974-1983.

77. Iciek, M., I. Kwiecien, and L. Wlodek, *Biological properties of garlic and garlic-derived organosulfur compounds.* Environ Mol Mutagen, 2009. **50**(3): p. 247-65.

78. O'Gara, E.A., D.J. Hill, and D.J. Maslin, *Activities of garlic oil, garlic powder, and their diallyl constituents against Helicobacter pylori.* Appl Environ Microbiol, 2000. **66**(5): p. 2269-73.

79. Rouf, R., et al., *Antiviral potential of garlic (Allium sativum) and its organosulfur compounds: A systematic update of pre-clinical and clinical data.* Trends Food Sci Technol, 2020. **104**: p. 219-234.

80. Katircioglu, B. and S. Navruz-Varli, *Effects of different preparation and cooking processes on the bioactive molecules of vegetables.* Frontiers in Nutrition, 2024. **11**.

81. Song, K. and J.A. Milner, *The influence of heating on the anticancer properties of garlic.* J Nutr, 2001. **131**(3s): p. 1054S-7S.

82. Ankri, S. and D. Mirelman, *Antimicrobial properties of allicin from garlic.* Microbes and Infection, 1999. **1**(2): p. 125-129.

83. Lin, L.H., et al., *Effects of Allicin on the Formation of Biofilm and the Production of Quorum-Sensing Controlled Virulence Factors.* Polish Journal of Microbiology, 2013. **62**(3): p. 243-251.

84. Nakamoto, M., et al., *Antimicrobial properties of hydrophobic compounds in garlic: Allicin, vinyldithiin, ajoene and diallyl polysulfides.* Experimental and Therapeutic Medicine, 2020. **19**(2): p. 1550-1553.

85. Kumar, A. and V.D. Sharma, *Inhibitory effect of garlic (Allium sativum Linn.) on enterotoxigenic Escherichia coli.* Indian J Med Res, 1982. **76 Suppl**: p. 66-70.

86. Bhatwalkar, S.B., R. Mondal, and R. Anupam, *Antibiofilm properties of garlic and its interaction with methicillin against methicillin-resistant.* Ars Pharmaceutica, 2024. **65**(3): p. 232-239.

87. Cai, Y., et al., *Antibacterial activity of allicin alone and in combination with β-lactams againsts spp. and.* Journal of Antibiotics, 2007. **60**(5): p. 335-338.

88. Melguizo-Rodríguez, L., et al., *Biological properties and therapeutic applications of garlic and its components.* Food & Function, 2022. **13**(5): p. 2415-2426.

89. Zhai, B., et al., *Hypoglycemic and hypolipidemic effect of S-allyl-cysteine sulfoxide (alliin) in DIO mice.* Sci Rep, 2018. **8**(1): p. 3527.

90. Nakamoto, M., et al., *Antimicrobial properties of hydrophobic compounds in garlic: Allicin, vinyldithiin, ajoene and diallyl polysulfides.* Exp Ther Med, 2020. **19**(2): p. 1550-1553.

91. Hirsch, K., et al., *Effect of purified allicin, the major ingredient of freshly crushed garlic, on cancer cell proliferation.* Nutrition and Cancer-an International Journal, 2000. **38**(2): p. 245-254.

92. Yang, C.S., et al., *Mechanisms of inhibition of chemical toxicity and carcinogenesis by diallyl sulfide (DAS) and related compounds from garlic.* Journal of Nutrition, 2001. **131**(3): p. 1041s-1045s.

93. Wallace, G.C.t., et al., *Multi-targeted DATS prevents tumor progression and promotes apoptosis in ectopic glioblastoma xenografts in SCID mice via HDAC inhibition.* J Neurooncol, 2013. **114**(1): p. 43-50.

94. Lai, K.C., et al., *Diallyl sulfide, diallyl disulfide and diallyl trisulfide affect drug resistant gene expression in colo 205 human colon cancer cells in vitro and in vivo.* Phytomedicine, 2012. **19**(7): p. 625-30.

95. Munchberg, U., et al., *Polysulfides as biologically active ingredients of garlic.* Organic & Biomolecular Chemistry, 2007. **5**(10): p. 1505-1518.

96. Arbach, M., et al., *Antimicrobial garlic-derived diallyl polysulfanes: Interactions with biological thiols in Bacillus subtilis.* Biochim Biophys Acta Gen Subj, 2019. **1863**(6): p. 1050-1058.

97. Rattanachaikunsopon, P. and P. Phumkhachorn, *Diallyl sulfide content and antimicrobial activity against food-borne pathogenic bacteria of chives (Allium schoenoprasum).* Biosci Biotechnol Biochem, 2008. **72**(11): p. 2987-91.

98. Avato, P., et al., *Allylsulfide constituents of garlic volatile oil as antimicrobial agents.* Phytomedicine, 2000. **7**(3): p. 239-243.

99. Yi, L. and Q. Su, *Molecular mechanisms for the anti-cancer effects of diallyl disulfide.* Food Chem Toxicol, 2013. **57**: p. 362-70.

100. Yousuf, S., et al., *Effect of diallyldisulphide on an antioxidant enzyme system in Candida species.* Can J Microbiol, 2010. **56**(10): p. 816-21.

101. Oosthuizen, C., et al., *Diallyl Polysulfides from Allium sativum as Immunomodulators, Hepatoprotectors, and Antimycobacterial Agents.* Journal of Medicinal Food, 2017. **20**(7): p. 685-690.

102. Yagdi Efe, E., et al., *Tubulin-binding anticancer polysulfides induce cell death via mitotic arrest and autophagic interference in colorectal cancer.* Cancer Lett, 2017. **410**: p. 139-157.

103. Jirousek, L. and J. Jirsak, *Antifungal Properties of Organic Polysulphides from Cabbage.* Naturwissenschaften, 1956. **43**(16): p. 375-376.

104. Han, C.Y., et al., *Ajoene, a stable garlic by-product, inhibits high fat diet-induced hepatic steatosis and oxidative injury through LKB1-dependent AMPK activation.* Antioxid Redox Signal, 2011. **14**(2): p. 187-202.

105. Ahmed, N., et al., *Ajoene, a garlic-derived natural compound, enhances chemotherapy-induced apoptosis in human myeloid leukaemia CD34-positive resistant cells.* Anticancer Research, 2001. **21**(5): p. 3519-3523.

106. Yoshida, H., et al., *Antimicrobial activity of a compound isolated from an oil-macerated garlic extract.* Biosci Biotechnol Biochem, 1998. **62**(5): p. 1014-7.

107. Thomaz, L., et al., *Experimental paracoccidioidomycosis: alternative therapy with ajoene, compound from Allium sativum, associated with sulfamethoxazole/trimethoprim.* Med Mycol, 2008. **46**(2): p. 113-8.

108. Lee, H.J., J.H. Jeong, and J.H. Ryu, *Anti-pancreatic cancer activity of Z-ajoene from garlic: An inhibitor of the Hedgehog/Gli/FoxM1 axis.* Journal of Functional Foods, 2019. **56**: p. 102-109.

109. Li, S.Y., et al., *Combination of rapamycin and garlic-derived S-allylmercaptocysteine induces colon cancer cell apoptosis and suppresses tumor growth in xenograft nude mice through autophagy/p62/Nrf2 pathway.* Oncology Reports, 2017. **38**(3): p. 1637-1644.

110. Xu, S.Q. and B.H.S. Cho, *Allyl mercaptan, a major metabolite of garlic compounds, reduces cellular cholesterol synthesis and its secretion in Hep-G2 cells.* Journal of Nutritional Biochemistry, 1999. **10**(11): p. 654-659.

111. Nian, H., et al., *Allyl mercaptan, a garlic-derived organosulfur compound, inhibits histone deacetylase and enhances Sp3 binding on the P21WAF1 promoter.* Carcinogenesis, 2008. **29**(9): p. 1816-24.

112. Franzke, A., et al., *Cabbage family affairs: the evolutionary history of Brassicaceae.* Trends Plant Sci, 2011. **16**(2): p. 108-16.

113. Bell, L. and C. Wagstaff, *Rocket science: A review of phytochemical & health-related research in Eruca & Diplotaxis species.* Food Chem X, 2019. **1**: p. 100002.

114. Bell, L., M.J. Oruna-Concha, and C. Wagstaff, *Identification and quantification of glucosinolate and flavonol compounds in rocket salad (Eruca sativa, Eruca vesicaria*

and Diplotaxis tenuifolia) by LC-MS: highlighting the potential for improving nutritional value of rocket crops. Food Chem, 2015. **172**: p. 852-61.

115. Lietzow, J., *Biologically Active Compounds in Mustard Seeds: A Toxicological Perspective.* Foods, 2021. **10**(9).

116. Torrijos, R., et al., *Phytochemical profiling of volatile and bioactive compounds in yellow mustard and oriental mustard seed flour and bran.* Lwt-Food Science and Technology, 2023. **173**.

117. Balke, D.T. and L.L. Diosady, *Rapid aqueous extraction of mucilage from whole white mustard seed.* Food Research International, 2000. **33**(5): p. 347-356.

118. Tian, Y. and F.M. Deng, *Phytochemistry and biological activity of mustard: a review.* Cyta-Journal of Food, 2020. **18**(1): p. 704-718.

119. Andrés, C.M.C., et al., *The Multifaceted Health Benefits of Broccoli-A Review of Glucosinolates, Phenolics and Antimicrobial Peptides.* Molecules, 2025. **30**(11).

120. Rahman, M., et al., *Brassicaceae Mustards: Traditional and Agronomic Uses in Australia and New Zealand.* Molecules, 2018. **23**(1).

121. Abdel-Massih, R.M., et al., *Glucosinolates, a natural chemical arsenal: More to tell than the myrosinase story.* Frontiers in Microbiology, 2023. **14**.

122. Ishida, M., et al., *Glucosinolate metabolism, functionality and breeding for the improvement of Brassicaceae vegetables.* Breeding Science, 2014. **64**(1): p. 48-59.

123. Fahey, J.W., A.T. Zalcmann, and P. Talalay, *The chemical diversity and distribution of glucosinolates and isothiocyanates among plants.* Phytochemistry, 2001. **56**(1): p. 5-51.

124. Blazevic, I., et al., *Glucosinolate structural diversity, identification, chemical synthesis and metabolism in plants.* Phytochemistry, 2020. **169**: p. 112100.

125. Nguyen, V.P.T., et al., *Glucosinolates: Natural Occurrence, Biosynthesis, Accessibility, Isolation, Structures, and Biological Activities.* Molecules, 2020. **25**(19).

126. Baldelli, S., et al., *Glucosinolates in Human Health: Metabolic Pathways, Bioavailability, and Potential in Chronic Disease Prevention.* Foods, 2025. **14**(6).

127. Dufour, V., M. Stahl, and C. Baysse, *The antibacterial properties of isothiocyanates.* Microbiology-Sgm, 2015. **161**: p. 229-243.

128. Rahman, M., et al., *Brassicaceae Mustards: Phytochemical Constituents, Pharmacological Effects, and Mechanisms of Action against Human Disease.* International Journal of Molecular Sciences, 2024. **25**(16).

129. Guarrera, P.M., *Traditional phytotherapy in Central Italy (Marche, Abruzzo, and Latium).* Fitoterapia, 2005. **76**(1): p. 1-25.

130. Kissen, R., J.T. Rossiter, and A.M. Bones, *The 'mustard oil bomb': not so easy to assemble?! Localization, expression and distribution of the components of the myrosinase enzyme system.* Phytochemistry Reviews, 2009. **8**(1): p. 69-86.

131. Stoewsand, G.S., *Bioactive organosulfur phytochemicals in Brassica oleracea vegetables--a review.* Food Chem Toxicol, 1995. **33**(6): p. 537-43.

132. Verkerk, R., et al., *Glucosinolates in Brassica vegetables: the influence of the food supply chain on intake, bioavailability and human health.* Mol Nutr Food Res, 2009. **53 Suppl 2**: p. S219.

133. Cataldi, T.R., et al., *Naturally occurring glucosinolates in plant extracts of rocket salad (Eruca sativa L.) identified by liquid chromatography coupled with negative ion electrospray ionization and quadrupole ion-trap mass spectrometry.* Rapid Commun Mass Spectrom, 2007. **21**(14): p. 2374-88.

134. Holst, B. and G. Williamson, *A critical review of the bioavailability of glucosinolates and related compounds.* Nat Prod Rep, 2004. **21**(3): p. 425-47.

135. Halkier, B.A. and J. Gershenzon, *Biology and biochemistry of glucosinolates.* Annu Rev Plant Biol, 2006. **57**: p. 303-33.

136. Khoobchandani, M., et al., *Antimicrobial properties and analytical profile of traditional Eruca sativa seed oil: Comparison with various aerial and root plant extracts.* Food Chemistry, 2010. **120**(1): p. 217-224.

137. Cavaiuolo, M. and A. Ferrante, *Nitrates and Glucosinolates as Strong Determinants of the Nutritional Quality in Rocket Leafy Salads.* Nutrients, 2014. **6**(4): p. 1519-1538.

138. Loizzo, M.R., et al., *LC-ESI/HRMS analysis of glucosinolates, oxylipins and phenols in Italian rocket salad (Diplotaxis erucoides subsp. erucoides (L.) DC.) and evaluation of its healthy potential.* Journal of the Science of Food and Agriculture, 2021. **101**(14): p. 5872-5879.

139. Prieto, M.A., C.J. Lopez, and J. Simal-Gandara, *Glucosinolates: Molecular structure, breakdown, genetic, bioavailability, properties and healthy and adverse effects.* Adv Food Nutr Res, 2019. **90**: p. 305-350.

140. Smolinska, U., et al., *Isothiocyanates Produced by Brassicaceae Species as Inhibitors of Fusarium oxysporum.* Plant Dis, 2003. **87**(4): p. 407-412.

141. Bhandari, S.R. and J.H. Kwak, *Chemical composition and antioxidant activity in different tissues of brassica vegetables.* Molecules, 2015. **20**(1): p. 1228-43.

142. Kamal, M.M., et al., *Sulforaphane as an anticancer molecule: mechanisms of action, synergistic effects, enhancement of drug safety, and delivery systems.* Arch Pharm Res, 2020. **43**(4): p. 371-384.

143. Park, M.H., et al., *Variation of glucoraphanin and glucobrassicin: anticancer components in Brassica during processing.* Food Science and Technology, 2013. **33**(4): p. 624-631.

144. Bennett, R.N., et al., *Identification of the major glucosinolate (4-mercaptobutyl glucosinolate) in leaves of Eruca sativa L. (salad rocket).* Phytochemistry, 2002. **61**(1): p. 25-30.

145. Moghaddam, N.S., et al., *Antimicrobial screening of some selected Turkish medicinal plants.* Pakistan Journal of Pharmaceutical Sciences, 2019. **32**(3): p. 947-951.

146. Testai, L., et al., *Cardiovascular benefits of Eruca sativa mill. Defatted seed meal extract: Potential role of hydrogen sulfide.* Phytother Res, 2022. **36**(6): p. 2616-2627.

147. Li, B.L., et al., *Synthesis and antitumor activity of erysolin and its metabolites.* J Asian Nat Prod Res, 2022: p. 1-10.

148. Nowicki, D., et al., *Induction of the Stringent Response Underlies the Antimicrobial Action of Aliphatic Isothiocyanates.* Front Microbiol, 2020. **11**: p. 591802.

149. Yamane, A., et al., *Isothiocyanates as alleopathic compounds fromRorippa indica Hiern. (Cruciferae) roots.* J Chem Ecol, 1992. **18**(11): p. 1941-54.

150. Radziejewska-Kubzdela, E., A. Olejnik, and R. Bieganska-Marecik, *Effect of pretreatment on bioactive compounds in wild rocket juice.* J Food Sci Technol, 2019. **56**(12): p. 5234-5242.

151. Barillari, J., et al., *Glucosinolates in the subantarctic crucifer Kerguelen cabbage (Pringlea antiscorbutica).* J Nat Prod, 2005. **68**(2): p. 234-6.

152. Nastruzzi, C., et al., *In vitro antiproliferative activity of isothiocyanates and nitriles generated by myrosinase-mediated hydrolysis of glucosinolates from seeds of cruciferous vegetables.* J Agric Food Chem, 2000. **48**(8): p. 3572-5.

153. Al-Gendy, A.A., et al., *Glucosinolates profile, volatile constituents, antimicrobial, and cytotoxic activities of Lobularia libyca.* Pharm Biol, 2016. **54**(12): p. 3257-3263.

154. Jahangir, M., et al., *Health-Affecting Compounds in Brassicaceae.* Comprehensive Reviews in Food Science and Food Safety, 2009. **8**(2): p. 31-43.

155. Fenwick, G.R., R.K. Heaney, and W.J. Mullin, *Glucosinolates and their breakdown products in food and food plants.* Crit Rev Food Sci Nutr, 1983. **18**(2): p. 123-201.

156. Musk, S.R., T.K. Smith, and I.T. Johnson, *On the cytotoxicity and genotoxicity of allyl and phenethyl isothiocyanates and their parent glucosinolates sinigrin and gluconasturtiin.* Mutat Res, 1995. **348**(1): p. 19-23.

157. D'Antuono, L.F., S. Elementi, and R. Neri, *Glucosinolates in Diplotaxis and Eruca leaves: diversity, taxonomic relations and applied aspects.* Phytochemistry, 2008. **69**(1): p. 187-99.

158. Vo, Q.V., et al., *Synthesis and anti-inflammatory activity of indole glucosinolates.* Bioorg Med Chem, 2014. **22**(2): p. 856-64.

159. Williams, D.E., *Indoles Derived From Glucobrassicin: Cancer Chemoprevention by Indole-3-Carbinol and 3,3'-Diindolylmethane.* Front Nutr, 2021. **8**: p. 734334.

160. Agerbirk, N., et al., *1,4-Dimethoxyglucobrassicin in Barbarea and 4-hydroxyglucobrassicin in Arabidopsis and Brassica.* J Agric Food Chem, 2001. **49**(3): p. 1502-7.

161. Haack, M., et al., *Breakdown products of neoglucobrassicin inhibit activation of Nrf2 target genes mediated by myrosinase-derived glucoraphanin hydrolysis products.* Biol Chem, 2010. **391**(11): p. 1281-93.

162. Burmeister, W.P., et al., *High resolution X-ray crystallography shows that ascorbate is a cofactor for myrosinase and substitutes for the function of the catalytic base.* J Biol Chem, 2000. **275**(50): p. 39385-93.

163. Winde, I. and U. Wittstock, *Insect herbivore counteradaptations to the plant glucosinolate-myrosinase system.* Phytochemistry, 2011. **72**(13): p. 1566-75.

164. Tarar, A., et al., *Anticancer Activity, Mechanism, and Delivery of Allyl Isothiocyanate.* Bioengineering-Basel, 2022. **9**(9).

165. Burmeister, W.P., et al., *The crystal structures of Sinapis alba myrosinase and a covalent glycosyl-enzyme intermediate provide insights into the substrate recognition and active-site machinery of an S-glycosidase.* Structure, 1997. **5**(5): p. 663-75.

166. Rask, L., et al., *Myrosinase: gene family evolution and herbivore defense in Brassicaceae.* Plant Mol Biol, 2000. **42**(1): p. 93-113.

167. Hopkins, R.J., N.M. van Dam, and J.J. van Loon, *Role of glucosinolates in insect-plant relationships and multitrophic interactions.* Annu Rev Entomol, 2009. **54**: p. 57-83.

168. Pardini, A., et al., *Kinetics of glucosinolate hydrolysis by myrosinase in Brassicaceae tissues: A high-performance liquid chromatography approach.* Food Chem, 2021. **355**: p. 129634.

169. Traka, M. and R. Mithen, *Glucosinolates, isothiocyanates and human health.* Phytochemistry Reviews, 2009. **8**(1): p. 269-282.

170. Agerbirk, N. and C.E. Olsen, *Glucosinolate structures in evolution.* Phytochemistry, 2012. **77**: p. 16-45.

171. Hanschen, F.S., et al., *Brassica vegetables as sources of epithionitriles: Novel secondary products formed during cooking.* Food Chem, 2018. **245**: p. 564-569.

172. Burow, M., et al., *Glucosinolate hydrolysis in Lepidium sativum--identification of the thiocyanate-forming protein.* Plant Mol Biol, 2007. **63**(1): p. 49-61.

173. Wittstock, U. and M. Burow, *Tipping the scales--specifier proteins in glucosinolate hydrolysis.* IUBMB Life, 2007. **59**(12): p. 744-51.

174. Belliveau, K.A. and L.B. Romero-Zeron, *Monitoring the enzymatic degradation of sinigrin from B. juncea meal using (1)H NMR spectroscopy.* Nat Prod Res, 2010. **24**(1): p. 24-33.

175. Eisenschmidt-Bonn, D., et al., *Structural diversification during glucosinolate breakdown: mechanisms of thiocyanate, epithionitrile and simple nitrile formation.* Plant J, 2019. **99**(2): p. 329-343.

176. Bones, A.M. and J.T. Rossiter, *The enzymic and chemically induced decomposition of glucosinolates.* Phytochemistry, 2006. **67**(11): p. 1053-67.

177. Agerbirk, N., C.E. Olsen, and H. Sorensen, *Initial and final products, nitriles, and ascorbigens produced in myrosinase-catalyzed hydrolysis of indole glucosinolates.* Journal of Agricultural and Food Chemistry, 1998. **46**(4): p. 1563-1571.

178. Grygier, A., *Mustard Seeds as a Bioactive Component of Food.* Food Reviews International, 2023. **39**(7): p. 4088-4101.

179. Angelino, D., et al., *Myrosinase-dependent and -independent formation and control of isothiocyanate products of glucosinolate hydrolysis.* Frontiers in Plant Science, 2015. **6**.

180. Kaiser, S.J., et al., *Natural isothiocyanates express antimicrobial activity against developing and mature biofilms of.* Fitoterapia, 2017. **119**: p. 57-63.

181. Bendary, M.M., et al., *Investigating Sulforaphane's anti-virulence and anti-quorum sensing properties against.* Frontiers in Pharmacology, 2024. **15**.

182. Romeo, L., et al., *Isothiocyanates: An Overview of Their Antimicrobial Activity against Human Infections.* Molecules, 2018. **23**(3).

183. Borges, A., et al., *Antibacterial activity and mode of action of selected glucosinolate hydrolysis products against bacterial pathogens.* J Food Sci Technol, 2015. **52**(8): p. 4737-48.

184. Dufour, V., M. Stahl, and C. Baysse, *The antibacterial properties of isothiocyanates.* Microbiology (Reading), 2015. **161**(Pt 2): p. 229-243.

185. Conrad, A., et al., *Broad spectrum antibacterial activity of a mixture of isothiocyanates from nasturtium (Tropaeoli majoris herba) and horseradish (Armoraciae rusticanae radix).* Drug Res (Stuttg), 2013. **63**(2): p. 65-8.

186. Kensler, T.W., et al., *Keap1-Nrf2 Signaling: A Target for Cancer Prevention by Sulforaphane.* Natural Products in Cancer Prevention and Therapy, 2013. **329**: p. 163-177.

187. Matusheski, N.V., J.A. Juvik, and E.H. Jeffery, *Heating decreases epithiospecifier protein activity and increases sulforaphane formation in broccoli.* Phytochemistry, 2004. **65**(9): p. 1273-1281.

188. Bhattacharya, A., et al., *Allyl isothiocyanate-rich mustard seed powder inhibits bladder cancer growth and muscle invasion.* Carcinogenesis, 2010. **31**(12): p. 2105-2110.

189. Kubo, E., et al., *Sulforaphane reactivates cellular antioxidant defense by inducing Nrf2/ARE/Prdx6 activity during aging and oxidative stress.* Scientific Reports, 2017. **7**.

190. Esteve, M., *Mechanisms Underlying Biological Effects of Cruciferous Glucosinolate-Derived Isothiocyanates/Indoles: A Focus on Metabolic Syndrome.* Frontiers in Nutrition, 2020. **7**.

191. Múnera-Rodríguez, A.M., et al., *Sulforaphane-mediated immune regulation through inhibition of NF-kB and MAPK signaling pathways in human dendritic cells.* Biomedicine & Pharmacotherapy, 2024. **177**.

192. Zhou, S.S., et al., *Evaluate the stability of synthesized allicin and its reactivity with endogenous compounds in garlic.* Npj Science of Food, 2025. **9**(1).

193. Marcinkowska, M.A. and H.H. Jelen, *Role of Sulfur Compounds in Vegetable and Mushroom Aroma.* Molecules, 2022. **27**(18).

194. Kubec, R., et al., *Sulfur-containing volatiles arising by thermal degradation of alliin and deoxyalliin.* Journal of Agricultural and Food Chemistry, 1997. **45**(9): p. 3580-3585.

195. Chen, Z., et al., *Thermolysis kinetics and thermal degradation compounds of alliin.* Food Chem, 2017. **223**: p. 25-30.

196. Weerawatanakorn, M., et al., *Reactivity and stability of selected flavor compounds.* Journal of Food and Drug Analysis, 2015. **23**(2): p. 176-190.

197. Chen, C.W. and C.T. Ho, *Thermal Degradation of Allyl Isothiocyanate in Aqueous Solution.* J Agric Food Chem, 1998. **46**(1): p. 220-223.

198. Borlinghaus, J., et al., *Allicin, the Odor of Freshly Crushed Garlic: A Review of Recent Progress in Understanding Allicin's Effects on Cells.* Molecules, 2021. **26**(6).

199. Gruhlke, M.C.H. and A.J. Slusarenko, *The biology of reactive sulfur species (RSS).* Plant Physiology and Biochemistry, 2012. **59**: p. 98-107.

200. Mocniak, L.E., K. Elkin, and J.M. Bollinger, *Lifetimes of the Aglycone Substrates of Specifier Proteins, the Autonomous Iron Enzymes That Dictate the Products of the Glucosinolate-Myrosinase Defense System in Brassica Plants.* Biochemistry, 2020. **59**(26): p. 2432-2441.

201. Albrecht, F., et al., *An Optimized Facile Procedure to Synthesize and Purify Allicin.* Molecules, 2017. **22**(5).

202. Mazumder, A., A. Dwivedi, and J. du Plessis, *Sinigrin and Its Therapeutic Benefits.* Molecules, 2016. **21**(4).

203. Botti, M.G., M.G. Taylor, and N.P. Botting, *Studies on the mechanism of myrosinase. Investigation of the effect of glycosyl acceptors on enzyme activity.* J Biol Chem, 1995. **270**(35): p. 20530-5.

204. Palmieri, S., O. Leoni, and R. Iori, *A Steady-State Kinetics Study of Myrosinase with Direct Ultraviolet Spectrophotometric Assay.* Analytical Biochemistry, 1982. **123**(2): p. 320-324.

205. Bjorkman, R. and B. Lonnerdal, *Studies on myrosinases. 3. Enzymatic properties of myrosinases from Sinapis alba and Brassica napus seeds.* Biochim Biophys Acta, 1973. **327**(1): p. 121-31.

206. Glaser, R., et al., *Near-silence of isothiocyanate carbon in (13)C NMR spectra: a case study of allyl isothiocyanate.* J Org Chem, 2015. **80**(9): p. 4360-9.

207. Mellon, F.A., et al., *Intact glucosinolate analysis in plant extracts by programmed cone voltage electrospray LC/MS: Performance and comparison with LC/MS/MS methods.* Analytical Biochemistry, 2002. **306**(1): p. 83-91.

208. Block, E., et al., *(E,Z)-Ajoene - a Potent Antithrombotic Agent from Garlic.* Journal of the American Chemical Society, 1984. **106**(26): p. 8295-8296.

209. Debouzy, J.C., et al., *Interaction of antiaggregant molecule ajoene with membranes. An ESR and 1H, 2H, 31P-NMR study.* Eur Biophys J, 1989. **17**(4): p. 211-6.

210. Chang, H.S., et al., *Sodium 2-propenyl thiosulfate derived from garlic induces phase II detoxification enzymes in rat hepatoma H4IIE cells.* Nutr Res, 2010. **30**(6): p. 435-40.

211. Fahey, J.W., Y. Zhang, and P. Talalay, *Broccoli sprouts: an exceptionally rich source of inducers of enzymes that protect against chemical carcinogens.* Proc Natl Acad Sci U S A, 1997. **94**(19): p. 10367-72.

212. Lawson, L.D. and B.G. Hughes, *Characterization of the formation of allicin and other thiosulfinates from garlic.* Planta Med, 1992. **58**(4): p. 345-50.

213. Nguyen, B.T., et al., *A rapid and simplified methodology for the extraction and quantification of allicin in garlic.* Journal of Food Composition and Analysis, 2021. **104**.

214. Popova, I.E. and M.J. Morra, *Sinigrin and sinalbin quantification in mustard seed using high performance liquid chromatography-time-of-flight mass spectrometry.* Journal of Food Composition and Analysis, 2014. **35**(2): p. 120-126.

215. Kwon, H.Y., et al., *Comparative Analysis of the Nutritional Components and Antioxidant Activities of Different Brassica juncea Cultivars.* Foods, 2020. **9**(6).

216. Dai, R. and L.T. Lim, *Release of allyl isothiocyanate from mustard seed meal powder.* J Food Sci, 2014. **79**(1): p. E47-53.

217. Song, F.F., et al., *The stability of isothiocyanates in broccoli extract: Oxidation from erucin to sulforaphane was discovered.* Food Chemistry, 2025. **480**.

218. Verkerk, R., S. Tebbenhoff, and M. Dekker, *Variation and Distribution of Glucosinolates in 42 Cultivars of Vegetable Crops.* International Symposium on Vegetable Safety and Human Health, 2010. **856**: p. 63-69.

219. Triska, J., et al., *Factors Influencing Sulforaphane Content in Broccoli Sprouts and Subsequent Sulforaphane Extraction.* Foods, 2021. **10**(8).

220. Bhatwalkar, S.B., et al., *Antibacterial Properties of Organosulfur Compounds of Garlic (Allium sativum).* Frontiers in Microbiology, 2021. **12**.

221. Cutler, R.R. and P. Wilson, *Antibacterial activity of a new, stable, aqueous extract of allicin against methicillin-resistant Staphylococcus aureus.* Br J Biomed Sci, 2004. **61**(2): p. 71-4.

222. Luciano, F.B. and R.A. Holley, *Enzymatic inhibition by allyl isothiocyanate and factors affecting its antimicrobial action against Escherichia coli O157:H7.* Int J Food Microbiol, 2009. **131**(2-3): p. 240-5.

223. Forman, H.J., H. Zhang, and A. Rinna, *Glutathione: overview of its protective roles, measurement, and biosynthesis.* Mol Aspects Med, 2009. **30**(1-2): p. 1-12.

224. Horn, T., et al., *S-allylmercaptoglutathione Is a Substrate for Glutathione Reductase (E.C. 1.8.1.7) from Yeast (Saccharomyces cerevisiae).* Antioxidants (Basel), 2018. **7**(7).

225. Thornton, J.M., *Disulphide bridges in globular proteins.* J Mol Biol, 1981. **151**(2): p. 261-87.

226. Wedemeyer, W.J., et al., *Disulfide bonds and protein folding.* Biochemistry, 2000. **39**(23): p. 7032.

227. Armstrong, D.A., Q. Kaas, and K.J. Rosengren, *Prediction of disulfide dihedral angles using chemical shifts.* Chem Sci, 2018. **9**(31): p. 6548-6556.

228. Benson, S.W., *Thermochemistry and Kinetics of Sulfur-Containing Molecules and Radicals.* Chemical Reviews, 1978. **78**(1): p. 23-35.

229. Yokozeki, A. and S.H. Bauer, *Structures of Dimethyl Disulfide and Methyl Ethyl Disulfide, Determined by Gas-Phase Electron-Diffraction - Vibrational Analysis for Mean-Square Amplitudes.* Journal of Physical Chemistry, 1976. **80**(6): p. 618-625.

230. Creighton, T.E., *Disulphide bonds and protein stability.* Bioessays, 1988. **8**(2): p. 57-63.

231. Sevier, C.S. and C.A. Kaiser, *Formation and transfer of disulphide bonds in living cells.* Nat Rev Mol Cell Biol, 2002. **3**(11): p. 836-47.

232. Yang, D., et al., *Disulfide bond creates a small connecting loop in aminoxy peptide backbone.* Chemistry, 2008. **14**(33): p. 10297-302.

233. Muller, A., et al., *Allicin Induces Thiol Stress in Bacteria through S-Allylmercapto Modification of Protein Cysteines.* J Biol Chem, 2016. **291**(22): p. 11477-90.

234. Wang, T.X., H. Liang, and Q.P. Yuan, *Separation and Purification of Sinigrin and Gluconapin from Defatted Indian Mustard Seed Meals by Macroporous Anion Exchange Resin and Medium Pressure Liquid Chromatography.* Separation Science and Technology, 2014. **49**(12): p. 1838-1847.

235. Recio, R., et al., *NMR study on the stabilization and chiral discrimination of sulforaphane enantiomers and analogues by cyclodextrins.* Carbohydrate Polymers, 2018. **187**: p. 118-125.

236. Liang, H., et al., *Separation and purification of sulforaphane from broccoli seeds by solid phase extraction and preparative high-performance liquid chromatography.* Journal of Agricultural and Food Chemistry, 2007. **55**(20): p. 8047-8053.

237. Kreiswirth, B.N., et al., *The toxic shock syndrome exotoxin structural gene is not detectably transmitted by a prophage.* Nature, 1983. **305**(5936): p. 709-12.

238. Treangen, T.J., et al., *Complete Genome Sequence of the Quality Control Strain Staphylococcus aureus subsp. aureus ATCC 25923.* Genome Announc, 2014. **2**(6).

239. Bauer, A.W., et al., *Antibiotic Susceptibility Testing by a Standardized Single Disk Method.* American Journal of Clinical Pathology, 1966. **45**(4): p. 493-+.

240. Balouiri, M., M. Sadiki, and S.K. Ibnsouda, *Methods for evaluating antimicrobial activity: A review.* Journal of Pharmaceutical Analysis, 2016. **6**(2): p. 71-79.

9 Appendix

Chapter 2

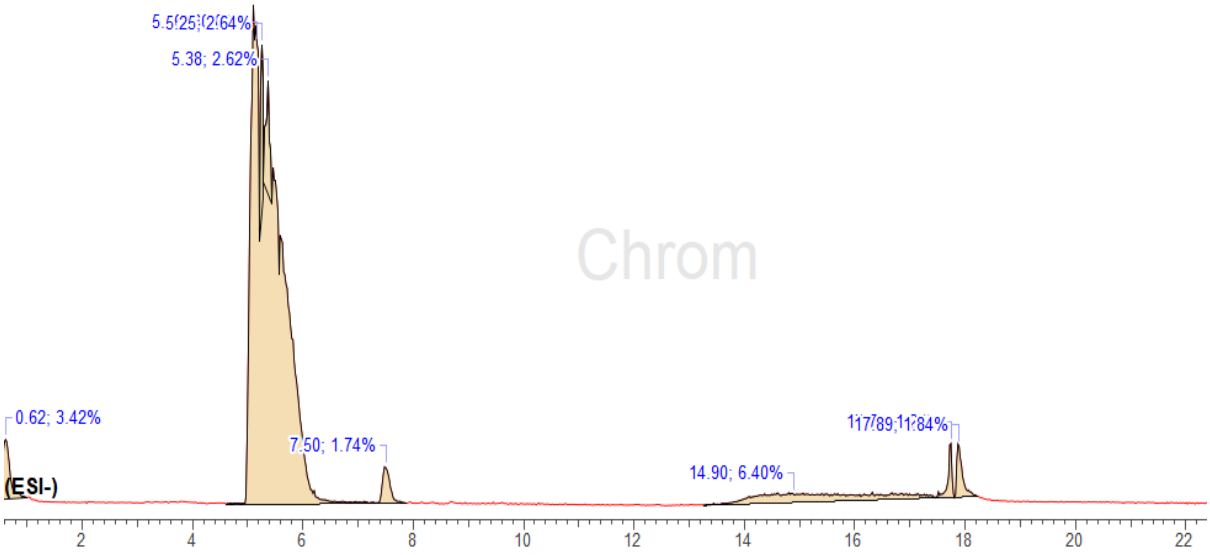

*Figure 9.1: HPLC chromatography of alligrin thermal treatment at 50-100 °C showing alligrin and compound **3**.*

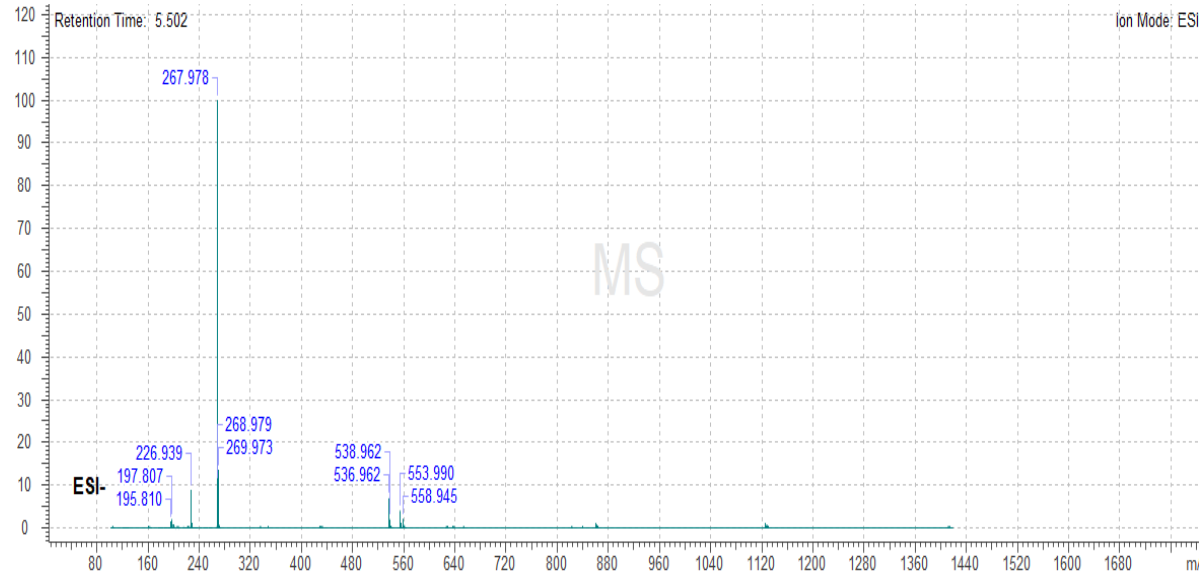

Figure 9.2: LC-MS of alligrin from thermal treatment of alligrin at 50-100 °C showing alligrin.

Appendices

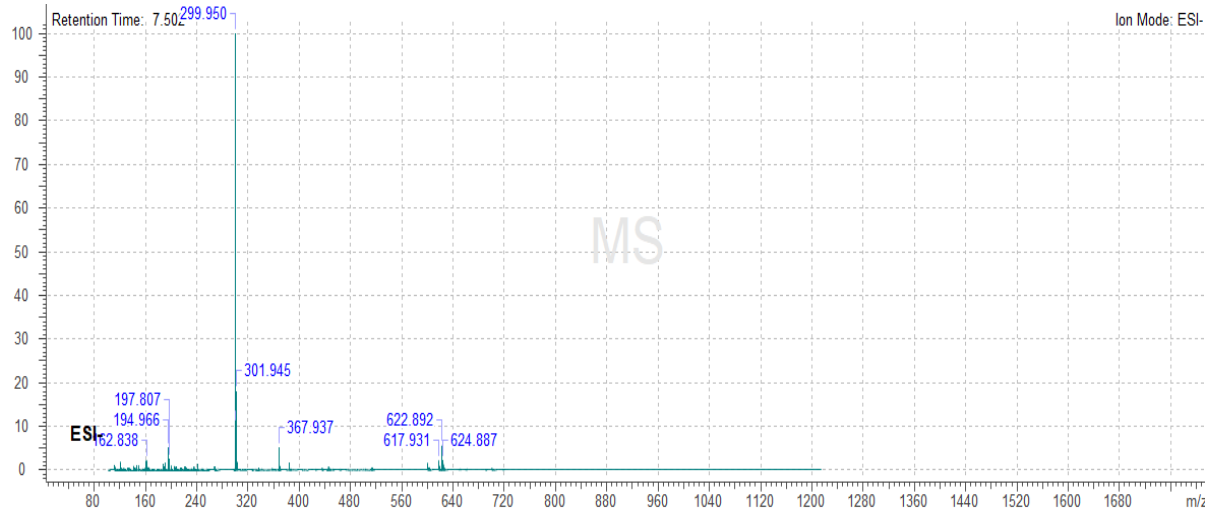

*Figure 9.3: LC-MS of compound **3** from alligrin thermal treatment at 50-100 °C showing compound **3**.*

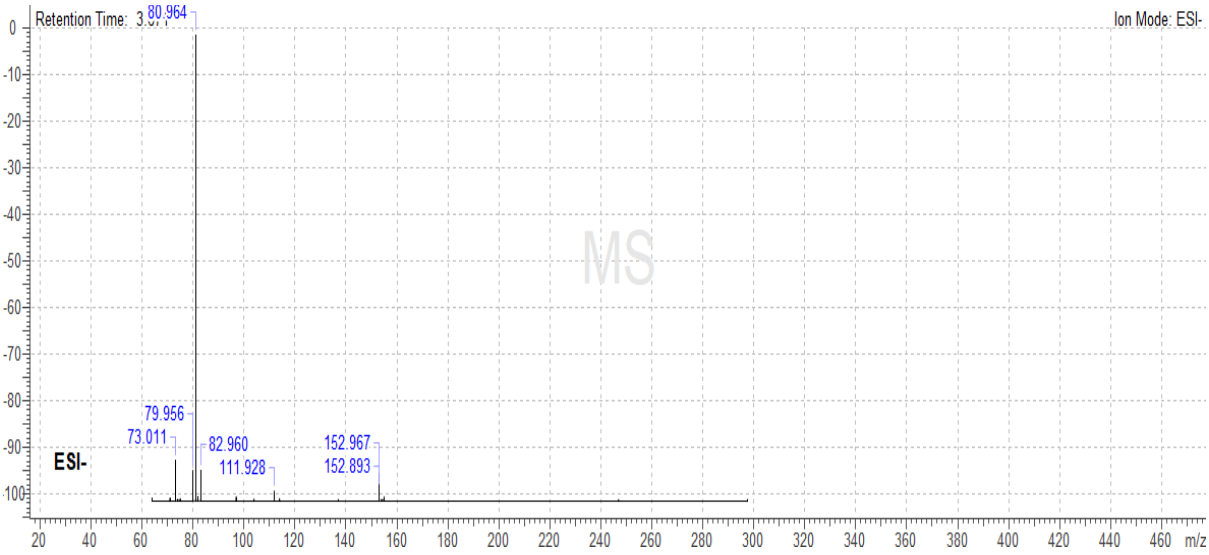

Figure 9.4: LC-MS of alligrin thermal treatment at 170-200 °C showing allyl thiosulfate ($C_3H_5O_3S_2$, m/z 152.96).

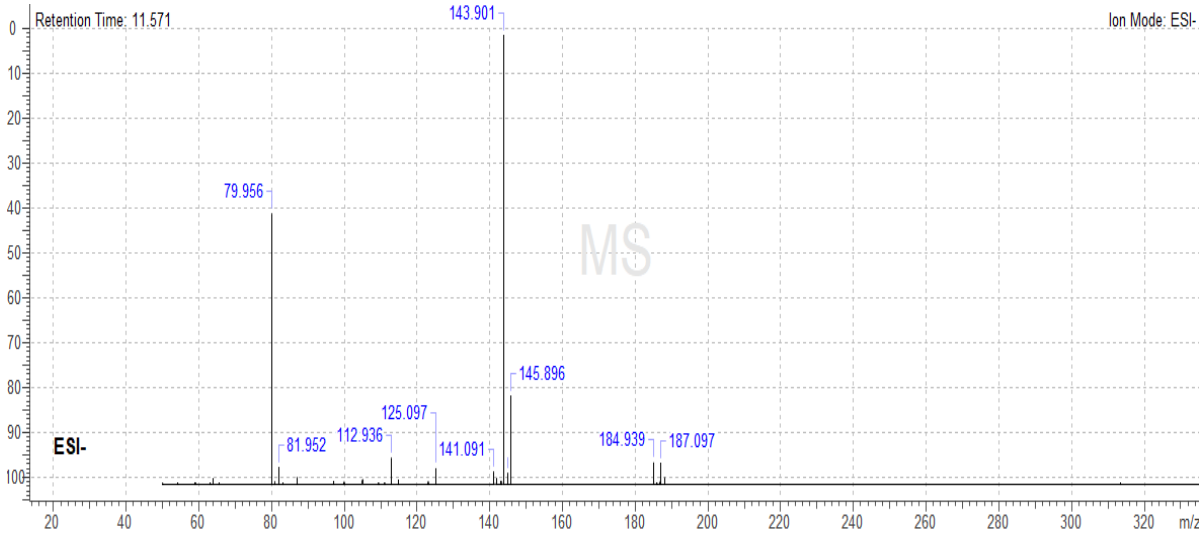

Figure 9.5: LC-MS of alligrin thermal treatment at 170-200 °C showing allyl dithiosulfate ($C_3H_5O_3S_3$, m/z 184.93).

Appendices

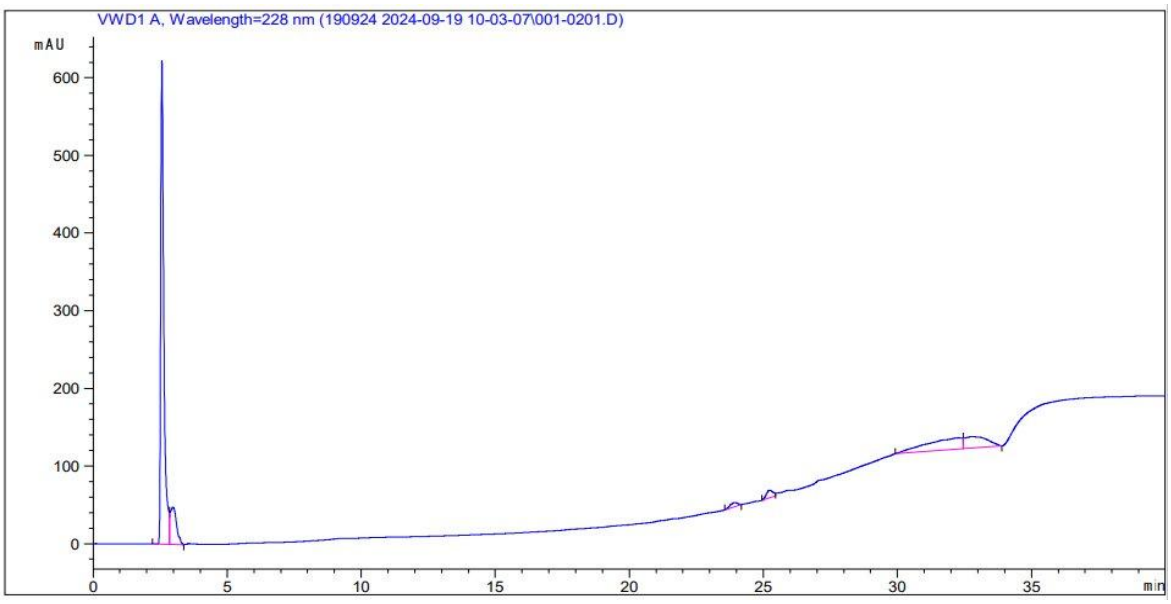

Figure 9.6: Analytical HPLC chromatography of glucoraphanin standard at retention time 2.6 min.

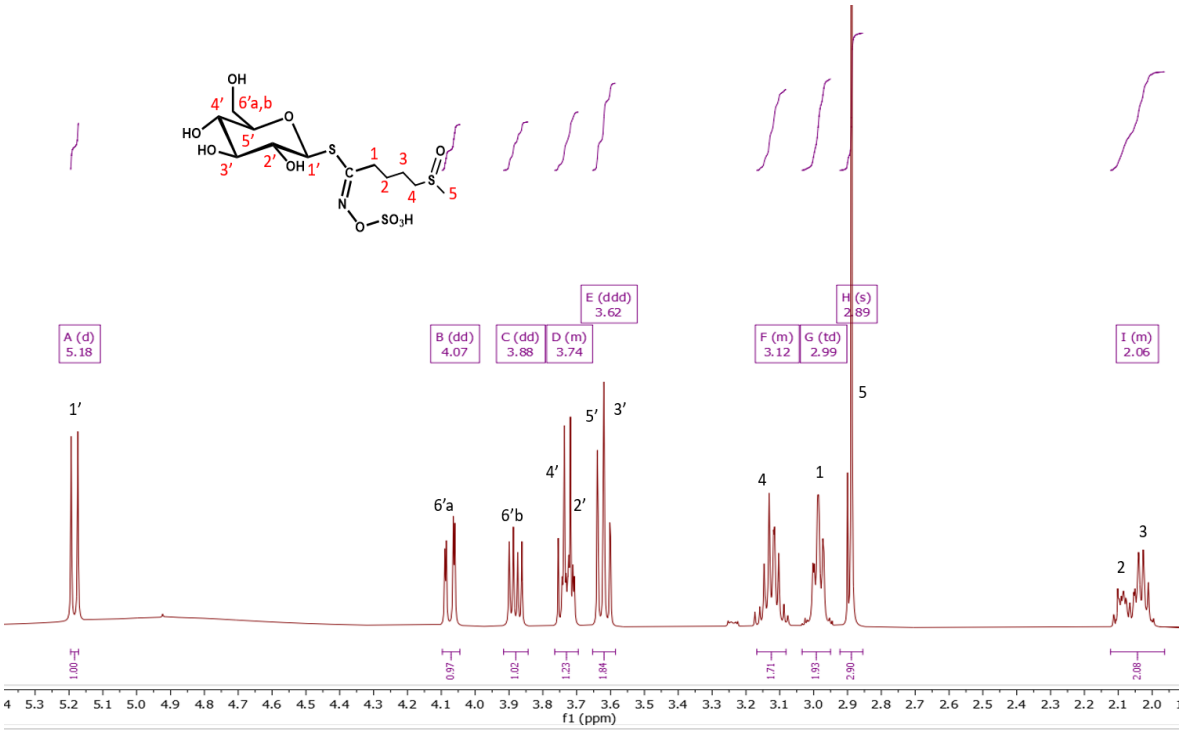

Figure 9.7: ^{1}H NMR (500 MHz, D_2O) of glucoraphanin standard.

Appendices

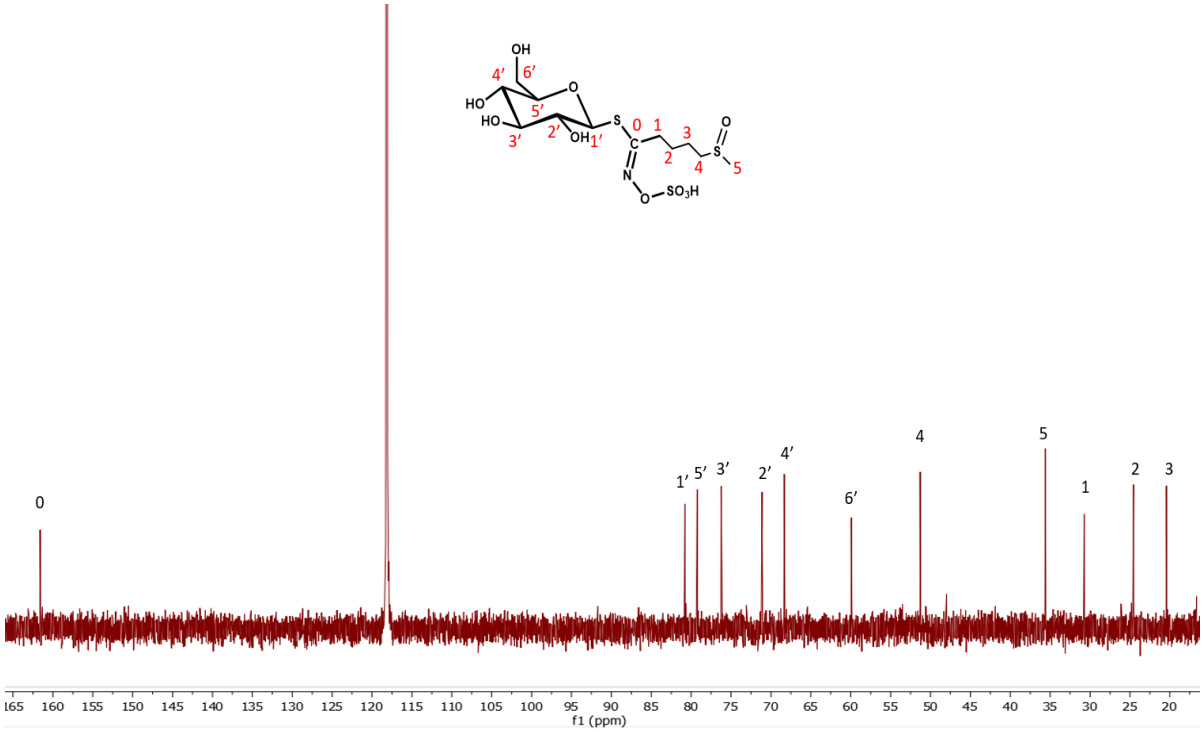

Figure 9.8: ^{13}C-NMR (500 MHz, D_2O) of glucoraphanin standard.

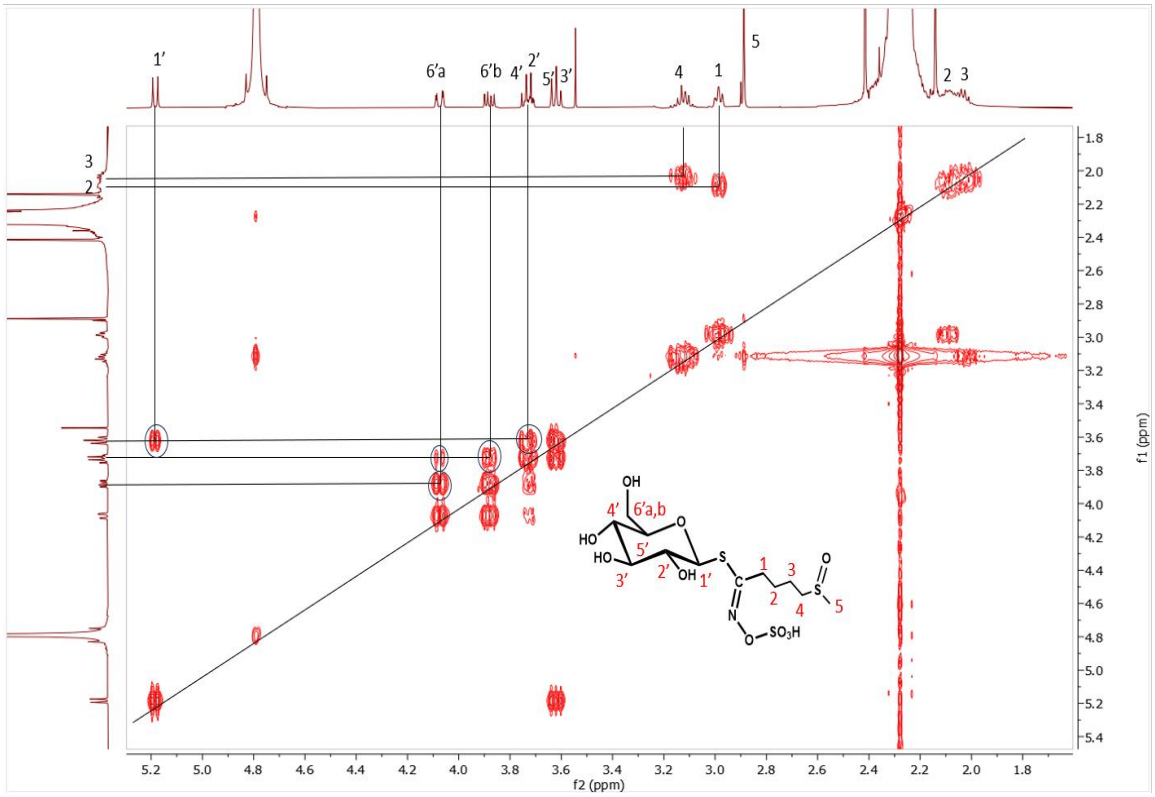

Figure 9.9: COSY-NMR (500 MHz, D_2O) of glucoraphanin standard.

Appendices

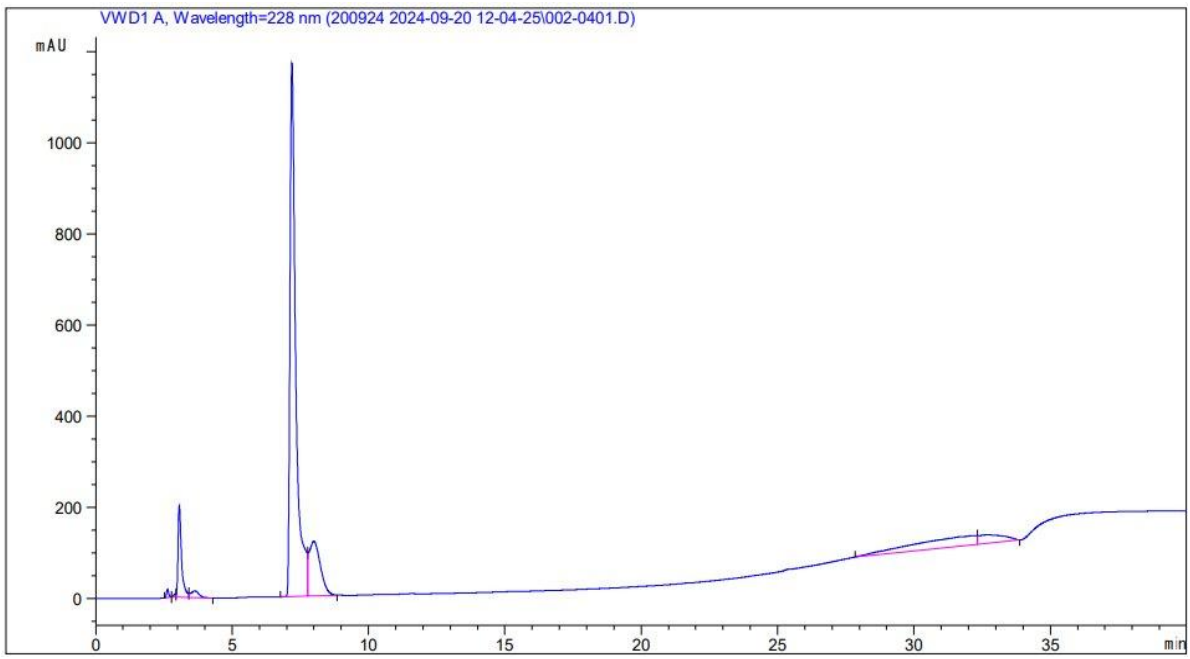

Figure 9.10: Analytical HPLC chromatography of sulphoraphane standard at retention time 7.2 min.

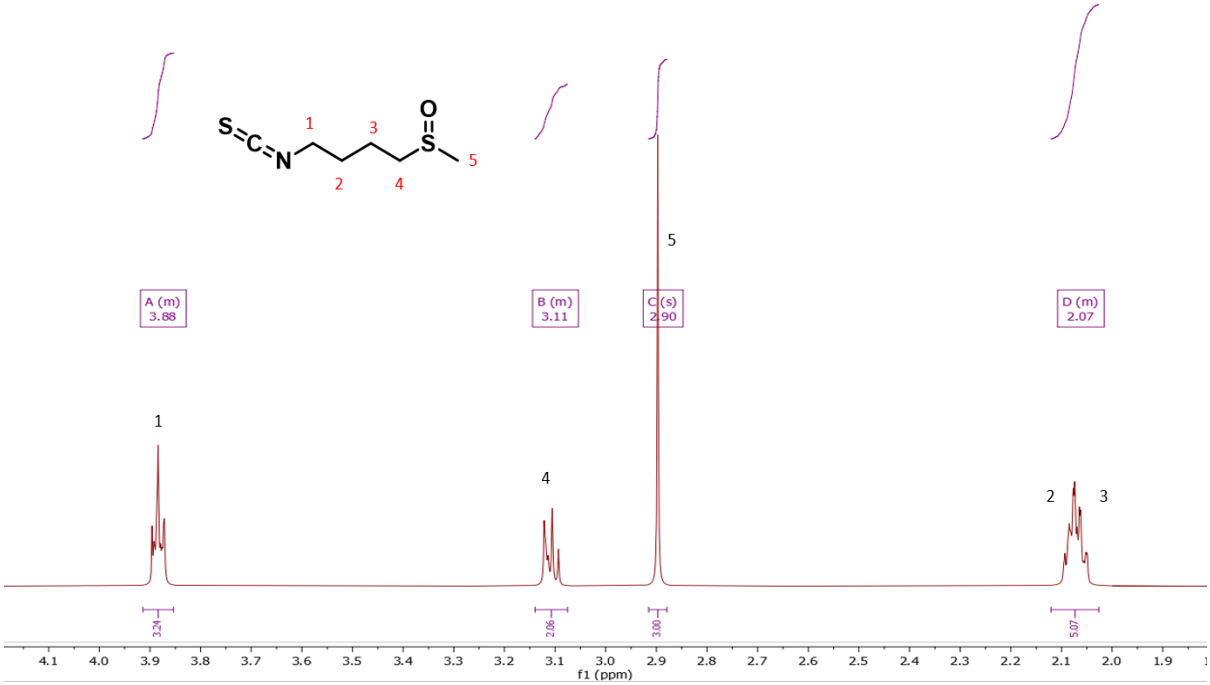

Figure 9.11: ^{1}H NMR (500 MHz, acetonitrile-d) of sulforaphane standard.

Appendices

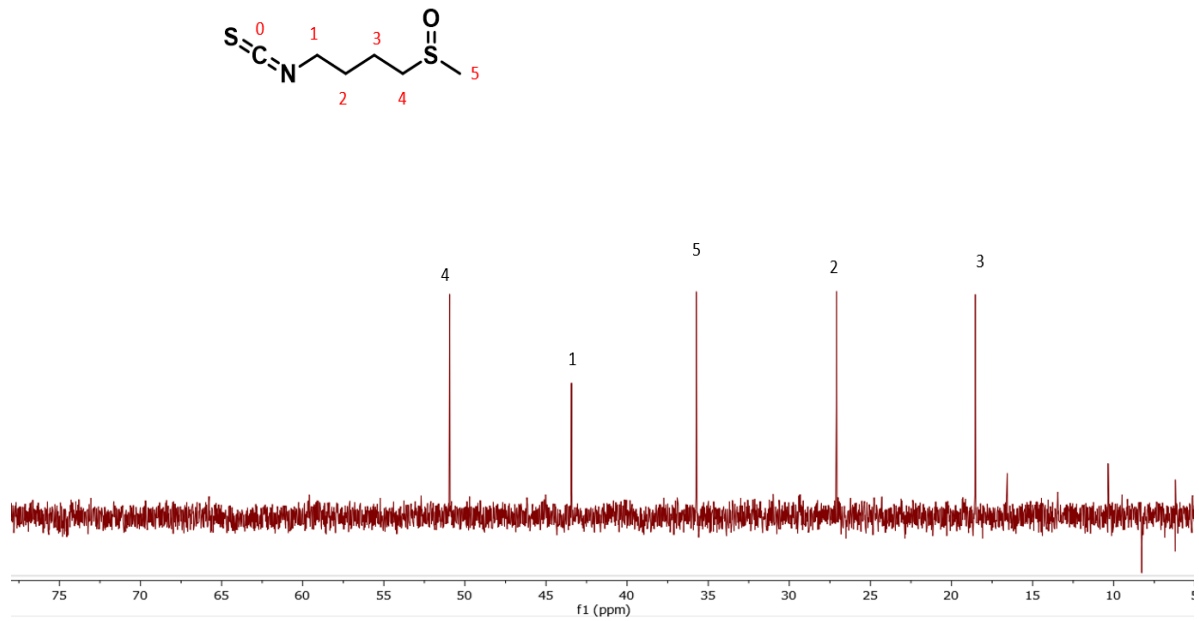

Figure 9.12: ^{13}C-NMR (500 MHz, D_2O) of sulforaphane standard.

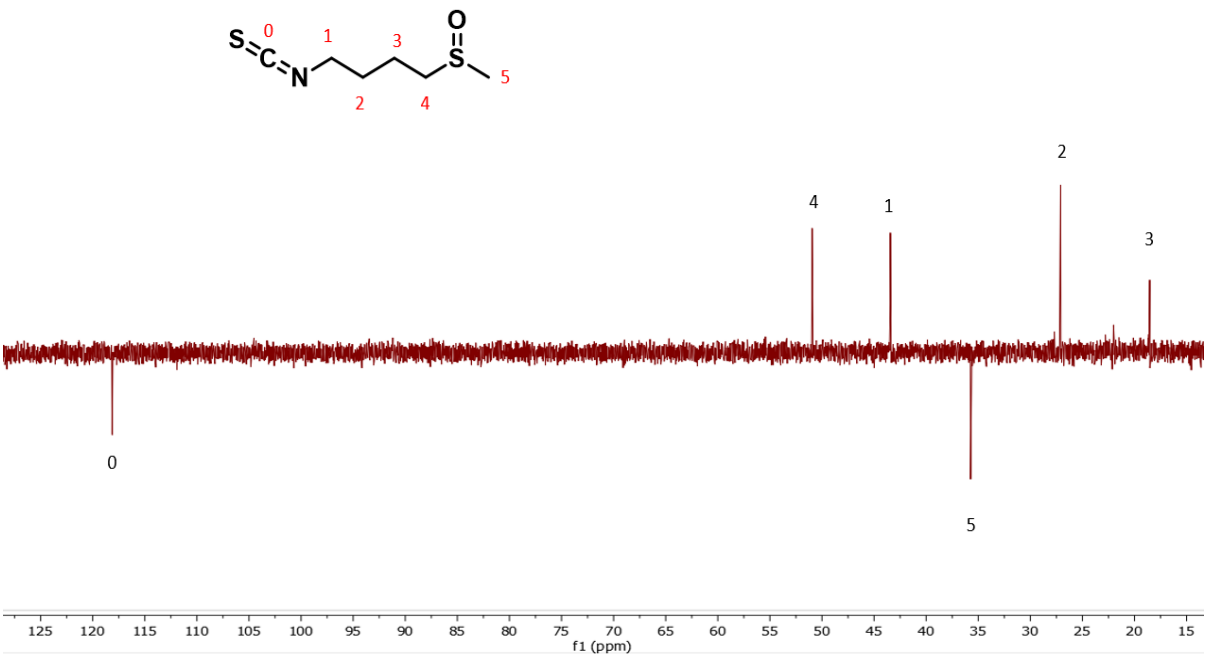

Figure 9.13: ^{13}C- DEPT 135 NMR (500 MHz, D_2O) of sulforaphane standard.

Appendices

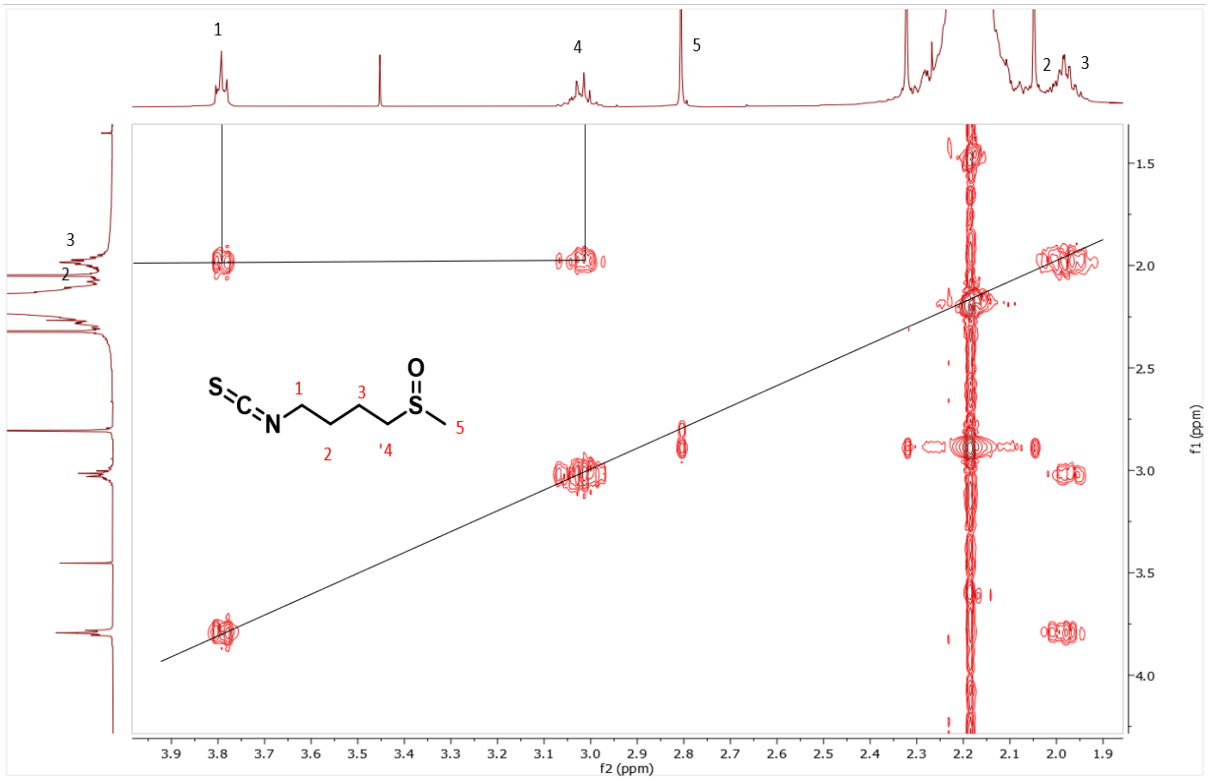

Figure 9.14: COSY-NMR (500 MHz, D_2O) of sulforaphane standard.

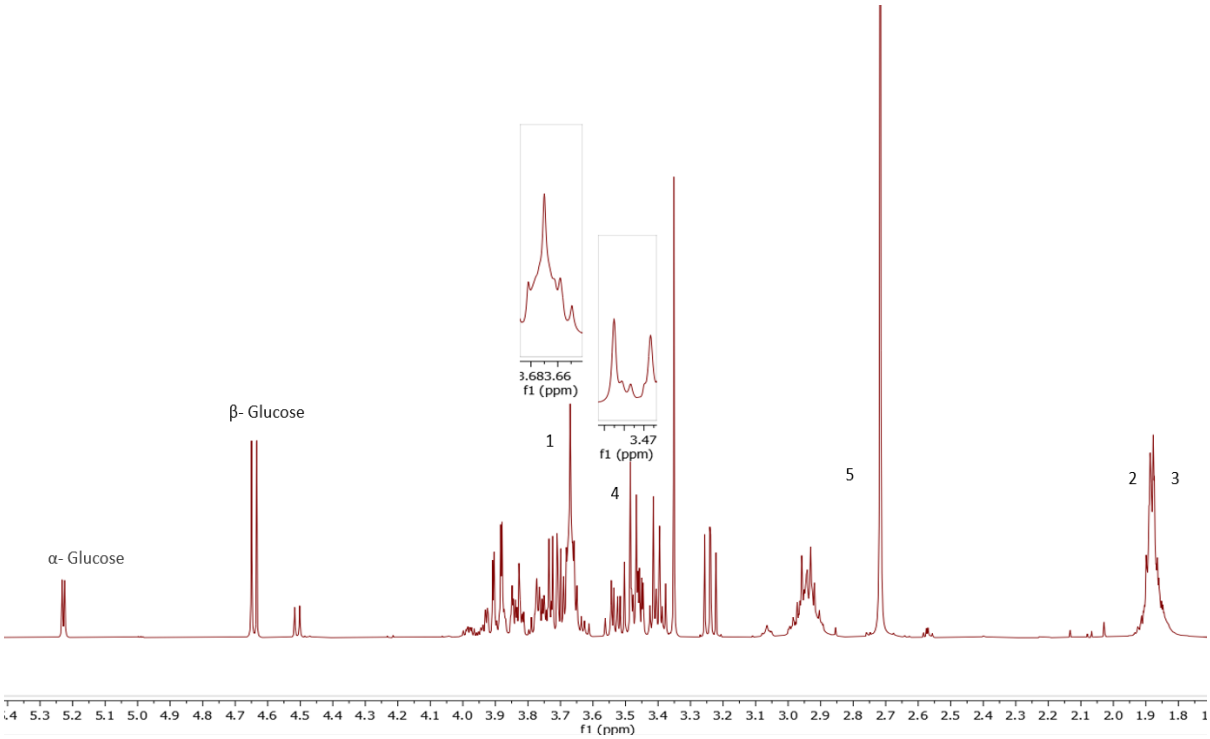

Figure 9.15: ^{1}H-NMR spectra (500 MHz, D_2O) of sulforaphane obtained by hydrolysis of glucoraphanin via myrosinase.

Appendices

Chapter 3

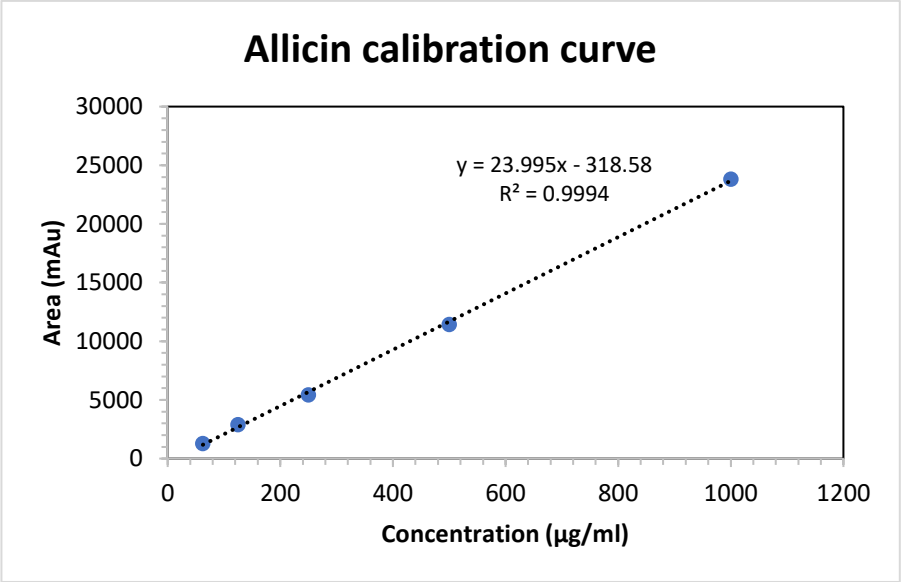

Figure 9.16: Calibration curve of synthetic allicin obtained by HPLC, showing a linear relationship between concentration (µg/mL) and peak area (mAU).

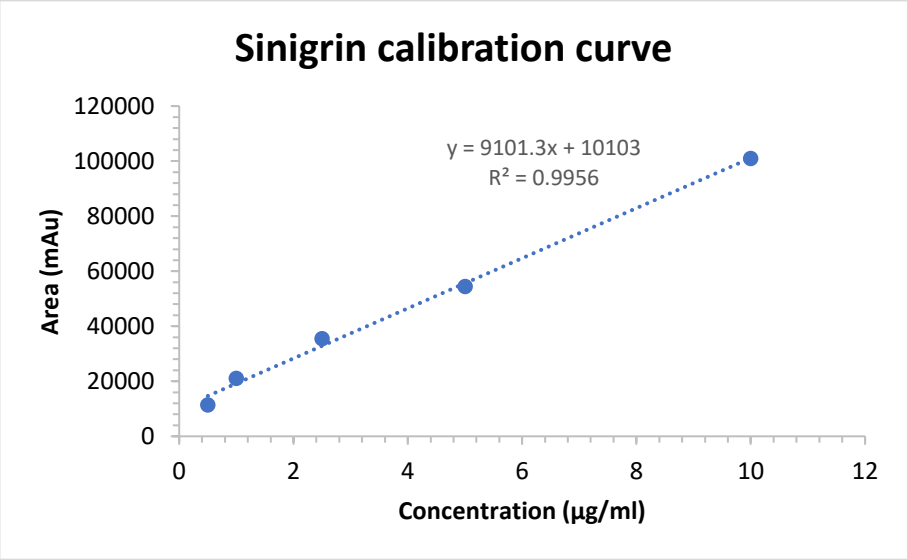

Figure 9.17: Calibration curve of sinigrin external standard showing the linear relationship between concentration (µg/mL) and HPLC peak area.

Appendices

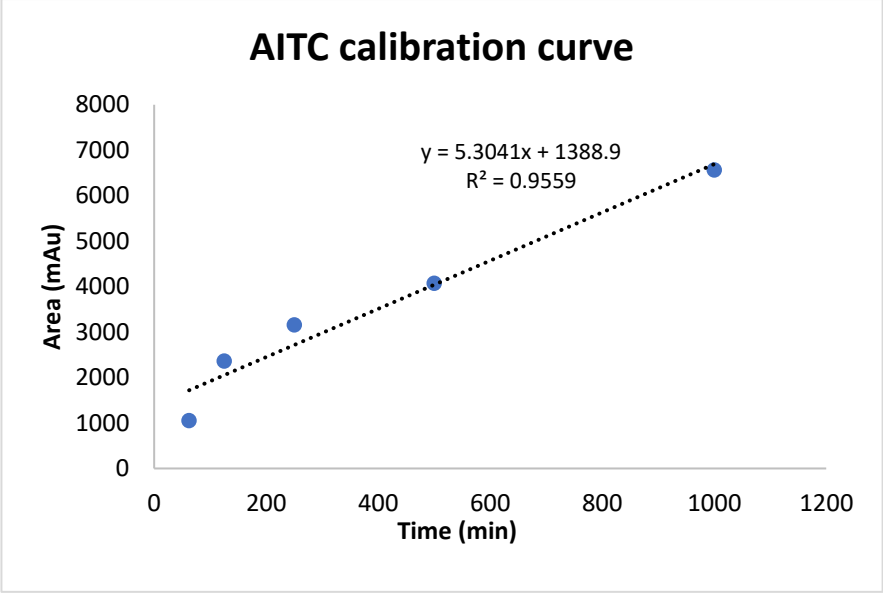

Figure 9.18: Calibration curve of allyl isothiocyanate (AITC) external standard showing the linear relationship between concentration (µg/mL) and HPLC peak area.

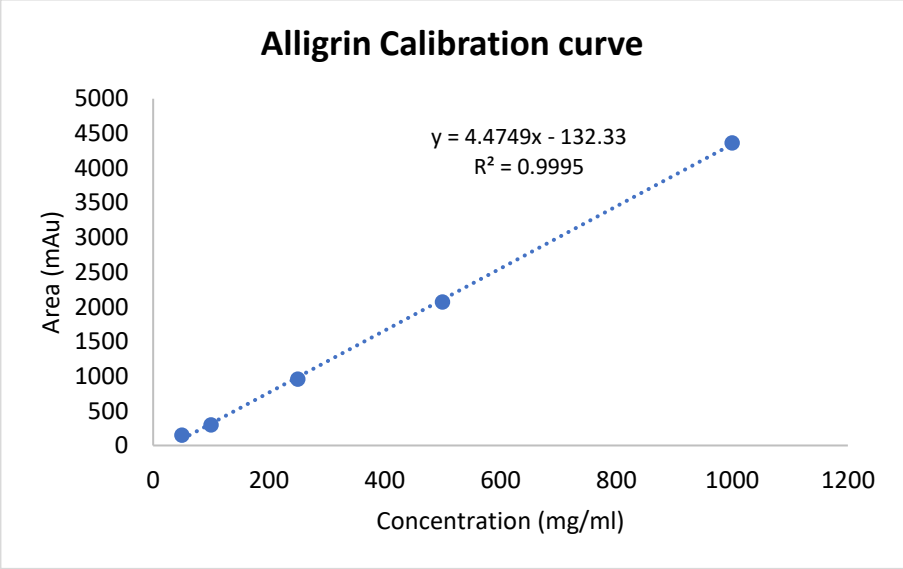

Figure 9.19: Calibration curve of purified alligrin showing a strong linear relationship between concentration and HPLC peak area.

Appendices

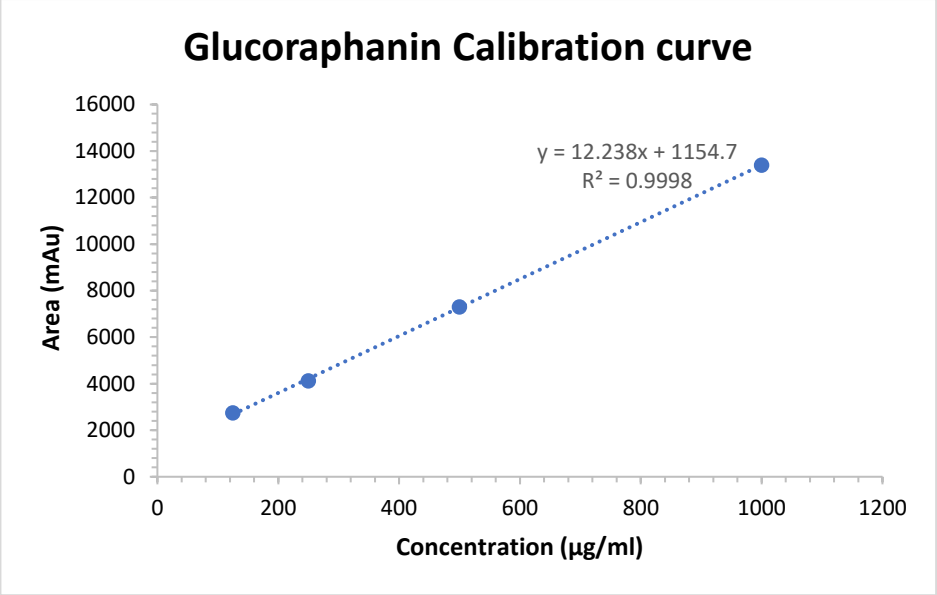

Figure 9.20: Calibration curve of Glucoraphanin external standard showing the linear relationship between concentration (µg/mL) and HPLC peak area.

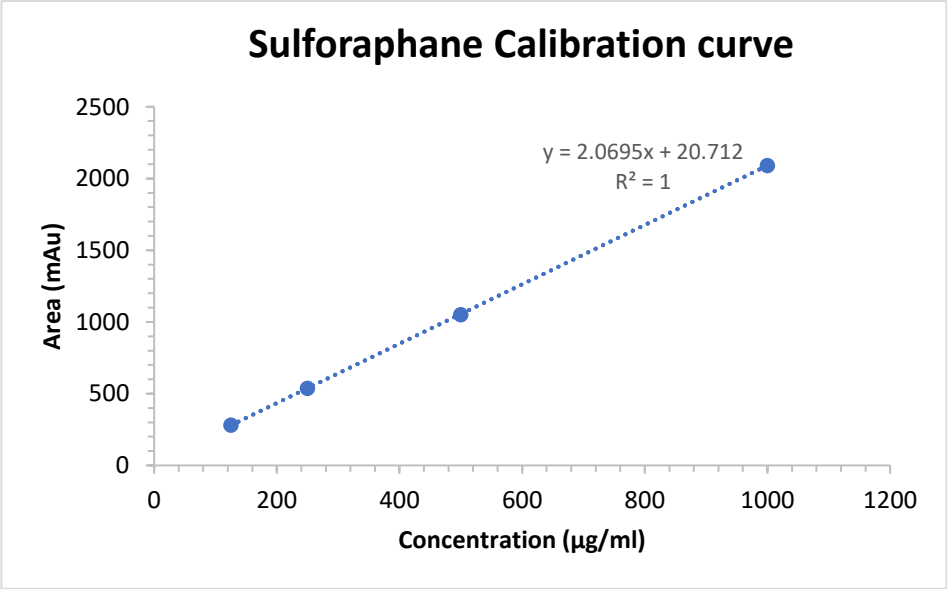

Figure 9.21: Calibration curve of Sulforaphane external standard showing the linear relationship between concentration (µg/mL) and HPLC peak area.

Appendices

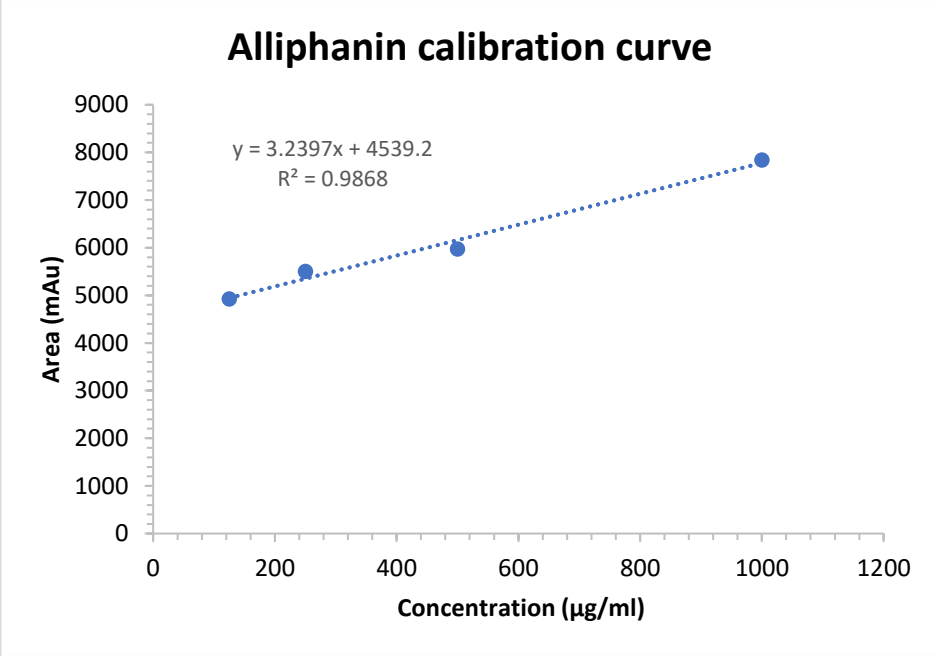

Figure 9.22: Calibration curve of Alliphanin showing the linear relationship between concentration (µg/mL) and HPLC peak area.

Chapter 4

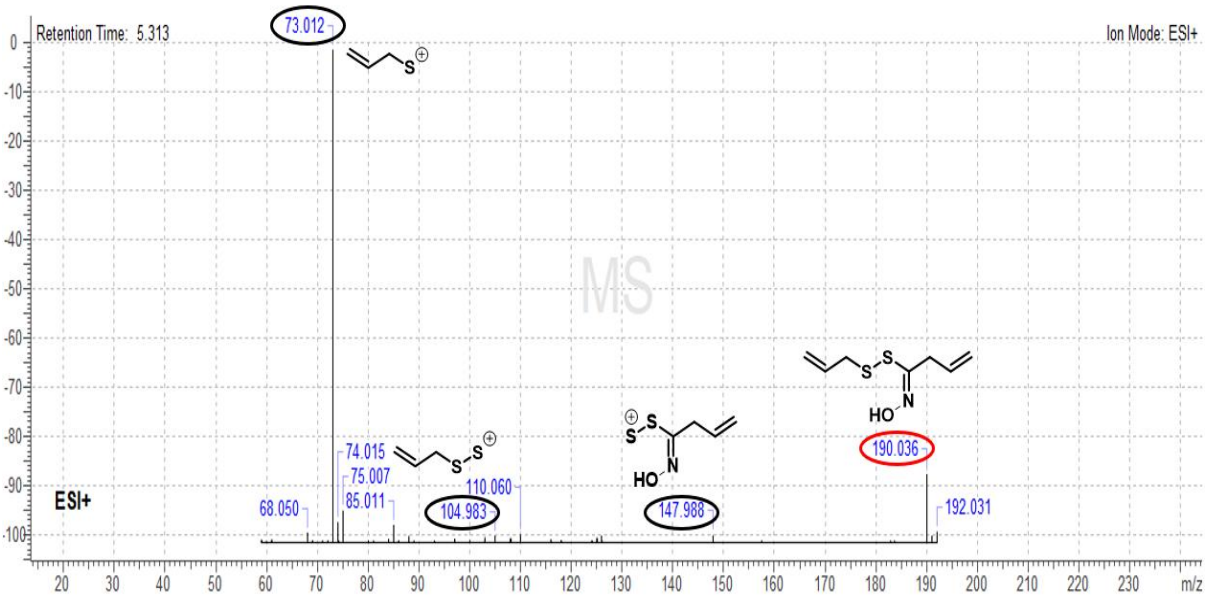

Figure 9.23: LC-MS data of desulfo-alligrin.

Appendices

Chapter 5

Table 9.1: Crystal Data and Structure Refinement for Alligrin

Parameter	Value
Crystal Information	
Empirical formula	$C_7H_{10}NO_4S_3 \cdot 0.222(NH_4)$
Formula weight	286.38
Crystal colour/habit	Clear white plate
Crystal size (mm)	0.435 × 0.165 × 0.068
Temperature (K)	100
Crystal System & Space Group	
Crystal system	Monoclinic
Space group	$P2_1/c$ (No. 14)
Z	4
Unit Cell Parameters	
a (Å)	7.2368(1)
b (Å)	6.4130(1)
c (Å)	27.5999(6)
α (°)	90
β (°)	95.341(2)

γ (°)	90
V (Å³)	1275.34(4)
Physical Properties	
$D^c_{al}{}^c$ (g cm^{-3})	1.492
Absorption coefficient μ (mm^{-1})	5.367
F (000)	600
Data Collection	
Radiation	Cu Kα (λ = 1.54184 Å)
Diffractometer	Rigaku XtaLAB Synergy Dualflex
Detector	HyPix Hybrid Pixel Array
θ range (°)	3.216 - 77.109
Absorption correction	Multi-scan (SCALE3 ABSPACK)
T_{min} / $T_{ma}{}^x$	0.710 / 1.000
Reflections collected	2693
Independent reflections	2479
R_{int}	0.0425
Completeness to $\theta_{ma}{}^x$	92.1%
Refinement	
Structure solution	SHELXT (Sheldrick, 2018)

Appendices

Refinement method	Full-matrix least-squares on F^2
Software	SHELXL 2019/3, Olex2 1.5
Parameters refined	162
R_1 [$I > 2\sigma(I)$]	0.0337 (2248 reflections)
wR_2 (all data)	0.0915 (2479 reflections)
Goodness-of-fit (S)	1.084
CCDC deposition no.	XXXXXXX